PN2022 INTERNATIONAL SUMMER SCHOOL PHOTONIC NANOMATERIALS

ABSTRACTS

Organizer:
St Petersburg State University

School Co-Chairs:
Vladimir G. Dubrovskii, St Petersburg State University, Russia
Frank Glas, CNRS and Universite Paris-Saclay, France

Sponsors:
Russian Science Foundation (project No. 19-72-30004)
St Petersburg State University

The Photonic Nanomaterials School
is organized as a part of 20th International Conference "Laser Optics" (ICLO-2022)

June 21–24 • 2022 • Saint Petersburg • Russia

TIMETABLE

Tuesday, June 21

Session R9-1

Ana Luisa Simões Gamboa (ITMO University, Russia)
Functions for describing non-exponential photoluminescence decay kinetics in semiconductor nanocrystals, *Invited*

Alexander Uskov (Lebedev Physical Inst. RAS, Russia)
Plasmon resonance broadening in hybrid structures, *Oral*

Olga Borovkova (Russian Quantum Center, Russia)
Transverse magnetophotonic intensity effect in plasmonic nanostructures with broken spatial symmetry, *Oral*

Akihiro Tomioka (Osaka Electro-Communication University, Japan)
Capillary-guided in-line fabrication of luminescent organic nanoparticles by visible laser processing of dye solution microdroplets, *Oral*

Muhammad Bkkar (ITMO University, Russia)
Perovskite-polymer nanocomposites based on nanofibers for flexible solar cells, *Oral*

Alexey Povolotskiy (St Petersburg State University, Russia)
Functional hybrid structures based on porphyrins and gold nanoparticles for optical sensors, *Oral*

Vlad Samyshkin (Vladimir State University, Russia)
The formation of one-dimensional LCC quasi-crystals deposited on a substrate, *Oral*

Wednesday, June 22

Poster Session

Thursday, June 23

Session ST1-1

Vladimir G. Dubrovskii (St Petersburg State University, Russia)
Growth modeling of III–V nanowires, *Invited*

George E. Cirlin (Alferov University, Russia)
Molecular beam epitaxy of semiconductor nanostructures

Session ST1-2

Ivan S. Mukhin (Alferov University, Russia)
Flexible light-emitting devices based on III–V and III–N nanowires encapsulated into polymer matrix

Rodion R. Reznik (St Petersburg State University, Russia)
III–V hybrid nanostructures on silicon: MBE growth and properties

Session ST1-3

Rodion R. Reznik (St Petersburg State University, Russia)
MBE growth and properties of AlGaAs nanowires with InGaAs quantum dots on silicon, *Oral*

Nickolay G. Sibirev (St Petersburg State University, Russia)
Droplet contact angle controlling the morphology and crystal phase of GaAs and GaP nanowires

Liliia Dvoretckaia (Alferov University, Russia)
Microspherical lithography for selective epitaxy, *Oral*

Vladimir G. Dubrovskii (St Petersburg State University, Russia)
Growth of III–V nanowires by molecular beam epitaxy: the role of material exchange with the substrate, *Oral*

Vladislav Gridchin (Alferov University, Russia)
Core-shell InGaN Nanowires: MBE growth and properties, *Oral*

Klochkov Ivan (ITMO University, Russia)
Investigation of the polymeric thin films deposed on the surfaces of optical elements using the laser multiparametric method, *Oral*

Functions for Describing Nonexponential Photoluminescence Decay Kinetics in Semiconductor Nanocrystals

A. L. Simões Gamboa[1], E. N. Bodunov[2]
[1]Centre of Optical Information Technologies, ITMO University, St. Petersburg, Russia
[2]Department of Physics, Emperor Alexander I St. Petersburg State Transport University, St. Petersburg, Russia

Abstract— We briefly review functions that we have proposed for the description of the experimentally observed nonexponential photoluminescence (PL) decay kinetics of colloidal quantum dots (QDs) at room temperature (RT) with parameters that have a straightforward physical meaning.

Keywords—colloidal quantum dot; photoluminescence kinetics; exciton; energy transfer; stretched exponential; trap; detrapping

I. Introduction

The dark-bright exciton model [1] predicts single-exponential kinetics of PL decay of an ensemble of nearly monodisperse II-VI and III-V QDs at RT [2] but this is rarely observed experimentally. A sum of exponential functions is commonly used for approximating the decays, with the choice of the number of exponentials being to a large extent arbitrary, or a single exponential, ignoring the long-time tails associated to charge detrapping processes leading to PL blinking [3]. We have proposed models and resultant functions with a minimum of physically meaningful parameters for the description of the PL decay kinetics of QDs at RT that have also been proven fruitful in the analysis of the nonexponential PL decays of other colloidal semiconductor nanocrystals.

II. Stretched exponential functional form

Based on the works by Förster and Ermolaev et al. [4,5] we have suggested that a stretched exponential functional form of the PL decay can be understood in terms of long-range resonance energy transfer from the QDs to energy acceptors randomly distributed in their surroundings (Förster kinetics), in particular anharmonic molecular vibrations, or by contact quenching by Poisson distributed quenchers on the surface of the QDs [2,6,7]. These approaches have provided a physically relevant framework for the analysis of the PL decays of nanocrystals of different composition [2,7,8] and shape (nanoplatelets, quantum rings) [9].

III. Reversible trapping of excited charge carriers

In another approach, we have suggested a model that considers reversible trapping of photogenerated charge carriers [10,11]. We assume (i) the trapped charge carriers can be either electrons or holes, (ii) the traps are not recombination centers, (iii) the number of traps per QD follows a Poisson distribution, and (iv) a single (average) trap depth. The resultant function has four physically meaningful parameters (characteristic radiative time constant of the exciton, trapping and detrapping rate constants, and average number of traps per QD), one of which (time constant) can be theoretically calculated [1]. Using this function it is possible to estimate the trap depth and obtain insight concerning the nature of the trap states involved in the recombination of the charge carriers in QDs with different core/shell architecture (sharp vs. compositionally graded interface) [10,11] and quantum confined materials of different shape [9]. We hope that our approach may be proven useful in the analysis of the nonexponential PL decays of other materials, beyond inorganic semiconductor nanocrystals.

References

[1] P. C. Sercel and Al. L. Efros, "Band-Edge Exciton in CdSe and Other II-VI and III-V Compound Semiconductor Nanocrystals - Revisited," Nano Lett., vol. 18, pp. 4061-4068, June 2018.

[2] E. N. Bodunov, V. V. Danilov, A. S. Panfutova, and A. L. Simões Gamboa, "Room-Temperature Luminescence Decay of Colloidal Semiconductor Quantum Dots: Nonexponentiality Revisited," Ann. Phys. (Berlin), vol. 528, pp. 272-277, April 2016.

[3] P. H. Sher, J. M. Smith, P. A. Dalgarno, R. J. Warburton, X. Chen, P. J. Dobson, S. M. Daniels, N. L. Pickett, and P. O'Brien, "Power Law Carrier Dynamics in Semiconductor Nanocrystals at Nanosecond Timescales," Appl. Phys. Lett., vol. 92, pp. 101111, March 2008.

[4] Th. Förster, "Experimentelle und Theoretische Untersuchung des Zwischenmolekularen Ubergangs von Elektronenanregungsenergie," Z. Naturforsch., vol. 4a, pp. 321-327, January 1949.

[5] V. L. Ermolaev, E. B. Sveshnikova, and E. N. Bodunov, "Inductive-Resonant Mechanism of Nonradiative Transitions in Ions and Molecules in Condensed Phase," Phys.-Usp., vol. 39, pp. 261-282, March 1996.

[6] E. N. Bodunov, Yu. A. Antonov, and A. L. Simões Gamboa,"On the Origin of Stretched Exponential (Kohlrausch) Relaxation Kinetics in the Room Temperature Luminescence Decay of Colloidal Quantum Dots," J. Chem. Phys., vol. 146, pp. 114102, March 2017.

[7] E. N. Bodunov and A. L. Simões Gamboa, "Luminescence Decay of Colloidal Quantum Dots and Stretched Exponential (Kohlrausch) Relaxation Function," Semiconductors, vol. 52, pp. 587-589, May 2018.

[8] O. Stroyuk, A. Raevskaya, F. Spranger, N. Gaponik, and D. R. T. Zahn, "Temperature-Dependent Photoluminescence of Silver-Indium-Sulfide Nanocrystals in Aqueous Colloidal Solutions," ChemPhysChem, vol. 20, pp. 1640-1648, April 2019.

[9] J. Xiao, Y. Liu, V. Steinmetz, M. Çağlar, J. Mc Hugh, T. Baikie, N. Gauriot, M. Nguyen, E. Ruggeri, Z. Andaji-Garmaroudi, S. D. Stranks, L. Legrand, T. Barisien, R. H. Friend, N. C. Greenham, A. Rao, and R. Pandya, "Optical and Electronic Properties of Colloidal CdSe Quantum Rings," ACS Nano, vol. 14, pp. 14740-14760, October 2020.

[10] E. N. Bodunov and A. L. Simões Gamboa,"Photoluminescence Decay of Colloidal Quantum Dots: Reversible Trapping and the Nature of the Relevant Trap States," J. Phys. Chem. C, vol. 123, pp. 25515-25523, September 2019.

[11] E. N. Bodunov and A. L. Simões Gamboa, "Kinetics of Photoluminescence Decay of Colloidal Quantum Dots: Reversible Trapping of Photogenerated Charge Carriers," Semiconductors, vol. 53, pp. 2133-2136, December 2019.

Plasmon Resonance Broadening in Hybrid Structures

A.V.Uskov[1], J.B. Khurgin,[2] I.V. Smetanin[1], I.E. Protsenko[1], N.V. Nikonorov[3]
[1]P. N. Lebedev Physical Institute, Russian Academy of Sciences, Leninskiy Pr. 53, Moscow, 119333, Russia
[2]Department of ECE, John Hopkins University, Baltimore, Maryland 21218, United States
[3]ITMO University, Kronverskiy av. 49, St. Petersburg 197101, Russia

Abstract— Landau Damping (LD) mechanism of the Localized Surface Plasmon (LSP) decay is studied for the hybrid nanoplasmonic (metal core/dielectric shell) structures. It is shown that LD in hybrid structures is strongly affected by the permittivity and the electron effective mass in the dielectric shell. The physical reason for this effect is identified as electron spillover into the dielectric where the electric field is higher than in the metal and as the presence of quasi-discrete energy levels in the dielectric. Our results indicate that by judicious selection of dielectric material and its thickness one can engineer decay rates and hot carrier production for important applications, such as photodetection and photochemistry.

Keywords— hot electron generation, Landau damping

I. Introduction

Recently [1], a new research area, "hybrid plasmonics", has been established, which studies the structures comprising of plasmonic metals, covered with a dielectric shell. These hybrid plasmonic structures are of great interest, and have many potential applications in photodetection, photovoltaics and photocatalysis [2-3]. The applications are based on photoexcitation of hot carriers in the metal with their transfer into surroundings. In small nanoparticles, the hot carrier generation is a result of collisions of metal electrons with metal border accompanied by light absorption and plasmonic resonance broadening – so called Landau Damping (LD).

II. Model

Fig. 1a illustrates hybrid nanoparticle, in which incident light of the frequency excites Localized Surface Plasmon (LSP). In calculations of LD in the hybrid structure, we follow the approach developed in [4] in which the Kreibig coefficient A, characterizing LD, is given as $A = A_{mat} A_{geom}$ where A_{mat} depends on the nanoparticle size and shape. On the other hand, A_{mat} depends on material parameters, and in particular, on characteristics of the interface between the metal nanoparticle and the surroundings. Here, we calculate A_{mat} for hybrid plasmonic nanostructures.

III. Results and Conclusion

Our calculations show strong dependence of the coefficient A_{mat} on the permittivity ε_d and the effective electron mass m_d in the dielectric shell, that is the effect of: (a) penetration of electron in dielectric where the electric field of LSP much stronger than in metal; (b) the presence of quasi-discrete levels in the dielectric. The theory indicates that the *transition* absorption at the interface metal-dielectric contributes dominantly into LD. Interference of electron wave functions at the quasi-discrete level and in metal ("bound state in continuum") leads to Fano-type resonances in absorption of photon by electrons.

Fig.1b maps the coefficient A_{mat} in the parameter space (m_d, ε_d) at given $\hbar\omega$=1.9eV and d=3nm, and shows that in hybrid plasmonic structures A_{mat} can be higher by several times compared with A_{mat} in conventional structures.

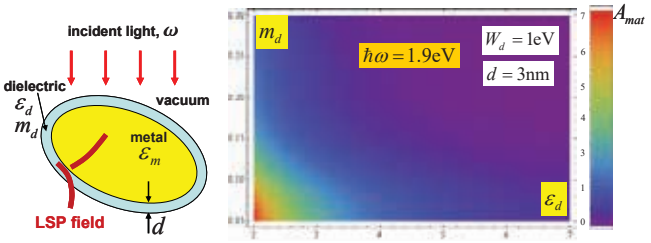

(a) (b)

Fig. 1. (a) Light of the frequency ω excites LSP in hybrid plasmonic nanoparticle. (b) A_{mat} as function of ε_d and m_d. $\hbar\omega$ =1.9eV, d=3nm. W_d is the work function from the metal to the dielectric.

As conclusion, proper choice of dielectric material and its thickness in hybrid structure one can substantially enhance hot carrier production for application in photodetection and photochemistry.

Acknowledgment

AVU, IVS and NVN thank Russian Science Foundation (20-19-00559) for support

References

[1] S. Linic, S. Chavez, and R.Elias, "Flow and extraction of energy and charge carriers in hybrid plasmonic nanostructures," Nat. Mater., vol. 20, pp. 916–924 (2021).

[2] M. Brongersma, N. Halas, and P. Nordlander, "Plasmon-induced hot carrier science and technology," Nature Nanotech., vol. 10, pp. 25–34, (2015).

[3] Y. Zhang, S. He, W. Guo, Y. Hu, J. Huang, J. R. Mulcahy, W. D. Wei, "Surface-Plasmon-Driven Hot Electron Photochemistry," Chemical Reviews, vol. 118, pp. 2927-2954 (2018).

[4] A. V. Uskov, I. E. Protsenko, N. A. Mortensen, and E. P. O'Reilly, "Broadening of Plasmonic Resonance Due to Electron Collisions with Nanoparticle Boundary: a Quantum Mechanical Consideration," Plasmonics, vol. 9, pp. 185–192 (2014).

Transverse magnetophotonic intensity effect in plasmonic nanostructures with broken spatial symmetry

O.V. Borovkova[1,2], H. Hashim[3,4], M.A. Kozhaev[1], S.A. Dagesyan[2], A.N. Kalish[1,2], A.N. Shaposhnikov[5], V.N. Berzhansky[5], V.I. Belotelov[1,2]

[1] Russian Quantum center, Skolkovo, Russia, o.borovkova@rqc.ru

[2] Faculty of Physics, Lomonosov Moscow state University, Moscow, Russia

[3] Physics Department, Faculty of Science, Tanta University, 31527, Tanta, Egypt

[4] Immanuel Kant Baltic Federal University, Kaliningrad 236004, Russia

[5] V.I. Vernadsky Crimean Federal University, 295007, Simferopol, Russia

***Abstract*—The transmittance of any nanostructure can be controlled by proper engineering of its dielectric and spatial properties. Applied magnetic field determines the dielectric properties of the ferrimagnetic nanostructures as well. We address the transverse magnetooptical intensity effect in two types of the nonsymmetric plasmonic nanostructures. It is shown that the effect depends on the asymmetry of the structure.**

***Index Terms*—magnetooptics, plasmonics, broken spatial symmetry, nanostructure**

I. Introduction

The transmittance of any material and structure depends on its dielectric properties and its geometry. This feature is widely used to explore the internal structure of materials and samples. If the sample has among its compounds a ferrimagnetic element, then the dielectric properties and the transmittance of the whole sample can be controlled by the external magnetic field. The so-called magnetooptical effects are related to the dielectric properties variations due to the change of the external magnetic field [1].

Apart from that, the nanostructuring facilitates the optical transmittance control via the optimization of geometrical parameters. Plasmonic nanostructures support a subwavelength localization of optical field via the excitation of the surface plasmon polaritons (SPPs) [2]. These optical modes are very sensitive to both dielectric properties of the materials and to the structure patterning. The latter can be clearly seen in the plasmonic nanostructures with spatial symmetry breaking that provide unidirectional propagation of the SPP modes [3], [4].

Recently, it was shown in [5], [6] that combination of the spatially nonsymmetric plasmonic nanostructures and the magnetic materials can give rise to the novel possibility of the transmittance and magnetooptical response control in the nanostructure.

This study was supported by Russian Science Foundation (project no. 20-72-10159). O.V.B. thanks the personal support by the Foundation for the Advancement of Theoretical Physics and Mathematics “BASIS”.

II. Results

We explore the magnetooptical properties of the magnetoplasmonic nanostructures with spatial symmetry breaking. Two types of the nanostructures are addressed. The first one contains plasmonic grating where the metal stripes of two different width alternate each other. Therefore, the grating with the double period has nonsymmetric unit cell, and the whole grating possesses the spatial symmetry breaking. The second considered structure is a comb-like plasmonic grating where the single unit cell includes one gold stripe with lateral modulation.

The transverse intensity magnetophotonic effect (TMPTE) shows the relative change of the transmittance of the nanostructure for two opposite directions of the magnetization of the structure. The magnetization of the structure is created by the external magnetic field. When the magnitude of the field is great enough to achieve the saturation the magnetization of the ferrimagnetic layer become directed along the magnetic field. It was shown that with the change of the asymmetry parameter the measured magnetophotonic effect changed. Moreover, for the comb-like magnetoplasmonic grating there was demonstrated the nanostructure with the optimal parameters when the magnetophotonic effect achieved its maximum.

References

[1] A.K. Zvezdin, V.A. Kotov, Modern Magnetooptics and Magnetooptical Materials, IOP, 1997.

[2] S.A. Maier, Plasmonics: Fundamnetals and Applications, Springer, 2007.

[3] X.Y. Zhu, Y.L. Xu, Y. Zou, X.C. Sun, C. He, M. H. Lu, et al., “Asymmetric diffraction based on a passive parity-time grating”, Appl. Phys. Lett., vol. 109, 111101, 2016.

[4] L. Feng, Y.-L. Xu, W.S. Fegadolli, M.-H. Lu, J.E.B. Oliveira, V.R. Almeida, et al., “Experimental demonstration of a unidirectional reflectionless parity-time metamaterial at optical frequencies”, Nat. Mater., vol. 12, p. 108, 2013.

[5] O.V. Borovkova, M.A. Kozhaev, H. Hashim, A.A. Kolosova, A.N. Kalish, S.A. Dagesyan, et al., “Transverse Magneto-Photonic Transmission Effect in Non-Symmetric Nanostructures with Comb-like Plasmonic Gratings,” Optical Materials Express, vol. 12, pp. 573–583, 2022.

[6] O.V. Borovkova, H. Hashim, D.O. Ignatyeva, M.A. Kozhaev, A.N. Kalish, S.A. Dagesyan, et al., “Magnetoplasmonic structures with broken spatial symmetry,” Phys. Rev. B, vol. 102, p. 081405(R), 2020.

Perovskite-polymer nanocomposites based on nanofibers for flexible solar cells

M.A. Bkkar [1], R. O. Olekhnovich [1] , M. V. Uspenskaya [1]
[1] ITMO University, Saint-Petersburg, Russia

Abstract— we study the crystallinity and light absorption properties of $CsPbI_3$: polyvinylpyrrolidone nanofibers, which can be used as active layers for solar cells. Experimental results show that the black phase of $CsPbI_3$ nanocrystals can be manipulated using the annealing parameters.

Keywords— crystallinity, light absorption, nanofibers, annealing, black phase.

In the field of renewable energy, organometal and non-organometal halide perovskite materials have attracted researchers, owning to their stunning optoelectronic and electrical properties. Unfortunately, the instability of these materials under room conditions limits their ability to leave the laboratory [1]. Perovskite-polymer nanocomposite engineering is a new approach to obtain more effective and stable perovskite solar cells. These nanocomposites have two types of nanostructures: nanolayers and nanofibrillar membranes. The former is usually prepared by a spin-coating method. The latter is obtained by an electrospinning method [1,2]. Perovskite nanofibrillar membranes are considered to be flexible, light-weight, and low-cost photoactive materials. Due to the internal reflection of light and optical cavities, perovskite-polymer nanocomposites based on nanofibers have higher light absorption properties than their thin-film counterparts [2]. Their optical and electronic properties are strongly dependent on various parameters related to the electrospinning and annealing processes [2]. Herein, the influence of annealing parameters on perovskite crystallinity and light absorption was studied.

The annealing temperature was changed from 60 °C to 350 °C, and the annealing time from 5 min to 90 min. XRD patterns confirm that stable α-$CsPbI_3$ nanocrystals embedded in polyvinylpyrrolidone nanofibers were obtained at annealing parameters 150-200 °C for 5 min. Increasing the annealing temperature up to 300 °C leads to the formation of β-$CsPbI_3$ nanocrystals. Whereas γ-$CsPbI_3$ perovskite was obtained after annealing at 350 °C for 5 min. The flexibility of nanofibrillar membranes decreases with increasing the annealing temperature. Increasing the annealing time from 5 min to 20 min at 350 °C results in lower crystallinity of γ-$CsPbI_3$. While annealing at 180 °C for 90 min leads to a little enhancement in the crystallinity of α-$CsPbI_3$. However, flexible nanofibers (see fig. 1) with stable α-$CsPbI_3$ or β-$CsPbI_3$ nanocrystals have resulted at annealing parameters 150-250 °C for 5-90 min. Light absorption results are consistent with XRD results. The bandgap

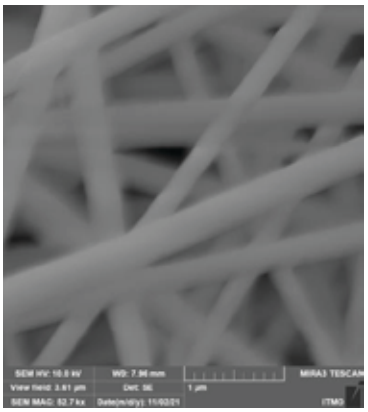

Fig. 1. The nanofibrillar membrane with stable α-$CsPbI_3$ nanocrystals obtained after annealing at 180 °C for 5 min.

was changed from 1.7 eV to 1.75 eV. It is slightly broader than reported in the literature [3,4].

The stability of perovskite nanofibers to environmental conditions was found to be up to 15 days, and the thermal stability up to 200-250 °C.

Finally, black-phase $CsPbI_3$ nanocrystals: polyvinylpyrrolidone flexible nanofibrillar membranes were successfully prepared by controlling annealing parameters. Perovskite phases were characterized by XRD patterns and light absorption spectra.

REFERENCES

[1] M. A. Bkkar, R. O. Olekhnovich, and M.V. Uspenskaya, "Perovskite nanocomposite layers engineering for efficient and stable solar cells," Journal of Nano Research. Switzerland, vol. 71, pp. 71-109, 2022.

[2] M. A. Bkkar, R. O. Olekhnovich, and M.V. Uspenskaya, "Obtaining nanofibers based on perovskite-polymer composites for applying in solar cells," SGEM2020. Hungary, vol. 20, pp. 129, 2020.

[3] H. Yao, J. Zhao, Z. Li, Z. Ci, and Z. Jin, "Research and progress of black metastable phase $CsPbI_3$ solar cells," Mater. Chem. Front., vol. 5, 1221-1235, 2021.

[4] Z. Yao, W. Zhao, S. (Frank) Liu, "Stability of the $CsPbI_3$ perovskite: from fundamentals to improvements," J. Mater. Chem. A, vol. 9, 11124, 2021.

Functional hybrid structures based on porphyrins and gold nanoparticles for optical sensors

A.V.Povolotskiy*[1], D.A.Soldatova[1], A.V.Povolotckaia[2], O.S. Smirnova[1], D.A.Lukyanov[1]
[1]Institute of Chemistry, Saint-Petersburg University, Saint-Petersburg, Russia
[2]Research Park, Saint-Petersburg University, Saint-Petersburg, Russia
*alexey.povolotskiy@spbu.ru

Abstract— The mechanisms of interaction between optically excited porphyrins and gold nanoparticles determine the functional properties of hybrid structures based on them and make it possible to create various optical sensors. The mechanisms of charge and energy transfer, luminescence quenching and the temperature dependence of the luminescence intensity have been studied.

Keywords — porphyrins, gold nanoparticles, hybrid nanostructure, oxygen sensor, luminescent thermometer, charge transfer, energy transfer

The interaction of organic molecules with metal nanoparticles (NPs) is of great interest for various scientific fields, including optics, laser physics, molecular plasmonics, medicine etc [1,2]. To date, a large number of publications have focused on the synthesis of noble metal NPs coated with organic molecules [3,4]. However, understanding the interaction mechanisms of organic stabilizing agents and ligands with the NP surface remains the main problem.

Synthesis of gold NPs was carried out by laser ablation in a liquid. The main advantage of this method is the highest chemical purity of the colloidal solution in comparison with other synthesis methods. The size of the obtained gold nanoparticles was about 20±5 nm.

Absorption spectroscopy and fluorescence spectroscopy were used to mechanisms study of binding of various natures porphyrins to gold NPs.

Porphyrins with amino groups effectively bind to the surface of gold. Cationic porphyrins cause the aggregation of gold NPs by reducing the stability of the colloidal solution. When gold nanoparticles are added to solutions of molecular components, static quenching of fluorescence is observed, which is a consequence of the formation of hybrid molecular-plasmon nanostructures. When gold NPs aggregate in solution, a combination of static and dynamic quenching is observed.

The effect of enhancing the generation of singlet oxygen by porphyrin molecules due to the surface plasmon resonance of gold nanoparticles was found (Fig. 1).

The dependence of the luminescent properties of porphyrins on temperature, including those in the composition of hybrid nanostructures, has been studied. It is shown that all considered systems can be used for ratiometric measurements with different efficiency (depending on solvent and temperature range).

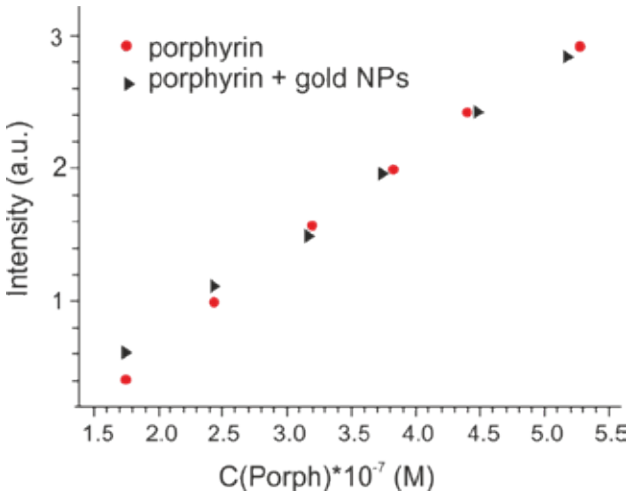

Fig. 1. Dependence of the singlet oxygen luminescence intensity on the porphyrin concentration.

ACKNOWLEDGMENT

Experimental part of the work was carried out with equipment of Center for Optical and Laser Materials Research, Research Park of Saint-Petersburg State University.

The work was supported by Saint-Petersburg University as part of the funding of a scientific laboratory under the guidance of a young scientist (ID: 92350587).

REFERENCES

[1] A. Csaki, T. Schneider, J. Wirth et al. “Molecular plasmonics: light meets molecules at the nanoscale,” Philosophical Transactions of the Royal Society A: Mathematical, Phys. and Eng. Sci., vol. 369, p. 1950, 2011.

[2] A. Povolotskaya, A. Povolotskiy, A. Manshina “Hybrid nanostructures: synthesis, morphology and functional properties,” Russian Chemical Reviews, vol. 84, p. 579, 2015.

[3] M. Kanehara, H. Takahashi, T. Teranishi, “Gold (0) porphyrins on gold nanoparticles,” Angewandte Chemie International Edition, vol. 47. iss. 2. pp. 307-310, 2008.

[4] A. Povolotskiy et al., “Molecular-plasmon nanostructures for biomedical application,” Springer Ser. in Chem. Phys., vol. 119, pp. 173–193, 2019.

The formation of one-dimensional LCC quasicrystals deposited on a substrate.

V. Samyshkin[1] , S Kutrovskaya[1,2,3], A. Osipov[1,3] , Igor Chestnov[1,2,3] , A. Kucherik[1]
1 Department of Physics and Applied Mathematics, Stoletov Vladimir State University, 600000, 87 Gorkii street, Vladimir, Russia
2- School of Science, Westlake University, 18 Shilongshan Road, Hangzhou 310024, China
3 Institute of Natural Sciences, Westlake Institute for Advanced Study, 18 Shilongshan Road, Hangzhou 310024, China

Abstract— A new method of deposition of spatially ordered polyyne filaments stretched by external fields during deposition has been proposed and described. An experimental setup has been designed that enables the creation of anisotropic nanostructured films composed of one-dimensional LCC (Linear Carbon Chains) quasicrystals by aerosol spraying of colloidal solutions in a constant electric field. The formation of these nanostructures is confirmed by TEM images and diffraction patterns.

Keywords—carbon chain; 1D crystal ; electric field; deposition.

Long linear carbon chains are formed due to the use of two-step irradiation method of colloidal solution [1]. Laser irradiation of an initial system with shungite (a natural mineral containing all kinds of allotropes of carbon) creates conditions for phase transformation of the material into a linear form of carbon[2]. Gold nanoparticles (NP) have been used as catalysts for chain growth and stabilizing anchors which prevent carbon chains from twisting and remaining in a stable state for a long time [2]. Such carbon-gold systems can be considered nanodipoles.

To form one-dimensional LLC quasicrystals on a substrate surface, the so-called Spray-Jet method was used, implemented in an experimental apparatus (Fig.1). Application of external electric field allowed to realize spatial orientation of LCC with gold nanoparticles on their ends[3].

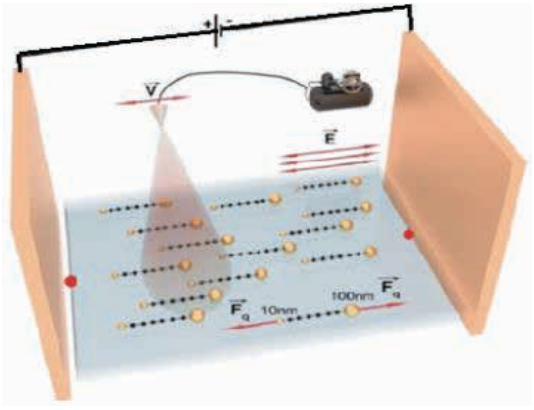

Figure 1. The scheme of the experimental setup used for the controlled deposition of carbon chains stabilised with gold NPs.

Figure 1 shows schematically our developed method of deposition of linear-chain carbon, followed by the formation of one-dimensional quasicrystals. After laser synthesis of the colloidal system, the stabilised linear-chain carbon was atomised at 70 kPa. The obtained nanodipoles CAu, passing through two plane-parallel electrodes, are exposed to an external electric field and in the process of deposition on a solid substrate they line up with lines of electric intensity of 10^5 V/m .

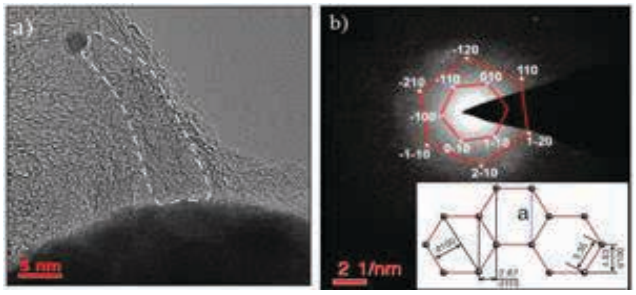

Figure 2. a) TEM image of linear carbon chains anchored between gold nanoparticles. The lower part of the image is occupied by a spherical gold nanoparticle with an average diameter of 25 nm, b) Diffraction pattern obtained from this region. The reflexes are indexed according to the Miller system.

The developed method for the formation of one-dimensional quasicrystals of linear-chain carbon has proven to be effective, as shown in (Fig. 2). An additional argument in favour of using this method, is the obtained diffraction pattern confirming the characteristic linear one-dimensional carbon phase (Fig. 2b).

ACKNOWLEDGMENT

Acknowledges support from the Ministry of Science and Higher Education within the State assignment Vladimir State University, project No. 0635-2020-0013.

The study was carried out using the equipment of the interregional multispecialty and interdisciplinary center for the collective usage of promising and competitive technologies in the areas of development and application in industry/mechanical engineering of domestic achievements in the field of nanotechnology (Agreement No. 075-15-2021-692 of August 5, 2021).

The support from the Grant of the President of the Russian Federation for state support of young Russian scientists No. MK-5318.2021.1.2 is acknowledged.

REFERENCES

1. Kucherik A. O. et al. Two-stage laser-induced synthesis of linear carbon chains //Quantum Electronics. – 2016. – T. 46. – №. 7. – C. 627.
2. Kucherik, A. et al. Laser-induced synthesis of metal–carbon materials for implementing surface-enhanced Raman scattering. Opt Spectrosc 121, 263–270 (2016).
3. Kutrovskaya S. et al. Electric field assisted alignment of monoatomic carbon chains //Scientific reports. – 2020. – T. 10. – №. 1. – C. 1-7.

Capillary-guided in-line fabrication of luminescent organic nanoparticles by visible laser processing of dye solution microdroplets

A. Tomioka[1], S. Arai[1], T. Okada[1] and Y. Tate[1]
[1]Graduate School of Engineering, Osaka Electro-Communication University, Osaka Japan

Abstract— We propose a novel procedure, liquid-phase laser processing based on a visible pulse laser resonant excitation [1], which is expected not to damage the organic material, but efficiently invoke the molecular vibration via strong electron-phonon coupling of π -conjugated organic dyes MEHPPV, leading to nanoparticle (NP) formation, after exposed to and cooled by insoluble water [2].

Keywords— liquid-phase laser processing; organic dyes; luminescent nanoparticles; microdroplet; capillary

I. Introduction

Here we imagine a practical palmtop projectors whose light source is a printed pattern of luminescent nanoparticles (NPs). That is a static image projector without the TFT circuitry. One can easily exchange the NP sheet after another printing to alter the image. High resolution images projected in front of the restaurants, shops, or ceremonial halls will attract the pedestrian's interest effectively with only a lighting power. For this purpose we need to prepare large volumes of luminescent NPs with homogeneous size distribution in an hour or so.

II. Results and Discussions

Fluorescence optical microscopy revealed that a large volume of fluorescent NPs were successfully fabricated. Dynamic light scattering apparatus revealed that NPs have unimodal size distribution in 100nm - 300nm. However, there are several issues to be solved in this original method [1]. The first issue is irregular suspension of the microdroplets: the hand-held homogenizer produced standing sonic waves with peak intensities positioned in a lattice. The difficulty of holding the dye solution injector tip at these peak positions brought about inhomogeneous suspension of dye droplets. It led to broad distribution of resultant NP size after laser processing, which is inadequate for application, e.g. printing ink to form a display pixel in a high-resolution static-image flexible digital signage device [2]. Furthermore, the second issue is that, during the laser irradiation, NPs randomly diffused into the water in a beaker, crossing the laser beam for a short time in a Brownian motion. It led to broad distribution of irradiation time among dye droplets, sometimes bringing about large irregular aggregates. The third issue is that if we took too much time for microdroplets suspension, the produced heat evaporated the chloroform and formed a solid MEHPPV film on the water surface which hindered the laser irradiation. Instead of this two-step fabrication [3], microdroplet suspension and laser irradiation, we propose a novel procedure which performs these two-steps simultaneously: we have devised a continuous fabrication machinery which utilizes a glass capillary as a flow path (Fig. 1): dye solution injected into the water flow in the capillary is dispersed as microdroplets by an ultrasonic agitation. The laser beam is guided through the capillary with a beam diameter larger than the capillary diameter. All the resultant dispersed dye microdroplets are laser processed with the same intensity and for the same duration of time while the microdroplets travel through the whole length of the capillary. This mechanism assures that every dye microdroplet is homogeneously laser processed and converted to solid NPs, which makes us expect homogeneous and narrow distribution of resultant NP size. Preliminary results of using this novel machinery suggested an improvement in the narrow distribution of resultant dye NP size. This machinery enabled a continuous and large volume production of dye NPs with homogeneous size, which can be applied to industrial production of well-dispersed dye NPs for a static image projector.

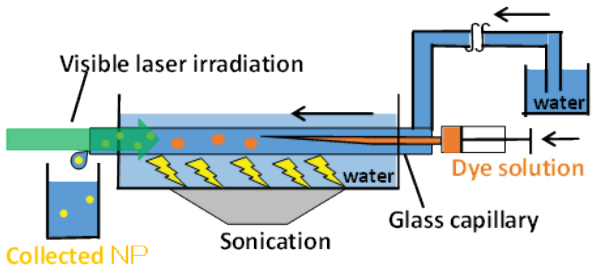

Fig. 1. Continuous NP fabrication by simultaneous suspension of and laser irradiation to microdroplets flowing through a glass capillary.

Acknowledgment

This research was supported by Amada Foundation and Electronics Fundamental Research Center in Osaka Electro-Communication University.

References

[1] K. Takada and A. Tomioka, "Solution-phase laser processing of π-conjugated polymers: Switching between different molecular states," J. Phys.: Conf. Ser., vol. 358 012012, pp. 1-7, 2012.

[2] S. Fushii, A. Tomioka, and Y. Matsuba, "Fabrication of ultrathin TiO_2 film with nanogrooves to trap organic dye nanoparticles," Phys. Status Solidi B, vol. 254, 1600720, pp. 1-6, 2017.

[3] Y. Matsuba, S. Fushii, M. Kawabata, and A. Tomioka, "Patterned deposition of luminescent organic nanoparticles fabricated by visible laser processing," Phys. Status Solidi, vol. B 254, 1600725, pp. 1-6, 2017.

Molecular beam epitaxy of semiconductor nanostructures

George Cirlin

Alferov University, Saint-Petersburg 194021, Russia
Saint-Petersburg State University, Saint-Petersburg 198504, Russia

Email: cirlin@ibeam.ioffe.ru
Keywords: III-N nanostructures, MBE, Si based substrate

In my talk I will briefly discuss the issues of MBE growth of different nanostructures. The main topics include the growth of heterostructures, quantum wells, quantum dots, multilayer structures as well as nanowires in different semiconductor systems. In the second part I will focus on various characterization techniques which are commonly used to study the grown structures. Different application areas are also discussed in a view of most important device structures.

III–V hybrid nanostructures on silicon: MBE growth and properties

R.R. Reznik[1-3], I.V. Ilkiv[1,], K.P. Kotlyar[1-3], V.O. Grodchin[1-3], E.V. Ubyivovk[1], N.S. Dragunova[2], N.V. Kryzhanovskaya[2], G.E. Cirlin[1-3]

[1]Faculty of Physics, St. Petersburg State University, St. Petersburg, Russia
[2]Alferov University, St. Petersburg, Russia
[3]Institute for Analytical Instrumentation RAS, St. Petersburg, Russia

Abstract— III–V hybrid nanostructures based on III–V materials including III–N has been grown by molecular-beam epitaxy on silicon.

Keywords— III–V semiconductors, nanowires, quantum dots, silicon, molecular-beam epitaxy.

I. Introduction

A combination of nanowires (NWs) with quantum dots (QDs), are promising building blocks for future optoelectronic devices, in particular, single-photon emitters [1]. The most studied epitaxially grown QDs are self assembled, i.e., grown by island nucleation in the Stranski-Krastanow growth mode. In common case, the size, shape, and density of self-assembled QDs can be changed by growth parameters, but it is a strain induced process and controlling the properties of the array independently is a challenging task. QDs in nanowires have in contrast shown great potential as a highly controllable system. The diameter, height, and density of the QDs are defined by the NW diameter, the growth time, and the NW density, respectively, and can be chosen more predictable.

In this paper we present the results of experimental studies on III-V hybrid nanostructures on silicon growth by molecular-beam epitaxy and physical properties of grown nanostructures.

II. Experimental

Experimentally, all the samples in the present work were grown by molecular beam epitaxy (MBE). For AlGaAs/GaAs material systems, different growth conditions were applied, but the strategy was the same: we have used Au-assisted in AlGaAs NWs. Comparison of photoluminescence spectra of grown GaN on hybrid and the most successful GaN NWs structures on silicon shows that the intensity of radiation from grown on SiC buffer layer GaN NWs is more than two times higher than the intensity from the best GaN structures on silicon. This fact leads to the conclusion that grown structures have fewer defects compared with GaN NWs on silicon sustrate. This is caused by a smaller lattice constant mismatch between GaN and SiC compared with GaN and Si. It should be noted that vicinal SiC/Si substrate were used for GaN NWs MBE growth. The results of morphological studies have shown that NWs on the slope and singular part of surface had different properties.

Finally, in this work we present the results of a set of experimental studies on the synthesis by molecular beam epitaxy and the study of the morphological and optical properties of InGaN nanostruc-tures of branched morphology (resembling nano-flowers, NF) directly on the surface of the silicon sub-strate. The results of morphological studies have shown that the growth occurs in several “stages.” The grown structures display an FL line in a wide wavelength range from 450 to 950 nm at room tempera-ture. All these facts indicate the prospects of such structures for optical applications, such as creating white LEDs based on a single material.

Acknowledgment

The samples were grown under financial support of Russian Science Foundation Grant № 21-72-00099. Morphological and structural properties of grown samples were studied under financial support of the research grant of St. Petersburg State University No. 75746688. Optical

growth of the NWs on Si(111) substrate, firstly we grew the AlGaAs base of the NW, secondarily, the GaAs nanoinsertion with lower bandgap, or QD, was formed and we end the structure with the core with the same material as the base. It was found that during the growth spontaneous, independently on the Al fraction, core-shell structures with lower aluminum con-tent in the cores are formed. Optically, our growth method results in the formation of GaAs QD in a Al-GaAs NW having very narrow spectral linewidth (< 10 μeV), single-photon emission in the wavelength range 750–820 nm in dependence on the QD growth recipe. Moreover, the emission wavelengths allows one to design light emission devices in a red range by simply changing of the Al fraction

properties of grown samples were studied under financial support of the Ministry of Science and Higher Education of the Russian Federation, research project no. 2019-1442.

REFERENCES

[1] V.G. Dubrovskii, G.E Cirlin and V.M. Ustinov, "Semiconductor nanowhiskers: Synthesis, properties, and applications" Semiconductors, vol 43, pp. 1539–1584, 2009.

MBE growth and properties of AlGaAs nanowires with InGaAs quantum dots on silicon

R.R.Reznik[1-4], I.V.Ilkiv[1,], K.P.Kotlyar[1-3], V.O.Grodchin[1-3], E.V. Ubyivovk[1], N.S.Dragunova[2], N.V.Kryzhanovskaya[2], N.Akopian[5], G.E.Cirlin[1-4]

[1]Faculty of Physics, St. Petersburg State University, St. Petersburg, Russia
[2]Alferov University, St. Petersburg, Russia
[3]Institute for Analytical Instrumentation RAS, St. Petersburg, Russia
[4]ITMO University, St. Petersburg, Russia
[5]Department of Photonics Engineering, Technical University of Denmark, Lyngby, Denmark

Abstract— AlGaAs nanowires with InGaAs quantum dots were grown on silicon by molecular-beam epitaxy under different growth conditions for the first time. The results of physical properties studies showed that by changing the quantum dots growth time, the ratio of III materials fluxes and the growth temperature it is possible to control the size and composition of quantum dots.

Keywords— III-V semiconductors, nanowires, quantum dots, silicon, molecular-beam epitaxy.

I. INTRODUCTION

Nowadays hybrid semiconductor nanostructures based on III-V nanowires (NWs) with quantum dots (QDs) are attracting increasing interest of researchers for creating optoelectronic applications [1]. Progress in the development of modern synthesis methods, such as molecular-beam epitaxy (MBE), makes it possible to controllably create high-quality QDs in the body of NWs within a single growth process. However, to increase the number of applications based on NWs with QDs, it is necessary to expand the set of materials of QDs and NWs.

In this paper we present the results of experimental studies on AlGaAs NWs with InGaAs QDs MBE growth on silicon surface and physical properties of grown nanostructures.

II. EXPERIMENTAL

AlGaAs NWs with InGaAs QDs were grown using MBE setup Riber Compact 21T. Si(111) S-I wafers were used as the substrates for MBE growth. On the preliminary stage Si surfaces were chemically cleaned using HF aqueous solution (1:10). Then substrates were loaded into metallization chamber of the MBE setup and heated to 950°C for thermal cleaning and removal of remaining native oxide layer from the Si surface. On the next step substrates temperature was decreased to 550℃ for deposition thin (~0.1 nm) Au layer with 1 minute pause for formation of Au droplets on the surface. After

The morphology of the grown NWs was studied by scanning electron microscopy (SEM). Structural properties and chemical composition of the grown NWs were investigated by transmission electron microscopy (TEM). Optical properties of grown nanostructures were studied by photoluminescence technique at room temperature and 4K.

III. RESULTS AND CONCLUTIONS

The results of studying the dependence of the nanostructures physical properties on growth conditions showed that by changing the quantum dots growth time, the ratio of III materials fluxes and the growth temperature, it is possible to control the size and composition of quantum dots. The possibility of AlGaAs nanowires growing at low temperatures makes it possible to synthesize InGaAs quantum dots with a high indium content and get closer to telecommunications wavelengths of radiation from quantum dots, which is difficult in case of GaAs nanowires growing. Moreover, studies of the grown nanostructures optical properties have shown the presence of narrow lines in the photoluminescence spectra at 4K. This fact indirectly indicates that the grown nanostructures can be promising for creating sources of single photons. Thus, the grown nanostructures with controlled properties are promising for creating applications in the field of quantum informatics, cryptography, and telecommunications.

ACKNOWLEDGMENT

The samples were grown under financial support of Russian Science Foundation Grant № 21-72-00099. Morphological and structural properties of grown samples were studied under financial support of the research grant of St. Petersburg State University No. 75746688. Optical properties of grown samples were studied under financial support of the Ministry of Science and Higher Education of the Russian Federation, research project no. 2019-1442.

cooling the samples to room temperature, substrates were transferred into the growth chamber with no vacuum brake. On the final stage, substrates temperature were increased to growth one (330-510°C), and sources shutters were opened for NWs growth. The QDs in the NWs body were formed by briefly (5-20 s) closing the Al shutter and opening the In shutter.

The samples were grown under financial support of Russian Science Foundation Grant № 21-72-00099. Morphological and structural properties of grown samples were studied under financial support of the research grant of St. Petersburg State University No. 75746688. Optical properties of grown samples were studied under financial support of the Ministry of Science and Higher Education of the Russian Federation, research project no. 2019-1442.

REFERENCES

[1] V. G. Dubrovskii, G. E Cirlin and V. M. Ustinov, "Semiconductor nanowhiskers: Synthesis, properties, and applications" Semiconductors, vol 43, pp. 1539–1584, 2009.

Droplet contact angle controlling the morphology and crystal phase of GaAs and GaP nanowires

V. G. Dubrovskii[1], N. V. Sibirev[1], V. V. Fedorov[2], L. N. Dvoretckaia[2], D. A. Kirilenko[3], I. S. Mukhin[2], A. Ghukasyan[4], N. I. Goktas[4], R. R. LaPierre[4]

[1] Faculty of Physics, St. Petersburg State University, Universitetskaya Emb. 13B, 199034, St. Petersburg, Russia
[2] Nanotechnology Research and Education Centre, Alferov University, Khlopina 8/3, 194021 St. Petersburg, Russia
[3]Ioffe Institute, Politekhnicheskaya 26, 194021 St. Petersburg, Russia
[4]Department of Engineering Physics, McMaster University, Hamilton, ON, Canada L8S4L7

Abstract — We discuss the droplet contact angle as the key parameter influencing the morphology and the related crystal phase of vapor-liquid-solid III-V nanowires. In particular, we show that twinning superlattice Te-doped GaAs nanowires are formed only when the droplet contact angle is above 130º, and that pure wurtzite sections in self-catalyzed GaP nanowires are obtained in the stage of Ga droplet consumption when the contact angle is within the range from 95º to 105º.

Keywords — droplet contact angle; twinning superlattice, crystal phase.

I. INTRODUCTION

Droplet contact angle resting on top of III-V nanowires (NWs), β, can easily be tuned by abruptly changing the V/III flux ratio or temperature. This property gives a useful control parameter for engineering the morphology and crystal phase of III-V NWs grown by the vapor-liquid-solid (VLS) method [1-3], particularly in the case of self-catalyzed VLS growth [3]. Here, we further investigate the possibilities of controlling the NW morphology and crystal phase by tuning the contact angle and show some new results on the twinning superlattice (TSL) Te-doped GaAs NWs [4] and pure wurtzite (WZ) sections in GaP NWs [5].

II. RESULTS AND DISCUSSION

Our modeling of the contact angle β versus the NW length, V/III flux ratio and temperature is based on the equation for the total volume of the droplet, V. According to Ref. [2], the volume V can be changed by either changing the NW top radius R or droplet contact angle β, depending on the surface energetics of a particular VLS system. The surface energetics is different for GaAs and GaP NWs due to the differences in the surface and interface energies involved [2]. The minimum surface energy configuration depends on β and favors different NW morphologies (vertical, tapered on inverse tapered) and the related crystal phases (zincblende (ZB) or WZ). In particular, WZ GaAs NWs with vertical sidewalls are formed within a relatively large range of β extending from ~ 100º to 125º [3]. high V/III flux ratios to decrease the droplet volume. Very importantly, the structural diagrams of GaAs and GaP NWs are insensitive to the growth temperature (due to a weak temperature dependence of the surface and interface energies of a VLS system) and catalyst type (Au or Ga).

We present the data and the corresponding modeling on the TSL Te-doped GaAs NWs along with the morphological diagram in terms of the growth temperature and V/III flux ratio corresponding to the TSL region [6]. We then elaborate on self-catalyzed GaP NWs, where pure WZ top sections are grown by MBE in the stage of droplet consumption under excessive V/III ratio of 3 [5]. It is shown that 610 ºC corresponds to the longest WZ sections of up to 500 nm length. In both cases, the phase diagrams are critically sensitive to the diffusion length of Ga adatoms on the NW sidewalls, which exhibits a maximum at a certain temperature. In particular, this explains a limited range of temperatures and V/III flux ratios corresponding to the TSL Te-doped GaAs NWs. In this range, the Ga diffusion flux from the NW sidewalls to the droplet is large enough to ensure that the droplet contact angle is greater than 130º [4,6].

Overall, the possibility to tune the NW morphology from vertical to tapered and crystal phase from WZ to ZB by varying the droplet contact angle during growth provides an interesting method for fabrication of WZ/ZB NW heterostructures, TSL III-V NWs in the ZB phase, and corrugated III-V NWs.

REFERENCES

[1] V. G. Dubrovskii, I. P. Soshnikov, G. E. Cirlin et al., "On the non-monotonic lateral size dependence of the height of GaAs nanowhiskers grown by molecular beam epitaxy at high temperature". Phys. Stat. Sol. (b), 2004, vol. 241, p. R30-R33, 2004.

[2] V. G. Dubrovskii. "Development of growth theory for vapor-liquid-solid nanowires: contact angle, truncated facets and crystal phase". Cryst. Growth Des., vol. 17, p. 2544–2548, 2017.

[3] F. Panciera, Z. Baraissov, G. Patriarche et al., "Phase selection in self-catalyzed GaAs nanowires". Nano Lett., vol. 20, p. 1669-1675, 2020.

[4] N. I. Goktas, A. Sokolovskii, V. G. Dubrovskii, and R. R. LaPierre. "Formation mechanism of twinning superlattices in doped GaAs nanowires". Nano Lett., vol. 20, p. 3344-3351, 2020.

For GaP NWs, the WZ range is much narrower, from 95° to 105°, while the stable contact angle of ~ 123° corresponds to ZB GaP NWs [5]. This explains why obtaining the pure WZ phase of GaP NWs is more difficult compared to GaAs, and requires

This research was supported by the research grant of St. Petersburg State University No. 75746688.

[5] V. V. Fedorov, L. N. Dvoretckaia, D. A. Kirilenko et al., "Formation of wurtzite sections in self-catalyzed GaP nanowires by droplet consumption", Nanotechnology, vol. 32, p. 495601, 2021.

[6] A. Ghukasyan, N. I. Goktas, V. G. Dubrovskii, R. R. LaPierre, "Phase diagram for twinning superlattice Te-doped GaAs nanowires", Nano Lett., vol. 22, p. 1345, 2022.

Microspherical lithography for selective epitaxy

L.N. Dvoretckaia[1], A.M. Mozharov[2], M.S. Gavrilov[1], V.V. Fedorov[1]

[1]Laboratory of Renewable energy sources, Alferov University, Khlopina str. 8/3A, 194021 St. Petersburg, Russia

[2]Faculty of Physics, St. Petersburg State University, Universitetskaya Emb. 13B, 199034 St. Petersburg, Russia

Abstract— The effect of focusing with microspheric lenses during the photolithography process is recently studied intensively due to the wide range of applications of this method. This paper presents the results of nanostructuring the silicon surface using photolithography on the hexagonal array of microspheric lenses and etching silicon in nanoholes. The possibility of epitaxial selective synthesis of semiconductor nanostructures A3B5 on silicon is demonstrated.

Keywords— microspherical lithography, MBE, selective epitaxy, GaP, InAs

I. Introduction

Light focusing by microlenses is widely used for fabrication and characterization at the micro- and nanoscale. Microsphere optical lithography can be employed solely or combined with other top-down or bottom-up methods, such as thin film deposition and etching, to provide the means for fabrication of nanostructures for various photonic, electronic and biosensor applications. A number of reports on successful microscopy or lithography applications consider the microspheres of specific size and material under illumination of specific wavelength [1]. In our work, we use microspheric photolithography to create patterned wafers for subsequent selective epitaxy A3B5 materials on silicon. These masks can be used in the synthesis of various epitaxial nanostructures, such as nanowires, nanocolumns, nanodiscs, etc. This approach to the preparation of growth wafers allows not only significantly reduce the exposure time of the resist in comparison with the traditional method of electronic lithography, but also provided the pattern of the large area wafers. The ordered array of nanowires can be used for light-emitting, light trapping or transistor structure [2,3]. In these cases, the distance between nanowires should be about a few micrometers. Alternatively to fabrication of oxide mask for GaP nanowire growth, our lithographic method can be used to prepare the substrates with graphene patches for selective area van der Waals epitaxy of GaN [4].

II. Results

Experiments on the creation of a pattern silicon surface were carried out using the method of microspheric photolithography and etching of the mask material. On the Si wafer <111> the thermal method was formed oxide with a thickness of 50 nm. A resist and quartz microspherical lenses from Micro Particles GmbH with a diameter of 1.5 um were coated to the Si/SiOx wafer with the spin-coating method to create a photomask. After the formation of a monolayer hexagonal microspheres array using the LED radiation source with a wavelength of 365 nm, the photoresist was exposed and developed. The size of the structures obtained by microspherical lithography is about 300 nm. Using the obtained photomask we were carried out etching the oxide layer in the CF4 plasma to a depth of 50 nm, after which the photomask was removed. To provided a smooth surface in the holes of the growth mask, a silicon etching process was carried out in a 20% alkali solution of the KOH within 10 min. Thus, hexagonal holes of fixed submicron sizes were formed. The silicon wafer with a patterned oxide layer was placed in a buffered fluorine hydrogen solution (BHF) to prepare for the epitaxy of the silicon surface in the holes of the oxide mask. The well-proven technology for making a growth mask was used for semiconductor nanostructure epitaxy. Using the MBE setup on a prepared patterned Si/SiOx wafer GaP and InAs nanocrystals in the growth mask holes were synthesized (Fig.1).

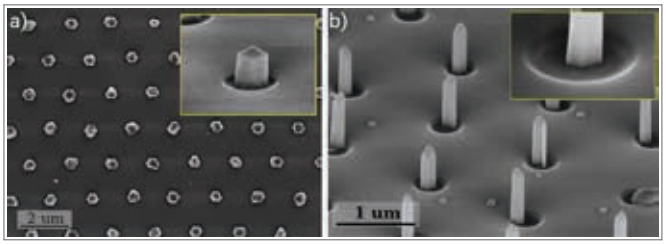

Fig. 1. SEM pictures of the selective MBE structures grown on patterned Si/SiOx wafer: a) GaP nanocolumns, b) InAs nanowires.

References

[1] L.N. Dvoretckaia, A.M. Mozharov, Y. Berdnikov, and I.S. Mukhin, "Optimization of microsphere optical lithography for nano-patterning," J. Phys. D: Appl. Phys., vol. 55.9, pp. 09LT01, November 2021.

[2] K. Tomioka, and F. Takashi, "Recent progress in integration of III–V nanowire transistors on Si substrate by selective-area growth,"J. Phys. D: Appl. Phys., vol. 47.39, pp. 394001, September 2014.

[3] M. Omelyanovich, and C.R. Simovski, "Wide-angle light-trapping electrode for photovoltaic cells," Optics letters, vol. 42.19, pp. 3726-3729, October 2017.

[4] M. Morassi, N. Guan, V.G. Dubrovskii, Y. Berdnikov, C. Barbier, L. Mancini, … & M. Tchernycheva, "Selective area growth of GaN nanowires on graphene nanodots," Crystal Growth & Design, vol. 20.2, pp. 552-559, December 2020.

MBE growth was carried out with the support of Russian Science Foundation № 19-72-30004 and postgrowth processing was carried out with the support Russian Federation President Council for grants SP-1152.2022.1.

Growth of III-V nanowires by molecular beam epitaxy: the role of material exchange with the substrate

N. V. Sibirev[1], V. G. Dubrovskii[1]

[1] Faculty of Physics, St. Petersburg State University, Universitetskaya Emb. 13B, 199034, St. Petersburg, Russia

Abstract — Growth theory of III-V nanowires fabricated by molecular beam epitaxy is developed to reveal the role of the substrate which can be either unpatterned or masked with an inert SiO_x layer. Axial and radial growths of nanowires are described in both cases, converging to the asymptotic stage which is independent of the substrate due to the shadowing effect. The nanowire lengths and radii are calculated as functions of time and the growth parameters. Good fits are obtained with the data on the growth kinetics of GaAs, GaP, InAs and InP nanowires.

Keywords — molecular beam epitaxy; growth modeling; shadowing effect.

I. Introduction

Modeling of III-V nanowire (NW) growth by molecular beam epitaxy (MBE) is required for the fine tuning of the NW morphology and crystal phase. Here, we present a generalization of the NW growth theory with an emphasize put on the material exchange of an ensemble of NWs with the substrate. Two mechanisms are considered: (i) surface diffusion of group III adatoms from an unpatterned substrate [1] and (ii) re-emission from an inert mask such as SiO_x on Si(111) with regular arrays of lithographically defined pinholes [2,3].

II. Results and Discussion

Axial and radial growths of cylindrical III-V NWs is analytically described in both cases. It is shown that in the absence of radial growth (stage 1), the NW length increases first linearly and then exponentially with time in MBE growth on unpatterned substrates. The elongation rate on masked substrates is faster due to re-emission, and more complex than exponential. In both cases, the length-radius correlation is decreasing due to surface diffusion of group III adatoms, as shown in Figure 1 for MBE-grown, Au-catalyzed InP NWs. When the radial growth starts (stage 2), the elongation rate decreases. The NW growth kinetics is strongly influenced by the shadowing effect originating from the neighboring NWs. As a result of the full shadowing of the substrate surface, the asymptotic stage of III-V NW growth by MBE (stage 3) is independent of the substrate.

In this late stage, the evolution of the NW length L with time t is given by

$$\frac{dL}{dh} = \frac{\chi}{\cos\alpha} + \varepsilon\left(\frac{L}{h}\right)^{1/2}, \quad \varepsilon = \frac{2\tan\alpha}{\sqrt{\pi}}\frac{\lambda}{P}.$$

Here, χ is the geometrical function which depends on the beam angle of group III flux α and the droplet contact angle β, λ is the diffusion length of group III adatoms on the NW sidewalls, and P is the pitch of regular arrays of pinholes.

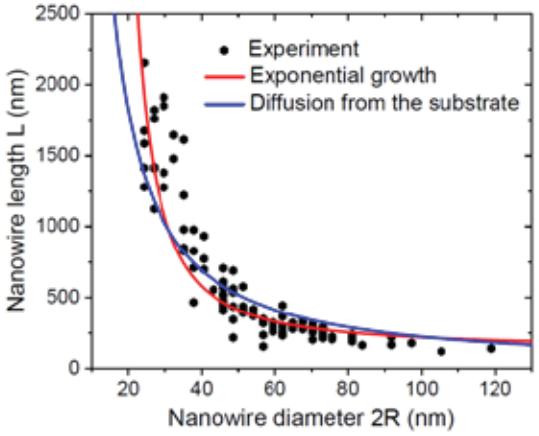

Fig. 1. Length of InP NWs versus their diameter [4], fitted by different growth models. The inverse length-radius correlation is due to surface diffusion on the unpatterned substrate and on the NW sidewalls.

III. Conclusions

To summarize, new effects have been reveled in MBE growth of III-V NWs. In particular, the non-linear evolution of the NW length and radius in different stages of growth has been revealed. The asymptotic stage of III-V NW growth has been described and good fits with the data for different III-V NWs grown by MBE have been obtained.

This research was supported by the research grant of St. Petersburg State University No. 75746688.

References

[1] G. E. Cirlin, V. G. Dubrovskii, N. V. Sibirev, I. P. Soshnikov, Yu. B. Samsonenko, A. A. Tonkikh, and V. M. Ustinov, "The diffusion mechanism in the formation of GaAs and AlGaAs nanowhiskers during the process of molecular-beam epitaxy". Semiconductors, vol. 39, p. 557, 2005.

[2] F. Oehler, A. Cattoni, A. Scaccabarozzi, G. Patriarche, F. Glas, J. C. Harmand, "Measuring and modeling the growth dynamics of self-catalyzed GaP nanowire arrays", Nano Lett., vol. 18, p. 701, 2018.

[3] V. G. Dubrovskii, "Theory of MBE growth of nanowires on reflecting substrates", Nanomaterials, vol. 12, p. 253, 2022.

[4] R.J. Yee, S.J. Gibson, V.G. Dubrovskii, and R.R. LaPierre, "Effects of Be doping on InP nanowire growth mechanisms". Appl. Phys. Lett., vol. 101, p. 263106, 2012.

Core-shell InGaN Nanowires: MBE Growth and Properties

V. O. Gridchin[1-3], R. R. Reznik[2], K. P. Kotlyar[1-3], V. V. Lendyashova[1,4], A. S. Dragunova[5], D. A. Kirilenko[4], N. V. Kryzhanovskaya[4], G. E. Cirlin[1-4]

[1]Alferov University, Saint-Petersburg, Russia
[2]St. Petersburg University, Saint-Petersburg, Russia
[3]IAI RAS, Saint-Petersburg, Russia
[4]Ioffe Institute, Saint-Petersburg, Russia
[5]HSE University, Saint-Petersburg, Russia

***Abstract* — The influence of the growth temperature on physical properties of InGaN nanowires grown by molecular beam epitaxy is considered. The growth conditions for synthesis of core-shell InGaN nanowires with a high In content are determined. The samples exhibit an intensive room temperature photoluminescence from green to orange spectral range.**

Keywords — InGaN, nanowires, Si, plasma-assisted molecular beam epitaxy

I. INTRODUCTION

Ternary InGaN alloys are promising for solid-state lighting and renewable energy sources due to the tunable energy band gap from 0.7 to 3.43 eV. However, the growth of homogeneously InGaN with a high In content (more than 0.3) is an extremely challenging task due to the large difference in interatomic spacing between InN and GaN. Besides, the growth of InGaN with high crystal quality is complicated by the lack of lattice-matched substrates. Much effort has gone into overcoming these challenges. Quasi-one-dimensional structures such as nanowires (NWs) have recently attracted particular attention as one of the approaches to growing InGaN alloys with the high In content [1]. On the way to receiving the high In content InGaN NWs, in this work, we study the influence of the growth temperature on the formation and physical properties of these nanostructures.

II. MATERIALS AND METHODS

InGaN NWs were grown directly on Si(111) substrates using plasma-assisted molecular beam epitaxy technique. The growth experiments were performed at the substrate temperatures from 650 to 670 °C. The growth conditions were described in detail in [2]. The structural properties were studied by scanning electron microscopy (SEM) and transmission electron microscopy (TEM). The optical properties were studied by photoluminescence (PL) measurements at room temperature.

III. DISCUSSION

Figure 1 shows the SEM image of the InGaN NWs grown at 655 °C. The NWs have an average length of 1.85 μm, an average diameter of 100 nm at the base and 30 nm at the top. It should be noted that the most part of NWs are separated from each other.

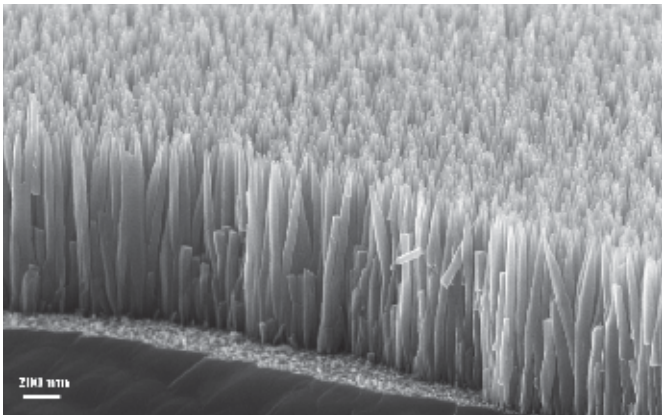

Fig. 1. SEM image of InGaN NWs grown at 655 °C.

When the growth temperature increases from 650 to 670 °C the NWs are transformed from separated to coalesced ones. The TEM studies of these samples shown that separated NWs have pronounced spontaneously formed core-shell structure with the core's diameter is similar to the NWs top diameter. Wherein, an average In content in the NWs core is about 40 % whereas in the shell is no more than 4%. The coalesced NWs are practically homogeneous in chemical composition. The In content in them is about 10 %. The PL results indicate an intensive emission from blue to orange spectral range in accordance with the chemical composition of the samples.

The results can be beneficial for the development of the growth model of spontaneously formed core-shell NWs with high In content and creation III-nitride nanowire lasers.

The work was carried out with the support of the Ministry of education and science of the Russian Federation within the State assignment No. 0791-2020-0003.

REFERENCES

[1] Kuykendall T. et al. "Complete composition tunability of InGaN nanowires using a combinatorial approach", Nature materials, vol. 6(12), pp. 951 (2007).

[2] Gridchin V. O. et al. "Multi-colour light emission from InGaN nanowires monolithically grown on Si substrate by MBE", Nanotechnology, vol. 32(33), pp. 335604 (2021)

Investigation of the polymeric thin films deposed on the surfaces of optical elements using the laser multiparametric method

A.V. Belikov[1], I. S. Klochkov[1,2], I.V. Alekseev[2], S. A. Kapralov[3]

[1] ITMO University, Saint Petersburg, Russia
[2] Joint Stock Company "Scientific and Production Corporation" Precision Instrumentation Systems ", St. Petersburg, Russian Federation
[3] Joint Stock Company "Scientific and Production Corporation" Precision Instrumentation Systems ", Velikiy Novgorod, Russian Federation

A laser multiparametric method based on the analysis of the parameters of the deposition zones is presented. The formation of deposition zones on the optical elements of the test-cuvette with the sample occurs during the interaction of volatile substances with laser radiation. Volatile substances are released from materials, elements and assemblies used in sealed volume under the influence of temperature. When the test-cuvette with the sample is heated up to 100 °C, the process of formation of deposition zones is accelerated. In current study, a solid-state YAG:Nd laser with a pulse repetition rate of 10 Hz, a pulse duration of 11–14 ns, a radiation wavelength of 1.064 µm, and a pulse energy of 100 mJ was used. The optical, geometric, and color parameters of the deposition zones and their resistance to the action of solvents have been studied. Silicone, activated carbon, and pressed anti-Stokes phosphor were used as samples. It is demonstrated that thin films with specified parameters can be created on the surfaces of optical elements using the laser multiparametric method.

Keywords— laser multiparametric method; sealed volume; test-cuvette; temperature; deposition zone; laser technology.

I. Introduction

At present time, polymer carriers have become widely known due to their use in biosensors and biochips. They are used in such areas of biomedicine as: control of gene expression in cell cultures, diagnostics, tissue engineering, antibacterial and anticancer therapy, drug delivery and others.

One of the promising carriers of biologically active substances are polymeric thin films. Such films are created by microlithography or by successive adsorption. The main feature of such films is the ability to seal biologically active substances for subsequent delivery and activation [1]. The relevance of the search for new technologies for the creation of polymeric thin films, adhesion control and an increase in the temperature range for the use of such films is explained by the great interest of biomedicine and laser technology in the creation of biosensors and nanomaterials.

II. Goal

The main goal of the current research is to study a new way of creating and control the properties of polymeric (silicone) thin films which are deposed on the surface of quartz glass as a result of the interaction of laser radiation with volatile substances released from silicone-containing materials placed inside sealed test-cuvette under the influence of temperature.

III. Method

The setup includes: 1 – YAG:Nd laser (JSC «SPC «PIS», Russia); 2 – telescope; 3 – beam splitter; 4 – test-cuvette with silicone-containing material; 5 – heating table Magistr S20T1 (LLD STC «Magistr-S», Russia); 6 – receiving head of Gentec QE25LP-S-MB-DO energy meter (Gentec Electro-Optics, Inc, Canada); 7 – laser radiation absorber; 8 – photodetector DET01CFC (THORLABS, Inc., USA); 9 – oscilloscope Wavesurfer 510R (Teledyne LeCroy, USA).

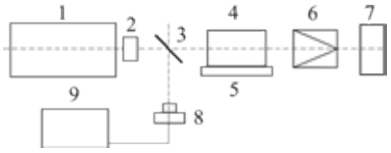

Fig. 1. Scheme of the setup for the polimeric (silicone) thin film deposition using the laser multiparametric method [2]

IV. Results

The polymeric (silicone) thin films were deposed and investigated. As results of the study, the following parameters of that deposed polymeric thin films were investigated: the coefficients of the area of deposition and attenuation, the resistance of the film to the action of solvents, the color of the films. The structure of the films was observed by the methods of scanning electron microscopy.

References

[1] M. Gai, J. Frueh, T. Tao et al. “Polylactic acid nano-and microchamber arrays for encapsulation of small hydrophilic molecules featuring drug release via high intensity focused ultrasound” // Nanoscale. vol. 9, N 21, pp. 7063–7070, 2017.

[2] Belikov A.V., Klochkov I.S., Alekseev I.V., Kapralov S.A. Laser multiparameter method for incoming inspection of the mounting elements used in the volume of sealed neodymium laser emitters. Scientific and Technical Journal of Information Technologies, Mechanics and Optics, 2021, vol. 21, no. 2, pp. 154–162. (in Russian). https://doi.org/10.17586/2226-1494-2021-21-2-154-162

Investigation of Volt-Ampere Characteristics of Crystalline Materials AgBr-AgI System

A.M.Turabi[1], N.N.Akif'eva [1], A.S.Korsakov[1], A.A.Yuzhakova[1], D.D.Salimgareev[1], J.O.Zelenkova[1], M.S.Korsakov[1], K.A.Karpov[1], L.V.Zhukova[1]

[1]Ural federal university named after the first President of Russia B. N. Yeltsin. 19 Mira str., Ekaterinburg 620002, Russia

Abstract— In this work, the dependence of the volt-ampere characteristics for optical infrared materials of the AgBr-AgI system solid solutions is studied depending on the composition of the material and temperature in the range of 298-423 K. It is established that an increase in the iodine content for crystalline materials of AgBr-AgI systems leads to a decrease in electrical conductivity.

Keywords— silver iodide, silver bromide, solid solution, volt-ampere characteristic.

I. Introduction

To date, promising optical materials for the manufacture of IR light guides, windows, lenses and other optical products that are widely used in various fields of science and technology, including laser, endoscopic and diagnostic medicine, are materials of AgBr-AgI systems, transparent in the middle infrared range from 0,5 to 40 μm [1]. Materials of AgBr-AgI systems have high photo resistance [2]. The application of crystalline materials of AgBr-AgI systems in optical and electrical devices, as well as in devices of laser technologies requires knowledge of basic physical, including electrical properties. Without knowledge of electrical properties it is impossible to design equipment using these materials, in particular automation devices designed to work in electromagnetic fields.

II. Investigation Volt-Ampere Characteristics

In this work, the dependence of the VAC of the material AgBr0.74I0.26 on temperature and on the thickness of the material for thin plates was studied. Plate specimens of two thicknesses were investigated: 1.7 mm and 0.5 mm. For each thickness specimen at each of the selected temperature values, a voltage was applied from 0.6 v to the breakdown voltage at a given temperature inarbitrary increments.

Figure 1, show the static volt-ampere characteristics obtained for the plate from the crystal of the system AgBr0.74-AgI0.26. For temperatures below 100°C, the dependence of the current on voltage is more typical for the dielectric. The current strength, when entrained, the voltage in a small degree will increase to the voltage of electrical breakdown. The value of the electrical breakdown voltage decreases as the temperature of the material increases. An electrical breakdown leads to a breakdown of the crystal, and the appearance of a silver 'track'.

The volt-ampere characteristics of the crystals of the systems AgBr-AgI, measured by applying voltage to plates of 500 microns and 1.7 mm of these materials, up to a certain voltage (about 2-3 volts) demonstrate a linear dependence of the current on the applied voltage. Further, a nonlinear dependence of current on voltage is observed, and a periodic section is observed in the transient current characteristics.

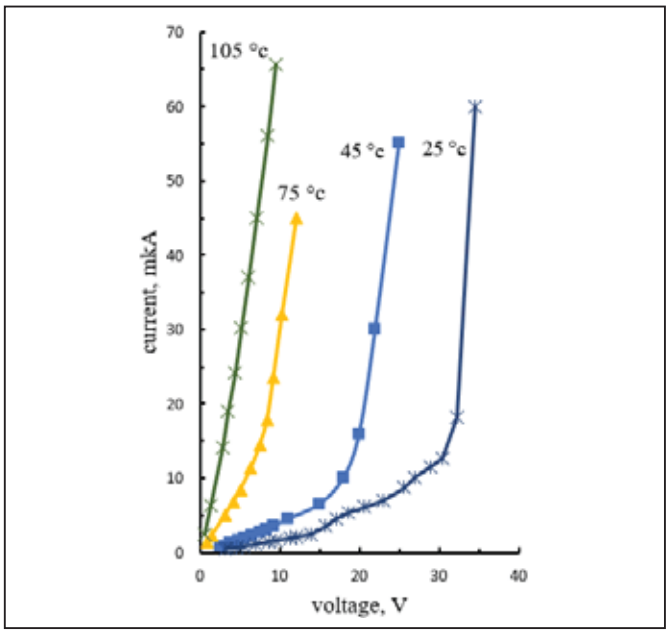

Fig. 1. Volt-ampere characteristics for the plate from the crystal of the system $AgBr_{0.74}I_{0.26}I$

References

[1] D. Salimgareev, A. Lvov, L. Zhukova, D. Belousov, A. Yuzhakova, D. Shatunova, A. Korsakov, A. Ishchenko, "Optical properties of the AgBr – AgI system crystals," Opt. Las. Tech. vol. 149, 107825, 2022.

[2] L. V. Zhukova, A. E. Lvov, D. D. Salimgareev, V. S. Korsakov, "Domestic Developments of IR Optical Materials Based on Solid Solutions of Silver Halogenides and Monovalent Thallium," Opt. and Spectrosc. vol. 125, iss. 6, pp 933–943, 2018.

This work was supported by the Ministry of Science and Higher Education of the Russian Federation, State Contract no FEUZ-2020-0058 (H687.42B.223/20).

Study of the electrical properties of InAs nanowires / Si substrate for IR photodetector

A.M.Mozharov[1], V.V.Fedorov[2], K.Yu.Shugurov[2], A.A.Vorobyev[2], D.A.Kudryashov[2]
[1]Faculty of Physics, St. Petersburg State University, Universitetskaya Emb. 13B, 199034 St. Petersburg, Russia
[2]Laboratory of Renewable energy sources, Alferov University, Khlopina str. 8/3A, 194021 St. Petersburg, Russia

Abstract— InAs nanowires are a promising form of material and can be used to create photodiodes and LEDs operating in the IR range, gas sensors and other electronic devices. We synthesized InAs NWs on a p-type Si substrate, formed ohmic contacts to the substrate and NWs, and performed electrical measurements of the fabricated structure. The current-voltage characteristic exhibits diode behavior with a low level of reverse current, indicating a low defect density at the InAs/Si interface.

Keywords— InAs nanowire, MBE, heterostructure

I. Introduction

InAs nanowires are a promising form of material and can be used to create photodiodes and LEDs operating in the IR range, gas sensors and other electronic devices [1]. Due to the small band gap, InAs-based photodiodes can be used in devices working in the NIR and SWIR ranges like fiber-optic communication systems, night vision systems and other. One of the main advantages of NWs over thin film devices is the possibility of their synthesis on substrates mismatched in lattice parameter, such as silicon, while maintaining a high crystalline quality. In turn, an important point in the design of devices based on NWs is to take into account the properties of the NW/substrate heterointerface. According to the literature [2], the reciprocal position of InAs and Si energy zones leads to the formation of a type-II heterojunction with a low barrier to holes, which qualifies the Si substrate as a p-type emitter for devices based on InAs NWs. The aim of this work was to synthesize InAs NWs on a p-type Si substrate and study the transport properties of the InAs/Si interface.

II. Results

Synthesis of InAs NWs was carried out using the method of molecular beam epitaxy on a Veeco GEN III setup on a p-type Si substrate with an 111 orientation. The SEM image of the formed structure is shown in the inset to Fig. 1. The typical length of the grown NWs is 500–1000 nm with a diameter of 100–250 nm. The formation of the measuring structure included several stages. At first, an aluminum layer 250 nm thick was formed on the back side of the Si wafer using the vacuum evaporation method. The activation of the ohmic contact was carried out using rapid thermal annealing at 300°C for 600 seconds. To electrically insulate the surface of the wafer and NW tips, a layer of light-cured epoxy resin SU8 was coated on the substrate followed by resist exposuring and curing. An ohmic contact to the NW tips was formed by deposition of a 100-nm thick ITO layer by magnetron sputtering method following the sample treatment in oxygen plasma to remove the insulator layer from the tips. A schematic picture of the fabricated structure is shown in the inset to Fig.1.

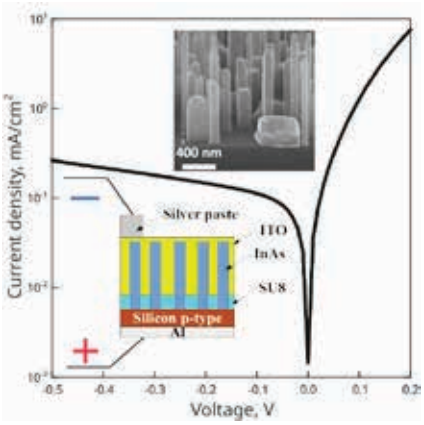

Fig. 1. Current-voltage characteristic of the fabricated structure. The inserts show the SEM image of grown NW array as well as schematic picture of the fabricated structure.

The electrical properties of the synthesized structure were measured with Keithley SourceMeter 2401 equipment. Fig. 1 shows the measured current-voltage characteristic of the fabricated structure on a semi-logarithmic scale. As can be seen, the measured dependence has a diode character. The value of the current density flowing through the diode under reverse bias corresponds to the expected level for the dark current in InAs NWs carring measured sizes, which indicates a low defect density at the InAs/Si interface. Summarizing, we can conclude that silicon is well suited to form a hole emitter for InAs NWs, which can be used to create devices based on this pair.

Authors gratefully acknowledges the Russian Science Foundation for financial support under the Grant 19-72-30004.

References

[1] T. Xu, H. Wang, X. Chen, M. Luo, L. Zhang, Y. Wang, F. Chen, C. Shan, and C. Yu, “Recent progress on infrared photodetectors based on INAS and InAsSb nanowires,” Nanotechnology, vol. 31, no. 29, p. 294004, 2020.

[2] S. Adachi, Properties of group-IV, III-V and II-VI semiconductors. Chichester: John Wiley & Sons, 2009.

Determination of Refractive Indices of the AgBr - AgI System Crystals in the Infrared Range

P.V.Pestereva[1], D.D.Salimgareev [1], A.E.Lvov[1], A.A.Yuzhakova[1], D.A.Belousov[1], A.S.Korsakov[1], L.V.Zhukova[1]
[1]Ural federal university named after the first President of Russia B. N. Yeltsin, Ekaterinburg, Russia

Abstract— This work is devoted to the determination of the refractive index of crystals with a composition from 0 to 36 mol. % AgI in AgBr. For measurements, we used polycrystalline plates based on the single crystals with a composition 3, 13, 25 and 36 mol. % AgI in AgBr. The samples refractive indices were determined by the spectroscopic method in the wavelength range from 3.0 to 14.0 μm.

Keywords— silver halides, refractive index, mid-infrared range, infrared optics

I. Introduction

Materials development for the manufacture of infrared (IR) fibers and laser optics that operate in the visible (from 0.38 to 0.74 μm), near-IR (from 0.74 to 2.0 μm), mid-IR (from 2.0 up to 50.0 μm) and far IR (up to 100.0 μm) ranges, is a promising direction for applications in various fields of science and technology [1]. At present, optical properties investigation of the AgBr - AgI system crystals have revealed that silver halide crystals have a wide transmission range, photo- and radiation resistance, are non-toxic and non-hygroscopic. Determination of the crystals refractive indices will allow the development of optical products, including fiber lasers operating in the IR range.

II. Refractive Index Measurement

To determine the refractive index of the AgBr - AgI system crystals, polycrystalline plates were prepared by hot embossing from single crystals with compositions of 3, 13, 25, 36 mol. % AgI in AgBr.

Common interference methods for determining the refractive index are direct (for example, the Michelson method) and indirect (spectroscopic method). The spectroscopic method makes it possible to study the refractive index of crystals in a wide wavelengths range. It is implemented using an IR-Fourier spectrometer from IRPrestige-21, Shimadzu.

The IR-Fourier spectrometer with MCT-detector makes it possible to obtain spectra with stable interference, with the help of which the crystals refractive indices are studied [1]. To calculate the indices with high accuracy, the thickness of each sample was determined, which ranged from 317 to 336 μm.

The study was carried out in the wavelength range (λ) from 3.0 to 14.0 μm. In the vicinity of a specific wavelength (3.0, 4.5, 5.0 μm, etc.), sections of the obtained spectra with a stable interference pattern were considered. This harmonic is used to determine the crystals refractive indices, which is possible due to the transparency of all samples in the studied wavelength range, and coherent radiation is preserved along the entire optical path. Under the condition that radiation is incident perpendicularly on the samples, the value of the refractive index can be determined as described in [3].

The measurement results are shown in Table 1. As can be seen from Table. 1 with increasing wavelength, a reduction in the refractive index is observed, which is typical for the normal index dispersion. There is also a growth in the index with an increase in the content of silver iodide in bromide. Errors are determined by the error in measuring the thickness, as well as errors introduced by the equipment and method. The obtained values are necessary for further design of optical products and devices based on them.

TABLE I. Dependence of the Refractive Index on the AgBr-AgI Solid Solution Composition

λ, μm	Composition				
	AgBr	$AgBr_{0.97}I_{0.03}$	$AgBr_{0.87}I_{0.13}$	$AgBr_{0.75}I_{0.25}$	$AgBr_{0.64}I_{0.36}$
3	2.167 ± 0.008	2.184 ± 0.008	2.190 ± 0.008	2.201 ± 0.009	2.208 ± 0.008
4.5	2.166 ± 0.007	2.181 ± 0.008	2.188 ± 0.008	2.199 ± 0.009	2.205 ± 0.008
5	2.166 ± 0.007	2.179 ± 0.008	2.187 ± 0.008	2.199 ± 0.009	2.205 ± 0.008
8	2.166 ± 0.007	2.177 ± 0.008	2.185 ± 0.008	2.196 ± 0.009	2.202 ± 0.008
10.6	2.165 ± 0.007	2.175 ± 0.008	2.183 ± 0.008	2.193 ± 0.009	2.201 ± 0.008
12	2.165 ± 0.007	2.173 ± 0.008	2.181 ± 0.008	2.191 ± 0.009	2.199 ± 0.008
14	2.165 ± 0.007	2.173 ± 0.008	2.179 ± 0.008	2.188 ± 0.009	2.197 ± 0.008

References

[1] D. Salimgareev, A. Lvov, L. Zhukova, D. Belousov, A. Yuzhakova, D. Shatunova, A. Korsakov, A. Ishchenko, “Optical properties of the AgBr – AgI system crystals,” Opt. Las. Tech. vol. 149, 107825, 2022.

[2] J.R. Rogers, M.D. Hopler, “Conversion of group refractive index to phase refractive index,” J. Opt. Soc. Am. A. vol. 5, № 10, pp. 1595-1600, 1988.

This work was supported by the Russian Science Foundation (No. 21-73-10108), https://rscf.ru/en/project/21-73-10108/.

High-sensitive dual-center ratiometric luminescence thermometers: co-doping vs mixture

I.E. Kolesnikov[1], E.V. Afanaseva[2], M.A. Kurochkin[1], E.I. Vaishlia[2]
[1]Center for Optical and Laser materials research, St. Petersburg State University, St. Petersburg, Russia
[2]Graduate School of Physics and Materials Technology, Peter the Great St. Petersburg Polytechnic University, St. Petersburg, Russia

Abstract— We report on dual-center ratiomentric luminescence thermometers $LuVO_4:Nd^{3+}/Yb^{3+}$ constructed via co-doping and mixing approaches. The suggested sensors were successfully demonstrated for temperature measurements within quite wide thermal range of 123-573 K. Effect of dispersion system type and Yb^{3+} doping concentration on thermometric characteristics including thermal sensitivity and temperature resolution was studied and discussed.

Keywords— Optical thermometry; Lanthanides; Nanoparticles; Dual-center phosphor

I. Introduction

Temperature is a widely used parameter that must be determined in different areas such as physics, biology, medicine, etc. Rapid progress in biomedicine and micro/nanoelectronics demands accurate thermal sensing, while traditional contact thermometry methods are useless in these applications as they require mechanical and reliable thermal contact. Non-contact methods do not need physical contact; therefore, the temperature measurement is not affected by electromagnetic noises, aggressiveness of environmental and the object movement. One of the most promising non-contact methods is the luminescence nanothermometry (LNTh). LNTh allows the temperature measurements in real time with high spatial and thermal resolution. Optical thermal sensing is generally based on the luminescence intensity ratio (LIR) between two thermally coupled lines. LIR makes it possible to obtain the temperature independently of external factors with high accuracy, fast response and high spatial resolution compared to other thermometers. Despite serious progress in the development of luminescence thermometers using thermally coupled levels, they have a fundamental limitation of thermal sensitivity ($S_r=\Delta E/kT^2$, $\Delta E<2000$ cm^{-1}). Herein, we suggested a new approach to create ratiometric luminescence nanothermometers using emission lines originating from two different active centers. This approach can potentially overcome the fundamental limitation of thermally-coupled levels and, as a result, lead to the development of LNTh with enhanced sensitivity.

II. Experimental Part

Co-doped and mixed $LuVO_4:Nd^{3+}/Yb^{3+}$ nanopowders were synthesized by the modified Pechini technique, which is based on the standard method with additional heat treatment in the melt salt medium [1]. X-ray powder diffraction studies were measured using Ultima IV powder diffractometer (Rigaku) with CuKα1 radiation (λ = 1.54059 Å) in the 2θ range from 10° to 85°. Zeiss Merlin microscope provided scanning electron microscopy. Steady-state and kinetics photoluminescence properties were studied by a modular fluorescence spectrometer Fluorolog-3. Temperature experiments were performed on the same spectrometer equipped with optical fibers and heating stage Linkam THMS 600 with thermal resolution of 0.1 °C.

III. Results and Discussion

XRD patterns of all synthesized $LuVO_4:Nd^{3+}/Yb^{3+}$ nanoparticles (NPs) confirm the formation of a pure tetragonal phase without any structural impurities. The prepared powders consist of weakly-agglomerated NPs with average size of 60 nm. Excitation spectra of co-doped and mixed NPs monitored at 983 nm (Yb^{3+} transition) and 1064 nm (Nd^{3+} transition) display a strong UV band and several longer-wavelength peaks. Comparing co-doped and mixed samples, it was concluded that the most significant difference was observed for Yb^{3+} excitation spectra. Yb^{3+} luminescence intensity was lower upon Nd^{3+} excitations in mixed phosphors compared with co-doped ones. Emission spectra of co-doped and mixed NPs display bands assigned to the electron transitions in both lanthanides. Relative emission lines intensities significantly vary for co-doped and mixed NPs. $^2F_{5/2}$–$^2F_{7/2}$ transition had lower intensity in mixed samples compared to the co-doped samples due to more efficient energy transfer from Nd^{3+} to Yb^{3+} ions in the case of co-doped NPs. Energy transfer between Nd^{3+} and Yb^{3+} ions were studied in detail using luminescence kinetics measurements.

Luminescence thermometry was realized through ratiometric technique based on monitoring LIR_1 = ($^4F_{3/2}$–$^4I_{9/2}$ / $^2F_{5/2}$–$^2F_{7/2}$) and LIR_2 ($^4F_{3/2}$–$^4I_{11/2}$ / $^2F_{5/2}$–$^2F_{7/2}$) within 123-573 K temperature range. Experimental data of both LIRs temperature evolution were fitted by exponential function, which makes luminescence thermal sensing simple. The best thermal sensitivity was 0.34 % K^{-1}@299K achieved for mixed Nd1+Yb1 NPs, while a better temperature resolution of 0.2 K was obtained for mixed Nd1+Yb4 NPs.

Acknowledgment

Experimental measurements were carried out in “Center for Optical and Laser materials research”, “Research Centre for X-ray Diffraction Studies”, “Interdisciplinary Resource Center for Nanotechnology” (St. Petersburg State University).

This research has been supported by the Russian Science Foundation (№ 21-79-10018).

References

[1] I. E. Kolesnikov *et al.*, “Multimode high-sensitivity optical YVO_4: Ln^{3+} nanothermometers (Ln^{3+}= Eu^{3+}, Dy^{3+}, Sm^{3+}) using charge transfer band features,” *Phys. Chem. Chem. Phys.*, vol. 22, no. 48, pp. 28183–28190, 2020.

Development of the alloyed quantum dots luminescence quenching based biosensor systems

D.D.Drozd, A.S.Moshkov, S.A.Mescheryakova, D.A.Kornilov, O.A.Goryacheva, I.Yu.Goryacheva
Department of General and Inorganic Chemistry, Saratov State University, Saratov, Russia

Abstract -Photoluminescent alloyed quantum dots are a promising material for biosensor development due to the high sensitivity of their optical properties to media conditions. Described sensing approaches based on quantum dots photoluminescence quenching. Discussed advantages and perspectives of alloyed quantum dots application.

Keywords — photoluminescence, alloyed quantum dots, biosensor systems

I. INTRODUCTION

Colloidal luminescent quantum dots (QDs) are quite a popular nanomaterial in assays and sensors development due to their unique optical properties. QDs show high photoluminescent efficiency in a wide range of exciting light wavelengths and have perfect thermal and photo- stability. The special type of QDs is the alloyed ones. In alloyed QDs semiconductor materials are distributed in the inner volume of the luminescent core and often form a gradient transition of the composition from center to the surface [1,2]. Due to this structural peculiarity alloyed QDs have higher quantum yield and narrow photoluminescence peak. This makes them sensitive to the media properties and composition that can be advantaging in sensors systems based on photoluminescence modulation. Already known application of the alloyed QDs in temperature and pH sensing [3].

II. QDS PHOTOLUMINESCENCE QUENCHING IN BIOSENSOR SYSTEMS

QDs photoluminescence quenching can be provided by the two pathways. The first pathway is based on energy transfer between donor QD and acceptor quencher and is reversible. The second pathway is based on particularly or full oxidative breakdown of stabilizing ligands layer and photoluminescent core [4]. Both pathways are high-sensitive, and selectivity is achieved by the combination of the quencher with the biorecognition molecules such as antibodies, streptavidin, protein A. Oxidative pathway based on enzymatic quencher generation. As enzymes can be used glucose oxidase (transforms glucose to the hydrogen peroxide and D-gluconic acid), catalase and horseradish peroxidase (decomposes hydrogen peroxide to water and oxygen) or their combination. This pathway has no required specific reagents and conjugation of the enzymes with biorecognition molecules runs by standard procedures. Known the applications of heterostructural and binary QDs as photoluminescent source material in such enzymatic systems for detection of glucose, pesticides, and disease markers [5].

III. ALLOYED QDS APPLICATION

Alloyed QDs were synthesized by the one-step high-temperature organometallic procedure and modified by functionalized thioalkyl ligands to provide colloidal stability in the aqueous media. The optical properties of obtained alloyed QDs were investigated. The efficiency of photoluminescence quenching by the direct addition of hydrogen peroxide and enzymatic generation was investigated. Quenching kinetics curves for the different concentrations of quencher for the batch of alloyed QDs were plotted. The quenching mechanism and analytical potential for biosensor development were discussed.

ACKNOWLEDGMENT

The work was supported by Russian Science Foundation (Project 20-13-00195).

REFERENCES

[1] K.H. Lee, C.Y. Han, H.D. Kang, H. Ko, C. Lee, J. Lee, and H. Yang, “Highly efficient, color-reproducible full-color electroluminescent devices based on red/green/blue quantum dot-mixed multilayer.” ACS nano, vol. 9(11), pp. 10941-10949, October 2015.

[2] X. Liu, D. Wen, Z. Liu, J. Wei, D. Bu, and S. Huang, “Thiocyanate-capped CdSe@ Zn1-XCdXS gradient alloyed quantum dots for efficient photocatalytic hydrogen evolution.” Chem. Eng. Journal, vol. 402, pp. 126178, December 2020.

[3] K. Susumu, L.D. Field, E. Oh, M. Hunt, J.B. Delehanty, V. Palomo, and I.L. Medintz, (2017). “Purple-, blue-, and green-emitting multishell alloyed quantum dots: synthesis, characterization, and application for ratiometric extracellular pH sensing.” Chem. Mater., vol. 29(17), pp. 7330-7344, August 2017.

[4] S.S.M. Rodrigues, D.S.M. Ribeiro, J.X. Soares, M.L.C. Passos, M.F.S. Saraiva, and J.L.M. Santos, “Application of nanocrystalline CdTe quantum dots in chemical analysis: Implementation of chemo-sensing schemes based on analyte-triggered photoluminescence modulation.” Coor. Chem. Rev., vol. 330, pp.127-143, January 2017.

[5] E.S.Speranskaya, D.D. Drozd, P.S. Pidenko, and I.Y. Goryacheva, “Enzyme modulation of quantum dot luminescence: Application in bioanalysis.” TrAC, vol. 127, pp. 115897, June 2020.

Design of a narrowband filter based on Fabry–Pérot etalon for implementing the undersamping method in terahertz time-domain spectrometer

A. A.Rybak[1,2], S.A.Kuznetsov[1,3], N. A. Nikolaev[1,2]
[1]Novosibirsk State University, Novosibirsk, Russia
[2]Institute of Automation and Electrometry, Novosibirsk, Russia
[3]Rzhanov Institute of Semiconductor Physics SB RAS, Novosibirsk Branch TDIAM, Novosibirsk, Russia

Abstract— In this paper, we consider an approach to the disign of a narrow-band quasi-optical filter with a center frequency ν = 806 GHz, designed to implement the undersampling method in pulsed terahertz spectroscopy.

Keywords— terahertz time-domain spectroscopy, metasurface, undersampling,

The time-domain spectroscopy (TDS) method is based on the coherent detection of the temporal form of the terahertz field, which allows one to directly determine its amplitude and phase, and in a wide frequency band. This in turn makes it possible to measure the complex permittivity or the complex refractive index of materials with high accuracy. A typical spectrometer signal is a one-period oscillation of the electromagnetic field with a duration of ~1 ps, carrying a wide frequency spectrum [1, 2]. We suposed that for TDS, the undersampling method [3] can be applied, which speeds up the measurement time by limiting the signal spectrum with a bandpass filter.

To check up the undersampling method, we chose the absorption line of CO molecular gas with a frequency about in the 806 GHz. This is since the gain in the application of this method is greater with an increase in the band frequency, since it is at higher frequencies that the increased TDS noise is observed; also, in the vicinity of 0.8 THz, the dynamic range of the spectrometer remains sufficient for measuring strong gas lines. Therefore, this work is devoted to the development of a narrow-band quasi-optical filter based on frequency-selective surfaces (FSS), designed to implement the undersampling method in pulsed terahertz spectroscopy.

The filter is based on the Fabry-Perot standard and is a polypropylene film with square-shaped aluminum chips applied on both sides. Numerical simulation was carried out using the ANSYS® HFSS R19 electrodynamic simulation package.

It was determined that the optimum ratio of the width of the metal bridge *a* to the period *g* of the FSS lies in the vicinity of *a*/*g*=0.5 (Fig. 1). When g is chosen to be less than half of the working wavelength λ, it is shown that the total width at half-height of the transmission of the resulting quasi-optical filter is less than 4%, which is sufficient to implement the undersampling method in time-domain terahertz spectrometers.

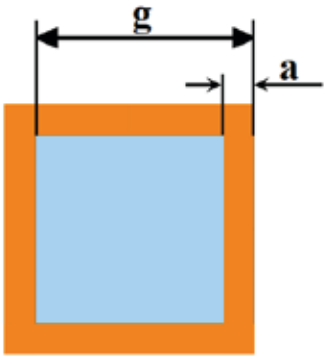

Fig. 1. Unit cell of the periodic structure of the Fabry-Perot filter with metal grid reflectors (orange) separated by a dielectric layer (blue), g is the lateral period of the grid, a is the width of the metal bridges between the cells.

ACKNOWLEDGMENT

The reported study was funded by RFBR according to the research project № 20-32-90137.

The authors acknowledge the NSU Shared Equipment Centers “Applied Physics” and “VTAN”.

REFERENCES

[1] В. Д. Анцыгин, А. А. Мамрашев, Н. А. Николаев, О. И. Потатуркин. Малогабаритный терагерцовый спектрометр с использованием второй гармоники фемтосекундного волоконного лазера. Автометрия. 2010, Т. 46, №3. С. 110-117.

[2] 2. B. Sartorius, H. Roehle, H. Künzel, J. Böttcher, M. Schlak, D. Stanze, H. Venghaus, and M. Schell. All-fiber terahertz time-domain spectrometer operating at 1.5 µm telecom wavelengths. Optics express. 2008, Vol. 16, No. 13, PP. 9565-9570.

[3] H. Harada, R. Prasad. Simulation and Software Radio for Mobile Communications. Artech House. 2002. P. 395

Ga_2O_3 and GaN nanoparticles synthesis by femtosecond laser ablation in ammonia environment

A.S. Chernikov, D.A. Kochuev, R.V. Chkalov, A.V. Egorova, D.G. Chkalova
Vladimir State University named after A. G. and N. G. Stoletovs, Vladimir, Russia

Abstract — In the present work beta-gallium oxide and gallium nitride nanoparticles have been synthesized on the silicon wafer surface by femtosecond pulsed laser ablation of a metallic gallium target in ammonia vapor environment of various concentrations under the action of an electrostatic field.

Keywords — femtosecond laser, laser ablation, nanoparticles, semiconductor compound, gallium oxide, gallium nitride, electrostatic field, ammonia environment

I. Introduction

In the last few decades, binary III-Nitride semiconductor compounds, in particular, gallium nitride (GaN), have been of great interest. These semiconductor compounds are widely used as a large variety of photonic and optoelectronic devices. Great interest is focused on the study of various methods for the synthesis of such compounds, the method of laser ablation synthesis in various media is worth mentioning separately.

Gallium oxide (Ga_2O_3) is a fairly promising semiconductor material which has the advantage of ultrawide bandgap, high breakdown electric field, good luminescence properties and is a good candidate for different application such as photodetectors, solar cells, power and high voltage electronic devices, etc [1].

II. Femtosecond Laser Ablation Synthesis of Ga_2O_3 and GaN in Ammonia Environment

Ga_2O_3 and GaN nanoparticles were obtained by pulsed laser ablation of a gallium metallic target in ammonia vapor environment of various concentrations using a femtosecond Yb:KGW laser operated at a wavelength of 1029 nm, with pulse duration of 280 fs and pulse repetition rate of 10 kHz. The laser beam is moving in the transverse plane along a given trajectory using galvanometer scanner, flat-field lens with a focal length of 200 mm is used as focusing optics. Schematic drawing of the experimental setup for femtosecond laser ablation synthesis in ammonia environment under the action of an electrostatic field presented in figure 1.

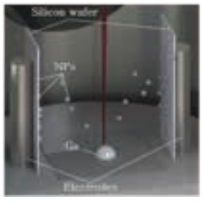

Fig. 1. Schematic drawing of the experimental setup for femtosecond laser ablation synthesis in ammonia environment under the action of an electrostatic field.

The process of laser ablation synthesis was carried out under the action of an electrostatic field, the presence of which provided to carry out the predicted deposition of ablation products which leave the area of laser radiation propagation, do not fall under repeated exposure and directly deposited on silicon wafer surface.

The synthesized nanomaterials were characterized by X-ray diffraction, the optical characterization of synthesized nanoparticles were also studied (photoluminescence properties).

Based on the obtained XRD-pattern it can be concluded that the synthesized nanoparticles characterized by a crystalline phase β-Ga2O3 (correlated with a diffraction pattern from JCPDS card number 76-0573) [2]. It was found that during the ablation of gallium in ammonia vapor environment (using aqueous ammonia with a concentration of 10%), the formation of gallium oxide is observed, and annealing at a higher temperature promotes the appearance of more pronounced peaks of gallium oxide phases.

Figure 2 presented XRD pattern of GaN nanoparticles, synthesized in ammonia vapor environment (aqueous ammonia with a concentration of 25%) and XRD pattern from JCPDS card number 50-0792.

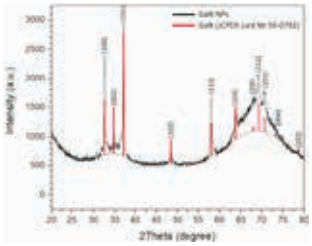

Fig. 2. XRD pattern of GaN nanoparticles, synthesized in an ammonia vapor environment (aqueous ammonia with a concentration of 25%) – black line; XRD pattern from JCPDS card number 50-0792 – red line.

When using aqueous ammonia with a concentration of 25% the obtained nanoparticles can be characterized as the hexagonal phase of the wurtzite GaN (full compliance with a JCPDS card diffraction pattern for wurtzite-type GaN [3]. It should be pointed out that there are no Ga_2O_3 phases, no cubic and other oxide phases were observed in the considered measurement range either.

References

[1] Stepanov S. I. et al. Gallium oxide: properties and applications—a review. Rev Adv Matter Sci 44: 63–86. – 2016.

[2] Reddy L. S., Ko Y. H., Yu J. S. Hydrothermal synthesis and photocatalytic property of β-Ga2O3 nanorods //Nanoscale Research Letters. – 2015. – Т. 10. – №. 1. – С. 1-7.

[3] Kang B. K. et al. Formation of highly efficient dye-sensitized solar cells by effective electron injection with GaN nanoparticles //Journal of The Electrochemical Society. – 2011. – Т. 158. – №. 7. – С. H693.

Laser-Induced Phase Transitions of GeTe and $Ge_2Sb_2Te_5$ Thin Films

A.A. Burtsev[1], V.V. Ionin[1], N.N. Eliseev[1], A.V. Kiselev[1], V.A. Mikhalevsky[1], A.A. Lotin[1]
[1] Institute on Laser and Information Technologies of Russian Academy of Sciences — Branch of Federal Scientific Research Center "Crystallography and Photonics" of Russian Academy of Sciences, Shatura, Russian Federation.

Abstract— Thin film phase-change materials (PCM) based on germanium telluride (GeTe, $Ge_2Sb_2Te_5$) are widely used in photonic and optoelectronic devices. We demonstrate a reversible change in the optical properties of thin-film samples associated with phase transitions under the influence of pulsed laser radiation according to the pump-probe scheme.

Keywords— phase-change materials, thin film, germanium telluride, laser-induced transitions

I. Introduction

Thin film chalcogenide materials based on germanium telluride (GeTe, $Ge_2Sb_2Te_5$ or GST) are widely used in photonic and optoelectronic devices [1]. These alloys have very high amorphization and crystallization rates in the order of nanoseconds which, combined with large cyclability and a pronounced property contrast between the crystalline and amorphous phases [2]. Today, the efforts of researchers are aimed at studying the possibility of using phase-change materials in the design of optical [3] and memristive [4] neuromorphic devices that combine memory and logic elements.

II. Experimental

A few series of 100 nm thick GeTe and GST films were grown by the thermal vacuum deposition method on SiO_2, Si and ZnSe substrates. The samples fabricated on SiO_2 and Si substrates were used for investigation of structural and dynamics properties, while the samples on ZnSe substrates were used for wide range spectrometry.

The thin films' dynamics of optical properties changing related with laser-induced phase transitions was studied using the pump-probe scheme [5,6]. The phase state of the sample was changed by pulsed laser radiation with 15 ns duration at a wavelength of 532 nm (pump). The dynamics of changes in the optical properties of the samples was studied using signals from photodetectors with a time resolution of at least 1 ns, which were recorded using a multichannel digital oscilloscope. Photodetectors recorded CW probe laser radiation reflected from the surface and transmitted through the sample under study at a wavelength of 980 nm. The pump laser radiation intensity profile was formed close to the top hat. The structural analysis of films was carried out by X-ray diffraction with a radiation wavelength of $\lambda = 0.709317$Å (MoKα).

The samples were exposed by crystallization and amorphization. The spectrometry data demonstrated the contrast of optical properties in a wide range from 200 to 22000 nm, and also determined the rates of change in optical properties lying in the range of tens of nanoseconds for both forward and reverse changes associated with laser-induced phase transitions. It should be noted that the reamorphization process is a glass transition that occurs during rapid cooling of the molten film. The glass transition temperature strongly depends on the cooling rate of the melt, and in order to achieve reamorphization over the entire film thickness, its values are 10^9–10^{11} K/s [7]. Therefore, the thermal conductivity of the substrate plays a key role here.

Acknowledgment

The work was supported by Ministry of Science and Higher Education: agreement №72/21-SYN1357 in a part of the samples' synthesis and State assignment of FSRC "Crystallography and Photonics" RAS in part of the samples' investigation.

References

[1] K.V. Sreekanth, M. ElKabbash, V. Caligiuri, R. Singh, A. De Luca, G. Strangi. New Directions in Thin Film Nanophotonics, Springer, 2019, pp.45-58.

[2] P. Guo, A. M. Sarangan and I. Agha. A Review of Germanium-Antimony-Telluride Phase Change Materials for Non-Volatile Memories and Optical Modulators. Applied Sciences, vol. 9, 2019, 530.

[3] W. Zhang, R. Mazzarello, M. Wuttig, E. Ma. Designing crystallization in phase-change materials for universal memory and neuro-inspired computing. Nature Reviews Materials, vol. 4, 2019, pp. 150-168.

[4] C.D. Wright, L. Wang, M.M. Aziz, J.A.V. Diosdado, P. Ashwin. Phase-change processors, memristors and memflectors. Physica Status Solidi (B), vol. 249, 2012, pp. 1978–1984.

[5] N.N. Eliseev, A.V. Kiselev, V.V. Ionin, V.A. Mikhalevsky, A.A. Burtsev, M.A. Pankov, D.N. Karimov, A.A. Lotin. Wide range optical and electrical contrast modulation by laser-induced phase transitions in GeTe thin films. Results in Physics, vol. 19, 2020, 10346.

[6] A.V. Kiselev, V.V. Ionin, A.A. Burtsev, N.N. Eliseev, V. A. Mikhalevsky, N.A. Arkharova, D.N. Khmelenin, A.A. Lotin. Dynamics of reversible optical properties switching of $Ge_2Sb_2Te_5$ thin films at laser-induced phase transitions. Optics & Laser Technology, vol. 147, 2022, 107701.

[7] S. Raoux, M. Wuttig (ed.). Phase Change Materials. Science and Applications. Springer, 2009, p. 206.

Assessment of cell viability of non-cadmium quantum dots

T.S.Ponomaryova, V.V.Olomskaya , E.A.Mordovina, D.V.Tsupka, A.S.Novikova, I.Yu. Goryacheva
Saratov State University, 83 Astrakhanskaya Street, Saratov, 410012, Russia

The small (<10 nm) size-selected thiol-capped $AgInS_2/ZnS$ quantum dots (QDs) were produced by precipitation from an aqueous colloidal ensemble. To demonstrate the potential of synthesized QDs for bioimaging, cellular uptake and localization within the cell lines were evaluated using L929 cells. These water-soluble $AgInS_2/ZnS$ QDs exhibited excellent biocompatibility and can be used for labeling the cell lines and in bioassay.

Keywords — cell viability, quantum dots, fluorescence, biocompatibility

INTRODUCTION

Quantum dots have been fascinating fluorescent materials for more than two decades in the field of biomedical technology due to their unique optical properties, such as broad absorption and narrow emission spectra, high extinction coefficients, high quantum yields, photostability, and large surface area, characteristics that are not observed in the bulk materials [1, 2]. However, in most of the cases of the main problems remains their biocompatibility and toxicity [3]. In this connection, the new approaches to synthesis in the aqua medium and the transition to ternary non-cadmium QDs will reduce the toxic effects [4]. In this work, we obtained hydrophilic quantum dots of the core/shell structure of the $AgInS_2/ZnS$ using an aqueous one-pot synthesis. Their cytotoxicity was evaluated on the L929 mouse fibroblast cell line with the aim of their potential bioanalytical use as a luminescent label.

1 – SYNTHESIS AND OPTICAL PROPERTIES QDs

Hydrophilic size-selective $AgInS_2/ZnS$ QDs were synthesized using a simple, cost-effective, eco-friendly synthesis approach according to procedure [4]. The fluorescence band maximum shifts from ~620 nm for the first fraction to ~540 nm for the last fraction in the series, while the fluorescence intensity is reduced by about an order of magnitude. The QDs reveal broadband photoluminescence with a quantum yield of up to 57 % for the most populated fraction of the core/shell $AgInS_2/ZnS$ QDs.

2 – CELL VIABILITY

To assess the viability of cells, the analysis of cellular redox status using the Alamar Blue reagent was used. This assay is based on the metabolic reduction of redox dyes. L929 cells were cultured in a nutrient medium (DMEM) supplemented with 10% fetal bovine serum and 1% antibiotic (streptomycin and penicillin) at 37 °C in a 5% CO_2 incubator for 24 hours in 96-well plates (in 1 well ~ $1 \cdot 10^4$ cells, 80 µl). Then 10 µl of the sample was added to the wells of the cells, in 4 parallel wells. It was left to incubate for 24, 48, 72, 96, 120 hours, after which AlamarBlue (10 µl) was added to the cells. The fluorescence intensity values were measured after a 4-hour incubation period at λ em. = 590 nm, λ ex = 560 nm. The result shows the percentage of cell viability after incubation with various concentrations of QD and surface ligand. Cytotoxicity was not observed under experimental conditions for all QD concentrations. The cell line L929 showed the viability of over 75%, which is critical for biological applications and indicates that QDs displays excellent biocompatibility. The results obtained are in good agreement with the data from the literature. (Fig 1).

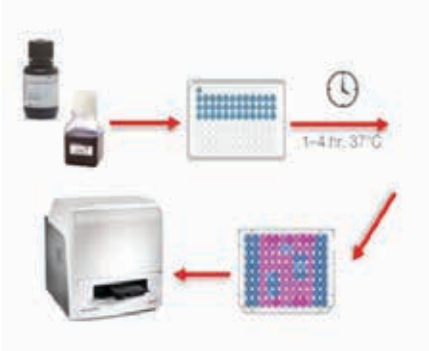

Fig. 1. Illustration of cell viability analysis using AlamarBlue

ACKNOWLEDGMENT

The reported study was funded by Russian Science Foundation, project number 21-73-00102.

REFERENCES

[1] R. Muñoz, E. M. Santos, C. A. Galan-Vidal, J. M. Miranda, A. Lopez-Santamarina, J. A. Rodriguez, "Ternary Quantum Dots in Chemical Analysis. Synthesis and Detection Mechanisms," Molecules, vol. 26(9), pp.2764, 2021.

[2] O. S. Oluwafemi, B. M. May, S. Parani, J. V. Rajendran, "Cell viability assessments of green synthesized water-soluble $AgInS_2/ZnS$ core/shell quantum dots against different cancer cell lines," Journal of Materials Research, vol. 34(24), pp. 4037-4044, 2019.

[3] W. M. Girma, M. Z. Fahmi, A. Permadi, M. A. Abate, J. Y. Chang, "Synthetic strategies and biomedical applications of I–III–VI ternary quantum dots," Journal Materials Chemistry B, vol. 5(31), pp. 6193-6216, 2017.

[4] A. Raevskaya, V. Lesnyak, D. Haubold, V. Dzhagan, O. Stroyuk, N. Gaponik, D. R. T. Zahn, A. Eychmüller, "A Fine Size Selection of Brightly Luminescent Water-Soluble Ag−In− S and Ag−In−S/ZnS Quantum Dots, " Journal Physical Chemistry, vol. 121, pp. 9032−9042, 2017.

Spectral properties of sodium-modified Bi-doped GeO_2 glasses

K.S. Serkina, I.V. Stepanova, A.A. Trofimova , D.V. Volkova
The Department of Chemistry and Technology of Crystals, D. Mendeleev University of Chemical Technology, MUCTR, Moscow, Russia

Abstract— Bismuth-germanium oxide glasses with the addition of sodium oxide have been synthesized and their spectral characteristics have been investigated. It is shown that modification with sodium leads to a decrease in the synthesis temperature and an increase in the optical quality of glasses with a low content of bismuth oxide.

Keywords— bismuth active centers; glass; sodium modification

I. INTRODUCTION

Bismuth-germanium oxide glasses emitting in the NIR-region are a promising material for modern fiber-optic technology. Bismuth active centers (BACs) are the source of NIR-luminescence [1] in these glasses. Various factors affect the properties of BACs: glass composition, synthesis and annealing conditions [2].

To obtain effective luminescence, a relatively small number and uniform distribution of BACs is required. The most important problem is the quite high synthesis temperature of GeO_2 glasses with a low content of bismuth oxide. High temperatures of glass synthesis lead to a significant increase in the number of bismuth centers, adversely affecting luminescence. Modification with sodium oxide should lower the synthesis temperature of these glasses [3] and improve their optical quality. Therefore, finding the optimal compositions and synthesis conditions for this type of glass is an urgent scientific problem.

II. EXPERIMENTAL SECTION

Sodium-modified Bi-doped GeO_2 glasses were synthesized by melt-quenching technique. The compositions can be described by the general formula xBi_2O_3–$(90-x)GeO_2$–$10Na_2O$ (x = 1, 2, 3, 4, 5 mol%). High purity Bi_2O_3, GeO_2 and Na_2CO_3 were used as starting components for the synthesis. The melt was kept at 1100 °C during 30 min, then hardened on a metal substrate. The absorption spectra of polished glass samples were recorded on a UNICO 2800 spectrophotometer (UV/VIS) (190-1100 nm).

The addition of the modifier reduced the synthesis temperature and favorably affected the quality of the glasses with a low content of bismuth oxide. All synthesized Bi-doped GeO_2–Na_2O glasses possessed the good optical quality and had no obvious coloration.

The absorption spectra of all glasses (Fig. 1) show no absorption bands in 400-1100 nm range. A light increase of absorption in the region of 500 nm for 5 mol.% Bi_2O_3-doped sample (Fig. 1, inset) associated with the presence of BACs.

In addition, an increase in the bismuth concentration leads to a shift of the short-wavelength absorption edge to the long-wavelength region.

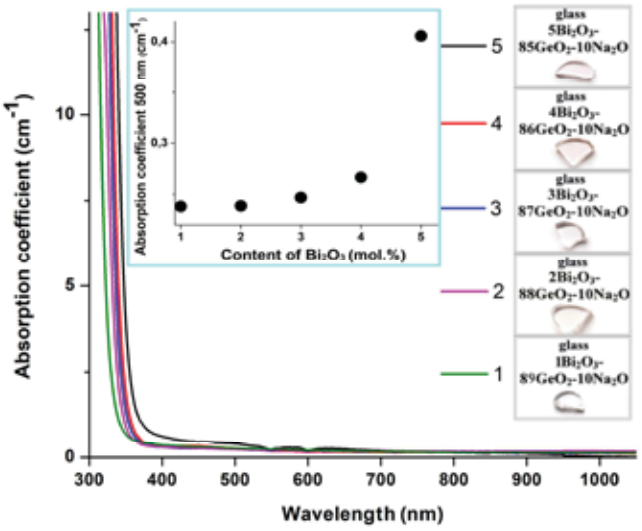

Fig. 1. The absorption spectra of sodium-modified Bi-doped GeO_2 glasses.

It was noted that the addition of sodium oxide to bismuth-germanium glasses decreases the absorption in the region of 500 nm, which may be associated with internal rearrangements of the glass structure [4]. As already mentioned, the absorption intensity in the region of 500 nm is related to the amount of BACs. Therefore, modification with sodium oxide can be used for control of the number of BACs in GeO_2 glasses.

The research was supported by the Ministry of Science and Higher Education of the Russian Federation by the project FSSM-2020-0003.

REFERENCES

[1] E. M. Dianov, “Nature of Bi-related near IR active centers in glasses: state of the art and first reliable results”, Laser Physics Letters. vol. 12, № 9, pp. 51–56, 2015.

[2] O. Sanz, E. Haro-Poniatowski, J. Gonzalo, and J. M Fernarndez Navarro, “Influence of the melting conditions of heavy metal oxide glasses containing bismuth oxide on their optical absorption”, Journal of Non-Crystalline Solids, vol. 352, pp. 761–768, 2006.

[3] S. I. Shornikov, Thermodynamic properties of the Na_2O–GeO_2 melts // Experiment in Geosciences. 2014. vol. 20. № 1. P. 48–51.

[4] H. J. Weber, “Bond volumes in crystals and glasses and a study of the germanate anomaly”, Journal of Non-Crystalline Solids, vol. 243, № 2-3, pp. 220–232, 1999.

Powder and thin-film hybrid materials emitting in the IR-range, based on tris(8-hydroxyquinolate) Yb (III) in CaF_2, PbF_2 and PbO matrices

K.I.Runina, A.U.Sekacheva, L.V.Popkova, O.B.Petrova, I.Ch.Avetissov
The Department of Chemistry and Technology of Crystals, D. Mendeleev University of Chemical Technology, MUCTR, Moscow, Russia
kristinarunina95@gmail.com

Abstract — Organic-inorganic hybrid materials based on ytterbium (III) tris(8-hydroxyquinolate) were obtained in fluoride and oxide inorganic matrices by solid-phase synthesis. Thin films were prepared using the obtained powder hybrid materials by capillary deposition technique. The films demonstrated photoluminescence in the visible and infrared regions.

Keywords — hybrid materials; photoluminescence; IR-region, ytterbium, 8-hydroxyquinolates, thin films

I. Introduction

Hybrid materials (HM), combining an inorganic matrix and an organic functional component (organic-inorganic HM), are used in devices for passive, active and integrated optics and photonics [1]. The use of rare-earth metal complexes in such materials can significantly increase the luminescence efficiency due to the transfer of excitation energy to trivalent rare-earth ions from organic ligands [2]. This energy transfer "antenna effect" is more efficient than direct excitation of RE ions, since organic ligands have broader absorption bands than RE ions due to low-intensity of *f-f* transitions. Synthesis of HM based on various Yb-complexes [3-4] by the melt technique resulted to the fabrication of glass HM with a wide intense photoluminescence (PL) band in the visible region and a very weak band in the NIR-region of 1 μm. This is due to the partial thermal destruction of the organic metal complex and the formation of new bonds between organic ligands and matrix components, leading to ligand-centered luminescence of new complexes.

II. Experimental Section

The initial materials were tris(8-hydroxyquinolate) ytterbium (III) and powders of CaF_2, PbF_2, and PbO with chemical purity better than 99.99 wt%. In order to obtain materials luminescent in the NIR region, we synthesized HM at lower temperatures by the solid-phase method. We grinded 1 wt% phosphor with an inorganic matrix and subjected to heat treatment at 200, 300, or 400 °C for 2 h.

The resulting powders demonstrated luminescence in the visible and NIR regions. An increase in the processing temperature resulted to the relative intensity of the NIR PL decreased, and the visible PL increased. The most stable powders with a high NIR PL intensity were obtained by heat treatment at 200 ° C (Fig. 1).

The research was financially supported by the Ministry of Science and Higher Education of the Russian Federation within the FSSM-2020-0005 project.

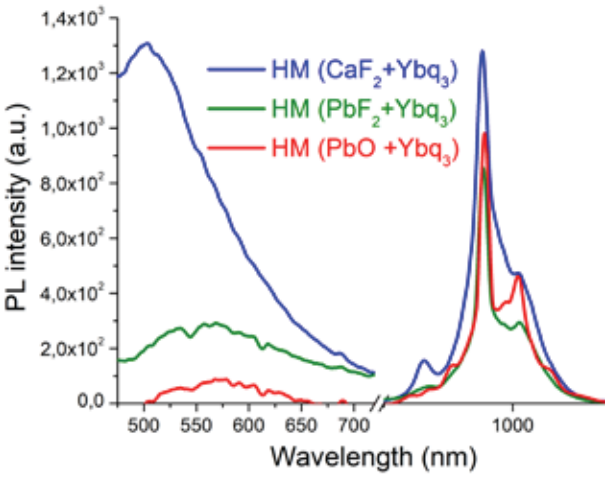

Fig.1 PL spectra of HMs, heat treatment at 200 °C (λ^{exc} = 377 nm).

Thin films based on HM powder were prepared by the capillary deposition technique. HM powders were dispersed in isopropanol and thoroughly mixed using an ultrasonic bath. The resulting suspension was poured into a capillary felt-tip pen (pore diameter 10 μm). The films were prepared on glass plates, corundum ceramic surfaces, and writing paper. Upon UV excitation, the films showed PL in the visible and NIR regions, which approved a good energy transfer from the ligands to Yb^{3+}.

References

[1] B.Lebeau, P.Innocenzi, "Hybrid materials for optics and photonics", Chemical Society Reviews, vol. 40, pp. 886–906, January 2011.

[2] P.Escribano, B.Julian-Lopez, J.Planelles-Arago, E.Cordoncillo, B.Viana, C. Sanchez, "Photonic and nanobiophotonic properties of luminescent lanthanide-doped hybrid organic–inorganic materials", Journal of Materials Chemistry, vol. 18, pp. 23–40, November 2008.

[3] M.O. Anurova, K.I. Runina, A.V. Khomyakov, I.V.Taydakov, I.Ch. Avetissov, "The effect of borate glass matrix on the luminescence properties of organic-inorganic hybrid materials", Physics and Chemistry of Glasses: European Journal of Glass Science and Technology Part B, vol. 60, № 4, pp. 140-145, August 2019

[4] K.I.Runina, L.V.Popkova, A.V.Khomyakov, R.I.Avetisov, O.B.Petrova, I.Kh.Avetisov, "Infrared Luminescent Hybrid Materials Based on Inorganic Glass Matrices", Glass and Ceramics, vol. 78, № 5-6, pp. 215–218, September 2021.

Down-Conversion Luminescence of Yb^{3+} Ions in $Yb:CaWO_4$ Single Crystals

K. A. Subbotin[1,2], A. I. Titov[1,2], D. A. Lis[1], E. V. Chernova[1], O. N. Lis[1], K. V. Kuleshova[2], Y. S. Didenko[2], Y. I. Zimina[2], and E. V. Zharikov[1]

[1]Prokhorov General Physics Institute of the Russian Academy of Sciences, Moscow, 119991 Russia
[2]Mendeleev University of Chemical Technology of Russia, Moscow, 125047 Russia

Abstract— Ytterbium and ytterbium –niobium doped sheelite single crystals have been grown by the Czochralski method in air and in protective atmospheres and subjected to additional annealing in air, in CO/CO_2 atmosphere, and in forevacuum. Comparative investigations of optical absorption and photoluminescence spectra of the crystals in the visible and near-IR spectral regions upon UV excitation were performed. A consistent pattern is proposed, explaining the nature of the donor centers involved into the process of down-conversion population of $^2F_{5/2}$ excited state of Yb^{3+} ions in the crystals.

Keywords — scheelite, single crystals, ytterbium, down-conversion, luminescence

I. Introduction

Yb doped Scheelite-like tungstate and molybdate single crystals, exhibit cooperative down-conversion process (quantum cutting) [1, 2] that can be used for increase the efficiency of solar cells based on crystalline silicon. In the frame of this process UV photons are absorbed by some donor centers of the crystal, and then, as a result of cooperative donor–acceptor interaction, the excited state energy of the donor is transferred into a doubled number of acceptors (excited state $^2F_{5/2}$ of Yb^{3+} ions), from which the emission of a doubled number of secondary photons at ~1 μm occurs. The nature of the donor centers involved in this process remained unknown. It was believed in [3] that in $Yb:CaMoO_4$ crystal these donor centers are molybdate complexes $[MoO_4]^{2-}$, which pass to the charge-transfer excited state (self-trapped exciton) under UVexcitation. However, it was convincingly proved later [4] that these complexes are not involved into the population of Yb^{3+} excited state in Scheelite-like crystals. A number of other versions of the possible nature of aforementioned donor centers were also considered and verified in [4]. Some of them (color centers at oxygen or cation vacancies, as well as partially reduced molybdenum/tungsten ions and uncontrolled impurities) were rejected. The aim of this research was to verify additionally some other versions, i.e., Yb^{2+} ion and self-trapped exciton at Yb^{3+} ion.

II. Experimental

$Yb:CaWO_4$ and $Yb,Nb:CaWO_4$ single crystals were grown by the Czochralski method in air, in N_2 and in argon atmospheres. A part of the grown crystals were then annealed in air, in CO/CO_2 atmosphere, and in forevacuum. The optical absorption spectra of the samples were measured in the range from 200 to 1500 nm. The down-conversion luminescence of the samples was measured in the range of 400–1050 nm upon UV excitation by four different LEDs with the following peak wavelengths: 255 nm, 285 nm, 315 nm, and 360 nm. The emission band FWHM was the same for all diodes: 15 nm.

III. Results

The performed investigations allowed us to make the following conclusions:

1. Additional introduction of Nb^{5+} into $Yb:CaWO_4$ crystal composition as the charge compensator of heterovalent substitution of Ca^{2+} by Yb^{3+} raises the Yb^{3+} segregation coefficient between Czochralski-grown $Yb:CaWO_4$ crystal and melt by an order of magnitude (almost to unity), in comparison to the case of solely Yb doped $CaWO_4$ (about 0.1).
2. $Yb:CaWO_4$ и $Yb,Nb:CaWO_4$ crystals exhibit down-conversion luminescence of Yb^{3+} near 1 μm under UV excitation (260 to 355 nm). An increase in oxidative potential of the samples synthesis atmosphere, as well as the introduction of niobium into the composition of $Yb:CaWO_4$ crystal suppresses the Yb^{3+} down-conversion luminescence.
3. The main donor center involved in the down-conversion population of $^2F_{5/2}$ excited state of Yb^{3+} in Scheelite crystal is Yb^{2+} ion. Another possible (although much less efficient) mechanism is population of this excited state from the high-lying charge-transfer excited state of Yb^{3+} ions.
4. It was additionally shown that the color centers at oxygen vacancies and partially reduced tungsten ions, as well as self-trapped excitons at tungstate complexes, are not involved into the process of down-conversion population of $^2F_{5/2}$ excited state of Yb^{3+} ions in scheelite crystals, whereas vacuum annealing of the crystals suppress both optical transparency, and ytterbium down-conversion luminescence of the crystal.

The research was financially supported by the Ministry of Science and Higher Education of the Russian Federation within the FSSM-2020-0005 project.

References

[1] Subbotin K.A., Lis D.A., Osipova Y.N., Khomyakov A.V. et. al.- *Opt. Spectrosc.* **2015**, 119, 974-981. DOI:10.1134/S0030400X1511022

[2] [30] K.A.Subbotin, Y.N.Osipova, D.A.Lis, V.A.Smirnov, et. al.- *Opt. Spectrosc.* **2017**, *123*, 49-55. DOI:10.1134/S0030400X17070256

[3] Cao X., Wei T., Chen Y., Yin M., Guo C., Zhang W..- *J. Rare Earths*, Vol. 29, No. 11 (2011), p.1029-1035. DOI: 10.1016/S1002-0721(10)60592-3

[4] K.A.Subbotin, A.I.Titov, D.A.Lis, E.Sani, V.A.Smirnov, O.K.Alimov, E.V.Zharikov, and I.A.Shcherbakov.- *Phys. Status Solidi* A 2020, 217, 1900659. DOI: 10.1002/pssa.201900659.

Few-layer graphene: growth and potential applications in optoelectronics.

V.Y. Aristov [1,2], A.N. Chaika [2,3], O.V. Molodtsova [1,4], S.V. Babenkov [1,5], D.V. Potorochin [1,4,6], A. Locatelli [7], T. Mentes [7], A. Sala [7], and D. Marchenko [8];

[1] Deutsches Elektronen-Synchrotron DESY, Hamburg, D-22607 Germany,
[2] Institute of Solid-State Physics, Russian Academy of Sciences, Chernogolovka, 142432 Russia,
[3] CRANN, School of Physics, Trinity College Dublin, Dublin 2, Ireland,
[4] University ITMO, Saint-Petersburg, 197101 Russia,
[5] LIDYL, CEA Saclay, Gif-sur-Yvette, 91191 France,
[6] Institut für Experimentelle Physik, Freiberg, D-09596 Germany,
[7] Elettra Sincrotrone, Trieste, I-34149 Italy,
[8] Helmholtz-Zentrum Berlin für Materialien und Energie, Berlin, D-12489 Germany

Abstract— Using SiC/Si(001) vicinal wafers, it is possible to synthesize self-aligned graphene nanoribbons with a transport gap on the order of 1 eV, a large in-plane positive magnetoresistance, and the potential to operate as a spin filter, opening up possibilities for electronic devices and applications of spintronics. This work demonstrates the ability to control the orientation of the lattice and boundaries, as well as the layer thickness in situ during low-layer graphene synthesis in ultrahigh vacuum.

Keywords—low-layer graphene, vicinal cubic SiC(001)/Si(001) wafers, nanoribbons, transport gap, magnetoresistance, spin filter, ARPES, LEEM, μ-LEED, XPS.

The mechanism of few-layer graphene growth on the technologically relevant cubic-SiC/Si(001) substrate is uncovered using high-resolution core-level and angle-resolved photoelectron spectroscopy, low-energy electron microscopy, and micro spot low-energy electron diffraction [1]. The thickness of the graphitic overlayer supported on the silicon carbide substrate and related changes in the surface structure are precisely controlled by monitoring the progress of the surface graphitization in situ during high-temperature graphene synthesis, using a combination of microspectroscopic techniques. The experimental data reveal gradual changes in the preferential graphene lattice orientations at the initial stages of the few-layer graphene growth on SiC(001) and can act as reference data for controllable growth of single-, double-, and triple-layer graphene on silicon carbide substrates.

We have presented [1] a step-by-step in situ studies of the UHV synthesis of few-layer graphene on β-SiC/Si(001) wafers performed using complementary high-resolution spectroscopic methods and low-energy electron diffraction. ARPES (Fig 1) and μ- LEED data demonstrate that graphitization of the β-SiC(001) surface starts from the formation of nanodomains with their graphene lattices aligned relative to the silicon carbide crystal lattice. The growth of such nonrotated graphene domains is favored by the small mismatch between the β-SiC(001)-c(2×2) and graphene lattices. At sub-monolayer coverages, these nonrotated graphene domains dominate, with the nonrotated and rotated domains coexisting in the first completed monolayer. The following graphene layers start growing from the linear defects of the substrate (steps or carbon atomic chains). The lattices in the top graphene layers are preferentially rotated by ±13.5° relative to the two orthogonal ⟨110⟩ directions of β-SiC. The in situ core-level μ- XPS studies conducted in the course of the few-layer graphene synthesis reveal only two components corresponding to the substrate and the overlayer, demonstrating the very small interaction between the few-layer graphene and β-SiC(001). The results of the C 1s spectra decomposition performed in this work can be used as a reference to distinguish between mono-, bi-, and trilayer graphene using XPS data obtained in the normal emission geometry with 330, 400, and 450 eV photon energies. They can also help to stop the synthesis procedure in fast dynamic-XPS stations with real-time control of the core level spectra shape when a desirable number of graphene layers (1, 2, or 3 ML) is synthesized.

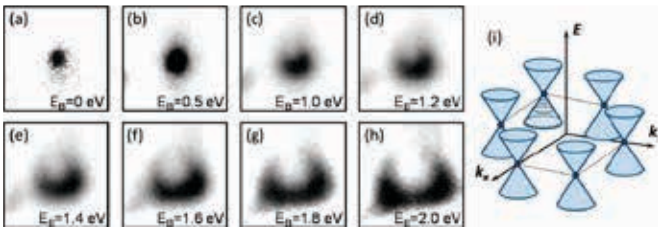

Fig. 1. ARPES constant-energy maps near the Fermi level measured for one of the Dirac cones. (a–h) Constant-energy ARPES intensity maps taken near one of the K points at binding energies (EB) from 0 to 2.0 eV, showing the electronic structure in the kx–ky plane (hν = 47 eV). (i) Schematic diagram of the E(k) dispersions near six corners of the Brillouin zone.

This work was supported by the Russian Foundation for Basic Research (grant no. 20-02-00489).

REFERENCES

[1] V. Y. Aristov, A. N. Chaika, O. V. Molodtsova, S. V. Babenkov, A. Locatelli, T. O. Mentes, A. Sala, D. Potorochin, D. Marchenko, B. Murphy, B. Walls, K. Zhussupbekov, and I. V. Shvets, Layer-by-Layer Graphene Growth on cubic-SiC/Si(001), ACS Nano 13, 526 (2019), doi: 10.1021/acsnano.8b07237

Hexagonal Ge on the side facets of GaAs and AlGaAs nanowires

I. V. Ilkiv[1], K. P. Kotlyar[1,2], D. A. Kirilenko[3], I. P. Soshnikov[2], S. V. Mikushev[1], V. G. Dubrovskii[1,3], George E. Cirlin[1-3]

[1] Faculty of Physics, St. Petersburg State University, Universitetskaya Emb. 13B, 199034, St. Petersburg, Russia
[2] Nanotechnology Research and Education Centre, Alferov University, Khlopina 8/3, 194021 St. Petersburg, Russia
[3]Ioffe Institute, Politekhnicheskaya 26, 194021 St. Petersburg, Russia

Abstract — Growth of hexagonal Ge stripes on the side facets of wurtzite AlGaAs and GaAs nanowires is considered. It is shown experimentally and explained within a model that Ge forms stripes on AlGaAs nanowires, while it covers conformally GaAs nanowires. The effect is explained by different surface and interface energies in the two material systems.

Keywords — hexagonal Ge; GaAs and AlGaAs nanowires, molecular beam epitaxy, surface energetics.

I. Introduction

Synthesis of hexagonal (HEX) Ge attracts great interest as Ge may become direct bandgap material in 2H HEX crystal phase. One of the methods is epitaxial growth of Ge on the sidewalls of wurtzite (WZ) III-V nanowires (NWs), where a WZ NW serves as a template for HEX Ge layer [1]. Here, we investigate the difference in the morphology of Ge layers on the side facets of AlGaAs and GaAs NWs and present a model explaining why Ge grows in the form of stripes on AlGaAs NWs, while it forms conformal shells on GaAs NWs.

II. Results and Discussion

Ge layers were grown by low-temperature molecular beam epitaxy (MBE) (at 320 ºC) on the side facets of AlGaAs and GaAs NWs, whose crystal phase was WZ. It was shown that Ge forms in 2H HEX phase in both cases. However, there was an important difference in the morphology of Ge layers. Ge formed ~ 17 nm wide stripes on 25 nm wide facets of AlGaAs NWs (see Fig. 1) [2], while it covered conformally the sidewalls of GaAs NWs. Since both material combinations are lattice-matched, the effect was explained based on the surface and interface energetics [3,4].

The simplified expression for the normalized surface energy of interest was obtained in the form

$$f = \frac{v}{x} + \alpha x.$$

Here, v is the volume of Ge stripe per unit length, and $\alpha \propto \gamma_{Ge} + \gamma_{Ge-AlGaAs} - \gamma_{AlGaAs}$ contains the difference of surface energies of Ge, Ge-AlGaAs interface, and AlGaAs materials (with or without Al). This α is negative for Ge-GaAs interface, meaning that Ge wets the side facets of GaAs NWs. The situation is reversed for Ga-AlGaAs interface, where Ge forms the stripe rather than the conformal shell on the side facets of AlGaAs NWs, as shown in Fig. 1. The observed formation of Ge stripes is interesting for obtaining 1D confinement of Ge in 2H HEX crystal phase.

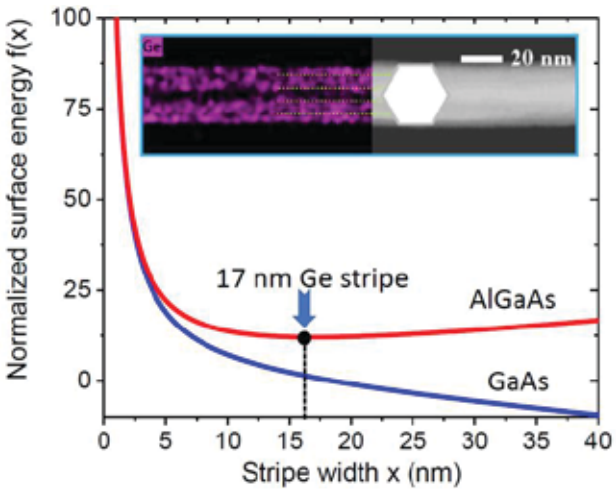

Fig. 1. (a) Normalized surface energy of HEX Ge stripe on the side facet of WZ AlGaAs (the curve with a minimum) and GaAs (the monotonically decreasing curve) NW versus the stripe width. Ge forms a 17 nm stripe on 25 nm wide side facet of AlGaAs NW, as shown in the insert. Conversely, Ge forms a conformal shell around GaAs NW.

This research was supported by the research grant of St. Petersburg State University No. 75746688.

References

[1] E. M. Fadaly, A. Dijkstra, J. R. Suckert, D. Ziss, M. A. van Tilburg, C. Mao, Y. Ren, V. T. Lange, K. Korzun, S. Kölling, M. Verheijen, D. Busse, C. Rödl, J. Furthmüller, F. Bechstedt, J. Stangl, J. J. Finley, S. Botti, J. Haverkort, and E. P. A. M. Bakkers, "Direct-bandgap emission from hexagonal Ge and SiGe alloys", Nature, vol. 580, p. 205-209, 2020.

[2] I. V. Ilkiv, K. P. Kotlyar, D. A. Kirilenko, A. V. Osipov, I. P. Soshnikov, S. V. Mikushev, V. G. Dubrovskii, and G. E. Cirlin, "Formation of hexagonal Ge stripes on the side facets of AlGaAs nanowires: Implications for near-infrared detectors". ACS Appl. Nanomaterials, vol. 4, p. 7289-7294, 2021.

[3] K. W. Ng, W. S. Ko, T.-T. D. Tran, R. Chen, M V. Nazarenko, F. Lu, V. G. Dubrovskii, M. Kamp, A. Forchel, and C. J. Chang-Hasnain, "Unconventional Growth Mechanism for Monolithic Integration of III–V on Silicon", ACS Nano, vol. 7, p. 100–107, 2013.

[4] V. G. Dubrovskii, N. V. Sibirev, X. Zhang, and R. A. Suris, "Stress-driven nucleation of three-dimensional crystal islands: from quantum dots to nanoneedles", Cryst. Growth Des., vol. 10, p. 3949-3955, 2010.

Terahertz Lasing Condition in the Cavity with Graphene Hyperbolic Medium: Optimisation.

O.N. Kozina[1], L.A. Melnikov[2]
[1]Kotel'nikov Institute of Radio-Engineering and Electronics of Russian Academy of Science, Saratov Branch, Saratov, Russia
kozinaolga@yandex.ru
[2]Yuri Gagarin State Technical University of Saratov, Saratov, Russia

Abstract— Complex resonator with thin hyperbolic media inside is investigated in the way of developing theory of THz laser. The eigen waves of the cavity contains asymmetrical hyperbolic medium have been calculated. Optimal conditions for efficient THz lasing have been clarified.

Keywords— terahertz emission, hyperbolic metamaterials

Developing the theory of a THz laser, we studied in detail the processes of wave propagation in a complex cavity with thin hyperbolic media (HM) inside. We employ asymmetrical hyperbolic medium (AHM) based on graphene-semiconductor multilayer structure with optics axis tilted with respect to outer boundary as an active media.

The transverse permittivity of the AHM with saturation is given as follow

$$\varepsilon_{\perp} = \varepsilon_{\parallel} + \frac{i}{d\omega\varepsilon_0}\left[\sigma'(\omega, E_0) + i\sigma''(\omega, E_0)\right],$$

where ω is the angular frequency, d is the period of the AHMM, E_0 is a component of the external electric strength vector transverse to the graphene plane, ε_0 is the vacuum permittivity, and $\sigma(\omega, E_0)$ *is* the surface conductivity of graphene [1]. THz wave emission in the cavity was investigated numerically using transfer matrix method [2,3]. The frequency of oscillation and field intensity have been calculated from the solution of equations for real and imaginary parts of log of eigenvalues κ_i of total transfer matrix of one period of the structure $P_t = P_0(l)P(h)$. l is total length of air gap in resonator; h is thickness of AHMM. Due to the linearity of the eigenvalues problem at a given E_0 the eigenvalues of the entire transfer matrix P_t are $\Lambda_i = e^{(i\varkappa_i L)}$, where $\varkappa_i = \ln \Lambda_i$ characterizes the phase delay at one pass ($L = l + h$). Mode frequency and mode intensity proportional to E_0 are the solutions of the equations:

$$\mathrm{Re}\left[\kappa_i(k_z, E)\right] = 0, \qquad \mathrm{Im}\left[\kappa_i(k_z, E)\right] = 0,$$

These equations may be solved numerically to find k_{z0} and E_0. The results of this calculation for different values of the period AHM d on the Fig.1

We have shown the existence of amplification of the THz waves in such structure [3]. We estimated the gain saturation effect and have shown that the gain saturation arises at the electric field strength about $2.7 \cdot 10^{12}$ V/m. The intensity of THz

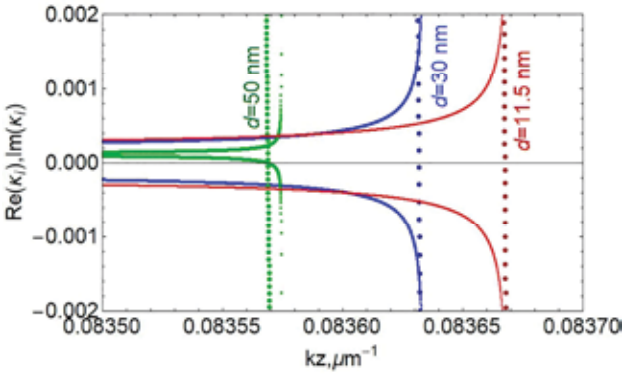

Fig. 1. Real (dotted curve) and imaginary (solid curve) parts of eigenvalues of the extraordinary wave κ_i vs k_z for one of extraordinary wave. L=1320μm, h=5μm. Euler angles φ=π/2, θ= 55°, incidence angle α=15°; E_F = 25 meV, τ = 10^{-12} c, T = 300º K.

radiation and the frequencies of oscillations have been calculated using recursive procedure.

Here we clarified optimal conditions for efficient THz lasing. The parameters of AHM were carefully analyzed to find ones providing the maximal gain of the THz radiation. The radiation incidence angle on processes taking place in the resonator containing AHM taken into account and was selected similarly to the Brewster angle for an active medium of a laser cavity to reduce the reflection from AHM. Selection of the incidence angle has been done simultaneously with selection of other parameters of the complex resonator, namely, the Euler angles, the period of AHM d, dynamic parameters of materials constituting AHM, and the lengths of air parts of the resonator. The region where considered AHM possess hyperbolic properties and amplification properties simultaneously was determined for different values of the AHM period.

ACKNOWLEDGMENT

This work was carried out at IREE RAS within the framework of the state task

REFERENCES

[1] J. B. Khurgin., "Graphene a rather ordinary nonlinear optical material," Appl. Phys. Lett., vol. 104, pp. 161116-161121, 2014.

[2] D. A. Yakovlev, V. G. Chigrinov, Modeling and optimization of the LCD optical performance, Hoi-Sing Kwok, Wiley, United Kingdom, 554, 2015.

[3] O.N. Kozina, L.A. Melnikov, I.S. Nefedov, "The theory for terahertz laser based on a graphene hyperbolic metamaterial," Journal of Optics, vol..22(9), pp.095003-095011, 2020.

The use of THz metamaterials for studying the adsorption of the SARS-CoV-2 virus spike protein by vibrational spectroscopy

M.R. Konnikova[1,2], O.P. Cherkasova [2,3,4], E.S. Dizer[2,5], A.A. Mankova[1], I.S. Vasilievskii[5], A.A. Butylin[1], A.P. Shkurinov[1]

[1]Faculty of Physics, Lomonosov Moscow State University, Moscow, Russia

[2]Institute on Laser and Information Technologies, Branch of the Federal Research Centre 'Crystallography and Photonics', Russian Academy of Sciences, Shatura, Russia

[3]Institute of Laser Physics, Siberian Branch, Russian Academy of Sciences, Novosibirsk, Russia

[4]National Research Tomsk State University, Tomsk, Russia

[5]National Research Nuclear University MEPhI, Moscow, Russia

Abstract—Adhesion of the SARS-CoV-2 virus spike protein was studied by vibrational spectroscopy using terahertz metamaterials. Specific features of metastructure absorption by histidine, albumin, and receptor-binding domain of spike protein films were investigated. An original method for quantitative estimation of the efficiency of virus adhesion on the surface of metamaterials has been proposed and experimentally tested.

Keywords— metamaterials, terahertz spectroscopy, viruses, adhesion

I. Introduction

The outer envelope of SARS-CoV-2-type coronavirus is formed by the spike (S) protein, which includes a receptor binding domain (RBD). The interaction of RBD with surfaces is largely due to weak non-specific intermolecular interactions, including hydrogen bonds [1]. The relaxation times of hydrogen bonds lie in the THz range. Special metasurfaces are widely used to increase the sensitivity of THz spectroscopy to thin molecular layers [2]. We demonstrate the applicability of THz metamaterials to estimate the adhesion efficiency of various molecular layers, including the RBD S protein SARS-CoV-2.

II. Experiments

We investigated thin films from solutions BSA and histidine (Sigma, USA) and RBD of the SARS-CoV-2 derived from the Chinese hamster ovary (CHO) recombinant line by THz spectroscopy [3, 4]. To improve the sensitivity of THz spectroscopy to thin films, we developed a THz metamaterial with resonance frequencies of 0.85 and 1.06 THz, whose single cell is shown in Fig. 1. To evaluate the adhesion efficiency, the films were extracted by ethanol and water with a certain sequence. After each extraction step, the THz transmittance of the metamaterial with the remaining molecules was measured (Fig. 1). The extraction fluids were also measured on a spectrophotometer after each extraction step.

III. Results

We investigated the adhesion efficiency of RBD S protein SARS-CoV-2 films compared to other films on surfaces by THz spectroscopy using metamaterials. After each step of film extraction, characteristic shifts of metastructure absorption resonances are observed. The results were confirmed by reference spectrophotometry of the extraction fluids. RBD has the highest effective adhesion.

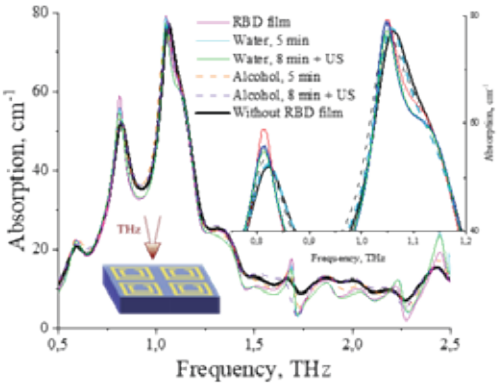

Fig. 1. Absorption spectra of THz metamaterials during sequential extraction of deposited RBD films. After the last extraction step, the position of the resonances returns to the initial one characteristic of the pure metastructure. Insertion of the developed THz metamaterial with resonance frequencies of 0.85 and 1.06 THz.

Thus, in this work, the IR and THz spectrum of the RBD of the SARS-CoV-2 derived from the CHO recombinant line were measured for the first time and a new method for determining the adhesion efficiency of substances based on THz metamaterials was proposed.

The work was supported by the RFBR (project No. 20-04-60505), the Ministry of Education and Science of the Russian Federation (project No. 0748-2020-0012), the Interdisciplinary Scientific and Educational School of Moscow University "Photonic and Quantum Technologies. Digital Medicine", as well as by the Government of the Russian Federation (Agreement No. 075-15-2021-615 of 04 June 2021).

References

[1] E. Joonaki et al. "Surface Chemistry Can Unlock Drivers of Surface Stability of SARS-CoV-2 in a Variety of Environmental Conditions, " Chem, vol. 6 (9), pp. 2135, 2020.

[2] Qin, W. Cheng, B. Han et al. "Ultrasensitive detection of saccharides using terahertz sensor based on metallic nano-slits, " Sci Rep, vol. 10, pp. 3712, 2020.

[3] M. R. Konnikova, O. P. Cherkasova, T. A. Geints, E. S. Dizer, et al., "Study of adsorption of the SARS-CoV-2 virus spike protein by vibrational spectroscopy using terahertz metamaterials", QUANTUM ELECTRON, vol. 52 (1), pp. 2–12, January 2022.

[4] M. R. Konnikova, O. P. Cherkasova, M. M. Nazarov, et al., "Malignant and benign thyroid nodule differentiation through the analysis of blood plasma with terahertz spectroscopy," Biomed. Opt. Express, vol. 12, pp. 1020-1035, February 2021.

The spectral properties of Er^{3+}/bismuth active centers co-doped germanate glasses

I.V.Stepanova, L.M.Savenko, A.V.Efimochkina
The Department of Chemistry and Technology of Crystals, D. Mendeleev University of Chemical Technology, MUCTR, Moscow, Russia

Abstract— Erbium-doped bismuth-germanate glasses have been synthesized and their spectral characteristics have been studied. The contour of the absorption spectra in the region of 450-550 nm is represented by the superposition of the bands of erbium and BACs. It was found that the addition of erbium does not destroy bismuth active centers, which in the future makes it possible to expand the range of NIR luminescence.

Keywords— bismuth active centers; glass; erbium oxide, luminescence

I. Introduction

Bi_2O_3-GeO_2 glasses have broadband NIR-luminescence, which makes them an attractive material for creating tunable lasers in the 1100–1500 nm range and for amplifying optical signals in the 1300–1500 nm range for fiber communication systems [1]. Luminescence in bismuth glasses is associated with bismuth active centers (BACs) [2], the number and properties of which depend on the composition of the glass matrix and on the glass synthesis conditions.

The spectral range of the luminescence of Bi-doped glasses can be further extended by introducing rare-earth ions into the glass, such as Er^{3+}, Yb^{3+}, Pr^{3+}, etc. [3–5]. Therefore, the study of the spectral characteristics of RE/BACs co-doped glasses is not of only scientific but also practical interest.

II. EXPERIMENTAL SECTION

High pure Bi_2O_3, GeO_2 and Er_2O_3 were mixed and calcined at T = 750°C, then melted at T = 1100°C for 30 min, and the melt was poured onto a metal substrate. The glass composition was described by the general formula $10Bi_2O_3$–$90GeO_2$ + xEr_2O_3 (x = 0; 0.1; 0.2; 0.3; 0.4 and 0.5 mol.%). Er_2O_3 was added in excess of 100%. The absorption spectra were fixed using an UNICO 2800 (UV/VIS) spectrophotometer (190 -1100 nm).

Erbium-free glass has a characteristic pale red color, and its absorption spectrum (Fig. 1) shows a broad absorption band around 500 nm, associated with the presence of BACs.

In erbium-containing glasses, characteristic lines of erbium at 378, 489, 522, 543, 653, 795 and 978 nm [3] appeared in the spectra, the intensity of which increases with increasing erbium concentration. In the region of 450-550 nm, the contour of the spectral lines of erbium-containing glasses is represented by the superposition of a wide absorption band of the BACs and Er^{3+} bands. Based on the analysis of the spectra, it can be concluded that an increase in the concentration of erbium does not lead to a decrease in the concentration of BACs (Fig. 1, inset).

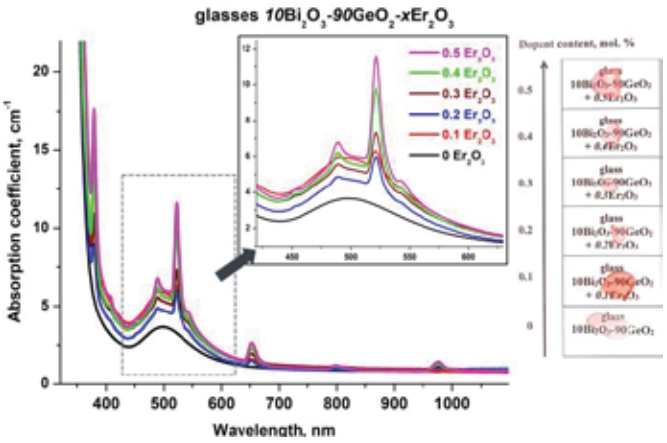

Fig. 1. The absorption spectra of synthesized Er^{3+}/BACs co-doped germanate glasses.

It was found that a further increase in the concentration of erbium leads to uncontrolled glass crystallization. Thus, for a given amount of bismuth in glass, the concentration of 0.5 mol.% Er_2O_3 is the maximum. The question of the effect of erbium on the NIR-luminescence in Er^{3+}/BACs co-doped germanate glasses requires further research.

The research was supported by the Ministry of Science and Higher Education of the Russian Federation by the project FSSM-2020-0003.

References

[1] E.M. Dianov, S.V. Firstov, V.F. Khopin, A.N. Guryanov, and I.A. Bufetov, “Bi-doped fibre lasers and amplifiers emitting in a spectral region of 1.3 μm”, Quantum Electronics, vol. 38, pp. 615-617, 2008.

[2] E. M. Dianov, “Nature of Bi-related near IR active centers in glasses: state of the art and first reliable results”, Laser Physics Letters. vol. 12, № 9, pp. 51–56, 2015.

[3] R.Ruamnikhom, P. Limsuwan, N. Chanthima, and J. Kaewkhao, “Preparation and properties of Er^{3+} doped with Bi_2O_3-BaO-B_2O_3”, Glass Advanced Materials Research, vol. 770, pp. 54-58, 2013.

[4] V.D.D. Cacho, L.R.P. Kassab, S.L. Oliveira, and P. Verdonck, “Near infrared and blue cooperative emissions in Yb^{3+}-doped GeO_2–PbO glasses”, Journal of Non-Crystalline Solids, vol. 352, pp. 56–62, 2006.

[5] G. Chinna Ram, T. Narendrudu, N. Veeraiah, C.K. Jayasankar, and D. Krishna Rao, “Influence of Bi^{3+} ions on optical and luminescence properties of multi-component P_2O_5–PbO–Ga_2O_3–Pr_2O_3 glass system”, Optical Materials, vol. 77, pp. 178–186, 2018.

Spectral properties of $CsPbI_3$ perovskite nanocrystals in borogermanate glass

R. Kharisova[1], A. Babkina[1], K. Zyryanova[1], N. Kuzmenko[1], A. Pavliuk[1], V. Klinkov[2], N. Nikonorov[1]
[1]Research Center for Optical Materials Science, ITMO University, St. Petersburg, Russia
[2]Laboratory of Applied Chemistry, Peter the Great St. Petersburg Polytechnic University, St. Petersburg, Russia

Abstract— The investigation results of spectral properties of $CsPbI_3$ perovskite nanocrystals in borogermanate glass are presented. The nanocrystals luminescence band shifts from 670 to 710 nm with crystal size increase from 6.3 to 17 nm. The maximum quantum yield obtained is 34%.

Keywords— perovskite quantum dots; cesium lead iodide perovskite; borogermanate glass; red phosphor.

I. Introduction

Perovskite nanocrystals $CsPbX_3$ (X = Cl, Br, I) have recently attracted much attention due to the optical and photoelectric properties. Unfortunately, these nanocrystals are not stable in air and are influenced by moisture and temperature; therefore, there is a need to search for various matrices that protect them from environmental influences [1]. One of such matrices that provide the greatest stability are glass matrices. And although the use of glasses does not allow the photovoltaic applications, there remains a possibility for their use as luminescent and laser media.

II. Experimental Section

Borogermanate glasses of the GeO_2-B_2O_3-ZnO-Na_2O-TiO_2-Cs_2O-PbO-KI system were synthesized by melt-quenching technique at 1000°C in air atmosphere using closed quartz crucibles. The STA6000 (PerkinElmer) differential scanning calorimeter was used to determine a glass transition temperature T_g=490°C. The glass samples were heat-treated (HT) at temperatures above T_g for 1 hour to promote the nucleation of the $CsPbI_3$ perovskite nanocrystals in glass matrix. The absorption and luminescence spectra were recorded on a Lambda 650 UV-Vis spectrophotometer and a LS-55 (PerkinElmer) spectrofluorimeter. Absolute quantum yield was measured using Absolute PL Quantum Yield Measurement System (Hamamatsu) with integrating sphere unit.

III. Results

The initial glass was transparent in the whole visible spectral range from 400 nm to 800 nm. After HT the absorption band at 654-688 nm region occurred corresponding to the exciton absorbance in $CsPbI_3$ perovskite nanocrystals that were formed during the HT. The 1S exciton band location shifted to the larger wavelengths from 654 to 688 nm while the HT temperature increased from 490 to 550°C. With an increase in the heat treatment temperature, the maximum of the luminescence band shifted from 670 to 710 nm (Fig. 1).

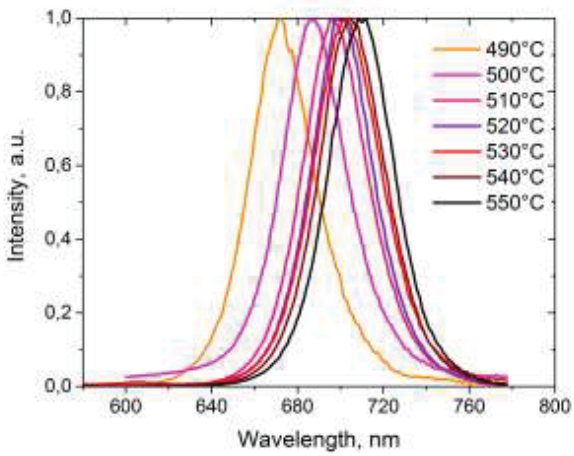

Fig. 1. Luminescence spectra of CsPbI3 nanocrystals nucleated at different temperatures in borogermanate glass matrix (excitation wavelength 460 nm).

A typical excitation spectrum of the iodine-containing glass coincided in shape with the absorption spectrum and had the pronounced band around 460 nm.

Due to the small size and low concentration of the nucleated crystalline phase, the results of the XRD study showed the presence of $CsPbI_3$ crystals of the cubic modification only after high-temperature heat treatment (550°C). The calculation of the mean crystal size from the XRD data gave a large error. Therefore, the mean crystal size was calculated from the location of the first exciton 1S maximum in the absorption spectrum recorded at liquid nitrogen boiling point. Wherein the mean crystal size calculated for the case of strong confinement and considering the spherical shape of the nucleated crystals [2] increased from 6.3 to 17 nm. The maximum quantum yield obtained was 34%, which is close to the best values indicated in the literature for pure $CsPbI_3$ perovskite crystals in glass [3].

The glass synthesis was supported by the grant of the President of the Russian Federation for young PhD scientists No. MK-2869.2021.1.2. Investigation of spectral properties was supported by the grant of the President of the Russian Federation for young PhD scientists No. MK-4235.2021.1.3.

References

[1] S. Seth, T. Ahmed, A. De, and A. Samanta, "Tackling the Defects, Stability, and Photoluminescence of $CsPbX_3$ Perovskite Nanocrystals," ACS Energy Lett., vol. 4, no. 7, pp. 1610–1618, 2019.

[2] A. L. Efros and A. L. Efros, "Interband absorption of light in a semiconductor sphere," Sov. physics. Semicond., vol. 16, no. 7, pp. 772–775, 1982.

[3] D. Chen *et al.*, "Promoting photoluminescence quantum yields of glass-stabilized $CsPbX_3$ (X = Cl, Br, I) perovskite quantum dots through fluorine doping," Nanoscale, vol. 11, no. 37, pp. 17216–17221, 2019.

Synthesis of luminescent hybrid materials in the PbF_2-La(Y)F_3- (8-hydroxyquinolate) lithium system by co-precipitation technique

P.V.Strekalov[1], M.N.Mayakova[2], M.U.Andreeva[1], K.I.Runina[1], O.B.Petrova[1], R.I.Avetisov[1]
[1] The Department of Chemistry and Technology of Crystals, D. Mendeleev University of Chemical Technology, MUCTR, Moscow, Russia
[2] A.M.Prokhorov General Physics Institute RAS, GPI RAS, Moscow, Russia

Abstract — Organic-inorganic luminescent hybrid materials with an inorganic matrix based on mixed lead and rare-earth fluorides and (8-hydroxyquinolate) lithium as an organic phosphor by co-precipitation from aqueous solutions have been synthesized. Their phase compositions and spectral characteristics have been investigated. The synthesized hybrid materials showed efficient broadband photoluminescence in the 390-700 nm region.

Keywords — hybrid materials; photoluminescence; lead fluoride, 8-hydroxyquinolates, co-precipitation, nanopowder

I. INTRODUCTION

Luminescent organic-inorganic hybrid materials (HM) contain nanoclusters of a highly efficient organic phosphor in a stable inorganic matrix. On the basis of PbF_2-containing matrices, HMs were synthesized by the melt method in low-melting glasses [1-2] and by the co-precipitation technique [3] using 8-hydroxyquinolate and β-diketonate organometallic phosphors. In the PbF_2-REF_3 system (RE = rare earth element), solid solutions of the $Pb_{1-x}RE_xF_{2+x}$ cubic phase of the fluorite *Fm3m* type can be formed. The high capacity of such solutions to RE, suggests the possibility of obtaining HM with a high concentration of organic components.

II. EXPERIMENTAL SECTION

The initial materials were lead, lanthanum; yttrium nitrates, 8-hydroxyquinolate lithium (Liq), and ammonium fluoride were used as a fluorinating agent.

At the first stage we mixed aqueous solutions of lead and RE nitrates and a solution of 8-hydroxyquinolate lithium in ethanol. We used two concentrations of nitrate solutions, namely, 1.43M or 0.8M. At the second stage, the final product was precipitated by ammonium fluoride; direct and reverse precipitations were used. As a result of co-precipitation, we got powder preparations, which contained both the low-temperature α-PbF_2 rhombic phase and solid solutions based on β-PbF_2 cubic phase, depending on the RE concentration and synthesis conditions. During the co-precipitation of nominally pure PbF_2 and HM (PbF_2+Liq), all powder preparations, regardless of the conditions, have the crystal structure of α-PbF_2.

Stable single-phase powders with the crystal structure of β-PbF_2 were obtained at RE concentrations of 20-25 mol%. For these samples, the photoluminescence (PL) spectra were studied (Fig. 1) by a Fluorolog 3D spectrofluorimeter (Horiba Jobin Yvon) at 377 nm excitation.

The research was financially supported by the Ministry of Science and Higher Education of the Russian Federation within the FSSM-2020-0005 project.

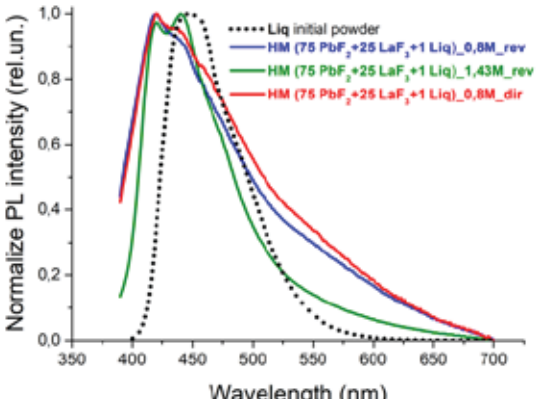

Fig.1 PL spectra of HM (PbF_2+LaF_3+Liq): dir - direct precipitation, rev - reverse precipitation (λ^{exc} = 377 nm).

The most intense PL is possessed by HM obtained by the reverse co-precipitation with a nominal LaF_3 concentration of 25 mol% and a concentration of the initial fluoride solution of 1.43M. The HM spectra are noticeably shifted to shorter wavelengths relative to the initial Liq. The short-wavelength component is obviously not associated with the centers of lanthanum or lead 8-hydroxyquinolates, which demonstrate PL in the longer wavelength region comparing to Liq. Besides, the center cannot be attributed to specific bonds in PbF_2 cubic phase. The PL intensity of HMs from the ternary PbF_2+LaF_3+Liq system turned out to be higher than that fabricated from binary (PbF_2+Liq, LaF_3+Liq) systems. Thus, HMs obtained from the ternary system are very promising due to a very short-wavelength and intensity PL.

REFERENCES

[1] M.O. Anurova, K.I. Runina, A.V. Khomyakov, I.V.Taydakov, I.Ch. Avetissov, "The effect of borate glass matrix on the luminescence properties of organic-inorganic hybrid materials", Physics and Chemistry of Glasses: European Journal of Glass Science and Technology Part B, vol. 60, № 4, pp. 140-145, August 2019

[2] O.B Petrova., M.O. Anurova, A.A. Akkuzina, R.R. Saifutyarov, E.V. Ermolaeva, R.I. Avetisov, A.V. Khomyakov, I.V.Taydakov, I.Ch. Avetissov, "Luminescent hybrid materials based on (8-hydroxyquinoline)-substituted metal-organic complexes and lead-borate glasses", Optical Materials, vol. 69, pp. 141-147, April 2017

[3] O.B.Petrova, K.I Runina., M.N.Mayakova, I.V.Taydakov, A.V.Khomyakov, R.I.Avetisov, I.Ch. Avetissov, "Luminescent hybrid materials based on metal-organic phosphors in PbF_2 powder and PbF_2-containing glass matrix", Optical Materials, vol. 88, pp. 378–384, February 2019

Plasmon–exciton interaction improves two-photon properties of semiconductor quantum dots

V.Krivenkov[1,2], P.Samokhvalov[2], I.S.Vasilyevskij[2], N.I.Kargin[2], Y.Rakovich[1,3,4], I.Nabiev[2,5]
[1]Centro de Física de Materiales (MPC, CSIC-UPV/EHU), Donostia - San Sebastian, Spain
[2]National Research Nuclear University MEPhI (Moscow Engineering Physics Institute), Moscow, Russian Federation
[3]Donostia International Physics Center, Donostia - San Sebastian, Spain
[4]IKERBASQUE, Basque Foundation for Science, Bilbao, Spain
[5]Laboratoire de Recherche en Nanosciences, LRN-EA4682, Université de Reims Champagne-Ardenne, Reims, France

To enhance the two-photon absorption (TPA) of quantum dots (QDs) we a designed plasmon–exciton hybrid material using plasmon nanoparticles (PNPs). We found that the effective The TPA of QDs near PNPs increased by an order of magnitude due to the nonlinear energy transfer from plasmons to excitons. We fabricated a near-infrared photodetector based on the designed material and found an order of magnitude increase in the photocurrent from the detector filled with QD–PNP hybrid material compared to the detector filled with QDs alone.

Keywords—quantum dots; two-photon absorption; plasmons; nonlinear energy transfer; near-infrared photodetector

I. Introduction

The engineering of efficient photodetectors with a nonlinear response to light is an important task for modern optoelectronics because this allows the fabrication of fully light-controlled devices. The two-photon absorption (TPA) phenomenon allows 3D confinement of excitation and, hence, the fabrication of 3D arrays of light-sensitive elements. Moreover, this type of excitation ensures the control of the response efficiency by tuning the intensity of light. Most current technologies use photodiodes based on bulk semiconductors, but the use of colloidal semiconductor quantum dots (QDs) is more advantageous due to easy processing, precisely controlled optoelectronic properties, quick response, and compatibility with flexible substrates [2]. Moreover, QDs have very large two-photon absorption cross-sections in a wide spectral range in the infrared region. However, activation of these photodetectors in the nonlinear optical mode still requires peak excitation intensities higher than 1 GW/cm^2. To reduce the excitation intensity, it is required to further increase the TPA.

II. Results

To achieve the plasmon-induced increase in the TPA of QDs, we designed a plasmon–exciton hybrid material containing plasmon nanoparticles (PNPs) with an absorption peak overlapping with the excitation band. We have fabricated thin-film hybrid materials based on QDs located near a PNP layer. The coating of the QD films with PNPs led to an order of magnitude increase in the TPA at the maximum of the plasmon spectrum. Moreover, we have shown that this increase is not related to the Purcell effect, but is entirely determined by nonlinear energy transfer from plasmons of the PNPs to excitons of the QDs [1]. To demonstrate a practical application of the effect, we designed a near-infrared plasmon–exciton photodetector based on the new plasmon–exciton hybrid material [2]. This device was fabricated by filling the gap between Au contacts patterned on a sapphire substrate with QDs and PNPs using the layer-by-layer deposition technique. Our experimental results showed that, under near-infrared excitation, the dependence of the photocurrent on the excitation power was quadratic relative to the corresponding dependence measured under one-photon excitation in the visible range, which indicates that the infrared excitation was two-quantum. Further experiments showed that the photocurrent was an order of magnitude higher in the detector filled with the QD–PNP plasmon–exciton hybrid material than in the detector filled with QDs alone. Additional measurements of the dark current in the designed QD–PNP photodetector and a reference photodetector (containing QDs alone) showed that the photocurrent enhancement in the presence of PNPs did not result from the formation of Ag-based conductive channels. Therefore, we interpreted this enhancement as a result of the nonlinear two-quantum energy transfer from linearly excited PNPs to the excitons of QDs.

Acknowledgments

This study was supported by the Russian Science Foundation, grant no. 18-72-10143 (plasmon–exciton materials design and investigation) and grant no. 21-79-30048 (nanoparticle synthesis and characterization). V.K. has received funding from the European Union's Horizon 2020 research and innovation programme under the Marie Skłodowska-Curie Actions, grant agreement no. 101025664 (QESPEM).

References

[1] V. Krivenkov, P. Samokhvalov, A. Sánchez-Iglesias, M. Grzelczak, I. Nabiev, and Y. Rakovich, "Strong increase in the effective two-photon absorption cross-section of excitons in quantum dots due to the nonlinear interaction with localized plasmons in gold nanorods," *Nanoscale*, vol. 13, no. 8, pp. 4614–4623.

[2] V. Krivenkov, P. Samokhvalov, I. S. Vasil'evskii, N. I. Kargin, and I. Nabiev, "Plasmon–exciton interaction strongly increases the efficiency of a quantum dot-based near-infrared photodetector operating in the two-photon absorption mode under normal conditions," *Nanoscale*, vol. 13, no. 47, pp. 19929–19935.

Single mode extruded silver halides fibers for CO_2 laser with losses less than 1 dB/m

A.L. Butvina, L.N. Butvina, A.G. Okhrimchuk

Prokhorov General Physics Institute of the Russian Academy of Sciences, Dianov Fiber Optics Research Center, Moscow, Vavilov 38. Russia

Abstract.

The optical loss of a extruded single-mode polycrystalline fiber AgCl0.5Br0.5\AgCl0.55Br0.45 was 0.8 dB / m. For the first time, a polycrystalline single-mode fiber at a wavelength of 10.6 µm with a step-index profile AgCl0.25Br0.75 / AgCl0.5Br0.5 and the world's lowest optical loss of 0.5 dB / m was extruded.

Summary.

For the first time, single-mode polycrystalline silver halides mid-IR optical fibers with a cutoff wavelength of 10 µm with an optical loss of the fundamental mode less than 1 dB / m at a wavelength of 10.6 µm of a CO2 laser were developed and manufactured by extrusion.

The measured optical loss of a segmented single-mode polycrystalline fiber with 0.01 a contrast of refractive index AgCl0.5Br0.5\AgCl0.55Br0.45 was 0.8 dB / m.

For the first time, a polycrystalline segmented single-mode fiber at a wavelength of 10.6 µm with a step-index profile and a high 0,05 contrast of refractive index AgCl0.25Br0.75 / AgCl0.5Br0. and, as we know, the world's lowest optical loss of 0.5 dB / m was developed and manufactured by extrusion. The threshold for laser destruction of this single-mode fiber from the power of a cw CO2 laser, which occurred in 20 min, was 200 kW / cm2.

For the first time, single-mode polycrystalline nano- and micro-structured extrusion fibers of silver halides with a core with a smallest diameter of 10 µm have been fabricated. Very high plastic elongation (1 000 000) of initial crystalline preform of silver halides with diameter 10 mm to 10 mkm core diameter of extruded polycrystalline co-clad fiber was achieved with low losses in mid IR and without mechanical necking.

The optical losses mechanisms of extruded polycrystalline silver halides will be discussed.

Investigation of the interaction of excitons with light in mesoscopic structures

A.B.Belonovskii[1,2], K.M. Morozov[1,2], E. I. Girshova[1,2], G. Pozina[3], M. A. Kaliteevski[1,2]
[1] St. Petersburg Academic University, 194021 St. Petersburg, Russia
[2] ITMO University, Kronverksky Pr. 49, 197101 St. Petersburg, Russia
[3]Department of Physics, Chemistry and Biology (IFM), Linköping University, SE-58183 Linköping, Sweden

Abstract— Interaction of cavity modes with exciton in meso-cavity (the structure supporting several cavity modes separated by energy interval comparable to Rabi-splitting of exciton and cavity modes) has been analyzed using a quantum-mechanical approach. Simultaneous interaction of exciton and several cavity modes results in a few novel effects.

Keywords— mesoscopic structures, exciton, Rabi-splitting, bistability

I. Introduction

In the case of electrons in a solid, consideration of mesostructures (structures whose size is comparable to the coherence length for electrons) has led to the discovery of new effects such as the Aharonov-Bohm effect and Universal fluctuations in conductivity. By analogy with electrons in a solid, the question arises whether there are mesoscopic effects in the interaction of light with matter?

One of the main characteristics of a microcavity is the existence of one high-Q photon mode that interacts with an exciton. The energy interval in such structures is much larger than the Rabi splitting. In bulk materials, there is a continuous spectrum of modes. However, little attention has been paid to the intermediate case, namely, the consideration of meso-cavities, structures that occupy an intermediate position between microcavities and bulk materials [1,2].

II. Theory

To theoretically describe the interaction of one exciton mode with several photon modes, we consider a model system consisting of one exciton mode with energy $\hbar\omega_0$ and several photon modes with energy $\hbar\omega_k$. The Hamiltonian describing the interaction of the exciton in the cavity with the optical modes of the resonator and the exciton-exciton interaction has the form:

$$\hat{H} = \hbar\omega_0 \hat{x}^+\hat{x} + \sum_k \hbar\omega_k \hat{a}_k^+\hat{a}_k + \sum_k \hbar g_k(\hat{a}_k^+\hat{x} + \hat{a}_k\hat{x}^+) + \hbar U\hat{x}^+\hat{x}^+\hat{x}\hat{x}, \quad (1)$$

where $\hat{x}^+, \hat{a}_k^+$ $(\hat{x}, \hat{a}_k)$ are the operators of creation (annihilation) of exciton and photons, respectively, obeying the commutation rule for bosons $[\hat{x}, \hat{x}^+] = 1$ and $[\hat{a}_k, \hat{a}_k^+] = 1$. In presence of dissipation, the system is upgraded to a Liouvillian description, with a quantum dissipative master equation for the density matrix.

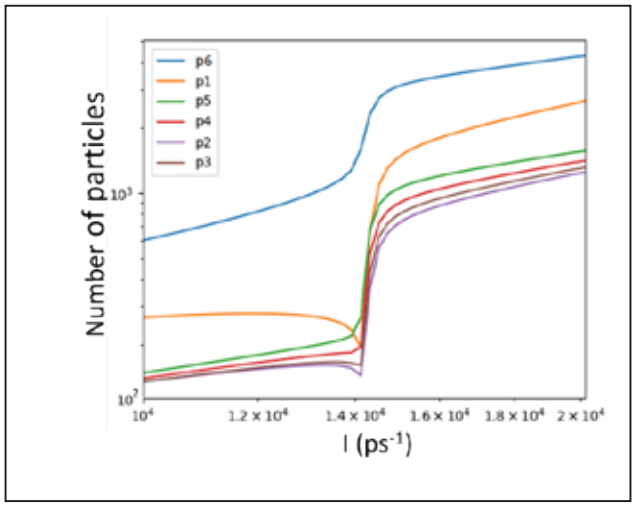

Fig. 1. Dependence of the population of polariton modes on pumping.

III. Polariton bistability

Figure 1 shows the dependences of the population of polariton modes in a mesoresonator supporting five photon modes interacting with an exciton mode in the presence of an exciton-exciton interaction. The polariton modes in Figure 1 are numbered in order of increasing energy. That is, the p1 mode has the lowest energy, and the p6 mode has the highest. As can be seen from Fig. 1, for low energy modes, a nonmonotonic dependence of the population on pumping is observed. This effect is observed for the p1, p2 and p3 polariton modes. In this case, the lower the mode energy, the stronger this effect.

Such an additional nonlinear dependence, demonstrated in this work, can be used to expand the range of application of polaritons.

Acknowledgment

This work has been supported by Russian Science Foundation Grant (16-12-10503).

References

[1] A. V. Belonovski et al. “Weak and strong coupling of photons and excitons in planar meso-cavities” Optics Express, vol. 29, no. 13, pp. 20724-20734 (2021).

[2] A. V. Belonovski et al. “Quantum analysis of luminescence of an exciton in a mesocavity” Optics Express, vol. 28, no. 9, pp. 12688-12698 (2020).

Thermodynamic Analysis of Borate Formation in the Synthesis of Glass-Ceramics Based on BaO – B_2O_3 – Bi_2O_3 and Er:YAG

A.D. Plekhovich, A.M. Kut'in, E.E. Rostokina, M.E. Komshina, K.V. Balueva, K.F. Ignatova
G.G. Devyatykh Institute of Chemistry of High Purity Substances of RAS, 49 Tropinina Str., Nizhny Novgorod, Russia

Abstract— The temperature conditions for the formation of aluminum, yttrium, erbium, barium, and bismuth borates from the glass-ceramic phase were determined by the Gibbs energy minimization method. The use of thermodynamic information in the interpretation of the results of thermal, XRD, and SEM analyzes of glass-ceramic samples contributed to the optimization of the modes of their sol-gel synthesis.

Keywords — glass-ceramics, Er:YAG, thermodynamics

I. Introduction

BaO – B_2O_3 – Bi_2O_3 (BBB) system is used for the synthesis of well-known nonlinear optical crystals: β-BaB_2O_4, α-BiB_3O_6, $BaBiBO_4$, as well as compounds $Ba_3Bi_2(BO_3)_4$ belonging to the $A_3REE_2(BO_3)_4$ phosphor family, where A = Ca, Ba [1,2]. Due to the additional crystalline phase YBO_3 formed from the BBB system in the presence of yttrium aluminum garnet [3], the material is also of interest as a matrix for phosphors.

The purpose of the intermediate stage of the work is to determine the temperature-time conditions for the formation of a new functional glass-crystalline material of optical quality at various ratios of the indicated glass phase and garnet (Er:YAG).

II. Results and discussion

Samples of glass-ceramics at this stage of the work were synthesized by impregnation of the Er:YAG ceramics obtained by the sol-gel method with pre-prepared $20Bi_2O_3$-$65B_2O_3$-15BaO glass at different ratios. The high intensity and completeness of impregnation at temperatures exceeding the T_m of glass is evidence of its chemical interaction with the Er:YAG surface. The component-selective depth of such interaction, experimentally recorded, first of all, by the XRD method, made it possible to establish the temperature and time conditions for the synthesis of new functional glass-ceramics with details of its composition. Note that the densest of a series of 7 samples were obtained at temperatures from 800 to 900 °C with a synthesis time of 30 minutes. The predictive thermodynamic factor in the characterization of the phase and component composition of new glass-ceramics, including by instrumental methods of DSC and spectroscopy, was a necessary component of the study.

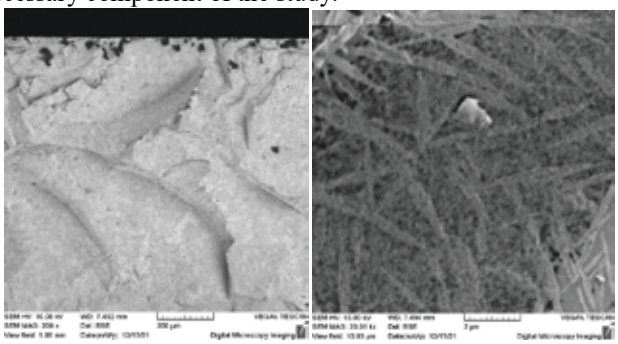

Fig. 1. SEM images of cleavage of glass ceramics.

References

[1] A. Khanna, K J S Sawhney, M K Tiwari, S. Bhardwaj, A.M. Awasthi Effects of melt ageing on the density, elastic modulus and glass transition temperature of bismuth borate glasses Journal of Physics: Condensed Matter.–2003.–V.15. № 40, pp. 6659.

[2] S.V. Krivovichev, R.S.Bubnova, S.N.Volkov, M.G.Krzhizhanovskaya, A.V. Egorysheva, S.K. Filatov Preparation, crystalstructureandthermalexpansionofanovel layered borate, $Ba_2Bi_3B_{25}O_{44}$ Journal of Solid State Chemistry, 196, pp. 11–16, 2012.

[3] E.Ye. Rostokina, A.D. Plekhovich, A.M. Kut'in, I.F. Georgiu, S.S. Balabanov, M.E. Komshina Kinetic effects of substitution Er^{3+} for Y^{3+} in $(Y_{1-x}Er_x)_3Al_5O_{12}$ garnet Journal of the European Ceramic Society, Volume 41, Issue 10, pp. 5324-5330, 2021.

This work was supported by the Russian Science Foundation (project No. 20-73-10110)

Up-conversion luminescence quantum yields of MF_2:Yb:R (M=Ca, Sr, Ba, Pb; R=Er, Tm, Ho) single crystals for photonics

S.V. Kuznetsov[1], V.A. Konyushkin[1], A.N. Nakladov[1], A.A. Alexandrov[1], E.I. Madirov[2], D. Busko[2] B.S. Richards[2], A. Turshatov[2]

[1]Prokhorov General Physics Institute of the Russian Academy of Sciences, GPI, Moscow, Russia
[2]Institute of Microstructure Technology, Karlsruhe Institute of Technology, Eggenstein-Leopoldshafen, Germany

Abstract — We present the measurements of up-conversion luminescence quantum yields of MF_2:Yb:R (M=Ca, Sr, Ba, Pb; R=Er, Tm, Ho) single crystals at 0.1-490.0 W/cm^2 pumping (976 nm). We revealed the solid solution compositions, which demonstrated the highest quantum yields.

Keywords—Up-conversion luminescence, quantum yield, alkali-earth fluorides, rare-earth elements, single crystals

Introduction

Up-conversion luminescence allowed to convert infrared irradiation in visible spectral range radiation which is promising for bioimaging, photodynamic therapy, theranostics, optical thermometry, anti-counterfeiting, increasing efficiency of perovskite solar cell and plastic sorting [1-3]. For different applications in industry used luminophores as powders and aqueous dispersion. Measurements of absolute quantum yield of up-conversion luminescence for powders and dispersion are very complicated technique. It is easier to measure the relative quantum yield of up-conversion luminescence in comparison to bulk reference materials with well-known absolute quantum yield. The classical reference crystalline materials are single crystals. One of the efficient up-conversion materials are fluorides, which allow low phonon energy of matrix. The purpose of our study was to determine the composition of single crystals, which demonstrated the highest quantum yields of up-conversion luminescence. The absolute quantum yield of up-conversion luminescence was measured by means of integrating sphere at 0.1-350.0 W/cm^2.

Experiments and results

The fluoride single crystals of MF_2:Yb:R (M=Ca, Sr, Ba, Pb; R=Er, Tm, Ho) were grown by the Bridgman technique in a vacuum furnace with CF_4 fluorinating atmosphere. The absolute quantum yields of up-conversion luminescence were measured in integrating sphere at 976 nm pumping in 0.1-490.0 W/cm^2.

The highest quantum yield (4.0%) for CaF_2:Yb:Er solid solution was recognized for 2,0 mol.Yb and 2.0 mol.%Tm at 350 W/cm^2.

The highest quantum yield (6.5%) for SrF_2:Yb:Er solid solution was recognized for 3,0 mol.Yb and 2.0 mol.%Tm at 230 W/cm^2.

The highest quantum yield (10.0%) for BaF_2:Yb:Er solid solution was recognized for 3,0 mol.Yb and 2.0 mol.%Er at 490 W/cm^2.

The highest quantum yield (3.2%) for PbF_2:Yb:Er solid solution was recognized for 1,5 mol.Yb and 1.5 mol.%Er at 350 W/cm^2.

The MF_2:Yb:Er (M=Sr, Ba) single crystals were successfully testified for increasing efficiency of perovskite solar cell and estimation of quantum yield of nanoparticle dispersion in comparison to single crystal.

Acknowledgment

The reported study was funded by RFBR (project numbe 21-53-12017) and DFG (project number TU 487/8-1).

References

[1] B.S. Richards, D. Hudry, D. Busko, A. Turshatov, I.A. Howard, "Photo upconversion for photovoltaics and photocatalysis: a critical review", Chem. Rev., vol.121, pp.9165-9195, 2021

[2] J. Woidasky, I. Sander, A. Schau, J. Moesslein, P. Wendler, D. Wacker G. Gao, D. Kirchenbauer, V. Kumar, D. Busko, I. A. Howard, B. S Richards, A. Turshatov, S. Wiethoff, C. Lang-Koetz, "Inorgani fluorescent marker materials for identification of post-consumer plasti packaging", Resour., Conserv. Recycl., vol.161, pp.104976, 2020.

[3] R. Singh, E. Madirov, D. Busko, I.M. Hossain, V.A. Konyushkin, A.N. Nakladov, S.V. Kuznetsov, A. Farooq, S. Gharibzadeh, U.W. Paetzold B.S. Richards and A. Turshatov, "Harvesting sub-bandgap photons vi up-conversion for perovskite solar cells", ACS Appl. Mater. Interfaces vol.13, pp. 54874–54883, 2021

Optical Properties of Composite ZnO-Er_2O_3-Yb_2O_3 Ceramics: Effect of Annealing

Elena Gorokhova[1,*], Olga Dymshits[1], Ivan Venevtsev[2], Liza Basyrova[3,**], Irina Alekseeva[1], Alexander Khubetsov[1], Sergey Eron'ko[1], Eugenia Oreschenko[1], Anna Seroglazova[4], Patrice Camy[3], Pavel Loiko[3], and Alexander Zhilin[5]

[1] S. I. Vavilov State Optical Institute, 192171 St. Petersburg, Russia

[2] Peter the Great St. Petersburg Polytechnic University, 195251 St. Petersburg, Russia

[3] CIMAP, UMR 6252 CEA-CNRS-ENSICAEN, Université de Caen Normandie, 6 Boulevard Maréchal Juin, 14050 Caen, France

[4] Saint-Petersburg State Institute of Technology, 190013 St. Petersburg, Russia.

[5] D.V. Efremov Institute of Electrophysical Apparatus, 196641 St. Petersburg, Russia

*e-mail: e.gorokhova@rambler.ru; **e-mail: liza.basyrova@ensicaen.fr

***Abstract*—Composite optical ceramics ZnO-Er_2O_3-Yb_2O_3 were prepared by uniaxial hot pressing of commercial oxide powders at 1180 °C in vacuum. Their structure, optical absorption and luminescence and X-ray induced luminescence (XRIL) have been studied. The annealing of ceramics at 1200 °C modified the ZnO grain morphology, enhanced up-conversion luminescence of Er^{3+} ions, affected the shape of the XRIL spectra and their decay kinetics.**

Keywords—zinc oxide; sesquioxides; erbium ions; optical ceramics; luminescence.

I. Introduction

Zinc oxide (ZnO) is a wide bandgap semiconductor attractive for photonics applications. ZnO materials exhibit two XRIL bands: a short-wavelength one near the absorption edge of the crystal, which is excitonic in nature, and a broad band in the visible, assigned to different defects. The solubility of rare-earth ions (RE^{3+}) in ZnO is very low, if any, however, there is a strong interaction between ZnO crystals and RE^{3+} ions located at their surface. One example of a material accommodating both ZnO and RE^{3+} ions is a composite optical ceramic ZnO-RE_2O_3 [1]. It is challenging to fabricate such ceramics, as ZnO is optically anisotropic. In the present work, we have fabricated and characterized ZnO-Er_2O_3-Yb_2O_3 optical ceramics.

II. Results and Discussion

ZnO ceramics codoped with 1 wt% Er^{3+} and 3 or 4 wt% Yb^{3+} were prepared by uniaxial hot pressing of commercial oxide powders (ZnO, RE_2O_3) at 1180 °C in vacuum. The ceramics were additionally annealed at 1200 °C for 2 h in air. The ceramics exhibited a maximum total transmission of ~40% in the visible, and it decreased by 10% after annealing. They were rose-colored. According to XRD studies, the ceramics are composite materials comprised of ZnO microcrystals (hexagonal, wurtzite-type structure, a = 3.251 Å, c = 5.201 Å, size: 10-15 μm) and nanocrystals (cubic, C-type structure, size: ~130 nm) of rare-earth sesquioxides, Er_2O_3 (a = 10.450 Å) and Yb_2O_3 (a = 10.555 Å). The unit-cell parameters of ZnO are independent of the RE^{3+} content indicating that these ions do not enter the zinc oxide. The microstructure of ceramics and their composition were studied by SEM-EDX, Fig. 1(a). The absorption spectra of Yb^{3+} and Er^{3+} ions characteristic for cubic sesquioxide crystals do not change after annealing, Fig. 1(b). The luminescence spectra are sensitive to annealing: (i) the intensity of green and red upconversion luminescence (UCL) of Er^{3+} ions increases for annealed ceramics, Fig. 1(c), and (ii) the shape and intensities of XRIL bands of excitonic and defect nature of ZnO, Fig. 1(d), as well as the XRIL lifetimes change. These changes are in line with the variation of the morphology and defectiveness of ZnO crystals induced by annealing.

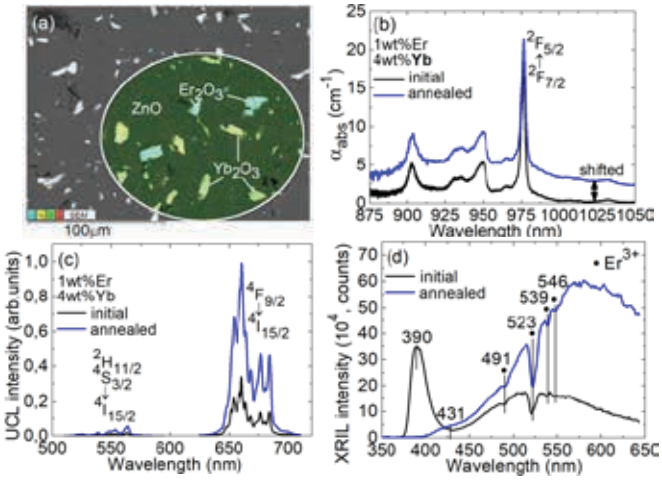

Fig. 1. Composite optical ceramics ZnO-Er_2O_3-Yb_2O_3: (a) a SEM image with EDX element mapping of RE^{3+} ions (1 wt% Er^{3+}, 3 wt% Yb^{3+}); (b-d) 1 wt% Er^{3+}, 4 wt% Yb^{3+}: (b) absorption spectra of Yb^{3+} ions; (c) UCL spectra of Er^{3+} ions, λ_{exc} = 980 nm; (d) XRIL spectra.

III. Conclusion

ZnO-Er_2O_3-Yb_2O_3 ceramics are promising optical materials with tailored emission properties in the visible (ZnO emissions, UCL of Er^{3+} ions) and infrared (Yb^{3+}, Er^{3+} emissions). Further work will focus on revealing the ZnO ↔ RE^{3+} energy transfers.

Acknowledgements

The SEM-EDX study was performed on the equipment of the Engineering Center of Saint-Petersburg State Institute of Technology.

References

[1] E. Gorokhova, *et al.,* "ZnO – Yb_2O_3 composite optical ceramics: Synthesis, structure and spectral-luminescent properties," J. Eur. Ceram. Soc., vol. 42, pp. 616-630, Feb. 2022.

Accurate optical detection of low-concentrated hydrogen halide vapors by $CsPbBr_3$ nanowire laser

D.I.Markina[1], A.P.Pushkarev[1], S.V.Makarov[1]
[1]School of Physics and Engineering, ITMO University, Saint-Petersburg, Russia

Abstract — A novel highly responsive optical sensor of hydrogen halide vapors based on an all-inorganic lead halide perovskite nanowire laser is developed and comprehensively studied. It is shown that a small spectral shift of high-Q lasing modes invoked by chlorine-rich shell formation on the $CsPbBr_3$ nanowire surface in presence of HCl in the atmosphere allows detection of extremely low amounts of hazardous hydrogen halide vapors in the surrounding air.

Keywords — perovskite nanolaser, optical sensing, hydrogen chloride

The rapid development of the chemical industry in recent decades has been accompanied by an increase in the level of chemical safety standards. Substances that are harmful in low concentrations require special attention, such substances include volatile hydrogen halides in particular hydrogen chloride and hydrogen iodide. Despite their toxicity, they are widely used to produce textiles and rubber, employed in electroplating, and different complex synthesis processes. The need to use them calls for the creation of sensors that can provide both low-cost production and ultra-high responsivity. In this sense, lead-halide perovskite nanostructures known for their unique optical properties, such as broad tunability of excitonic emission [1], thermo- and moisture stability [2] and high-quality laser generation at low thresholds [3] are great candidates to be utilized as a sensing platform. In particular perovskite nanowire lasers integrated with the nanostructured substrate are capable to demonstrate a sensitive optical response to small changes in the environment.

Herein, we perform the study of the optical sensor of low-concentrated hydrogen chloride vapor based on perovskite $CsPbBr_3$ nanowire laser on nanostructured alumina substrate. The optical sensing mechanism is relied on the formation of a chlorine-rich shell on the surface of the $CsPbBr_3$ core nanowire structure due to an anion exchange process between the original nanowire and hydrogen chloride vapors that is confirmed by XPS spectroscopy data. A noticeable difference in the refractive indices of the core and shell leads to a hypsochromic spectral shift of high-Q laser modes of the nanowire. Results of optical experiment are supported with accurate numerical modeling of the spectral position of the core-shell cavity eigenmodes. The proposed design (Fig.1) allows the detection of HCl vapor at less than 100 ppm concentrations.

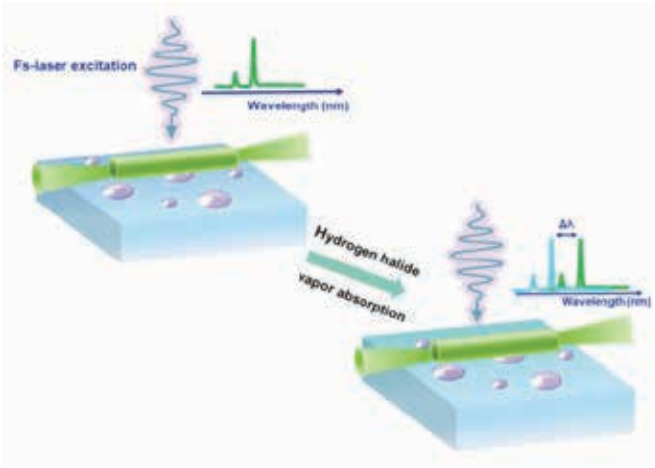

Fig.1. Schematic diagram of a sensing mechanism based on $CsPbBr_3$ NW laser integrated with nanostructured alumina substrate.

ACKNOWLEDGMENT

This work was supported by the Russian Science Foundation, project no. 20-73-10183.

REFERENCES

[1] E.Yu. Tiguntseva, D.G. Baranov, A.P. Pushkarev, B. Munkhbat, F. Komissarenko, M. Franckevicius, A.A. Zakhidov, T. Shegai, Yu.S. Kivshar, S.V. Makarov, "Tunable hybrid Fano resonances in halide perovskite nanoparticles", Nano Letters, vol.18, pp. 5522-5529, 2018.

[2] S. W. Eaton, M. Lai, N.A. Gibson, A.B. Wong, L. Dou, J. Ma, L.-W. Wang, S.R. Leone, P. Yang, "Lasing in robust cesium lead halide perovskite nanowires.", Proc. Natl. Acad. Sci. U. S. A., vol. 113, pp. 1993−1998, 2016.

[3] D.I. Markina A.P. Pushkarev, I.I. Shishkin, F.E. Komissarenko, A.S. Berestennikov, A.S. Pavluchenko, I.P. Smirnova, Irina, L.K. Markov, M. Vengris, A.A. Zakhidov, S.V. Makarov, "Perovskite nanowire lasers on low-refractive-index conductive substrate for high-Q and low-threshold operation", Nanophotonics, vol.9, pp. 3977-3984, 2020.

Optical Nonlocality in Dynamics of Ultrashort Laser Pulses in Hyperbolic Metamaterials

V.B. Novikov, T.V. Murzina
Department of Physics, M. V. Lomonosov Moscow State University, Moscow 119991, Russia
e-mail: vb.novikov@physics.msu.ru

***Abstract*—We reveal theoretically the effects of fast and slow light in transmission of femtosecond laser pulses through a metal nanorod-based hyperbolic metamaterial (HMM) and confirm the decisive role of optical nonlocality of HMMs in the appearance of these phenomena in the spectral vicinity of the epsilon-near-zero regime of HMM. Numerical simulations demonstrate that strong spatial HMMs dispersion leads to the appearance of additional wave accompanying common p-polarized one, and it is the interference of these waves that governs the dynamics of the laser pulses propagating in the HMMs. The obtained results sustain recent experimental investigations of fast and slow light effects in similar structures.**

***Index Terms*—hyperbolic metamaterials, nonlocality, ultrashort laser pulses, slow light, superluminality**

I. Introduction

Hyperbolic metamaterials (HMMs) conquer the realm of photonics due to plephora of the optical effects exhibited by these structures. In particular, pioneering expriments on both superluminal and slow laser pulse propagation in HMMs has been demonstrated recently [1]. Fascinating HMMs properties are achieved due to strong optical anisotropy of these media typically consisted of metal-dielectric multilayers or arrays of metal nanorods in a dielectric matrix, which provide both the hyperbolic dispersion of light in HMMs and epsilon-near-zero (ENZ) regime. The latter corresponds to the case when one of the principal components of effective dielectric tensor of the optical composite is close to zero. It was shown that nonlocality of the HMM optical response can become significant in the spectral vicinity of ENZ [2].

Here we demonstrate theoretically that nonlocality in metal-nanorod based HMMs is responsible for superluminal and slow light effects for femtosecond laser pulses propagating in these metamaterials.

II. Details and results

We investigate the dynamics of ultrashort laser pulses in a HMM slab consisting of the hexagonal array of silver nanorods in anodic alumina. The diameter of nanorods oriented along the normal to the HMM interface was 28 nm, their packing period was 95 nm and the HMM thickness was $L = 1100$ nm. These parameters correspond to the experimental structures used previously for the investigation of the pulse dynamics in HMMs [1].

This optical composite demonstrates the ENZ regime close to the wavelength of 760 nm. Carried out finite element based numerical calculations of the eigenmodes of light in the array of metal-nanorods demonstrate the existence of an additional wave associated with nonlocality of optical response of the HMM, which accompanies the two main waves related to s- and p-polarized light. In the vicinity of the ENZ, the main and additional waves are excited resulting in the interference features in the transmitted light. It is demonstrated at calculated map of the HMM transmittance as a function of the incident wavelength and the angle of incidence (θ) for the p-polarized light [Fig. 1(a)]. As seen besides pronounced decrease of the transmission inherent to the ENZ spectral region, a set of minima appears as a result of the mode interference.

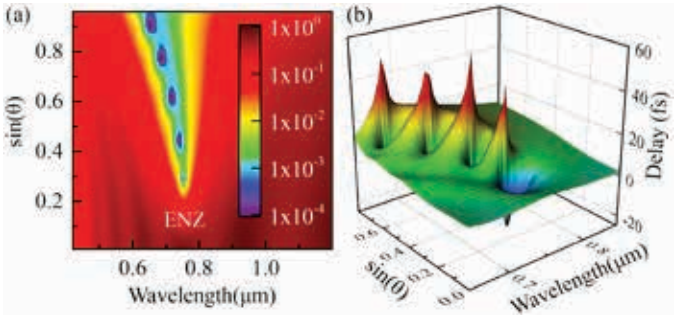

Fig. 1. (a) Transmission spectrum of the HMM for p-polarized light, (b) the pulse delay in the HMM with subtracted delay in the air slab of thickness L.

Simulations of the propagation of 60 fs laser pulses through the HMM carried out by the bind of (i) the transfer matrix method adapted for media supporting the additional waves and of (ii) fast Fourier transform demonstrate pronounced change of the delay of the pulse maximum in the spectral vicinity of the ENZ [Fig. 1(b)]. The HMM exhibits both superluminal pulse advance (negative delay) of about 25 fs and slow light regime with the pulse retardation of about 40 fs. The transition between these dynamical regimes takes place at variation of the angle θ near the transmission dips driven by the optical nonlocality of the HMM. The obtained results are in agreement with the recent experimental results of the investigations of fast and slow light effects in similar structures [1].

References

[1] V. B. Novikov, A. P. Leontiev, K. S. Napolskii, and T. V. Murzina, "Superluminal and slow femtosecond laser pulses in hyperbolic metamaterials in epsilon-near-zero regime," Opt. Lett. vol. 46, p. 2276, 2021.

[2] R. J. Pollard, A. Murphy, W. R. Hendren, P. R. Evans, R. Atkinson, G. A. Wurtz, A. V. Zayats, and V. A. Podolskiy, "Optical Nonlocalities and Additional Waves in Epsilon-Near-Zero Metamaterials," Phys. Rev.Lett. vol. 102, p. 127405, 2009.

Luminescent properties of Er/Lu-codoped transparent lead fluoroborate glass-ceramics

O.B.Petrova, D.A.Butenkov, A.V.Bakaeva, K.I.Runina
Department of Crystals Chemistry and Technology, Mendeleev University of Chemical Technology of Russia (MUCTR), Moscow, Russia
petrova@proriv.ru

***Abstract* — Lead fluoroborate glasses codoped with Er^{3+}/Lu^{3+} - have been synthesized. Glass-ceramics have been made by heat-treatment. In a glass-ceramic the rare-earth ions were located in fluoride crystal nanoparticles distributed in a glass. The changes in structural, mechanical, optical and luminescent properties of the glass-ceramics were revealed in comparison with the initial glasses.**

Keywords* — *fluorescence, nanophotonics, glass-ceramic, fluoride, erbium, lutetium

I. Introduction

Recently, special attention has been paid to halide glass-ceramics (GC) based on glasses from heavy metal compounds [1]. In systems containing PbF_2, the formation of the cubic phase β-PbF_2 is possible, which, when doped with ions of rare earth elements (RE), has outstanding spectral characteristics. However, the orthorhombic phase α-PbF_2 often crystallizes together with β-PbF_2, which adversely affects the optical characteristics of glass-ceramics [2].

Stabilization of β-PbF_2 can be carried out due to the mechanism of heterovalent substitution with trivalent rare earth ions of the divalent lead ion. In this case, one ion does not have *f-f* transitions and plays only the role of a stabilizer of the cubic phase, while the second ion is an optical functional center. This makes it possible to avoid concentration quenching of the luminescence. Successful application of this approach for co-activation of Nd/La [3] and Eu/Gd [4] was previously demonstrated. In this work, the crystallization and luminescence properties of glasses and GCs coactivated with Er/Lu are studied.

II. Experimental Section

Glasses were synthesized in the $66PbF_2$-$30B_2O_3$-$4REF_3$ system, co-activated with ErF_3 and LuF_3 in various ratios, as well as only with erbium or lutetium. Samples weighing 10 g were melted in closed corundum crucibles at a temperature of 1100 °C in air for 0.25–0.3 h. GC was obtained by controlled crystallization of glasses under various temperature and time conditions.

In GC, a significant change in the luminescence spectra is observed in comparison with the initial glass. However, in contrast to the glass-ceramics activated only with Er, in codoped GC, the luminescence intensity in the 1550 nm region increases significantly (Fig.1), and the upconversion luminescence in the visible region is insignificant. This can be explained by the lower Er concentration in the forming cubic crystallites of the $Pb_{1-x-y}Lu_yEr_xF_{2+x+y}$ solid solution. The total concentration of Er+Lu in solid solution crystallites is 20-25 at%.

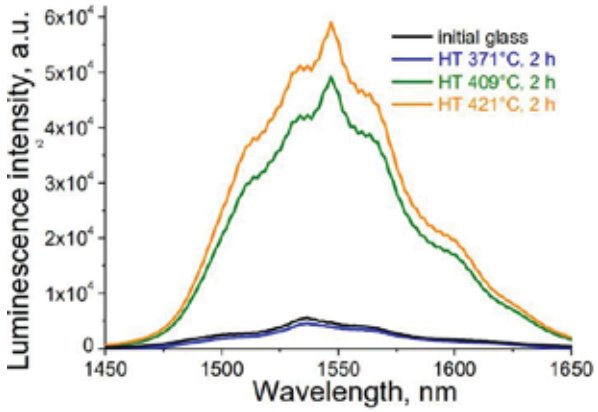

Fig.1. The PL spectra Er^{3+} on the $^4I_{13/2} \rightarrow {}^4I_{15/2}$ transition heat-treatment (HT) and initial glass $66PbF_2$-$30B_2O_3$-$3LuF_3$-$1ErF_3$. λ^{exc} = 973 nm.

Thus, the heterovalent stabilization of the cubic phase based on PbF_2 by codoping Er and Lu in different ratios makes it possible to control the probability of transfer of the excitation energy of the Er^{3+} ion from the $^4I_{11/2}$ level either to $^4I_{13/2}$ or to $^4I_{9/2}$, $^2H_{11/2}$, and $^4S_{3/2}$.

The research was financially supported by the Ministry of Science and Higher Education of the Russian Federation within the FSSM-2020-0003 project

References

[1] M.A. Hughes, T. Suzuki, and Y. Ohishi, "Compositional dependence of the optical properties of bismuth doped lead-aluminum-germanate glass", Optical Materials, vol. 32, № 9, pp. 1028–1034, July 2010.

[2] O. Sanz, E. Haro-Poniatowski, J. Gonzalo, and J. M Fernarndez Navarro, "Influence of the melting conditions of heavy metal oxide glasses containing bismuth oxide on their optical absorption", Journal of Non-Crystalline Solids, vol. 352, pp. 761-768, June 2006.

[3] O.B. Petrova, D.A. Velichkina, M.P. Zykova, A.V. Khomyakov, M.A. Uslamina, K.N. Nischev, A.A. Pynenkov, R.I. Avetisov, I.Ch. Avetissov, "Nd/La, Nd/Lu-co-doped transparent lead fluoroborate glass-ceramics", Journal of Non-Crystalline Solids, vol. 531, pp. 119858-119864, March 2020.

[4] D.A.Velichkina, K.I.Runina, M.P.Zykova, O.B. Petrova, "Transparent Glass-Ceramic Materials Based on Lead Fluoroborate Glasses Co-Activated by Eu/Gd", Glass and Ceramics, vol. 78, № 1-2, pp.14–17, May 2021.

Influence of laser radiation on carbon nanostructures in order to improve their electrophysical characteristics

A.V. Kuksin[1], Y.P. Shaman[2], E.P. Kitsyuk[2], O.E. Glukhova[3,4], A.Yu. Gerasimenko[1,3]
[1]Institute of Biomedical Systems, National Research University of Electronic Technology, MIET, Zelenograd, Russia
[2]Scientific-Manufacturing Complex "Technological Centre", Zelenograd, Russia
[3]Institute for Bionic Technologies and Engineering, I.M. Sechenov First Moscow State Medical University, Moscow, Russia
[4]Department of Physics, Saratov State University, SGU, Saratov, Russia

Abstract— This paper presents a method for creating electrically conductive nanostructures from carbon nanotubes (CNT) and reduced graphene oxide (rGO) on a Si substrate by laser irradiation and a method for structuring vertical CNT arrays. Electrically conductive CNT/rGO network was obtained under the action of pulsed laser radiation. Also, laser radiation in combination with the chemical BaO treatment led to the structuring of a vertically grown CNT array with improved emission characteristics.

Keywords— carbon nanotubes, graphene oxide, laser radiation, electrical conductivity, electron emission

I. Introduction

Currently, the number of areas using carbon modifications such as carbon nanotubes (CNT) and graphene is actively growing. CNT have high electrical conductivity, mechanical strength and thermal conductivity and are used for creation of energy storage devices, optical limiters [1]. Graphene has no less unique characteristics and is used to create capacitors, aerogels, sensors. Nanostructures based on CNT and graphene can combine the unique properties of these nanomaterials and will find application in micro- and nanoelectronics, bioelectronics, and flexible electronics [2]. CNT have a low work function, which makes it possible to use CNT arrays as efficient field emission sources [3].

II. Materials and Methods

Dispersion of multi-walled carbon nanotubes (MWCNT) and reduced graphene oxide (rGO) with concentrations 0.05/0.05 mg/ml in the bio-surfactant sodium cholate hydrate solvent was prepared and deposited by sputtering method onto a Si substrate. Pulsed Nd:YAG laser (λ=266 nm, pulse duration 100 ns, frequency 30 kHz, energy density 0.5 J/cm^2), was used to influence the CNT/rGO film in the Ar medium.

Vertical MWCNT array was synthesized by the plasma enhanced chemical vapor deposition from the gas phase method using the Oxford PlasmaLab System 100 setup in an H_2+He gas medium. The array height was ~8 μm. Then, the array was uniformly coated with a $Ba(NO_3)_2$ solution followed by annealing at 800°C for 15 minutes. Laser structuring was performed using a pulsed Yb laser (λ=1064 nm, pulse duration 100 ns, frequency 30 kHz, energy density 1.5 J/cm^2).

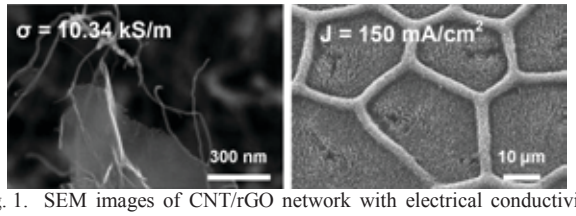

Fig. 1. SEM images of CNT/rGO network with electrical conductivity 10.34 kS/m (left) and structured CNT array with emission current density 150 mA/cm^2 (right)

III. Results and Discussion

As a result of high-intensity laser treatment, the effect of CNT nanowelding with graphene sheets was achieved. Figure 1 shows an rGO sheet with CNT welded to it. Electrical conductivity of resulting CNT/rGO film after laser treatment was increased by 1.8 times compared to the initial film.

It has been determined that chemical BaO and laser treatment of vertically grown CNT array leads to an improvement in its emission characteristics. Figure 1 shows the general morphology of the array after structuring. The emission current density increased by 2.3 times compared to the as-grown array.

Acknowledgment

This work was supported by grants of the Russian Science Foundation No. 21-19-00226 and the Ministry of Science and Higher Education of the Russian Federation No. 075-03-2020-216 from 27.12.2019.

References

[1] S.A. Tereshchenko, V.M. Podgaetskii, A.Yu. Gerasimenko, M.S. Savel'ev, "Threshold effect under nonlinear limitation of the intensity of high-power light," Quantum Elec., vol. 45, pp. 315-320, 2015.

[2] A.Y. Gerasimenko, A.V. Kuksin, Y.P. Shaman, E.P. Kitsyuk, Y.O. Fedorova, A.V. Sysa, A.A. Pavlov, O.E. Glukhova, "Electrically Conductive Networks from Hybrids of Carbon Nanotubes and Graphene Created by Laser Radiation," Nanomaterials, vol. 11(8), pp. 1875, 2021.

[3] A.Yu. Gerasimenko, E.P. Kitsyuk, A.V. Kuksin, R.M. Ryazanov, A.I. Savitskiy, M.S. Saveliev, A.A. Pavlov, "Influence of laser structuring and barium nitrate treatment on morphology and electrophysical characteristics of vertically aligned carbon nanotube arrays," Diam. Relat. Mater., vol. 96, pp. 104-111, 2019.

Optical characterization of CdTe/CdMgTe quantum well structure containing ultrathin manganese layers at interfaces

V.F. Agekyan[1], N.G Filosofov[1], G. Karczewski[2], A.Yu. Serov[1], and I.V. Shtrom[1]

[1] St.-Petersburg University, Universitetskaya nab. 7/9, St. Petersburg, 199034 Russia

[2] Institute of Physics, Polish Academy of Science, Ał. Lotnikov 32/46,Warsaw, 02-668 Poland

Abstract — The aim of this work was to grow and study the optical properties of heterostructures with ultrathin inclusions at interfaces, which improve the quality of interfaces.

Keywords — Exciton, cadmium telluride, quantum well

I. Introduction

Heterostructures containing four CdTe quantum wells (QWs) 4, 8, 16, and 32 monolayers (ML) thick, separated by CdMgTe barriers 62 ML thick were grown by MBE. Manganese layers 1 ML thick (sample #1) and 2 ML thick (sample #2) were formed at the interfaces.

II. Results

The optical studies reveal the higher quality of sample #2 in the following parameters:

– the emission of free excitons is observed in sample #2 at T = 5 K, while in sample #1 only the emission of localized excitons is observed at low temperatures;

– exciton resonances in the luminescence spectrum of sample #2 have a smaller width;

– exciton radiation from the sample #2 QWs is more resistant to the sample heating;

– the exciton resonances of the QW are more pronounced in the reflection spectrum of sample #2.

The study of the luminescence excitation spectra of QW excitons in samples #1 and #2 made it possible to study the following questions:

– efficiency of the energy transfer from CdMgTe barrier layers to CdTe QWs of different thicknesses through the exciton mechanism and through free carriers;

– transfer of excitons and free carriers between CdTe QWs of different thicknesses and its temperature dependence.

Samples #1 and #2 show the paramagnetic properties due to a vertical diffusion of manganese atoms [1, 2].

Comparison of the properties of samples #1 and #2 with the properties of similar nanostructures shows that the formation of additional ultrathin layers at the interfaces can improve the quality of nanostructures.

Authors gratefully acknowledge financial support of St.Petersburg State University research grant No. 75746688

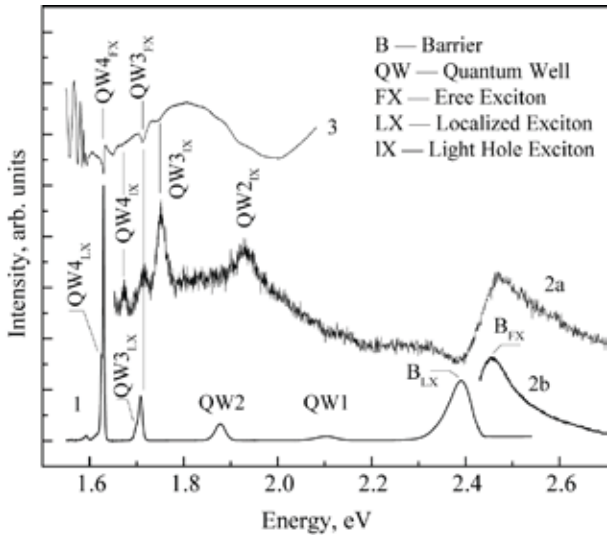

Fig. 1. Sample #2. Photoluminescence spectrum — 1; QW4 free exciton photoluminescence excitation spectrum— 2a; barrier localized exciton photoluminescence excitation spectrum — 2b, reflectance spectrum — 3. T = 5 K

Acknowledgments

Authors gratefully acknowledge financial support of St. Petersburg State University research grant No. 75746688.

References

[1] G. Prechtl, W. Heiss, S. Mackowski, A. Bonanni, G. Karczewski, H. Sitter, and W. Jantsch, Semicond. Sci. Technol. vol. 15, pp. 506–510, 2000.

[2] V. Agekyan, P. Holz, G. Karczewski, V. Katz, E. Moskalenko, A. Serov, and N. Filosofov, Semiconductors, vol. 45, pp. 1301–1305, 2011.

Synthesis, crystallization and luminescent properties of lead chlorosilicate glasses and glass-ceramics Nd-doped

D.A.Butenkov, K.I.Runina, A.M.Slastuhina, O.B.Petrova
The Department of Chemistry and Technology of Crystals, D. Mendeleev University of Chemical Technology, MUCTR, Moscow, Russia
dabutenkov@gmail.com

Abstract — Nd-doped lead oxochloride silicate glasses were synthesized and their spectral characteristics were studied. Glass-ceramics, including those with lead chloride phase, were obtained using heat treatments. The influence of controlled crystallization on the spectral-luminescent properties of glasses has been investigated.

Keywords — oxochloride glasses, lead chloride, neodymium, luminescence, glass-ceramics

I. Introduction

Silicate glasses containing $PbCl_2$ are known as solid electrolytes [1]. However, there is no information in the literature on the doping of such systems by RE and their study as matrices for applications in photonics. Crystalline lead chloride has a short phonon spectrum (phonon energy 230 cm^{-1}), an extended transparency range and the ability to generate luminescence in spectral regions in which it is impossible in oxide and oxofluoride systems [2-4]. The preparation of glass-ceramics with $PbCl_2$ crystalline phase activated by Nd^{3+} ions is an urgent task, since such a material is of great interest for IR device technologies.

II. Experimental Section

To synthesize oxohalide glasses, we used $PbCl_2$, PbO, SiO_2, and NdF_3 commercial preparations with chemical purity not less than 99.99 wt%. The synthesis was carried out for 15 min at 1100 °C in closed corundum crucibles, the melt was poured into a brass mold at room temperature and covered with a steel plate. High-quality glasses were obtained with nominal lead chloride content of 10 to 60 mol%. Spectral studies were carried out at room temperature. Absorption spectra werer measured using a UNICO 2800 instrument (UV/VIS), photoluminescence (PL) spectra were measured by a QE65000 spectrometer (Ocean Optics). Based on the DSC data (STD Q600, TA Instruments), the initial glasses were heat treated. The formed crystalline phases were identified by XRD analysis using an Equinox 2000 diffractometer (Inel).

The absorption spectra of Nd-doped glasses have all absorption bands specific for the Nd^{3+} ion. The short-wavelength cut lies in the 355-380 nm range. The optical band gap decreases while SiO_2 content in the glass composition reduces.

The research was financially supported by the Ministry of Science and Higher Education of the Russian Federation within the FSSM-2020-0005 project.

There are several crystallization peaks in the glass derivatograms. According to XRD data, $Pb_5O_2Cl_2$ phase is released in all cases, while in the samples with $PbCl_2$ content more than 40 mol%, the lead chloride phase predominates. The PL spectrum of the heat-treated sample (Fig. 1) exhibits a significant narrowing of the spectral line and a shift of the λ_{PL}^{max} to longer wavelengths in comparison with the original glass.

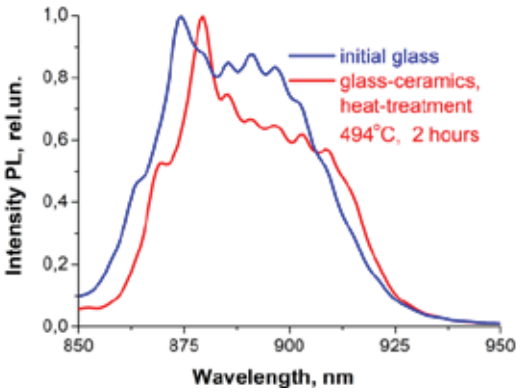

Fig. 1. The PL spectra Nd^{3+} on the $^4F_{3/2} \rightarrow {}^4I_{9/2}$ transition heat-treatment and initial glass $50PbCl_2–25PbO – 24SiO_2–1NdF_3$. λ^{exc} = 785 nm.

This changes indicate a change in the environment of Nd^{3+} ions from oxide to chloride, which is promising for generating luminescence in the mid-IR range.

References

[1] I. A. Sokolov, I. V. Murin, H. D. Wiemhiifer, and A. A. Pronkin, “The Nature of Current Carriers and Electric Conductivity in the $PbCl_2$-$2PbO*SiO_2$ Glasses”, Glass Physics and Chemistry, vol. 26, No. 2, pp. 148-157, January 2000.

[2] T.T. Basiev, Yu.K. Danileiko, L.N. Dmitruk, B.I. Galagan, L.V. Moiseeva, V.V. Osiko, E.E. Sviridova, N.N. Vinogradova, “The purification, crystal growth, and spectral-luminescent properties of $PbCl_2$:RE”, Optical Materials, vol. 25, pp. 295–299, April 2004.

[3] E. Brown, U. Hömmerich, A. G. Bluiett, S. B. Trivedi, and J. M. Zavada “Synthesis and spectroscopic properties of neodymium doped lead chloride” Journal of Applied Physics, vol. 101, pp. 113103, June 2007.

[4] D.A.Butenkov, K.I.Runina, O.B. Petrova, “Synthesis and Properties of Nd-doped Chlorofluorosilicate Lead Glasses”, Glass and Ceramics, vol. 78, № 1-2. pp. 135–139, July 2021.

Phase and Chemical Transformations Kinetics in the Synthesis of a $BaO-B_2O_3-Bi_2O_3 - (Y_{1-x}Er_x)_3Al_5O_{12}$ Functional Glass-Ceramics

A.D. Plekhovich, A.M. Kut'in, E.E. Rostokina, M.E. Komshina, K.V. Balueva, K.F. Ignatova
G.G. Devyatykh Institute of Chemistry of High Purity Substances of RAS, 49 Tropinina Str., Nizhny Novgorod, Russia

Abstract— The kinetics chemical and phase transformations in the interaction of the glass-forming system $BaO-B_2O_3-Bi_2O_3$ with $(Y_{1-x}Er_x)_3Al_5O_{12}$ in the glass-ceramics formation process were studied by DSC. The samples were characterized by powder X-ray diffraction and scanning electron microscope methods. The presence of devitrification according to DSC data proves that the samples synthesized in the temperature range 800-1300ºC are glass-ceramic materials.

Keywords— glass-ceramics, Er:YAG, crystallization.

I. Introduction

Nonlinear-optical glass-ceramics with transition metal ions are in demand in frequency converters of IR/UV radiation into visible, and also find wide application in personal dosimetry and as laser media. Note that the size of crystals and their volume fraction affect the spectral luminescent and other properties of glass-ceramic materials. The main attention in this work is directed to the study of the kinetic aspects of crystallization, which are directly related to the formed crystalline phase size.

The purpose of the work: to study chemical and phase transformations to detail the conditions for obtaining a new functional glass-ceramic material based on $BaO-B_2O_3-Bi_2O_3$ and $(Y_{1-x}Er_x)_3Al_5O_{12}$.

II. Results and Discussion

Fig.1 shows thermograms of a series of synthesized samples (Fig. 2), on which glass transition is noted, which clearly indicates the presence of a glass phase. According to XPA data, the samples contain the garnet phase along with the most thermodynamically favorable yttrium and erbium borates phases. For the sample synthesized at a temperature of 800 °C, the decreasing section on the thermogram after a temperature of 700 °C indicates the "formation" of the garnet phase and its modification with borates.

The thermogram (Fig. 3) shows the synthesis result of a glass-ceramic sample from a dispersed mixture of glass $20Bi_2O_3–65B_2O_3-15BaO$ and $(Y_{0.5}Er_{0.5})_3Al_5O_{12}$, which takes place under nonisothermal conditions in DSC instrument. The glass transition temperature (T_g = 463.3 °C) practically corresponds to the original glass. The deepest peaks at temperatures lower than 900 °C and 1080 °C refer to the previously studied [1,2] process of Er:YAG formation.

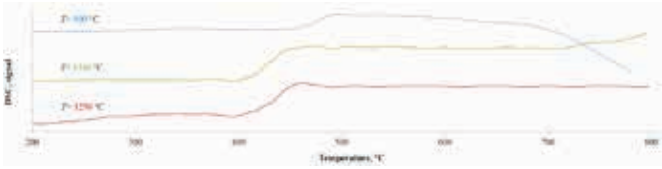

Fig. 1. Thermograms of samples synthesized at temperatures of 800, 1100, 1250 °C at a heating rate of 10 °C/min.

Fig. 2. Translucent samples of glass-ceramics after annealing at temperatures of 800, 1100, 1250 °C for 30 min.

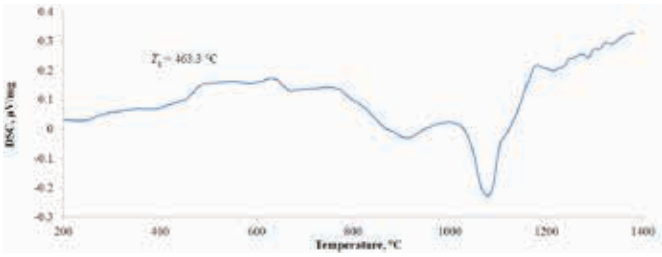

Fig.3. Thermogram of non-isothermal synthesis of glass-ceramics.

References

[1] A.M. Kutyin, E.Ye. Rostokina, E.M. Gavrishchuk, V.V. Drobotenko, A.D. Plekhovich, P.A. Yunin Kinetics and formation mechanism of yttrium aluminum garnet from an amorphous phase prepared by the sol–gel method, Ceramics International, Vol. 41, Part A, pp. 10616-10623, 2015.

[2] E.Ye. Rostokina, A.D. Plekhovich, A.M. Kut'in, I.F. Georgiu, S.S. Balabanov, M.E. Komshina Kinetic effects of substitution Er^{3+} for Y^{3+} in $(Y_{1-x}Er_x)_3Al_5O_{12}$ garnet Journal of the European Ceramic Society, Volume 41, Issue 10, pp. 5324-5330, 2021.

This work was supported by the Russian Science Foundation (project No. 20-73-10110)

Sensitivity of random array of gold nano islands for biosensing applications

J. P. Cuanalo-Fernández[1], J.A. Urrutia-Anguiano[2], S.F. Guerra-Hernández[1], N. Korneev[1], M.B. De-la-Mora-Mojica[3], A. Reyes-Coronado[2], I. Cosme-Bolaños[1], S. Mansurova[1] and R. Ramos-García[1],

[1]Dep. Óptica, INAOE, Puebla, México.
[2]Dep. Física, Facultad de Ciencias, UNAM, Ciudad de México, México.
[3]Dep. micro y nanotecnologías, Instituto de Ciencias Aplicadas y Tecnología, UNAM, Ciudad de México, México.

Abstract This work presents the results of experimental and theoretical study of the sensing characteristics of disordered arrays of gold nanoisland (Au NI) on top of glass substrate. The influence of the Au NI array parameters (average NI size and fill factor) on bulk refractive index sensitivity was analyzed.

Keywords— Localized Surface Plasmonic Resonance; gold nano-island, biosensor.

I. Introduction

Localized surface plasmon resonance (LSPR) is an ideal candidate for real-time label-free sensing applications of small biomolecules. Recently, a sensing method based on LSPR induced in a self assembly monolayer (SAM) of Au NI by evanescent wave in attenuated total internal reflection (ATR) configuration has been reported showing the possibility of highly sensitive detection of SARS-CoV-2 genetic material [1]. The method uses phase interrogation mode, where LSPR differential phase between s and p polarization component is measured directly using spectral interferometer (SI) based detection scheme. Despite promising results, the properties of such a sensor are still largely unexplored, preventing rational design and optimization of sensor's performance characteristics. One of the main issues is that for LSPR (unlike SPR) both s and p polarization components contribute to the observed differential phase response. In addition, resonance characteristics (e.g. resonance position or differential phase shift) are nonlinear function of refractive index and its response strongly depends on the characteristics of metasurface (such as NI average radius, fill factor, etc).

This work presents the results of experimental and theoretical study of the plasmonic response of disordered arrays of Au NI with varying arrays characteristics (average NI size and fill factor). The influence of the metasurface´s characteristics on bulk refractive index sensitivity of SAM AuNI was analyzed.

II. Results

SAM AuNI were fabricated by depositing a thin film of gold (5 -13 nm) on a low-cost corning glass, followed by thermal annealing at high temperature (~ 550°C) for three hours. The experimental set up used to study the plasmonic response of the obtained nanostructure is based on a common path interferometer in the ATR configuration. It has been shown, that plasmonic response of SAM AuNI and relative contribution of s and p polarization components critically depends on the diameter of the nanoparticles and the fill factor. In order to quantify the sensing characteristics of SAM AuNI the sensitivity defined as $S = \frac{\Delta\lambda}{\Delta n}$, was measured.

It was found that, unlike SPR, the dependence of resonance position on variations of the refractive index in the vicinity of nanoparticles is highly nonlinear, may present the change of the sign and its shape vary strongly with the angle of incidence upon the substrate. In addition, it was shown, that the characteristics of the SAM AuNI should be chosen carefully, since for certain combination of the parameters s and p phase contribution can cancel each other. This behavior qualitatively agrees with the results of theoretical model describing plasmonic response in the similar system using Coherent Scattering Model formalism [2].

III. Conclusions

Influence of array characteristics on bulk refractive index sensitivity of SAM AuNI has been studied both theoretically and experimentally. The results of this study can provide guidance in choosing right transducer characteristics for bioanalytical tasks.

References

[1] G. Qiu et al., ACS Nano, 14 (5), pp. 5268-5277, 2020.
[2] A. Reyes-Coronado et al., Optics Express, 9594:6697-6706, 2018

Photostimulation of thin C-Au films

A. Lelekova[1], V.Samyshkin [1,2], A. Osipov [1], S. Kutrovskaya [1,3,4], A. Kucherik[1]

[1] Department of Physics and Applied Mathematics, Stoletov Vladimir State University, 600000 Gorkii street, Vladimir, Russia
[2] Institute of Chemistry, St. Petersburg State University,198504, Ulianovskaya str. 5, St. Petersburg, Russia
[3] School of Science, Westlake University, 18 Shilongshan Road, Hangzhou 310024, China
[4] Institute of Natural Sciences, Westlake Institute for Advanced Study, 18 Shilongshan Road, Hangzhou 310024, China

Abstract— Studies have conducted on the stimulating effect of laser radiation on the hybrid thin-film gold-carbon system. Gold nanoparticles stabilized by a porous carbon matrix demonstrate a stable response at frequencies close to plasmon resonance.

Keywords— hybrid thin-film, gold nanoparticle, carbon

We to study the electrophysical properties of the deposited film on a substrate. In research employed a setup based on the Ntegra Aura device operating in the tunneling mode. The research films were obtained from the C-Au colloidal system by spraying in atmospheric air with deposition on a substrate [1]. The experimental scheme of photostimulation of the hybrid film has shown in Fig. 1.

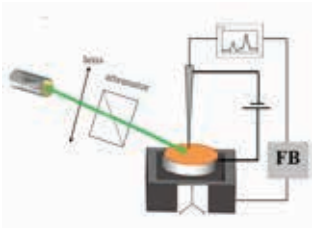

Fig. 1. The experimental scheme of photostimulation of the hybrid film

The focused laser beam has been directed at a thin Au-C film with a wavelength in the range of 500-570 nm because only at these wavelengths possible to excite surface plasmon resonance in Au nanoparticles. The measured current-voltage curves have shown in Fig. 2a

The thickness of the film was enough to neglect the substrate contribution to the collecting data of the tunneling current. It demonstrates a nearly linear behavior in the selected voltage range from -1 to 1 V (see the black curve in Fig.2a) The I/V curve for a thing hybrid C-Au film looks similar to also linear. However, the value of the locking voltage increased significantly and reached 0.27 V (see the red curve in Fig.2a). We detected a significant increase in the tunneling current in the case of the laser illumination of the tunneling probe area (see the blue curve in Fig.2a). The observed current amplification was caused by the increase of the free charge carrier concentration due to the resonant absorption of the laser radiation of the 532 nm wavelength by gold nanoparticles.

The resistance of various points on the hybrid film was estimated from a sample of measured data (fig. 3). Based on these data, the behavior of electronic conductivity in the mode of electronic photostimulation is analyzed. The evaluation of the resistance of the Au-C thin film showed that with an increase in the laser radiation power, the conductivity of the hybrid film changes proportionally.

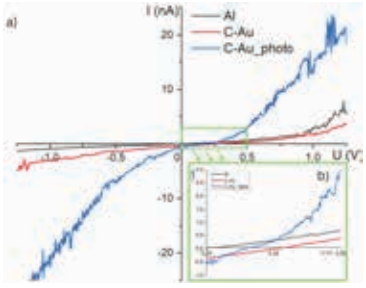

Fig. 2. The tunneling current as a function of the voltage applied to the deposited free-standing C-Au films: a) The current-voltage curves measured at various samples: the black line corresponds to the I/U curve of a pure aluminum substrate, the red curve corresponds to the C-Au thin film and the blue curve shows the I/U dependence of the C-Au thin film subjected to the excitation at the wavelength of 532 nm. b) The inset presents the behavior of the tunneling at a low applied voltage level

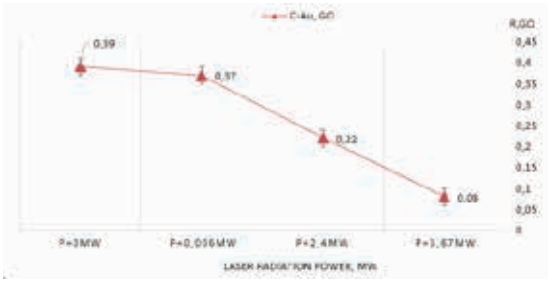

Fig. 3. A resistance diagram behavior of the Au-C thin-film on laser excitation power

ACKNOWLEDGMENT

The study was carried out using the equipment of the interregional multispecialty and interdisciplinary center for the collective usage of promising and competitive technologies in the areas of development and application in industry/mechanical engineering of domestic achievements in the field of nanotechnology (Agreement No. 075-15-2021-692 of August 5, 2021).

The paper was prepared within the framework of the state task of VlSU № 0635-2020-0013. This work was also partially supported by RFBR grants 20-21-00038 and by the Grant of the President of the Russian Federation for state support of young Russian scientists No. MK-5318.2021.1.2

REFERENCES

[1] Kucherik, A.O., Arakelyan, S.M., Vartanyan, T.A., Laser-induced synthesis of metal–carbon materials for implementing surface-enhanced Raman scattering, Opt. Spectrosc, (2016)

Nanostructure assisted laser desorption of Au+/Au- ions from gold surface below plasma threshold

I.I. Kuzmin[1], P.K. Laptinskaya[2], S.M. Nikiforov[2], A.V. Pento[2], Ya.O. Simanovsky[2]
[1]V.I. Vernadsky Institute of Geochemistry and Analytical Chemistry, Russian Academy of Sciences, Moscow, Russia
[2]Prokhorov General Physics Institute of the Russian Academy of Sciences, Moscow, Russia

Abstract - The process of Au+ and Au- ions formation on a surface of nanostructured gold plate under pulsed laser irradiation with energy density below plasma threshold is studied. The role of nanoscale objects produced on the surface under laser irradiation higher than the plasma threshold in the ion formation process is discussed.

Keywords - Laser desorption, laser mass spectrometry, nanoparticles.

The main mechanism leading to the appearance of a flux of ions of the target material when exposed to high-power laser radiation is the formation of plasma at the target surface. At the same time, it is known [1] that the target metal ions begin to be registered at the laser radiation power density that is lower than the plasma threshold value when the plasma radiation occurs and fast increasing of fluorescence emitted from neutral atoms and ions of the target metal is observed. It is also known that high power pulsed laser radiation produces structures on the metal surface of the wide range of sizes [2].

A gold plate 3x3x0.5 mm in size was installed inside the vacuum chamber of a linear time-of-flight mass spectrometer. The third harmonic radiation (355 nm) of a diode pumped solid state Nd: YAG laser (pulse duration of 0.37 ns, maximum pulse energy of 40 uJ, and repetition rate of 174 Hz) was focused on the surface of the plate by a lens with a focal length of 30 cm. To increase the area of the exposed surface, a two-mirror scanner was installed in the optical path, providing scanning motion of the focal spot over the surface within a rectangle of 0.4 x 0.45 mm. The surface was preprocessed using exposure to the same laser radiation with energy density elevated 1.5 times higher than plasma threshold which led to nanostructuring of the surface. The ion yield measurements were preceded with such preprocessing for each value of the laser energy.

It has been shown that the dependences of ion yield on the laser energy density are the same both for Au^+ and Au^- ions and Au_n clusters and can be approximated by the power function $N \sim F^9$. The ion formation threshold (~1 ion per 10 laser pulses) is at least 5 times lower than the plasma threshold. The ion formation threshold for the gold surface region that has not been processed before, is at least 2 times higher (see fig.). The ion signal decreases gradually for an order of magnitude after the same surface area is being exposed to approximately 10 successive laser pulses (see fig.).

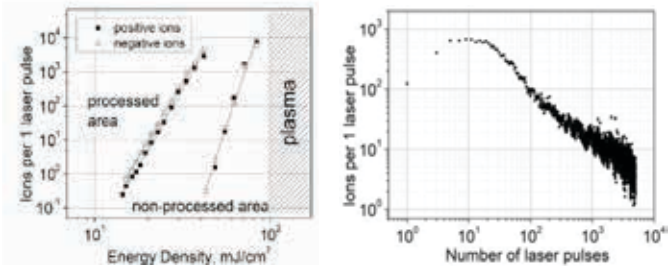

Fig. 1. Left - the dependence of the ion yield from the gold plate under pulsed laser exposure at the wavelength 355 nm. Right - the dependence of the ion yield from the processed gold plate on the number of laser pulses (positive ions, energy density 17 mJ/cm^2)

Nanostructuring of the surface changes its reflectivity, heat conductivity, melting temperature and vapor pressure thus governs the process of ion formation. Long term laser processing with the energy density below the plasma threshold leads to the change of the surface structure size distribution and decreases the ion yield. The effect of ion formation at low power densities can be caused by plasmon resonance, Coulomb explosion or multiphoton excitation and ionization of quantum dots.

ACKNOWLEDGMENT

This work was supported by the Russian Federation Ministry of Science and Higher Education grant No. 075-15-2020-912 for the creation and development of World-class research centers.

REFERENCES

[1] Usmanov, D., et al. Int. J. of Mass Spectrom. 2013, V. 341, pp. 45-51
[2] Zavedeev, E.V., et al 2006 Quantum Electron. 2006, V. 36, p. 978

The excitation modes of porous silicon microcavities with an embedded conjugated polymer for detecting vapors of nitroaromatic compounds

T. A. Kharinoeva, O. K. Malyshev, I. L. Martynov, A. A. Chistyakov
National Research Nuclear University MEPhI, Moscow, Russia

Abstract — Currently, fluorescent sensors for detection of explosives are being actively developed. One of the important issues, along with the sensitivity and speed of analysis, is the stability of the fluorescence of a sensitive luminophore, and the natural degradation of its fluorescence under the action of exciting radiation. In this work, we study the fluorescence response of MDMO-PPV embedded in a porous silicon microcavity to trinitrotoluene vapors under the action of exciting radiation with different intensities and wavelength of 450 nm. The conclusion is made about the preferred mode of the luminophore excitation.

Keywords— porous silicon, microcavity, fluorescent sensors

I. Introduction

Currently, a fluorescent method for detecting explosives is being actively developed [1]. To improve the efficiency of fluorescence collection and increase the effective surface area of the sensor, the sensitive luminophore can be embedded in porous matrix with properties of photonic crystals, for example in porous silicon (por-Si) microcavity (MC) [2]. In this work, we investigate the fluorescence of sensitive polymer poly[2-methoxy-5-(3′,7′-dimethyloctyloxy)-1,4-phenylenevinylene] (MDMO-PPV) into por-Si MC under different intensities of exciting radiation. Trinitrotoluene (TNT) vapors were used as target quenching agent.

II. Experimental

The standard electrochemical anodizing of monocrystalline silicon wafer in water-alcohol solution of fluoric acid ($HF:C_2H_5OH$ – 3:7) was used to fabricate por-Si MCs. Silicon p-type wafers doped with boron with orientation (100) and resistivity of 0.003-0.005 Ω·cm were used for etching. The MCs consisted of two Bragg mirrors and a cavity layer. The Bragg mirrors were formed by alternation of layers with high and low porosity with typical pore size about 7 and 30 nm respectively. After fabrication, the MCs were thermally oxidized at a temperature of 700 °C. The embedding of MDMO-PPV into por-Si MCs was made from a solution in toluene with concentration of 0.5 mg/ml at an excess pressure of 3 atm [3]. The reflection and fluorescence spectra of fabricated samples were measured by Ocean Optics USB2000+ spectrometer. The laser diode (LD) with a wavelength of 450 nm was used for fluorescence excitation. The concentration of TNT vapors was in range about 0.1-0.5 of the saturated vapor pressure.

III. Results

The fluorescence spectra of the fabricated samples had a narrow peak with FWHM ~ 7 nm corresponding to the eigenmode of por-Si MC. Their fluorescence demonstrated natural photodegradation, which accelerated with an increase in the intensity of the exciting radiation (I_{ex}). The presence of trinitrotoluene molecules in the environment led to an additional significant fluorescence quenching of the samples. The rate of this quenching was weakly dependent on the I_{ex}. At a higher value excitation intensity the signal-to-noise ratio improved and the fluorescence response to the presence of TNT vapor accelerated, which is associated with an increase in the average number of the MDMO-PPV molecules in the excited state. At the same time, at I_{ex} higher than ~ 5 W/cm^2, the rate of natural photodegradation of MDMO-PPV into por-Si MC exceeded the fluorescence quenching rate under the action of TNT vapors. It is expected that at lower TNT vapor concentrations, proportionally lower I_{ex} should be used. Thus, for applications of the fabricated structures for detecting vapors of nitroaromatic compounds at vapor concentration in range ~10^{-14} g/cm^3 the intensity of exciting radiation in continuous mode should be < 5 W/cm^2. As an alternative, a pulsed mode of excitation and fluorescence registration can be considered.

IV. conclusion

The fluorescence structures based on por-Si MC with embedded MDMO-PPV, which is sensitive to vapors of nitroaromatic compounds, have been fabricated. The quenching of their fluorescence under the action of TNT vapors at different intensities of exciting radiation has been investigated. The data obtained can be used in the development of fluorescent sensors of explosives.

References

[1] X. Sun, Y. Wang and Y. Lei, “Fluorescence based explosive detection: from mechanisms to sensory materials,” Chem. Soc. Rev, vol, 44, pp. 8019–8061, September 2015.

[2] I. A. Levitsky, W. B. Euler, N. Tokranova and A. Rose, “Fluorescent polymer-porous silicon microcavity devices for explosive detection,” Appl. Phys. Lett., vol. 90, 041904, January 2007.

[3] E. V. Osipov, I. L. Martynov, M. N. Kur’yanova and A. A. Chistyakov, “The embedment of conjugated MDMO−PPV polymer in microcavities of porous silicon at excess pressure from solution,” Tech. Phys. Lett., vol. 44, pp. 392–394, June 2018.

Anion Exchange in Yb-Doped All-Inorganic Perovskite NCs

A.S. Sokolova[1], D.A. Tatarinov[1], S.A. Cherevkov[1], A.P. Litvin[1]
[1] Laboratory 'Optics of Quantum Nanostructures', ITMO University, Saint Petersburg, Russia

Abstract - Perovskite nanocrystals have demonstrated an excellent possibility of tuning their optical properties in the visible and near-infrared ranges (NIR). At present, Yb-doped perovskites $CsPbCl_3$ are popular optical nanomaterials for the development of the next-generation electronic devices due to the sharp electronic transition of ytterbium in the NIR. Here, we have developed anion exchange procedures with usage of different chemical compounds and studied optical properties in visible and near-infrared ranges of obtained nanocrystals.

Keywords— perovskite nanocrystals; anion exchange; ytterbium; lanthanide; near-infrared emission

I. Introduction

Perovskite nanocrystals (NCs) have gained a great deal of attention as the next-generation fluorophores for medicine, photovoltaic devices, and optical sensors. Photoluminescence (PL) of metal halide perovskite nanocrystals can be easily tuned in the visible range by anion exchange. For this purpose, a wide range of halide molecules can be applied, both organic (e.g. OlAmX, where X = Cl, Br, I) and inorganic (e.g. lead halide salts) [1]. However, due to the high surface activity of the mentioned compounds, the anion exchange can lead to the better surface passivation as well as to the degradation of the ionic structure of perovskite nanocrystals [2]. Therefore, this work aimed to investigate the influence of different Br sources on the optical properties of anion-exchanged $CsPb(Cl/Br)_3$ and $CsPb(Cl/Br)_3$:Yb^{3+} perovskites.

II. Results

Undoped and ytterbium-doped perovskite nanocrystals $CsPbCl_3$ were synthesized as previously reported [3]. The obtained nanocrystals were investigated with absorption and photoluminescence spectroscopy in the visible and near-infrared ranges. Both samples possessed a PL signal at 407 nm that corresponds to the transitions of perovskite structure while $CsPbCl_3$:Yb^{3+} NCs have more intensive NIR luminescence at 990 nm. For further anion exchange, the nanocrystal solutions with the absorbance of 0.1 at 375 nm were prepared. Afterwards, a certain amount of Br source was added. As a Br source, the following chemical compounds were used: hydrobromic acid (HBr), tetraoctylammonium bromide (TOAB), bromotrimethylsilane (TMS-Br) and didodecyldimethylammonium bromide (DDAB).

As a basic experiment, an excess amount of HBr (38% aqueous solution) was added to the $CsPbCl_3$:Yb^{3+} NCs in toluene. Prepared nanocrystals showed two PL signals at 510 and 990 nm. The intensity of the PL signal in the visible range increased, while the PL QY in NIR decreased from 52% to 14%. Moreover, the next day the photoluminescence signal in the near-infrared range was not observed. This can be explained by the high water-affinity of ytterbium and, hence, its diffusion from nanocrystals. Due to this observation, other organo-bromide molecules were investigated.

TMS-Br is a popular bromide source that is usually used in perovskite synthesis. In contrast to HBr, anion exchange reaction with TMS-Br proceeded overnight with continuous stirring. Obtained nanocrystals showed the same two PL peaks at 510 and 990 nm as in the first experiment. Nevertheless, the PL QY in the NIR drastically reduced to 0.8%. For better understanding of the anion exchange with TMS-Br, photoluminescence in the visible and NIR was measured every hour that gave evidence of the non-uniformity of the process. Due to this, for further experiments TOAB and DDAB molecules were chosen as it was experimentally shown that they have a higher reactivity.

Anion exchange reaction with TOAB and DDAB occurred immediately, so their application allows one to investigate the optical properties of nanocrystals with different Cl:Br ratios. The addition of TOAB leads to the red shift of the host PL up to 425 nm. Further increase of TOAB concentration is followed by the appearance of the side PL maximum at 560 nm, which can be related to the formation of defect states or by-products in the solution. At the same time, anion exchange with DDAB solution allows PL maximum to be shifted in the visible range up to 510 nm for both undoped and ytterbium-doped perovskites. With increasing of DDAB concentration PL QY in visible range for undoped and Yb-doped NCs was changing in a similar way, while PL QY in NIR was decreased by only 12%.

Acknowledgments

The work was supported by the Russian Science Foundation (21-73-10131)

References

[1] Nedelcu G. et al. "Fast Anion-Exchange in Highly Luminescent Nanocrystals of Cesium Lead Halide Perovskites (CsPbX3, X = Cl, Br, I)", Nano Lett.,vol. 15, pp 5635–5640, July 2015.

[2] Gualdrón-Reyes A.F., Masi S., Mora-Seró I., "Progress in halide-perovskite nanocrystals with near-unity photoluminescence quantum yield", Trends Chem., vol. 3, pp 499–511, April .2021

[3] Zhang X. et al. "Yb3+ and Yb3+/Er3+ doping for near-infrared emission and improved stability of CsPbCl3 nanocrystals", J. Mater. Chem. C. The Roy. Soc. of Chemistry, vol. 6, pp 10101 – 10105, August 2018

Role of kinetics in spontaneous segregation of group III elements in arsenide nanowires

N. V. Sibirev[1], Y. S. Berdnikov[1], R. R. Reznik[1,2], E. V. Ubuivovk [1,2], G. E. Cirlin [2]
[1] The Faculty of Physics, Saint-Petersburg University, Saint Petersburg, Russia
[2] Alferov University, St. Petersburg, 194021, Russia

Abstract— A model of spontaneous formation of the radial heterostructure in arsenide nanowire in single process is proposed. Good agreement of theory and experiment was demonstrated for (In,As)As nanowires. This could be considered as an alternative approach to formation of core-shell heterostructure.

Keywords— ternary nanowires, radial nanowire heterostructures, arsenide.

III−V nanowires (NWs) are promising building blocks for scalable bottom-up nanoelectronics and nanophotonics. Among all the nanostructures used as templates for bandgap engineering, semiconductor nanowires are one of the most promising. Because NW geometry offers a lot of capacity for strain relaxation without formation of dislocations or other defects.

In the NW growth via vapor-liquid-solid mechanism the composition of the forming monolayer (ML) is controlled by the kinetics of atom incorporation into the steps rather than by nucleation[1-2]. If the growth of ternary NW proceeds at low concentration of at least one type of the species in the liquid phase, the catalytic droplet depletes during the ML formation [1]. Thus, the region of forming ML near the nucleus should be enriched by an easily crystallized (poorly soluble) element. This allows formation of radial nanowire heterostructures in single process [2]. Here we demonstrate and discuss this effect in the case of (In,Ga)As NWs.

InGaAs NWs were grown on Si(111) substrates using a gold catalyst in Riber Compact 21 MBE system in nearly self-catalyzed regime [2]. The growth temperature was about 220°C. Growth rate was set at 0.8 ML/s. Figure 1a show the high-angle annular dark field transmission electron microscopy (HAADF TEM) image of the NW cross-section with the composition-sensitive contrast. Figure 1b illustrates the variation of the share of In inside the NW along the dotted lines marked in the inset.We observe In concentration to be below ⅓ in the core, about ½ in the dark ring and stripes and ⅔ near the edge.

The formation of the observed core/shell-like structures is explained within our growth model which assumes the NW composition to be determined by the rates of In and Ga incorporation into the moving steps of the forming MLs [2]. While the incorporation rates are proportional to the elements concentrations in the catalyst. In turn, In and Ga concentration are determined by the balance of incoming flux from the vapor phase and their incorporation rate into the steps. Altogether these considerations allow us to calculate In and Ga concentrations inside the ML (shown in Figure 1c) by solving a closed-form system of equations. In this way we model quantitively the spontaneous formation of core/shell-like structure inside the (In,Ga)As NWs in a single-stage process.

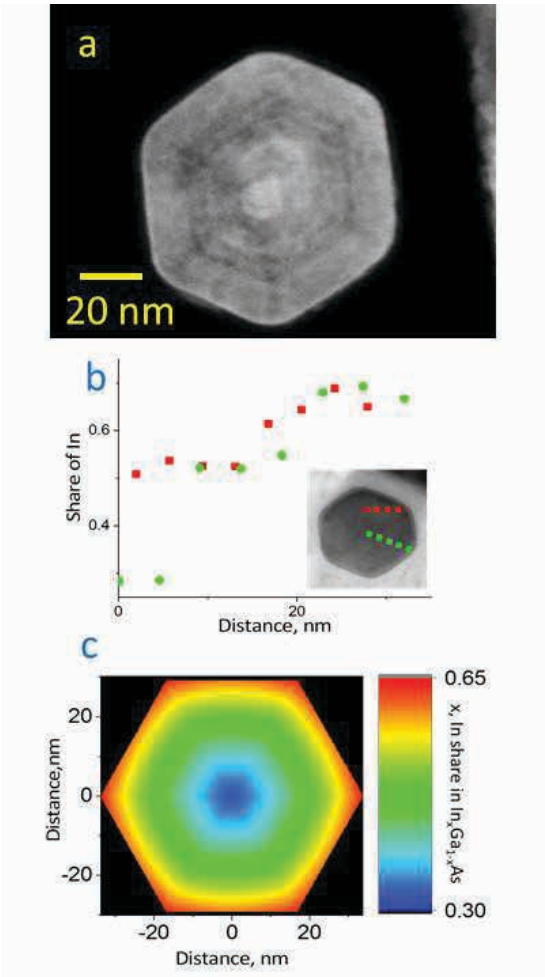

Fig. 1 (a) HAADF TEM image of (In,Ga)As NW cross-section. (b) In composition profiles along the red and green lines (c) The calculated In distribution in NW cross-section.

Nanowire growth and modelling was done with the support of SPbU grant № 75746688. TEM and EDX measurements were carried out in Resource Centre for Nanotechnology.

REFERENCES

[1] F. Glas, V. G. Dubrovskii, “Energetics and kinetics of monolayer formation in vapor-liquid-solid nanowire growth” Phys. Rev. Mater. vol. 4, p. 083401, August 2020

[2] N.V.Sibirev, Y.S. Berdnikov et.al. ”Kinetics of spontaneous formation of core shell structure in (In,Ga)As nanowires” Tech. Phys. Lett. vol 48(3), 2022

Luminescent oxide nanoparticles for security applications

D.V. Mamonova[1], A.A. Kalinichev[2] ,I.E. Kolesnikov[2], V.A. Medvedev[1], M.D. Mikhailov[3]
[1]Chemical Institute, St. Petersburg State University, St. Petersburg, Russia
[2]Center for Optical and Laser materials research, St. Petersburg State University, St. Petersburg, Russia
[3]Graduate School of Physics and Materials Technology, Peter the Great St. Petersburg Polytechnic University, St. Petersburg, Russia

Abstract— We report the synthesis of fluorescent markers based on YVO_4:Er^{3+}, Tm^{3+}, Nd^{3+} and the implantation of the markers into a steel plate by laser processing. We demonstrate that the luminescent properties of the particles can be used for creating an ID spectral code based on the energy transfer between different ions.

Keywords— Luminescence; Rare earth ions; Spectral coding; Laser beam marking

I. Introduction

The fast development of the computer technologies and their accessibility forces trademark owners to design increasingly sophisticated anti-counterfeiting programs. Nowadays different types of the anti-counterfeit protection, such as holograms, smart cards, magnetic stripes, special inks, RFID tags, are used. But all the above-mentioned protection elements require an additional enclosure and frequently are installed using an intermediate carrier (paper, plastic, etc.), which can be easily forged or lost during operation. The most effective protection method is the insertion of the marks directly in the product, when the protective element becomes an integral part of the product. A special class of products requiring the authenticity protection system is the steel products. Their hard-operational conditions need special marking techniques. The protection level of a serial number or a bar code is not high because it does not include the invisible protection and it can be easily repeated. We propose to use luminophores that are characterized by unique spectra to increase the complexity of the protection elements.

II. Experimental Part

The synthesis of particles was carried out using a salt melt (KCl) for formation the complex oxide according to the modified Pechini method [1]. Marking of steel plate with the surface implantation of the luminescent nanomarkers has been implemented using laser system Coherent MBD266 (266 nm, 60 mW power). The size distribution of the synthesized particles was measured with the static light scattering method using a particle size analyzer Marveln Mastersizer 3000. The structure of the synthesized materials was analyzed with a powder diffractometer Bruker "D8 DISCOVER" with CuKα1 line (1.54056 Å). Photoluminescence properties were studied with a spectrofluorimeter Horiba Jobin Yvon Fluorolog-3 equipped with a Xe-arc lamp (450 W power), a Raman spectrophotometer Horiba Jobin-Yvon LabRam HR800 equipped with He-Cd laser (325 nm, 20 mW power) and confocal luminescence microscope Nikon Ti2-E.

III. Results and discussion

All diffraction lines of XRD analysis correspond to tetragonal phase of YVO_4 (JCPDS 17-0341). The distribution curve confirms that the particle sizes in the resulting suspension are approximately between 25 nm and 200 nm, and the average size is found to be 50 nm. Direct excitation of rare earth ions (λ_{ex} = 595 nm for Nd, 526 nm for Er, 692 nm for Tm) produces the emission spectra of triply doped system YVO_4:Er^{3+}, Tm^{3+}, Nd^{3+} includes all the emission peaks corresponding to the set of rare earth ions Nd^{3+}, Er^{3+} and Tm^{3+}. Energy transfers in triply doped powder between Nd^{3+}, Er^{3+} and Tm^{3+} ions were detected upon direct REI excitation. The digital identification spectral code was created using non-overlapping emission bands, for which emission intensities depend on the doping concentration. The wide range of relative values makes it possible to obtain a high coding capacity with this system (>10^{25}). Laser beam marking of steel plate was realized with integration of oxide nanoparticles in the melting area. Luminescence microscopy results confirms the presence of luminescent particles in the area of laser action. The emission spectra measured on the surface of the steel plate allow the ID spectral code of the integrated particles to be decoded.

Acknowledgment

Authors are grateful to “Center for Optical and Laser materials research”, “Research Centre for X-ray Diffraction Studies”, “Interdisciplinary Resource Center for Nanotechnology”, "Innovative technologies of composite nanomaterials”, “Centre for Geo-Environmental Research and Modelling (GEOMODEL)” (St. Petersburg State University).

References

[1] V.A. Medvedev, D.V. Mamonova, I.E. Kolesnikov, A.R. Khokhlova, M.D. Mikhailov, A.A. Manshina, Synthesis and luminescence properties of YVO4: Nd3+, Er3+ and Tm3+ nanoparticles, Inorganic Chemistry Communications. 118 (2020) 107990. https://doi.org/10.1016/j.inoche.2020.107990.

This research has been supported by the Russian Science Foundation (№ 20-79-00101).

Optical properties of the $TlBr_{0.46}I_{0.54}$ – AgI and $TlCl_{0.67}Br_{0.33}$ – AgI system crystals

D.D.Salimgareev[1], A.E.Lvov[1], A.A.Yuzhakova[1], V.M.Kondrashin[1], A.S.Korsakov[1], L.V.Zhukova[1]
[1]Ural federal university named after the first President of Russia B. N. Yeltsin. 19 Mira str., Ekaterinburg 620002, Russia

Abstract— The present work is devoted to the synthesis of the $TlBr_{0.46}I_{0.54}$ – AgI and $TlCl_{0.67}Br_{0.33}$ – AgI systems optical nanoceramics and the study of their optical properties. The spectral transmission range was determined, and the refractive indices at the wavelength of the short-wavelength absorption edge and the carbon dioxide laser (10.6 μm) were calculated. The results are the basis for the development of new infrared optics based on monovalent thallium halides doped with silver iodide.

Keywords— silver halide, thallium halide, optical ceramics, nanoceramics, refractive indices, infrared range

I. Introduction

New optical materials research for the infrared (IR) and especially the terahertz (THz) range is one of the priority goals in the development of materials science. Modern studies have shown that crystals and nanoceramics based on thallium (I) and silver halides are promising optical materials for the manufacture of IR and THz fibers, because they are transparent from visible and IR range without absorption windows and in THz range with absorption windows.

II. Synthesis of Optical Ceramics and Investigation of Their Properties

The first step in the synthesis of the $TlBr_{0.46}I_{0.54}$ – AgI and $TlCl_{0.67}Br_{0.33}$ – AgI systems optical nanoceramics is the raw materials preparation with given composition and high purity. Synthesis was carried out using a high-tech method of thermozone crystallization-synthesis (TZKS). By TZKS was used to synthesize a raw materials of compositions 5, 10, 15, and 20 wt. % AgI in $TlCl_{0.67}Br_{0.33}$ and 5.10 wt. % AgI in $TlBr_{0.46}I_{0.54}$. From this raw materials using the method of directional crystallization at the PKB installation (Bridgman Furnace) optical nanoceramics were synthesized. Polycrystalline plane-parallel plates with a diameter of 10–15 mm and a thickness of 295–348 nm were manufactured using the hot embossing method. On these plates, both the spectral transmission ranges and the refractive indices were calculated.

The refractive indices determination was carried out at the short-wavelength absorption edge (λ_L) and a carbon dioxide laser (10.6 μm). In the first case transmission spectra were taken on a Shimadzu UV-1800 UV spectrophotometer (operating range from 190 to 1100 nm). Using the method of two tangents, the samples' short-wavelength absorption edges were determined, which increases from 0.398 to 0.448 μm for ceramics of the $TlCl_{0.67}Br_{0.33}$ –AgI system and from 0.408 to 0.418 for ceramics of the $TlBr_{0.46}I_{0.54}$ – AgI system. Further, according to the modified Planck-Einstein equations, the refractive indices at the short-wavelength absorption edge were calculated. The results are presented in Table 1.

This work was supported by the Russian Science Foundation (No. 21-73-10108), https://rscf.ru/en/project/21-73-10108/.

TABLE I. PCF's Fundamental Mode Parameters

Content of AgI in $TlCl_{0.67}Br_{0.33}$, mol. %	λ_L	$n(\lambda_L)$	n at 10,6 μm
0	398	2.348±0.002	2.179±0.008
5	436	2.401±0.002	2.194±0.008
10	444	2.412±0.002	2.204±0.008
15	446	2.415±0.002	2.213±0.008
20	448	2.419±0.002	2.233±0.008

In the second case refractive indices were obtained using a Shimadzu IRPrestige-21 IR Fourier spectrometer (operating range 7800 – 240 cm^{-1} or 1.28 – 41.7 μm) and at the 10.6 μm were calculated. The results are also presented in Table 1. Detailed methods for determining the refractive indices at the studied wavelengths are presented in [1].

Also using a spectrophotometer Shimadzu UV-1800 and a IR-Fourier spectrometer Shimadzu IRPrestige-21, the transmission spectra of the investigated non-ceramic samples were obtained (Fig. 1). Fig. 1 shows that the samples are transparent from 0.4 - 0.45 to 40.0 μm and no longer have absorption windows. It should be noted that the transparency is more than 60 - 75%.

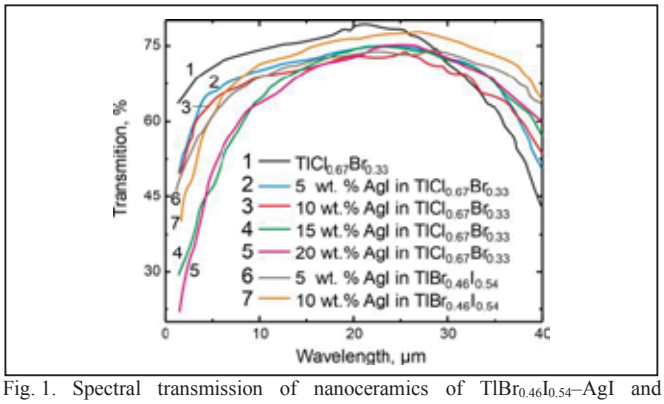

Fig. 1. Spectral transmission of nanoceramics of $TlBr_{0.46}I_{0.54}$–AgI and $TlCl_{0.67}Br_{0.33}$–AgI systems

The results show that the optical materials of the $TlBr_{0.46}I_{0.54}$–AgI and $TlCl_{0.67}Br_{0.33}$ – AgI systems are excellent candidates for manufacturing of infrared photostable optical fibers that will not be destroyed over time due to the effect of recrystallization.

References

[1] D. Salimgareev, A. Lvov, L. Zhukova, D. Belousov, A. Yuzhakova, D. Shatunova, A. Korsakov, A. Ishchenko, "Optical properties of the AgBr – AgI system crystals," Opt. Las. Tech. vol. 149, 107825, 2022.

Pseudomagnetic excitonic brightening via shear strain in monoatomic transition metal dichalcogenide

H.Y. Hwang[1], S.H. Lee[2], H. Lee[2], Y.D. Jho[2,*]
[1]Clarendon Laboratory, Department of Physics, University of Oxford, Oxford OX1 3PU, United Kingdom
[2]School of Electrical Engineering and Computer Science, GIST, Gwangju, South Korea
*jho@gist.ac.kr

***Abstract*— We experimentally demonstrate a drastic photoluminescence (PL) enhancement (reduction) in WSe2 (MoSe2) monolayers under pseudomagnetic out-of-plane shear strain. The shear strain-induced spin-state mixing at K valley is associated with brightening of dark exciton in the WSe2 and darkening of bright exciton in the MoSe2. Our results present an important advance toward manipulating the luminescence switching in nanomaterials device via strain engineering.**

Keywords*— Photoluminescence; spin flipping; pseudomagnetic field

The straintrionically controllable properties of low-dimensional nanomaterials have great potential to expand the degrees of freedom for a wide variety of engineering applications. [1, 2] Particularly, strain engineering in these transition metal dichalcogenides (TMDCs) aims to manipulate band structure related to spin and valley dynamics and therein to modify their optoelectronic properties. Intervalley scattering focused mainly on the application of normal strain and biaxial strain while the intra-band mixing at K valley influenced by shear strain have remained unclear in the TMDCs.

Here, by employing monolayered WSe2-MoSe2 lateral heterostructures, we experimentally demonstrate a drastic photoluminescence (PL) enhancement (reduction) in WSe2 (MoSe2) under applying simultaneously uniaxial normal strain (up to ~1%) and out-of-plane shear strain (OSS; up to ~6%) in terms of crystal axis. As established by previous studies, the uniaxial normal strain can tune the band structure of the TMDC materials to induce indirect-to-direct transition. On the other hand, the effect of shear strain on energy and intensity changes in PL spectra is newly related to the spin flipping coefficient according to shear deformation potential and spin orbit splitting of the TMDC materials.

The change in PL peak energy and PL intensity according to the shear deformation of the armchair axis was more significant because, unlike the zigzag axis, the contribution from the residual shear deformation was added directionally. The spectra further revealed a dependency on the bending direction that was consistent in the negative (compressive) strain case and then striking with positive (tensile) strain. Such strain-sign-dependent characteristics of the PL was accompanied by the tendency to break the optical selection rules of the lowest-lying excitons.

From the viewpoint of correspondence between the inversion symmetry breaking from in-plane magnetic field and the OSS-induced spin-flipping perturbation to subbands, the OSS can be formulatively converted into the in-plane magnetic field. By adapting the reported material parameters [3, 4], we estimate that the field equivalent to OSS of 6% is given as 140 T [5].

[1] Z. Peng *et al.*, "Strain engineering of 2D semiconductors and graphene: from strain fields to band-structure tuning and photonic applications." Light: Science & Applications 9, 1-25 (2020).

[2] S. Deng, A. V. Sumant and V. Berry "Strain engineering in two-dimensional nanomaterials beyond graphene" Nano Today 22, 14–35 (2018).

[3] C. Robert *et al.* "Fine structure and lifetime of dark excitons in transition metal dichalcogenide monolayers" Phys. Rev. B 96 155423 (2017).

[4] M. Koperski *et al.*, "Orbital, spin and valley contributions to Zeeman splitting of excitonic resonances in MoSe2, WSe2 and WS2 Monolayers" 2D Mater. 6, 015001 (2018).

[5] H. Y. Hwng *et al.*, "Shear-strain-mediated Photoluminescence Manipulation in Two-dimensional Transition Metal Dichalcogenides" 2D Mater. 9, 015011 (2022).

Two approaches to two-stage growth of GaP nanowires

Y. Berdnikov[1,2], V.V. Fedorov[1], N.V. Sibirev[2], A.D. Bolshakov[1], S.V. Fedina[1], G.A. Sapunov[1], L.N. Dvoretckaia[1], and I.S. Mukhin[1]

[1] Renewable energy sources laboratory, Alferov University, St. Petersburg, Russia
[2] Faculty of Physics, St. Petersburg State University, St. Petersburg, Russia

Abstract— We compare the two approaches to the growth of ensembles of self-catalyzed GaP nanowires, which both allow independent control of the length and diameter

Keywords— GaP nanowires; two-stage growth

III-V nanowires (NWs) find the applications as basic elements of photonic and optoelectronic devices, which mostly require high uniformity within NW ensemble and sufficiently large (~λ/2n) NW diameter to obtain efficient light localization in the NW volume [1]. The majority of the previous efforts were focused on improving the uniformity in ensembles of GaAs NWs, while fewer works studied GaP material system, which shows large nonlinear coefficients and optical transparency in a broad range. Therefore, highly controllable synthesis of GaP NWs is of great interest for nonlinear optical and photonic devices. Here we discuss two strategies for tailoring morphology of GaP NWs in the two-staged self-catalyzed growth on Si(111) substrates by molecular beam epitaxy.

We have found that the increase of vertical yield and NW diameter cannot be achieved simultaneously within a single-stage growth [2]. However, this restriction can be overcome in a two-stage approach with the decrease of the V/III flux ratio at the second growth step following the formation of NW stems at a higher V/III ratio and growth temperature. In this case, the subsequent expansion of the catalyst droplet results in the increase of NW diameter, while the uniform radial growth allows obtaining NWs with vertical sidewalls.

At the first growth stage the "Seed" arrays of NWs were synthesized at 640 ˚C and fixed V/III. Next, within the first approach ("Two-stage I"), we decreased the growth temperature by 20C and halved the P_2 flux down to V/III ratio of 12 at the second stage, while keeping Ga flux rate constant. For comparison, a single-stage reference sample was also grown under growth conditions identical to the seed growth. Corresponding scanning electron microscopy (SEM) images together with the results of the morphological analysis can be found in Fig.1 (a-d). The two-stage growth leads to the increase of the NW diameter from 70 to 105 nm and length reduction from 6 to 4 μm with respect to reference single-stage growth.

In the second two-stage approach ("Two-stage II") theV/III ratio was reduced from 30 to 12 by a smooth Ga 2.5-fold flux ramp from 180 nm/hr up to 450 nm/hr within 200 seconds while keeping P_2 flux and the growth temperature constant. Fig. 1 (e-h) illustrates the results obtained in this case. In contrast to the first approach, we observe no significant change in the NW length while the mean diameter increases from 100 to about 150 nm in comparison with the reference single-stage growth.

The authors gratefully acknowledge financial support of the research grant of St. Petersburg State University No. 75746688.

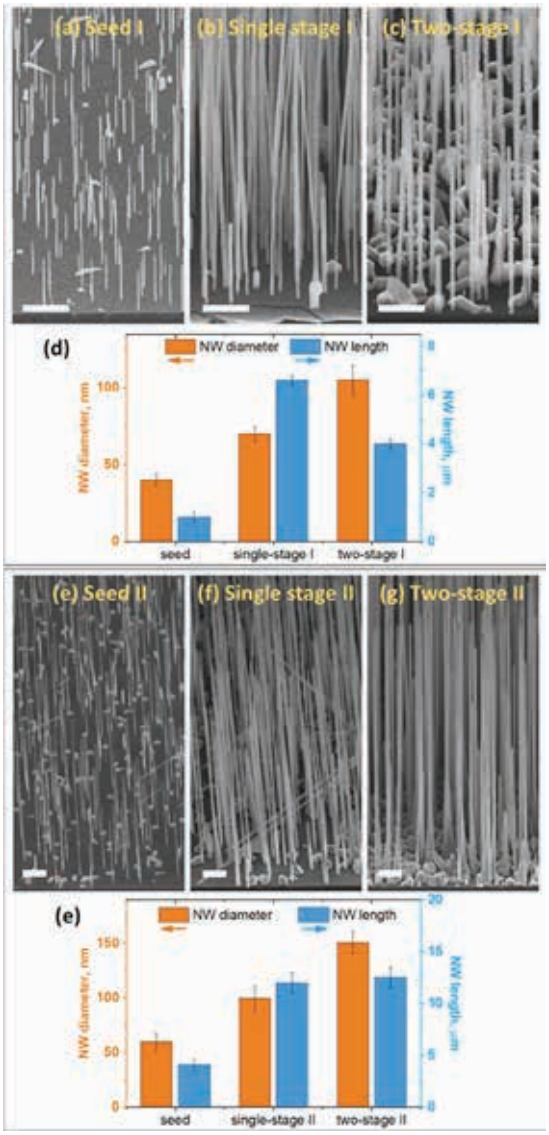

Fig. 1. SEM images of GaP NWs obtained in Seed (a,e), Single-stage (b,f), and Two-stage growths. (d, h) mean values of the NW diameters and lengths.

REFERENCES

[1] A. Kuznetsov et al "Anisotropic Radiation in Heterostructured "Emitter in a Cavity" Nanowire" Nanomaterials, vol. 12, p. 241, 2022

[2] V.V. Fedorov et al. "Tailoring morphology and vertical yield of self-catalyzed GaP nanowires on template-free Si substrates" Nanomaterials, vol. 11, p. 1949, 2021.

Optical Methods for Controlling the $CaSO_4 \cdot 2H_2O$ Crystallization Process in the Presence of a Seed

Kovalenko A.E., Kekin P.A., Vasil'ev A.S., Morozov A.N., Pochitalkina I.A., Popov K.I.
D. Mendeleev University of Chemical Technology of Russia (MUCTR), Moscow, Russia

To elucidate crystallization mechanism of $CaSO_4 \cdot 2H_2O$ the characteristics of a dispersed impurity in water of various degrees of purification and initial solutions prepared on its basis were determined (Table 1).

Table 1. Characteristics of the studied samples

Liquid	χ, μS/cm	Particle size, nm			
		< 100	101-200	201-300	301-500
		Suspended particle concentration in 1 ml			
Distilled water	5	7600	1570	420	320
Bidistilled water	3	4550	900	250	200
Bidistylate S-A	2	3040	630	170	130
Deionized water	0,056	660	75	36	13
$CaCl_2$, 0,02 mol/l	-	4150	1900	890	470
Na_2SO_4, 0,02 mol/l	-	5170	4300	3100	2500

Analytical control of the parameters of the solid phase was carried out by the methods of dynamic light scattering "Nanotrac ULTRA" (Fig. 1) and optical microscopy "Levenhuk", transmission (TEM) and scanning electron microscopy SEM "Talos L120C" "JEOL JSM-6510 LV".

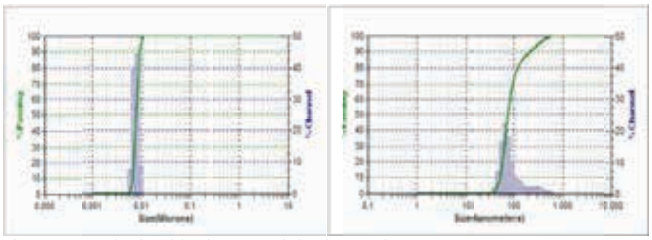

Fig. 1. Data obtained by laser particle size analyzer "Nanotrac ULTRA"

The results of processing the kinetic curves of nucleation obtained by independent methods of analysis of the solid and liquid phases are consistent and indicate the formation of a solid phase on a seed from a dispersed admixture of nanoparticles.

To determine the effect of the content of the dispersed phase on the kinetics of $CaSO_4 \cdot 2H_2O$ crystallization, 2 groups of model solutions were prepared on deionized water against the background of an initial ionic strength of 0.15 mol/l NaCl: group I – initial solutions ($CaCl_2$ and Na_2SO_4) with a concentration of 0.0598 mol/l, double degree of supersaturation; group II – initial solutions with a concentration of 0.1196 mol/l, a fourfold degree of supersaturation.

According to the kinetic dependences of the induction period on the content of the dispersed phase in the volume of solutions, it was found that the total content of the dispersed impurity is determined by the degree of contamination of the substance and solvent. Purification of the initial solutions of $CaCl_2$ and Na_2SO_4 using membranes with a pore size of 200 nm provides a decrease in the content of the dispersed phase from 10^6 to 10^3 particles/ml and a twofold increase in the induction period.

Despite the large amount of work devoted to the theory and practice of the crystallization process, there is no consensus among scientists on the mechanism of solid phase formation in aqueous solutions, therefore alternative options are considered in the scientific literature: homogeneous, heterogeneous and mixed mechanisms [1–3]. The heterogeneous mechanism of crystallization assumes the presence in the solution of a dispersed phase, which is a seed.

Visual determination of particle size was conducted using optical microscope concurrently. Set of micrograph were taken within a fixed period of time during the whole experiment. These micrographs were processed with special software which shows the average particle size at a given time.

This slide represents the dynamics of particle growth in time, which was obtained by combination of 2 independent methods (dynamic light scattering and optical microscopy). Both methods show matching a result at the borders of working ranges (Fig. 2).

Using the example of calcium sulfate nucleation, the effect of microimpurities contained in water used to prepare initial solutions is shown:

$$CaCl_2 + Na_2SO_4 + 2H_2O = CaSO_4 \cdot 2H_2O + 2NaCl$$

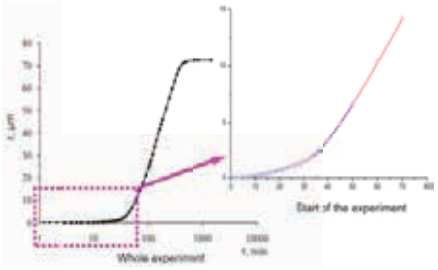

Fig. 2 Kinetic dependence of the average particle size of solid phase

Analytical grade reagents were used in this study: $CaCl_2$ (GOST 4460-79), Na_2SO_4 (GOST 83-79). The initial supersaturated solutions were prepared from $c(CaCl_2) = c(Na_2SO_4) = 1.0$ mol/l against the background of electrolyte c(NaCl) = 0.15 mol/l, which provided constant values of ionic strength (I = const) and activity coefficients of individual ions ($\gamma_\pm$ = const) [1–3].

The solid phase parameters were determined by instruments implementing optical methods of analysis, and the parameters of the liquid phase were determined by the methods of electrochemical analysis and complexometric titration (Mettler Tolledo) [1].

Particular attention is paid to the determination of water parameters (Table 1) for the preparation of initial solutions of $CaCl_2$ and Na_2SO_4. It has been established that the electrical conductivity of distilled water and its resistance are, respectively: for fresh distillate 5 μS/cm and 205 kOhm·cm, for bidistylate (Sigma-Aldrich) 2 μS/cm and 590 kOhm·cm, deionized water 0.0749 μS/cm and 15.5 MOhm·cm [2–3].

On Fig. 3 shows the results of the kinetic experiment of the $CaSO_4 \cdot 2H_2O$ nucleation process from initial solutions prepared in water before (a, c) and after its deionization (b, d). Designation of experimental points corresponds to parallel measurements of model solutions with $CaSO_4 \cdot 2H_2O$ concentrations of 0.05 (left) and 0.03 (right) mol/l.

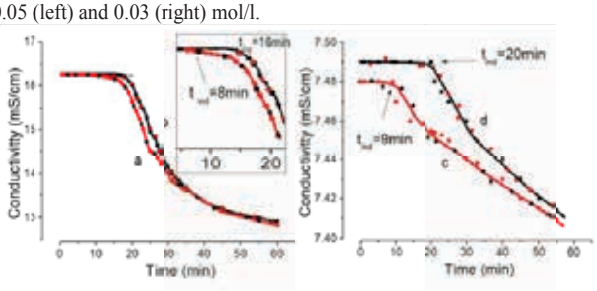

Fig. 3. Crystallization kinetics of $CaSO_4 \cdot 2H_2O$ from initial solutions before (a, c) and after filtration (b, d)

The induction time measured from the value of the electrical conductivity of solutions of one degree of supersaturation confirms its dependence on the content of nanoparticles: with an increase in their concentration in the bulk solution, the induction period decreases and the rate of nucleation increases at a constant state of saturation and temperature. Thus, the reaction of calcium sulfate formation occurs due to the sorption of $[Ca^{2+}]$, $[SO_4^{2-}]$ and $[CaSO_4]^0$ particles on the surface of nanoparticles.

[1] Pochitalkina I.A., Kekin P.A., Kovalenko A.E. Study of the crystallization process of low-soluble compounds using laser analyzers. 2020 International Conference Laser Optics, LO 2020, p. PD1, 2020.

[2] Oshchepkov Maxim, Popov Konstantin, Kovalenko Anna, Redchuk Anatoly, Dikareva Julia, Pochitalkina Irina. Initial Stages of Gypsum Nucleation: The Role of Nano/Microdust // Minerals. Scopus. 2020. vol. 10. № 12, pp.1083–1096.

[3] K. Popov, M. Oshchepkov, A. Kovalenko, A. Redchuk, J. Dikareva and I. Pochitalkina. The Scale Nucleation Natural Precursors: a Case Study of "Micro/Nanodust" Impurities Nature in Laboratory Aqueous Samples, obtained from Moscow TAP water// International Jornal of Corrosion and Scale Inhibition (Int. J. Corrosion Scale Inhibition). Scopus. vol. 9. № 3. pp. 1097–1112.

Investigation of obtaining ZnSe nanopowders by means of a fiber ytterbium laser.

V.V. Osipov[1] , V.V. Platonov[1] , E.V. Tikhonov[1] , V.V. Lisenkov[1.2]

[1] Institute of Electrophysics of the Ural Branch of the Russian Academy of Sciences, Yekaterinburg, Russia

[2] Institute of New Materials and Technologies, Ural Federal University named after the first President of Russia B.N Yeltsin, Yekaterinburg, Russia

Abstract — The production of zinc selenide nanopowder using repetitively pulsed radiation from a ytterbium fiber laser has been studied. With an average radiation power of 300 W and a pulse duration of 120 μs, the productivity of nanopowder production was ≈100 g/h. The nanopowder contains weakly agglomerated particles that have a spherical shape, as well as the shape of polyhedrons. Their arithmetic average size is 18 nm. Nanoparticles have two crystalline phases: cubic (40 wt.%), and hexagonal (60 wt.%).

Keywords— laser ablation, nanopowder, fiber ytterbium laser, gas-p *IPG Photonics* ***hase method for obtaining nanoparticles***

I. INTRODUCTION

Polycrystalline zinc selenide is a popular material for optical elements for CO_2 lasers, active media of mid-IR lasers, scintillators . Today, CVD technology is used to manufacture these products . An alternative is ceramic technology using nanopowders ZnSe . To do this, you need to use weakly agglomerated nanoparticles with an average size of <100nm. In addition, ZnSe is one of the quantum dot materials having the same dimensions. Nanopowders with such properties can be obtained using a high-power laser by evaporating a target of the required composition and subsequent condensation of vapors in a gas flow [1]. Previously, this method was used to produce nanoparticles of refractory oxides, and it was practically not used for synthesis non-oxide nanopowders. In this work, for the first time, the production of a ZnSe nanopowder is studied using a laser.

II. RESULTS AND DISCUSSION

To obtain a nanopowder , an experimental setup based on an LS-07N ytterbium fiber laser (IPG Photonics) described in [1] was used. The synthesis of the nanopowder was carried out in argon pumped through the setup from a gas cylinder. The targets were fabricated from ZnSe micropowder by pressing and subsequent sintering in an H_2 atmosphere. The targets had a porosity of ≈70 %.

Evaporation of zinc selenide using a fiber ytterbium laser is hampered by the high transparency of this material at the wavelength of its radiation (1.065 nm). Ablation is possible if the radiation intensity in the target exceeds the radiation damage threshold of the material. In a porous target, laser radiation is scattered, which leads to its concentration in some local areas [2]. As our calculations have shown, with the intensity of the incident radiation I=0.46 MW/cm ^{2} , grain size 0.55÷4.6 μm and their packing density of in the target is ≈50 %, the scattered radiation intensity in such places can reach ≈110 MW/cm^2. This allows us to evaporate the target under our conditions.

The productivity of obtaining ZnSe nanopowder using an ytterbium fiber laser can decrease due to splashing of melt droplets larger than 10 μm [1]. Therefore, the process of target evaporation using a single laser pulse was photographed. These experiments have shown that droplet spraying can be significantly reduced if the intensity of radiation focused on the target is reduced to 0.21 MW/cm^2 and the pulse duration is less than 400 μs. Taking into account these data, the ZnSe nanopowder was obtained under the following laser operating mode: the duration of the radiation pulses is 120 μs, the follow-up period is 240 μs, the pulse power is 600 W, the radiation intensity at the target is 0.18 MW/cm^2.

The productivity of ZnSe nanopowder production and its mass yield during the evaporation of one target were 100 g/h and 32÷34 wt.%. The nanopowder consists of weakly agglomerated particles with an average size of 18 nm, which have the shape of polyhedra, and sometimes spheres. The nanoparticles had both a cubic crystal lattice (40 wt.%) and a metastable hexagonal lattice (60 wt.%).

ACKNOWLEDGMENT

The work was performed as part of State Task No. AAAA - A 19-119020790031-5, was supported in part by RFBR Grant No. 20-08-00054 A.

REFERENCES

[1] VV Osipov, VV Platonov, VV Lisenkov, EV Tikhonov, AV Podkin / Study of nanoparticle production from yttrium oxide by pulse-periodic radiation of ytterbium fiber laser // Applied Physics A, 2018, vol. 123, article 3, DOI: 10.1007/s00339-017-1348-9

[2] VV Osipov, VV Lisenkov, VV Platonov, EV Tikhonov / Processes of interaction of laser radiation with porous transparent materials during their ablation // Quantum Electronics, 2018, vol. 48, N3, pp. 235 - 243

Investigation of the Resistance to Ionizing Radiation of Optical Products Based on the AgBr - AgI System Crystals

A.A.Yuzhakova[1], D.D.Salimgareev [1], A.E.Lvov[1], P.V.Pestereva[1], I.V.Yuzhakov[1], A.S.Korsakov[1], L.V.Zhukova[1]
[1]Ural federal university named after the first President of Russia B. N. Yeltsin, Ekaterinburg, Russia

Abstract— The photo- and radiation resistance of optical windows and fibers based on the AgBr–AgI system crystals has been studied. The greatest optical loss during irradiation with ultraviolet for 530 min does not exceed 40% in the entire transmission range. The transmission spectra show the resistance of fibers to electron irradiation with doses up to 400 kGy.

Keywords— silver halide, IR window, IR fiber, photostable, radiation resistance

I. INTRIDUCTION

The search and creation of an element base for fiber optics in the mid-infrared (IR) range is an urgent task, since the IR spectral region covers many applications from molecular fingerprint analysis to thermal imaging.

Today, as materials that provide transmission in the visible, IR, terahertz (THz) and millimeter ranges, crystals based on metal halide can be used [1]. In particular, crystals of the AgBr - AgI system, due to the introduction of heavier iodine into the crystal lattice of silver bromide, promise high resistance to ionizing radiation, as well as high optical properties.

The study of their transmission range showed that the AgBr - AgI system crystals with the composition from 1 to 36 mol.% AgI in AgBr cover the region from 0.46 to more than 42 microns. Infrared fibers based on them transmit IR radiation in the range from 3 to 25 μm without absorption windows. In this case, the optical losses in crystals are 0.1 dB/m, and in optical fibers - 0.46 dB/m. For the application of optical products based on the AgBr – AgI crystals system, a more comprehensive study of the properties is required. This paper presents the study results of the products' resistance to ultraviolet and β-radiation.

II. PHOTO- AND RADIATION RESISTANCE STUDY

The photoresistance study of the AgBr - AgI system crystals was carried out by stage-by-stage samples irradiation with increasing doses for 20, 50, 170, 530 min. Before irradiation and after each irradiation stage, transmission spectra were taken from the samples using a IR-Fourier spectrometer IRPrestige-21, Shimadzu. On Fig. 1 shows the relative transmission obtained by comparing the spectra of irradiated samples with different doses and unirradiated sample.

The investigation of resistance to β-radiation was carried out on IR fibers with a doses set of 50, 100, 200, 400 kGy. Irradiation was carried out on the UELR-10-10S installation and had a cumulative character. Before irradiation and after each stage (taking each dose), transmission spectra were taken. The measurement results are shown in Fig. 2.

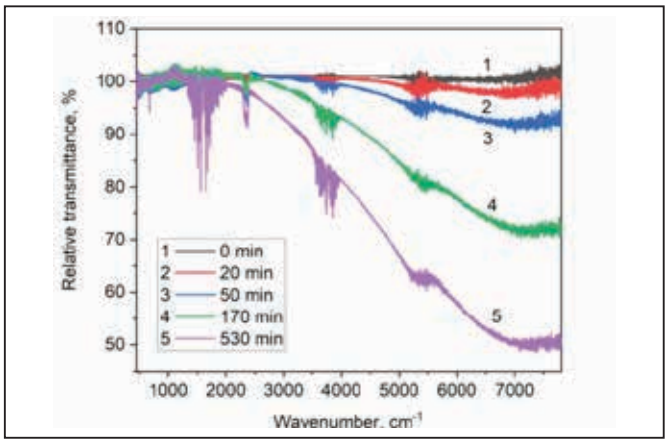

Fig. 1. Relative transmission spectra, sample of $AgBr_{0.64}I_{0.36}$

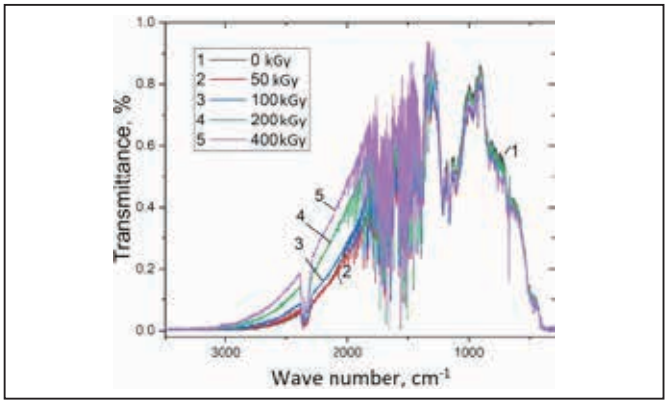

Fig. 2. Transmission spectra of the waveguide based on crystalline $AgBr_{0.92}I_{0.08}$

All samples showed high photostable and resistance to β-irradiation, thus they can be used without additional protective coatings, in rough environmental conditions such as hot cells of nuclear power plants, devices operating in space, etc.

This work was supported by the Ministry of Science and Higher Education of the Russian Federation, State Contract no FEUZ-2020-0058 (H687.42B.223/20).

REFERENCES

[1] L. Zhukova, D. Salimgareev, A. Korsakov, N. Yudin, G. Komandin, I. Spektor, A. Lvov, A. Yuzhakova, "The optical transparency investigation of crystals based on the AgHal – TlHal solid solutions systems in the terahertz range," Opt. Mat. vol. 113, pp.110870, 2021.

Low-cost magnetic Fe alloy based THz polarization filters in EVA matrix

D.M.Ezhov, E.S.Savelyev, A.I.Olekhnovich, V.N.Cherepanov
Optics and Spectroscopy Department, Tomsk State University, Tomsk, Russia

Abstract— We present the dependence of the concentration of magnetic driven 5BDSR alloy of THz filters in EVA matrix, on absorption and reflection properties in the extended THz range of 0.2-2 THz. Transmittance dependence on particles concentration and orientation was studied using a custom-made THz-TDS spectrometer. The extinction coefficient of up to 20 was obtained using 15 mass.% of 5BDSR alloy.

Keywords— Fe alloy; 5BDSR; THz polarization; THz—TDS; magnetic driven particles.

I. SUMMARY

In this work, we demonstrate the dependence of the polarization efficiency of modulators based on soft magnetic submicron particles of the 5BDSR alloy [1] on the concentration of nanoparticles in the ethylene-vinyl acetate (EVA) matrix.

Previously we found the optimal concentration of 5BDSR particles in the liquid THz attenuator, but 80W-90 oil leads to a significant decrease of initial transmittance in the long-wavelength THz range [2].

In this work, we create polymer polarization modulators based on the EVA polymer matrix, which are almost completely transparent up to 2 THz. Polymer solution with particles was deposited in the presence of a magnetic field, by analogy with [3]. A series of films with different concentrations of 5BDSR particles and thickness of about 300 μm were obtained as a result of deposition. To obtain all THz properties we made a series of polymer foils: without particles, with an isotropic distribution of particles, and with particles that were oriented along the lines of the magnetic field. We used a permanent magnet with a magnetic force of about 100 G to form an external magnetic field. Using this method, we obtained pseudo lattices with a non-uniform distribution over the distance between the lines of 5BDSR particles. Un-uniform distribution of the 5BDSR particles leads to the fact that the radiation is modulated in a wide spectral range. The maximal extinction coefficient occurs in the region of 1.4 THz.

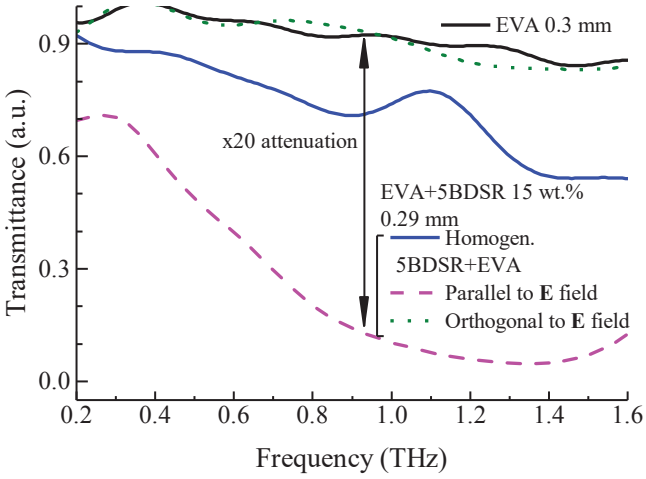

Fig. 1. Dependance of the transmittance of 15 wt. % of 5BDSR on the o

Spectral properties of these filters were studied using a custom-made THz-TDS spectrometer. We use Zomega electro-optical sensor as a THz detector and a Batop iPCA-21-05-1000-800-h antenna coupled with a femtosecond Chameleon Vision 2 laser (Coherent, USA). To obtain reliable data, THz polarizers from [4] were also used. The combination of two types of gratings makes it possible to obtain highly efficient THz polarizers in a wide spectral range. It is also worth noting that the use of particles of different sizes allows you to control the range of the maximum efficiency of the filters.

REFERENCES

[1] M. Rubinstein, V. G. Harris, and P. Lubitz, "Ferromagnetic resonance in nanocrystalline Fe73.5CuNb3Si13.5B9 (Finemet)," *J. Magn. Magn. Mater.*, vol. 234, no. 2, pp. 306–312, Sep. 2001

[2] Ezhov D.M. et al. Variable THz attenuator based on 5BDSR microparticles in synthetic 80W-90 oil // 2020 45th International Conference on Infrared, Millimeter, and Terahertz Waves (IRMMW-THz). IEEE, 2020. P. 1–2.

[3] Fragouli, A. Das, C. Innocenti, Y. Guttikonda, S. Rahman, L. Liu, V. Caramia, C. M. Megaridis, and A. Athanassiou, "Polymeric Films with Electric and Magnetic Anisotropy Due to Magnetically Assembled Functional Nanofibers," *ACS Appl. Mater. Interfaces*, vol. 6, no. 6, pp. 4535–4541, Mar. 2014.

[4] Mamrashev A. et al. Terahertz Time-Domain Polarimetry for Principal Optical Axes of Anisotropic Crystals // Photonics. 2021. Vol. 8, № 6. P. 213.

This study was supported by the Russian Science Foundation (RSF), Project # 18-19-00268.

Quantum Engineering of Bright-Dark Optical States of Resonantly Interacting Rare Earth Ions with Nanolocal Stark Effect

K.K.Pukhov[1], S.K.Sekatskii[2]
[1]Prokhorov General Physics Institute of the Russian Academy of Science, Moscow, Russia
[2]Laboratory of Biological Electron Microscopy (LBEM), IPHYS, Swiss Federal Institute of Technology (EPFL), and Department of Fundamental Biology, Faculty of Biology and Medicine, University of Lausanne, Lausanne, Switzerland

Abstract— Earlier an idea to use controlled with modern Scanning Probe Microscopy (SPM) technique resonant interaction of dipoles (fluorescent rare earth (RE) ions in crystals) was put forward. Here we discuss the possibility to exploit nanolocal Stark effect, caused in such systems by strong inhomogeneous electric fields of sharp SPM electrodes (tips), to engineer the dark – bright states of resonantly interacting dipoles: their energies and decay (decoherence) rates can be strongly influenced by such fields.

Keywords— nanostructured materials, rare-earth ions, dipole-dipole resonant interaction, Scanning Probe Microscopy, quantum computing

I. Introduction

An idea to use resonant interaction of dipoles (fluorescent rare earth (RE) ions in crystals), controlled with modern Scanning Probe Microscopy (SPM) technique, was put forward in 2003 [1]. Immediately afterwards, clusters and superlattices of resonantly interacting RE ions were proposed and analysed as a prospective quantum computer hardware. In particular, the use of pair, quartic and sextet neodymium ions, respectively $(Nd^{3+}– F^{-}_{i})_{2,4,6}$, in fluoride crystals CaF_2, SrF_2 и CdF_2 for the quantum information processing was considered. Especially interesting is the possibility to *engineer dark – bright states* of resonantly interacting ions using nanolocal Stark effect, induced by an electric field of sharp conducting tip of SPM, sf. [1]. Dark - bright states can be considered as a qubit, and they appear as a truly interesting element of quantum logic networks [2].

To solve this problem, we need to design novel optical materials and methods to modify them. To be more specific, the consideration is undertaken for the case of $(Nd^{3+}– F^{-}_{i})_2$ pair centers in CaF_2 crystal, but the very setting of the problem of the use of local Stark effect for the quantum computing is much more general.

II. Quantum Network

The idea of our approach is illustrated in the Fig. 1 below. The quantum state of a pair of resonantly interacting excited by external laser radiation dipoles (ions) *a* and *b* separated by a small (nano- or subnanometer) distance can be changed ("engineered") as a result of the nanolocal Stark effect caused by application of certain potential onto one of three electrodes shown in Fig. 1. For identical ions, resonant interaction leads to the splitting of excited state of the pair into "pure" optically bright and optically dark states. (The latter does not interact with light in a dipole approximation and hence is (almost) decoherence-free). When interacting ions are non-identical, the picture is much more complicated, and different superpositions of bright – dark states, having interesting for the Quantum Information Processing properties, are created.

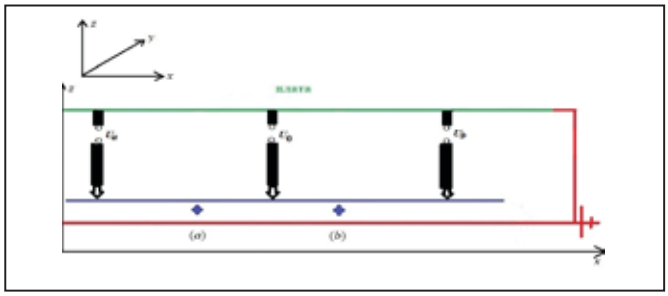

Fig. 1 A building block element of the proposed quantum network

In our approach, exactly this aforementioned (nano)local Stark shift is used as a factor introducing required controllable non-identity of ions. SPM tip is quite sharp (with the radius of curvature of up to a few nm and even better), which enables to "tune" the wavelength of the optical transition of RE ion in many crystals up to 50 MHz [1]. The peculiarities of pair centers of RE ions in crystals (e.g. their Kramers or non-Kramers nature) also should be taken into account.

References

[1] S.K. Sekatskii, M. Chergui, and G. Dietler, "Coherent fluorescence resonance energy transfer: construction of nonlocal mukltiparticle entangled states and quantum computing", Europhys. Lett., vol. 63, pp. 21-27, 2003.

[2] D. Petrosyan and G. Kurizki, "Scalable solid-state quantum processor using subradiant two-atom states", Phys. Rev. Lett., vol. 89, p. 207902, 2002.

Fluorescent nanostructures for targeted biological visualization

E. A. Mordovina, D. V. Tsyupka, A. A. Bakal, A. M. Abramova, O. A. Goryacheva, I. Yu. Goryacheva
Saratov State University, Saratov, Russia

Abstract— The fluorescent properties of products obtained by the hydrothermal treatment of organic raw materials are of great interest. Such products usually have high colloidal stability in water and photostability, as well as low cytotoxicity. One of their advantages is the wide range of starting materials and the relative simplicity of synthesis. The use of folic acid as a precursor for fluorescent nanostructures opens up the possibility of targeted imaging. This work shows a one-step scheme for the synthesis of fluorescent nanostructures from folic acid and citrates, as well as the effect of the citrate on the optical properties of the obtained particles.

Keywords—fluorescent nanostructures, one-step synthesis, hydrothermal synthesis, folic acid, citric acid, biological imaging.

I. Introduction

Folic acid (FA) is involved in many biological processes, which determines its vital necessity. Cells metabolize FA using specific folate receptors. FA molecules interact with receptors is via a pterin fragment [1]. As it is known, the activity of folate receptors of cancer cells is significantly higher than that of healthy ones [1,2], which allows the use of FA as a targeting ligand. As a result of the functionalization of various carriers with FA, were developed magnetic-resonance contrast agents [3,4], radiopharmaceutical imaging agents [5], chemotherapy [6], etc. Obtaining such systems is usually a difficult task; therefore, it is necessary to develop new approaches to the synthesis.

As a result of hydrothermal treatment of FA, the initial molecule partially destructs, while the pterin fragment of the molecule remains unchanged, which makes it possible to further use it for targeted fluorescence imaging. Hydrothermal co-treatment of FA and other organic precursors can lead to the formation of structures that are sensitive to folate receptors and possess the necessary properties (e.g., intense fluorescence) [7].

II. Results and Discussion

Fluorescent nanoparticles were obtained by the hydrothermal co-treatment of FA and citrates (citric acids (CA) and sodium citrate) [7]. The concentration of citrates ranged from 0.05 to 2 mol/L, concentration of FA was constant (10^{-3} mol/L).

The obtained samples have bright fluorescence in the blue-green region of the spectrum (fig. 1).

An increase in the concentration of CA leads to an increase in emission at an excitation wavelength of 410 nm, which indicates the presence of several fluorescent fractions.

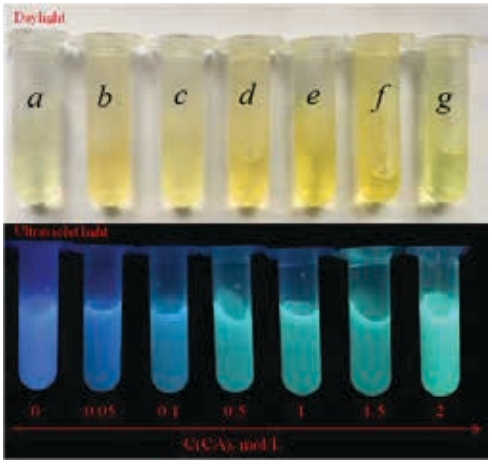

Fig. 1. Image samples in daylight and ultraviolet light: a – folic acid sample (10^{-3} mol/L) without any additives, b–g – samples with citric acid additives 0.05, 0.1, 0.5, 1, 1.5, and 2 mol/L, respectively

Acknowledgment

The work was supported by RSF, project 21-73-10046.

References

[1] Bhalerao, K.D. A folic acid-based functionalized surface for biosensor systems / K.D. Bhalerao, S.C. Lee, W.O. Soboyejo and A.B.O. Soboyejo // J. Mater. Sci. Mater. Med. – 2007. – Vol. 18, № 1. – P. 3–8.

[2] Chen, C. Structural basis for molecular recognition of folic acid by folate receptors / C. Chen, J. Ke, X.E. Zhou, W. Yi, J.S. Brunzelle, J. Li, E.L. Yong, H.E. Xu, and K. Melcher // Nature. – 2013. – Vol. 500, № 7463. – P. 486–489.

[3] Cheng, Z. Gadolinium-Conjugated Dendrimer Nanoclusters as a Tumor-Targeted T1 Magnetic Resonance Imaging Contrast Agent / Z. Cheng, D.L.J. Thorek and A. Tsourkas // Angew. Chem. – 2010. – Vol. 122. – P. 356–360.

[4] Konda, S.D. Specific targeting of folate-dendrimer MRI contrast agents to the high affinity folate receptor expressed in ovarian tumor xenografts / S.D Konda, M. Aref, S. Wang, M. Brechbiel, and E.C. Wiener // Magn. Reson. Mater. Physics, Biol. Med. – 2001. – Vol. 12. – P. 104–113.

[5] Wang, S. Synthesis, Purification, and Tumor Cell Uptake of ^{67}Ga-Deferoxamine-Folate, a Potential Radiopharmaceutical for Tumor Imaging / S. Wang, R.J. Lee, C.J. Mathias, M.A. Green, and P.S. Low // Bioconjug. Chem. – 1996. – Vol. 7, № 1. – P. 56–62.

[6] Lee, J.W. Synthesis and Evaluation of Taxol-Folic Acid Conjugates as Targeted Antineoplastics / J.W. Lee, J.Y. Lu, P.S. Low and P.L. Fuchs // Bioorg. Med. Chem. – 2002. – Vol. 10. – P. 2397–2414.

[7] Mordovina, E.A. Fluorescent nanostructures based on folic acid and citrate: Synthesis and properties / E. A. Mordovina, D. V. Tsyupka, A. A. Bakal, A. M. Abramova, I. Yu. Goryacheva // Izvestiya of Saratov University. Physics – 2021. – Vol. 21. P. 285–292.

Modeling the formation of self-catalyzed GaAs and GaP nanowires

A.A.Koryakin[1]
[1]St. Petersburg State University, St. Petersburg, Russia

Abstract — We present a theoretical model to depict the formation of self-catalyzed GaAs and GaP nanowires. The growth regimes of monolayer on the nanowire top facet are investigated.

Keywords— III-V nanowires; VLS growth

Owing to the recent development of in-situ TEM (transmission electron microscopy) techniques of III-V nanowire (NW) growth the growth mechanisms of III-V nanocrystals have attracted increasing attention [1]. In this paper, we use the model of self-catalyzed NW growth [2] to investigate the growth regimes of monolayer (ML) on the NW top facet. The nucleation-limited growth rate of NW which is calculated within the framework of the classical nucleation theory is considered. It is also assumed that the ML growth proceeds via the volume diffusion mechanism and that the group V fluxes limit the ML growth. The nucleation statistics and the faceting of the NW top facet are not considered.

To investigate the growth regimes of GaAs and GaP ML having the zincblende structure we calculate the dependences of group V content in the droplet on the growth time. ML growth cycle at different growth conditions is shown in Fig. 1 and Fig. 2. The values of the model parameters used are the same as in [3] (β=125° is droplet contact angle, α_V=30° is the angle between the direction of the direct group V flux and the substrate normal, the interphase energy γ=0.394 Jm^{-2} for GaAs and γ=0.47 Jm^{-2} for GaP; the NW radius equals 20 nm). It is seen that at high group V fluxes, the ML growth proceeds via the fast growth regime (limited by volume diffusion). In the opposite case, both the fast growth regime and the slow growth regime (limited by vapor fluxes) can be realized. The dependences for GaAs and GaP are qualitatively the same. The difference is that the desorption flux of phosphorus is higher than that of arsenic, however, the solubility of phosphorus in gallium is lower than that of arsenic. As a result, the slow growth regime is more likely to be realized in the GaP system. At a high temperature, the droplet refilling stage can take a very long time due to the high desorption of group V species (there is no NW growth when the desorption flux is equal to the total group V flux). Also, as seen from the figures, the ML growth rate is higher for GaAs. It should be noted that the duration of the droplet refilling stage is sensible to the diffusion coefficients of group V in gallium. Unfortunately, the known values of these coefficients relate to very high temperatures, and, at the NW growth temperature, these quantities should be specified in further studies.

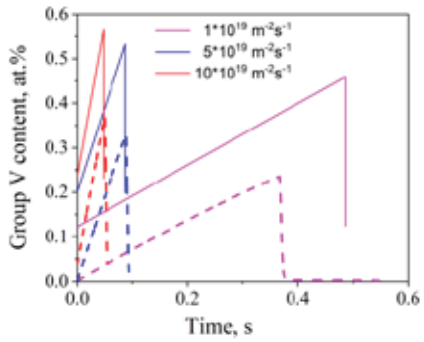

Fig.1. The dependences of the group V molar fraction on the growth time of GaAs ML (solid lines) and GaP ML (dashed lines) at different values of the total group V flux. The growth temperature is 500°C.

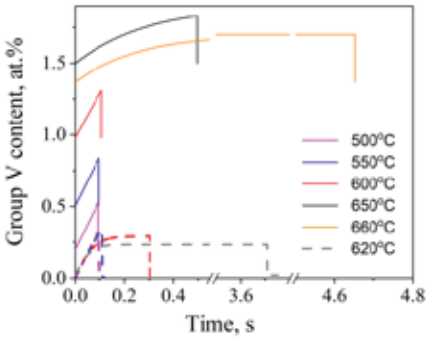

Fig. 2. The dependences of the group V molar fraction on the growth time of GaAs ML (solid lines) and GaP ML (dashed lines) at different values of the growth temperature. The total group V flux is 5·10^{19}m^{-2}s^{-1}.

ACKNOWLEDGMENT

The author acknowledges financial support of the Russian Science Foundation under the Grant 19-72-30004.

REFERENCES

[1] F. Panciera, Z. Baraissov, G. Patriarche, V.G. Dubrovskii, F. Glas, L. Travers, U. Mirsaidov, J.-C. Harmand, Nano Lett., vol. 20, pp. 1669-1675, 2020.

[2] A.A. Koryakin, S.A. Kukushkin, Phys. Status Solidi B, vol. 258, pp. 2000604, 2021.

[3] A.A. Koryakin, Y.A. Eremeev, S.V. Fedina, V.V. Fedorov, Tech. Phys. Lett., vol. 48, pp. 20-23, 2022.

Optical properties of a hybrid films of J-aggregates and aluminum oxide formed on an island Ag film

I.I.Nikitin, R.D.Nabiullina, L.N.Borodina, A.A.Starovoytov, I.A.Gladskikh
School of Physics and Engineering, ITMO University, St. Petersburg, Russia

Abstract— The synthesis technique of nanoporous aluminum oxide on an island silver film has been developed. Such a structure was coated with J-aggregates and optical properties were studied for it. The transfer of optical excitation energy from oxygen vacancies of aluminum oxide to J-aggregates was observed.

Keywords—aluminum oxide; island film; plasmon; J-aggregates; nanoparticles; reflection; absorption; fluorescence

I. Introduction

The development of solid-state microlasers based on organic compounds and nanoparticles as an active medium is an urgent problem of modern photonics. The J-aggregates of pseudoisocyanine dye (PIC) characterized by the high quantum yield, which can be enhanced with plasmonic nanoparticles due to the action of the near field. Anodic aluminum oxide (AAO) is a promising matrix for the uniform distribution of the dye. In the work, the hybrid film was synthesized in successive stages: the Ag island film was deposited on substrate, then a solid layer of aluminum was deposited and anodized, then PIC was coated and its optical properties were studied.

II. Object and techniques

The island silver film of the equivalent thickness of 15 nm was obtained by vacuum thermal deposition on a quartz substrate, the was annealed on air at a temperature of 150 °C. Then, an aluminum layer of 160 nm thickness was deposited by the electron beam method. The resulting Ag/Al film was anodized for 45 seconds in 0.4 M oxalic acid. Then the Ag/AAO film was immersed in PIC saturated ethanol solution for impregnation. Then the hybrid film was dried in air at room conditions

III. Results

The absorption of the Ag/AAO film corresponds to Ag island film, while the reflection is more similar to spectrum of AAO film (Fig. 1). At the same time, the shape of the reflection spectrum of the hybrid structure may coincide with the shape for the AAO film. The wavelength of the absorption maximum and reflection minimum of the Ag/AAO are the same, due to the scattering of light in the pores of aluminum oxide. The Ag/AAO film have luminescence maximum with a wavelength of 500 nm, which was associated with the formation of F-centers of oxygen vacancies during anodizing. The comparison of the luminescence spectra of a hybrid film, Ag/AAO film and dye layer on bare substrate with excitation in the absorption bands of oxygen vacancies and J-aggregates shows the presence of a luminescence maximum at 583 nm responsible for the emission of J-aggregates, shows the transfer of optical excitation from oxygen vacancies to J-aggregates.

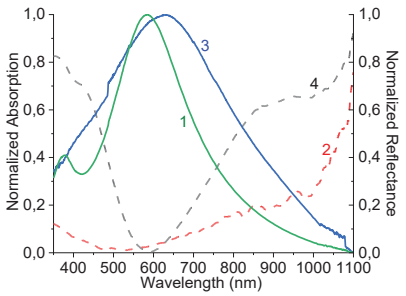

Fig. 1. Normalized spectra: absorption of the Ag island film (1), reflection of the AAO film (2), absorption (3) and reflection (4) of the Ag/AAO film

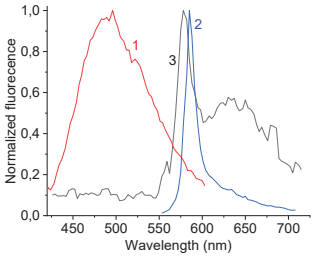

Fig. 2. Normalized luminecence spectra of the Ag/AAO (1) and hybrid (3) films with excitation wavelength of 405 nm, and dye layer on bare substrate with excitation wavelengths of 543 nm (2)

Acknowledgment

Mr. Nikitin and Ms. Nabiullina are grateful to RPMA grant of School of Physics and Engineering of ITMO University; Prof. Starovoytov and Dr. Gladskikh are grateful to Russian Science Foundation (Project 21-72-10098).

References

[1] W. Zhang, J. Yao, Y.S. Zhao, “Organic Micro/Nanoscale Lasers,” Acc. Chem. Res., vol. 49, pp. 1691-1700, 2016.

[2] A.K. Zeinidenov, N.K. Ibrayev, A.K. Aimukhanov, “The Laser Active Element Based on Dye on Porous Alumina,” Eurasian Chem.-Technol. J., vol. 16, pp. 73-78, 2014.

Optical Properties of Spinel Based Glass-Ceramics of the ZnO-Al_2O_3-Ga_2O_3-SiO_2 System Doped with Co^{2+} Ions

I.V. Glazunov[1], A.M. Malyarevich[1], K.V. Yumashev[1], O.S. Dymshits[2*], I.P. Alekseeva[2], A.A. Zhilin[2]

[1]Center for Optical Materials and Technologies, Belarusian National Technical University, 65/17 Nezavisimosty Ave., Minsk 220013, Belarus

[2]S.I. Vavilov State Optical Institute, 36 Babushkina St, 192171, St. Petersburg, Russia

Abstract. Transparent glass-ceramics containing Co^{2+}:$Zn(Al,Ga)_2O_4$ spinel nanocrystals with sizes of 6-11 nm were studied. Absorption band of the Co^{2+} ions in the material is shifted to longer wavelengths as compared with glass-ceramics with no Ga_2O_3 addition. Absorption saturation at 1.54 μm was observed and its characteristics (absorption recovery time, ground-state and excited-state absorption cross-sections) were measured. The developed glass-ceramics are promising as saturable absorbers for 1.6 μm erbium lasers.

Keywords — transparent glass-ceramics; spinel nanocrystals; absorption saturation; cobalt ions; gallium oxide

I. Introduction

Materials doped with cobalt Co^{2+} ions placed in tetrahedral sites are well known as saturable absorbers for lasers emitting in 1.3-1.6 μm spectral region (see e.g. [1]). For this purpose saturation of absorption in the band related to the $^4A_2(^4F)\rightarrow{}^4T_1(^4F)$ transition of tetrahedrally coordinated Co^{2+} ions is used. Among such materials Co^{2+}:$MgAl_2O_4$ spinel single crystal is the most widely applied for passive Q-switching of erbium glass lasers emitting at 1.54 μm.

Spectral region of 1.5-1.7 μm attracts attention for range-finding, environmental sensing, telecom applications, etc. due to low propagation losses of light in the atmosphere and silica fiber. Several crystalline materials doped with Er^{3+} ions were recently developed as laser ones with emission wavelengths in the 1.6-1.7 μm spectral region (see e.g. [2]). For such lasers passive Q-switching with Co^{2+}:$MgAl_2O_4$ spinel single crystal is not very efficient. This is due to low absorption in the range of the $^4A_2(^4F)\rightarrow{}^4T_1(^4F)$ transition of Co^{2+} ions and consequently, low saturable absorption contrast at the lasing wavelength. Therefore, new materials containing Co^{2+} ions with high absorption in the range of 1.6-1.7 μm are needed.

Spectral properties of transition metal ions are sensitive to their surrounding, and this is used to adjust position of the absorption bands by designing the proper environment of the transition metal ion. Therefore, if the addition of gallium oxide (in our case) to the composition of the initial zinc aluminosilicate glass results in crystallization of the gallium-containing gahnite spinel, such material will provide a desired spectral shift of the Co^{2+} absorption band to longer wavelengths.

II. Samples Preparation

Initial glass of the composition 25 ZnO, 23 Al_2O_3, 2 Ga_2O_3, 50 SiO_2, (mol%) nucleated by 7 mol% TiO_2 and doped with 0.1 wt% CoO, both added above 100% of the base composition, was prepared from the reagent grade raw materials. The glass was melted in a laboratory furnace with Globar heating elements at temperature T of 1580 °C for 6 h. Then the initial transparent violet-colored glass was cut into pieces and heat-treated in the muffle furnace by two-stage heat-treatments with the first hold at 720 °C and the second hold in the temperature range of 750-1000 °C. Transparent glass-ceramics contained crystals of $Zn(Al_xGa_{1-x})_2O_4$ solid solutions with spinel structure with sizes of 6-11 nm and the lattice parameter *a* ranging from 8.107 to 8.130 Å. The zinc aluminogallate nanocrystals were homogeneously distributed within the highly silicate residual glass.

III. Absorption Saturation

Typical experimental data on initial absorption recovery after power light excitation demonstrates monoexponential nature with relaxation time τ=790±10 ns for the glass-ceramic prepared by heat-treatment at 1000 °C.

The experimental data on dependence of transmission of the glass-ceramics at λ=1.54 μm on the input energy fluence was modelled with a slow saturable absorber model. This is due to the characteristic recovery time for Co^{2+} ions is few hundreds of ns (see e.g. [3]) that is much longer than the duration of the excitation pulse (70 ns in our case).

The best fitting curve results for ground-state absorption cross-section, σ_{GSA} are $(2.5 – 2.6)\times10^{-19}$ cm^2 for glass-ceramics prepared by the heat-treatment at 850 and 900 °C. The absorption saturation contrast, $\sigma_{GSA}/\sigma_{ESA}$ increases from 3 (for T = 800 °C) to 12.5 (for T = 1000 °C)

References

[1] M.B. Camargo, R.D. Stultz, M. Birnbaum, "Co^{2+}:YSGG saturable absorber Q switch for infrared erbium lasers", Opt. Lett., vol. 20, 1995, pp. 339–341.

[2] K.N. Gorbachenya, V.E. Kisel, A.S. Yasukevich, A.A. Pavlyuk, N.V. Kuleshov, "In-band pumped room-temperature Er:$KY(WO_4)_2$ laser emitting near 1.6 μm", Laser Phys., vol. 23, 2013, pp. 125005-125009.

[3] I.A. Denisov, Yu.V. Volk, A.M. Malyarevich, K.V. Yumashev, O.S. Dymshits, A.A. Zhilin, U. Kang, K.-H. Lee, "Linear and nonlinear optical properties of cobalt-doped zinc aluminum glass ceramics", J. Appl. Phys., vol. 93, 2003, pp. 3827-3831.

High-speed video recording of liquid melt spraying during ablation of the Y_2O_3 target using a fiber ytterbium laser.

V.V. Osipov[1], G.S. Evtushenko[3], V.V. Platonov[1], E.V. Thikhonov[1], M.V. Kremenetskii[1], N.A. Vasnev[2], P.I. Gembukh[2], M.V. Trigub[2].

[1] Institute of Electrophysics of the UB of the RAS, Yekaterinburg, Russia

[2]Institute of New Materials and Technologies, Ural Federal University named after the first President of Russia B. N. Yeltsin, Yekaterinburg, Russia

3 - Federal Research Centre for Projects Evaluation and Consulting Services, Moscow, Russia

Abstract— A Highspeed video shooting of liquid melt splashing during the ablation of Nd:Y2O3 target with the ytterbium fiber laser was made. Using the CuBr laser monitor for shooting allowed to eliminate bright laser plasma luminescence on pictures and to see splashing of drops right from the target crater. The splashing of liquid melt is a difficult hydrodynamic process. Usually the melt splashes out in separate jets, splitting into droplets already in the air, but sometimes single droplets form immediately.

Keywords— laser ablation, nanopowder, fiber ytterbium laser, splashing of melt droplets, projection laser microscope (laser monitor).

I. Introduction

The laser method for obtaining weakly agglomerated oxide nanoparticles with average dimensions of 10-20 nm consists in laser evaporation of a target of the required composition and in the formation of nanoparticles during vapor condensation in a gas flow.

By using powerful ytterbium fiber laser (λ=1,06 um) it's possible to get nanopowder in amount of several kilograms. However, the productivity of making nanopowder can strongly decrease because of splashing of numerous melt droplets with size 10-100 um. [1].

In this work, the splashing of the melt during ablation of a target made of Nd:Y_2O_3 in air by a fiber laser LS-07H radiation using high-speed video recording is investigated. The observation of the dynamics of the melt spraying is complicated by the very bright glow of vapor in a laser plume. The use of a laser monitor based on a brightness amplifier based on CuBr vapor for shooting made it possible to eliminate the influence of illumination and observe the splashing of the melt directly from the crater with a large optical magnification.

II. Results and discussion

In our experiments, the same experimental setup was used as in [2]. However, now the video was taken with a large optical magnification, which allowed us to study the formation of droplets in more detail. Shooting frequency of AOS Q-PRI camera was 22 kHz. Single radiation impulses of fiber laser were focusing on the target by lens with the focus F= 400 mm under 45° and 90°.

Usually, the melt is sprayed by separate jets, which are divided into droplets in the air. Sometimes single drops are sprayed. At a pulse duration of 1300 μs, radiation power P=670 W (I=0.46 MW/cm^2), melt splashing begins 70–200 μs after the start of target evaporation. When the radiation power decreases to a value of P=260 W (I=0.18 MW/cm^2), the delay increases to 570÷850 μs. Finally, the radiation power P=205 W (I=0.14 MW/cm^2) turns out to be close to the threshold value for a given pulse duration. Under these conditions, in half of the cases, the melt did not have time to spray. After the end of the laser pulse, the surface of the melt quickly calmed down and solidified in the form of a breastwork. In one case only single droplet was formed with the delay of 60±23 μs. In this way, the splashing of liquid melt is a difficult hydrodynamic process which has threshold nature. Probably, there are several mechanisms of droplets splashing and it requires additive theoretical researches to establish them.

Acknowledgment

The work was performed as part of State Task № AAAA—A19-119020790031-5, was supported in part by RFBR Grant № 20-08-00054 A.

References

[1] V.V. Platonov, E.A. Kochurin, V.V. Osipov, V.V. Lisenkov, N.M. Zubarev / Characteristic properties of laser ablation of translucent targets // Laser Physics, 2018, vol. 28, article number 076002

[2] V.V.Osipov, G.S.Evtushenko, V.V.Lisenkov, V.V.Platonov, A.V.Podkin, E.V.Tikhonov, M.V.Trigub, K.V.Fedorov / Laser plume evolution in the process of nanopowder preparation using an ytterbium fibre laser // Quantum Electronics, 2016, vol.46, N9, pp.821–82

Synthesis and properties of luminescent carbon nanostructures/SiO_2 composites

Yu. A. Podkolodnaya, A.A.Kokorina, I.Yu. Goryacheva
Saratov State University, 83 Astrakhanskaya Street, Saratov, 410012, Russia

Abstract - We have developed a method for the synthesis of carbon nanostructures/SiO_2 composite nanoparticles. The obtained composites have luminescent properties, colloidal stability, and are promising as markers for immunochemical analysis.

Keywords— luminescent composite particles; carbon nanostructures; luminescent carbon-based nanomaterials; silica nanoparticles; luminescence

I. Introduction

Nowadays, many scientific groups have a great interest in the development of carbon-based nanomaterials due to their optical properties, structural features, and a large variety of possible applications [1,2]. However, current synthetic ways lead to obtaining CNSs as a mixture of different structures with various properties. The known techniques for the CNSs' purification and fractionation in some cases are ineffective, multistage, and costly [3]. This problem can be solved by using a matrix for CNSs. In this work, we reported the facile hydrothermal method for the synthesis of luminescent composite nanoparticles from carbon nanostructures/SiO_2.

II. Synthesis and properties of luminescent composite nanoparticles

In this work, we reported the facile hydrothermal method for the synthesis of luminescent composite nanoparticles. The silica nanoparticles with surface amino and carboxyl groups were prepared by the reversed microemulsion method. The obtained silica nanoparticles were hydrothermally treated with citric acid. As a result of the synthesis were obtained luminescent composite nanoparticles. The scheme of the proposed process is shown in Figure 1 A. The use of the matrix agents leads to an increase in the PL signal, since the PL intensity of several CNSs is higher than the intensity of a single structure. We used dialysis to purification luminescent composite nanoparticles from unreacted components. Figure 1 B, C shows the absorption, photoluminescence, and normalized spectrum photoluminescence after dialysis.

The resulting composite nanoparticles had the maximum luminescence in the region of 450 nm with a quantum yield of 53±4 %. The average size of luminescent composite nanoparticles was (43±2) nm, polydispersity index (0.17±0.01), zeta potential (-27±2) mV. The resulting composite nanoparticles meet the basic requirements for markers in immunochemical analysis: they are characterized by a high PL signal; colloidal and chemically stable; the surface of nanoparticles is rich in functional groups necessary for subsequent conjugation.

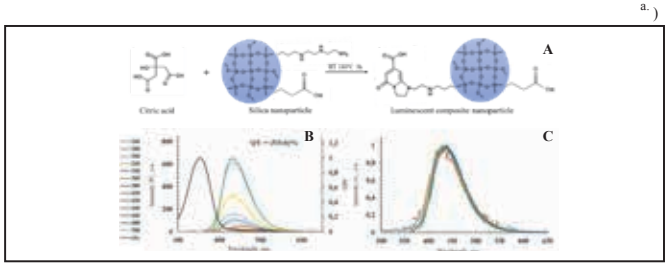

Fig. 1. Scheme of formation of luminescent composite nanoparticles (A), absorption spectrum, photoluminescence (B) and normalized photoluminescence spectrum (C) of luminescent composite nanoparticles after dialysis

Acknowledgment

This work was supported by the Russian Science Foundation (grant 20-13-00195).

References

[1] A. A. Kokorina, E. S. Prikhozhdenko, G. B. Sukhorukov, A. V. Sapelkin, I.Y. Goryacheva, "Luminescent carbon nanoparticles: synthesis, methods of investigation, applications," Russian Chemical Reviews, vol. 86(11), pp. 1157-117, 2017.

[2] I. Y. Goryacheva , A. V. Sapelkin, G. B.Sukhorukov, "Carbon nanodots: mechanisms of photoluminescence and principles of application," TrAC Trends in Analytical Chemistry. vol. 90, pp. 27-37, 2017.

[3] A. A. Kokorina, A. V. Sapelkin, G. B Sukhorukov, I. Y. Goryacheva , "Luminescent carbon nanoparticles separation and purification," Advances in colloid and interface science, vol. 274, p.102043, 2019.

Quantum dots for control the concentrations of anthracycline antibiotics.

Goryacheva O.A.[1], Drozd D.D. [1,], Ponamareva T. S.[1]

[1]Chemistry Institute, Department of General and Inorganic Chemistry, Saratov State University, Saratov, Russia

Abstract - Quantum dots (QDs) can be an optimal material for creating systems for determining the residual concentration of anthracycline antibiotics in blood, urine and tissues to optimize the dosage of chemotherapy drugs. The selection of the optimal composition of the structure and surface of QDs allows to achieve the best energy transfer and, as a result, the most reliable analytical system

Keywords— Quantum dots, quenching, electron transfer, surface modification, mitoxantrone

I. Introduction

Quantum dots are semiconductor nanocrystals that actively replace standard fluorescent dyes in bionalysis and medicine. Ability to change fluorescence wavelength, high chemical and physical stability. as well as the ability to change the surface of the crystal simplifies interactions with biological molecules and pharmaceuticals. QDs are capable of nonradiative energy transfer and can be both an acceptor and an energy donor. Analytical systems based on the photoinduced electron-transfer mechanism use QDs as an energy donor. The analyte is an acceptor of energy and the recognition of the target molecule will be shown as quenching QDs fluorescence [1].

Mitoxantrone (MTX) is used to treat certain cancers and multiple sclerosis. Its dosage is mainly based on the patient's body volume and results in a large excess of the drug with a high cytostatic effect. However, the development of targeted delivery has led to the need to monitor the working concentrations for each type of tumor. MTX is unstable, easily oligomerized and attached to biological molecules in difficult matrixes[2]. It makes it difficult to use classical methods.

The fluorescence of QDs decreases when MTX is attached to its surface. We select the composition, structure and surface of QDs for the best quenching of fluorescence in the presence of MTX.

II. Methods

A. AgInS2/ZnS QDs syntheis

Hydrophilic QDs AgInS2/ZnS with emission in the range from 500 to 750 nm were synthesized during One-pot synthesis in aqueous solutions by a two-stage procedure to obtain core-shell structure. The fractionation were used for the segmentation of QDs according to the size and color of fluorescence[3].

B. CdSe/CdS and CdSeS/ZnS QDs syntheis

Synthesis of core/shell QDs by high-temperature organic synthesis with subsequent surface passivation with a wider-gap semiconductor[4][5].

III. Results

Three types of QDs, differing in composition, peak shape and width, wavelength and fluorescence intensity were obtained to consider the optimal structures as an energy acceptor for the MTX molecule (fig. 1).

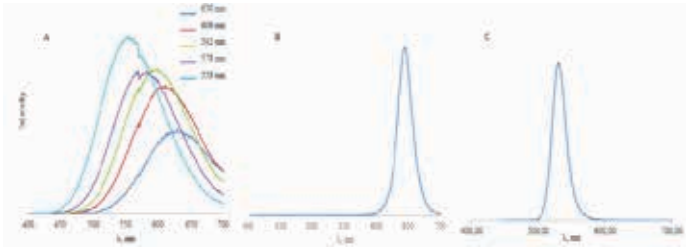

Fig. 1. Fluorescence intensity and peak position of A) AgInS/ZnS, B) CdSe/CdS, C) CdSeS/ZnS QDs

Acknowledgment

This research was funded by the Russian Science Foundation, grant number 21-73-10046.

References

[1] O.A. Goryacheva, N. V. Beloglazova, I.Y. Goryacheva, S. De Saeger, Homogenous FRET-based fluorescent immunoassay for deoxynivalenol detection by controlling the distance of donor-acceptor couple, Talanta. 225 (2021) 121973.

[2] M. Enache, A.M. Toader, Insights Into Molecular Interaction of Antitumor Drug Mitoxantrone With Anionic Surfactant Sodium Dodecyl Sulfate at Different Temperatures, J. Surfactants Deterg. 21 (2018) 31–41..

[3] A.S. Novikova, T.S. Ponomaryova, I.Y. Goryacheva, Fluorescent AgInS/ZnS quantum dots microplate and lateral flow immunoassays for folic acid determination in juice samples, Microchim. Acta. 187 (2020) 1–9.

[4] O.A. Goryacheva, C. Guhrenz, K. Schneider, N. V. Beloglazova, N. V. Beloglazova, I.Y. Goryacheva, S. De Saeger, N. Gaponik, Silanized Luminescent Quantum Dots for the Simultaneous Multicolor Lateral Flow Immunoassay of Two Mycotoxins, ACS Appl. Mater. Interfaces. 12 (2020) 24575–24584.

[5] D.D. Drozd, P.S. Pidenko, K.Y. Presnyakov, P.D. Strokin, E.S. Speranskaya, I.Y. Goryacheva, Dihydrolipoic acid coated alloyed quantum dots, in: V. V. Tuchin, E.A. Genina (Eds.), Saratov Fall Meet. 2019 Opt. Nano-Technologies Biol. Med., SPIE, 2020: p. 60.

Phase Composition Study of the AgBr – AgI – TlBr – TlI System for the Infrared Materials Creation

D.D.Salimgareev[1], A.E.Lvov [1], A.A.Yuzhakova[1], D.A.Belousov[1], A.S.Korsakov[1], L.V.Zhukova[1]
[1]Ural federal university named after the first President of Russia B. N. Yeltsin. 19 Mira str., Ekaterinburg 620002, Russia

Abstract— AgBr – AgI – TlBr – TlI isothermal cross section of the Ag – Tl – Br – I concentration tetrahedron has been studied. Inside cross section concentration regions are marked, where both single crystals and optical nanoceramics can be synthesized. In the obtained regions, single crystals of various compositions, as well as optical nanoceramics transparent in the infrared and terahertz ranges, were synthesized.

Keywords— silver and thallium halide, single crystal, optical ceramics, infrared range, terahertz range

I. Introduction

To date, a limited number of optical materials for the infrared (IR) and terahertz (THz) spectral regions is known. For the infrared range, chalcogenide (transmission range 0.62 - 25.0 μm) and fluoride (from 0.2 to 7.0 - 12.0 μm) glasses, ceramics based on borates and aluminum-magnesium spinels and some other materials are known. For the terahertz range (0.1 - 10 THz), the number of materials is even narrower and is limited to high-resistance silicon, crystalline quartz, sapphire, and some polymers. However, there are materials that are transparent in the visible, infrared and terahertz ranges. Such optical materials are crystals and optical nanoceramics based on silver and thallium (I) halides of the system AgBr - AgI - TlBr - TlI [1].

II. Phase Diagram Investigation

The phase diagrams of the systems AgBr – TlI, AgBr – $TlBr_{0.46}I_{0.54}$, AgBr – AgI and $TlBr_{0.46}I_{0.54}$ – AgI were studied. The isothermal section AgBr – AgI – TlBr – TlI of the concentration tetrahedron of the four-component system Ag – Tl – Br– I was constructed from these diagrams (Fig. 1). It has been found that single crystals with the Fm3m and Pm3m structure can be grown in the orange and bright red regions, respectively. Here the least influence of foreign phases with the R-3 structure, including chemical compounds Tl_2AgBr_3, $TlAgI_2$, Tl_2AgI_3 and their derivatives, is observed [1]. The influence of these compounds can be minimized by varying the synthesis modes, as a result of which stable solid solutions can be obtained. For the AgBr – TlI system, the stable solid solutions are observed from 0 to 20 and from 67 to 98 mol. % TlI in AgBr, for the system AgBr - $TlBr_{0.46}I_{0.54}$ from 0 to 31 and from 83 to 100 mol. % $TlBr_{0.46}I_{0.54}$ in AgBr, in the AgBr – AgI system from 0 to 40 mol. % AgI in AgBr, and in the system $TlBr_{0.46}I_{0.54}$ – AgI from 0 to 18 mol. % AgI in $TlBr_{0.46}I_{0.54}$. However, beyond these compositions, the influence of foreign phases becomes more significant. In view of this, single crystals (with the Fm3m structure) and crystalline ceramics for optics (Fm3m + R-3) can be obtained in the yellow region. Single crystals (Pm3m) and crystalline ceramics with the Pm3m + R-3 structure type can be obtained in the red region.

This work was supported by the Russian Science Foundation (No. 21-73-10108), https://rscf.ru/en/project/21-73-10108/.

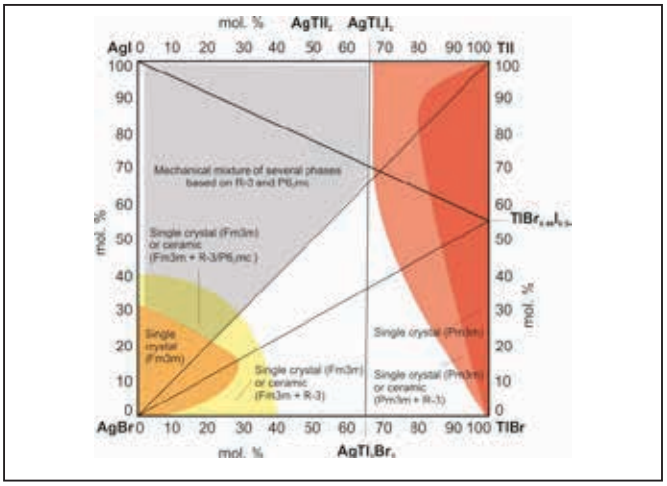

Fig. 1. AgBr – AgI – TlBr – TlI isothermal cross section of the Ag – Tl – Br – I concentration tetrahedron

The variation of the crystalline modification (crystal or ceramic) occurs due to the synthesis modes, ranging from obtaining a high-purity raw materials by the method of thermozone crystallization-synthesis (TZKS) and ending directly with the growth of single crystals or the synthesis of optical ceramics. In particular, the growth of single crystals is possible when a high degree of mixture homogeneity is achieved and the optimal growth modes with lower crystallization rates are selected. These measures make it possible to minimize the probability of the formation or incorporation of an orthorhombic phase (R-3). Also they make it possible to push the doping orthorhombic phase into the crystal's cap or to its periphery. Further, the formed R-3 phase is removed mechanically. The same is true in the opposite direction.

It should be noted that the choice of material type is determined by the requirements for transparency, hardness, strength, as well as the technological features of their production. The possibility of obtaining both crystals and ceramics from the same chemical composition makes it possible to optimize the process of manufacturing optical products for a specific applied task, making it economical, environmentally friendly and resource-saving.

References

[1] L. V. Zhukova, D. D. Salimgareev, A. E. Lvov, A. A. Yuzhakova, A. S. Korsakov, D. A. Belousov, K. V. Lipustin, V. M. Kondrashin, " Highly transparent ceramics for the spectral range from 1.0 to 60.0 μm based on solid solutions of the system AgBr-AgI-TlI-TlBr," Chin. Opt. Lett. vol. 19, iss. 2, pp. 021602, 2021.

Using the steepness of the localized surface plasmon resonance phase response for highly sensitive detection of molecular binding events

J.P. Cuanalo-Fernández[1], J.A. Urrutia-Anguiano[2], S.F. Guerra-Hernández[1], N. Korneev[1], M.B. De-la-Mora-Mojica[3], A. Reyes-Coronado[2], I. Cosme-Bolaños[1], S. Mansurova[1] and R. Ramos-García[1],

[1]Dep. Óptica, INAOE, Puebla, México.
[2]Dep. Física, Facultad de Ciencias, UNAM, Ciudad de México, México.
[3]Dep. micro y nanotecnologías, Instituto de Ciencias Aplicadas y Tecnología, UNAM, Ciudad de México, México.

Abstract— This study demonstrated the capabilities of method which uses the steepness of the localized surface plasmon resonance phase response for sensing of molecular binding event.

Keywords— Localized Surface Plasmonic Resonance; gold nano-island.

I. Introduction

It is well known [1], that surface plasmon resonance (SPR) phase interrogation can - under optimal condition - provide orders of magnitude better sensitivity than intensity or wavelength interrogation. In addition, phase interrogation based on surface plasmon resonance interferometry opens up the possibilities for the sensors that combine both ultra-high sensitivity and wide dynamic range. As it was pointed out in pioneering work of Nikitin et al. [2], phase dependence extracted from interferometric measurements offers three information sources and, respectively, three levels of sensitivity. The lowest sensitivity can be realized by the measurement of a resonance wavelength shift just as it is usually done in the traditional SPR sensors. An intermediate level of sensitivity relates to the steepness of phase jump at resonance. The highest sensitivity is provided by the monitoring of the phase jump inversion which occurs around the optimal resonance conditions. However, the highest sensitivity mode is difficult to achieve in practice because of tough tuning requirement needed to reach the optimal regime and - once it is achieved - high signal instability. This study demonstrated the capabilities of method which uses the steepness of the localized surface plasmon resonance phase response for sensing of molecular binding event.

II. Results

LSPR transducer was fabricated by magnetron sputtering deposition of Au nanofilms on a top of a glass substrate, Followed by a thermal annealing at 580°C for 3 hours. As a result, randomly distributed Au nanoislands (AuNI) were obtained. LSPR was excited in AuNI by evanescent wave in attenuated total internal reflection configuration. Common path spectral interferometer detection scheme was used to analyze LSPR phase response. The differential phase between s and p polarization components was recovered from a spectral interferogram in real time using a homemade LabVIEW interface. The sensitivity data to the molecular binding event were obtained using electrostatic sequential layer-by layer self-assembly of alternatively charged polymers – poly(allylamine hydrochloride) (PAH) and poly(sodium 4-styrenesulfonate) (PSS) – resulting in multilayers of defined thickness and number. Fig 1 shows the experimental dependence of resonance wavelength position and phase slope versus the number of molecular layers N. It is seen, that resonance wavelength dependence is non-linear: it grows with the increasing N, reach a maximum and then decrease. On its turn, the slope of the phase at resonance grows linearly at low and then starts to saturate.

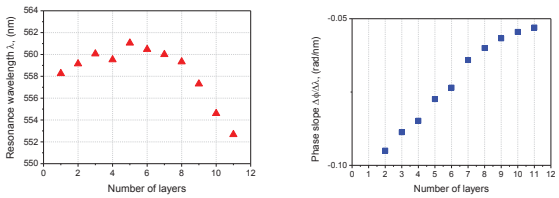

Figure 1a) Resonance wavelength position and b) phase slope vs. number of molecular layers deposited on top of AuNI

III. Conclusions

In conclusion, experimental comparison between conventional wavelength interrogation and the method which uses the steepness of the localized surface plasmon resonance phase response was performed.

References

[1] A. V. Kabashin et al., *Opt. Express*, vol. 17, no. 23, p. 21191, Nov. 2009.

[2] P. I. Nikitin et al., Sensors Actuators B Chem., vol. 54, no. 1–2, pp. 43–50, Jan. 1999, doi: 10.1016/S0925-4005(98)0032

The modeling of the “dry” foam laser probinge

A. V. Pantyukov[1], E. A. Isaeva[1], A. A. Isaeva[1], D.A. Zimnyakov[1]
[1]Yuri Gagarin State Technical University of Saratov, Saratov, Russia

Abstract—A software package for constructing the structure of "dry" foams and foam-like materials was developed. The possibility of the evaluation of the cell morphology is realized. This knowledge is necessary to determine the system stability and its internal dynamics. The limits of developed software application were also analyzed.

Keywords—foam-like materials, foam evolution, Monte Carlo method, optical probing

I. Introduction

The foams and foam-like porous media are of great interest because of the wide application of such materials in different technical and biomedicine applications. The functionality of the foam-like materials depends on the morphological parameters of the internal structure. The actual approaches to study the three-dimensional structure of foam-like media are optical and acoustic methods. But the internal dynamics and complexity of the structure make it difficult to analyze the results of the optical and acoustic probing of such media. A detailed model of such media could simplify the analysis of their morphological properties. A software package been developed for constructing the structure of "dry" foams and foam-like porous materials. It allows us to directly evaluate the morphological parameters of the medium model cells and simulate the scattering of laser radiation.

Such studies play an important role for the development of the methods for the diagnostic of the morphological and functional characteristics of nonstationary systems, for the problems of creating functional materials with determined properties, in particular, for the creating the optimal technologies for the synthesis of highly nanoporous materials for the regenerative medicine and tissue engineering.

II. Foam-like medium model

At the initial stage, the dimensions of the system, the number of cells and their morphological parameters are set. Coordinates of the centers of future cells are randomly generated to build foam cells and distribute them in the system with the help of repulsive forces. The cell faces are defined as tangent planes taking into account the thickness of the Plateau channel. The input parameters regulate the morphology of the resulting cells. It allows us to directly evaluate the morphological parameters of the medium model cells (for example, angular and dimensional characteristics, volume and surface area).

The constructed cell shapes of the foam-like medium correlates with the data of literary sources (fig. 1). The results of the simulation of the laser radiation scattering by the Monte Carlo method through a foam-like medium can be compared with the experiment results.

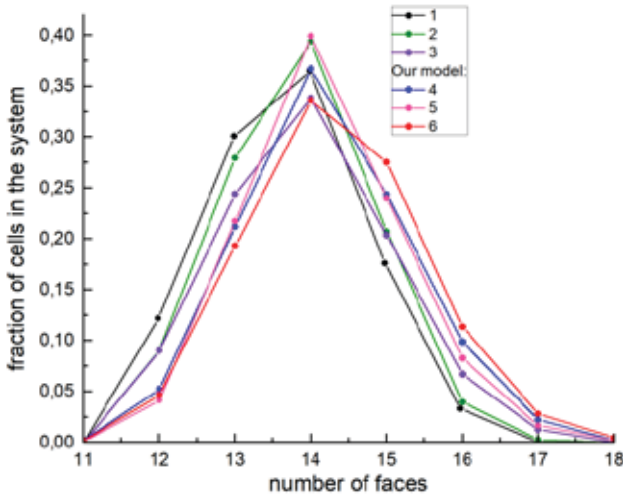

Fig. 1. Distribution of cells with number of faces. 1 – Matzke experiment[1], volume fraction if the cells are spheres: 2 – 64% R-RCP[2], 3 – 36% R-RSA[2]. 4 – 36%, 5 – 50%, 6 – 64%.

Acknowledgment

The research is supported by grant of the Russian Science Foundation (project № 21-79-00051, https://rscf.ru/en/project/21-79-00051/)

References

[1] E.B. Matzke, Am. J.Botany 33, 58 (1946)

[2] A.M. Kraynik, D.A. Reinelt, Frankvan Swol "Structure of random monodisperse foam" // Physical Review E 67, 031403 (2003)

Funding: grant of the Russian Science Foundation (project №21-79-00051)

Laser-induced optical chirality in planar plasmonic nanostructures

D.R. Dadadzhanov[1],*, N.A. Toropov[1, 2], A.A. Starovoytov[1], R.A. Zakoldaev[1], G. Alexan[1], A.A. Gladskikh[1], T.A. Vartanyan[1] and I.A. Gladskikh[1]
[1]School of Physics and Engineering, ITMO University, St. Petersburg, Russia
[2]Living Systems Institute, University of Exeter, Exeter EX4 4QD, United Kingdom
*e-mail: daler.dadadzhanov@gmail.com

Abstract— Demonstration of optical chirality in plasmon nanostructures made of silver on a dielectric substrate prepared by subsequent annealing and laser treatments was shown for the first time.

Keywords— silver nanoparticles, chirality, plasmonics, circular dichroism, spectral hole burning

I. Introduction

Circular dichroism (CD) spectroscopy is a powerful technique that allows distinguishing the enantiomers of chiral molecules and revealing of chiral nanoparticles [1]. The chiral dissymmetry in biological molecules can be explored by measuring of the difference between the left and right circularly polarized light absorption. This chiral-optical effect has found its way into pharmaceuticals and plays a decisive role there since living cells can specifically uptake only a specific form of molecules, usually referred to as the L and D-isomers. In their turn, metal nanostructures also can show chiral-optical effects that can arise from either their own intrinsically chiral structure or chiral ligands that break the symmetry of achiral nanostructures. Here we report on the novel method of fabrication of supported chiral plasmonic nanostructures.

II. Method

Our method is based on the spectral hole burning technique applied to plasmonic nanostructures with the inhomogeneously broadened extinction spectra [2]. Contrary to all previous implementations of this technique, we used laser pulsed radiation with circular polarization. Laser irradiation with a certain circular polarization state selectively affects chiral nanoparticles and/or their groups with the corresponding chirality spontaneously formed in the course of deposition, leading to their heating, melting and, finally, shape-changing. Hence, the balance between the nanostructures with opposite chirality is broken and the whole ensemble becomes chiral. The proposed novel method of preparation of the chiral plasmonic nanoparticle arrays paves the new route toward new concepts and the design of novel materials for biosensing application. First, thin silver films with the mass thickness of 12 nm were formed on the quartz support by the physical vapor deposition at high vacuum. After annealing at 200° C an array of nanoparticles with sizes from 20 to 150 nm was obtained.

This work was supported by the Russian Science Foundation (Project 21-72-10098).

III. Results and Discussion

Linear and circular polarized light derived from the second harmonic of the nanosecond Nd:YAG laser (wavelength 532 nm) was used to burn spectral holes in the plasmon absorption band of silver nanoparticles arrays. Independently of the laser polarization, a clear dip in the optical density spectrum is formed. On the other hand, linear dichroism induced by linearly polarized light is much larger than that induced by the circularly polarized light. Most importantly, circular dichroism is induced solely by circular polarized irradiation (Fig.1, upper panel). Thus, the possibility to modify the spontaneously formed achiral array of metal nanoparticles into a circular dichroic film via irradiation by circular polarized light is demonstrated.

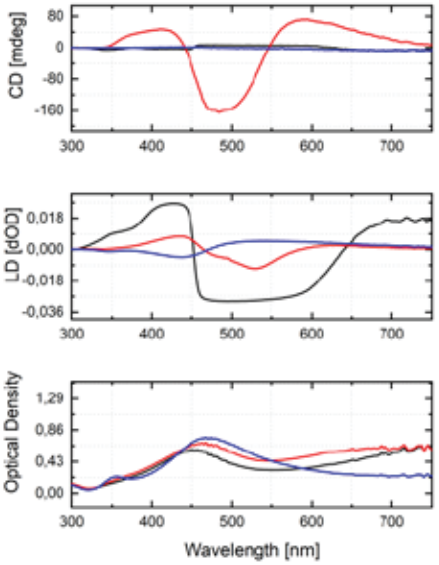

Fig. 1. Spectra of optical density, linear dichroism (LD) and circular dichroism (CD) of the prepared silver nanostructures before laser irradiation (blue curves), after irradiation with linearly polarized light (black curves) and after irradiation with circularly polarized light (red curves). The laser irradiation parameters were as follows: the wavelength was 532 nm, laser pulse duration 10 ns, repetition rate 10 Hz, duration of illumination 1 min, fluence 180 mJ/cm^2.

References

[1] Hentschel, Mario, et al. "Chiral plasmonics." *Science advances* 3.5 (2017): e1602735.

[2] Bosbach, J., et al. "Spectral hole burning in absorption profiles of metal nanoparticles prepared by laser assisted growth." *The European Physical Journal D-Atomic, Molecular, Optical and Plasma Physics* 16.1 (2001): 213-217

Electro-optical properties of modulators based on nematic LC composites with quantum dots

I.S.Chekulaev[1], A.D.Kurilov[1,2], R.N.Kucherov[2], A.A.Belyaev[1], V.V.Osipova[3], Y.G.Galyametdinov[3], V.V.Belyaev[1,4], D.N.Chausov[1,2]

[1]Education & Science Lab for Theoretical & Applied Nanotechnology, Moscow Region State University, Mytishi, Russia;
[2]Biophotonics Center, Prokhorov General Physics Institute of the Russian Academy of Sciences, Moscow, Russia
[3]Department of Chemistry, Kazan National Research Technological University, Kazan, Russia
[4]RUDN University, Moscow, Russia

Abstract— For to-date modulators in different laser applications electro-optical performances of liquid crystals (LC) should be enhanced. Effect of CdSe:Mn quantum dots (QD) on the dielectric, electro-optical, and rheological parameters of the ZhK-1289 LC mixture has been studied. The influence of the CdSe:Mn concentration on phase transitions, fluorescence intensity and, as a consequence, the changes in the electro-optical properties of the composite, has been investigated. According to the results obtained in this work, the best values of the physical parameters of LC composites based on QDs for applied purposes are achieved in the concentration range of 0.2-0.4 wt%.

Keywords— modulators, quantum dots, liquid-crystal mixture, electro-optical properties

I. Introduction

LC matrices with quantum dots find application in optical and display technologies and electronics. Most research in this area is focused on finding changes in a wide range of parameters depending on the different composition of nanoparticles, their size and shape [1]. At the same time, the question of finding the optimal concentration of quantum dots (QD) remains open in order to increase the efficiency of the composite based on the LC material itself by a number of parameters and to establish the nature of the concentration behavior of the system.

II. Results and Discussion

Measurements of the electro-optical and dielectric parameters of ZhK-1289 LC composites with CdSe:Mn QD were carried out in accordance with the technique [2–5].

Figure 1 shows that the anisotropy of the refractive index depends on the concentration of CdSe:Mn QD and has a maximum at moderate concentrations. The bell-shaped behavior of the anisotropy of the refractive index and dielectric permittivity can be explained by the appearance of the orientation ordering of the LC near QD. The orientational ordering of the LC near QDs also affected the thermodynamic and fluorescent properties of the composite.

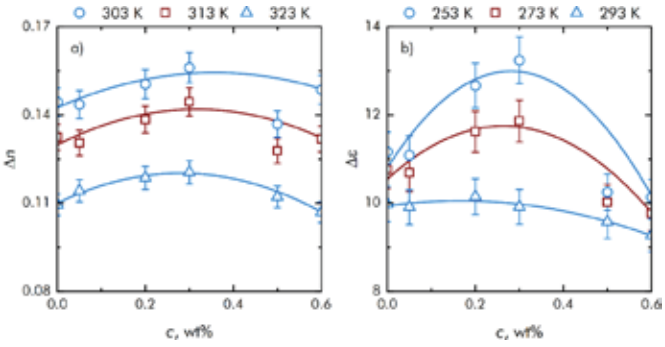

Fig. 1. Dependences of the anisotropy of the refractive index (a) and dielectric permittivity (b) on the mass fraction of CdSe:Mn quantum dots in ZhK-1289 at different temperatures.

III. Conclusions

Composites with synthesized CdSe:Mn QD based on the ZhK-1289 NLC have been obtained. It has been found that the fluorescence intensity of LC upon doping with nanoparticles depends on the QDs concentration. The range of existence of the mesophase during doping changes and has a concentration dependence. The dielectric spectroscopy of ZhK-1289 and LC composites with QD have revealed no changes in both the molecular relaxation frequency and the activation energy of this process for all synthesized samples. There is a limit concentration of QDs at which the efficiency of the LC composite is significantly increased.

Acknowledgment

The study was performed under partial support of Russian Science Foundation, project No. 20-19-00201.

References

[1] Qi, H., Kinkead, B., & Hegmann, T. (2008). In Emerging Liquid Crystal Technologies III (Vol. 6911, p. 691106). SPIE.

[2] Chausov, D. N., et al. (2020). Journal of Physics: Condensed Matter, 32(39), 395102.

[3] Chausov, D. N., et al. (2018). Opto-Electronics Review, 26(1), 44-49.

[4] Belyaev, V. V., et al. (2020). Applied Optics, 59(27), 8443-8449.

[5] Kurilov, A. D., et al. (2021). Journal of Molecular Liquids, 339, 116747.

Anisotropic Rhodium Nanoparticles for Ultraviolet Biomolecule Sensing

R.K.Soni
Department of Physics, Indian Institute of Technology Delhi, New Delhi 110016, India

***Abstract*—Transition metal rhodium exhibits surface plasmon resonance in ultraviolet. In this work, we report the synthesis of Rh nanocubes and tripod-star nanoparticles (NPs) with controlled shapes and sizes by the polyol reduction method and their plasmonic properties. The absorption spectra displayed single and broad plasmonic peak at 278 nm for nanocubes, 326 nm for concave nanocubes and 292 nm for tripods. Thin films of as-synthesized Rh NPs as surface-enhanced Raman spectroscopy substrate were prepared by self-assembly on silane treated glass substrate. The femtomolar detection limit of adenine molecules deposited on the Rh coated substrates was achieved under ultraviolet excitation at 325 nm.**

Keywords*— *Rhodium nanoparticles; UV Plasmonics; polyol synthesis; SERS.

I. Introduction

Rhodium (Rh) is a perfect metal for ultraviolet (UV) plasmonic applications with the advantages of its oxide-free nature and strong plasmon resonant modes at short wavelengths. The synthesis of shape-controlled Rh nanocrystals can offer an efficient route to optimize their plasmonic response. Shape anisotropy in nanoparticles can provide tunable localized surface plasmon resonance (LSPR) wavelengths, highly localized electric field at the tips, corners, and edges for enhancing plasmonic and surface-enhanced Raman spectroscopy (SERS) activity and selectivity. The shape of the nanostructures is controlled by the type of seed formation during nucleation and capping agent driving facet selective adsorption for further growth. Also, controlling the reaction kinetics can play a major role in controlling the seed and the final shape of the metal nanoparticles. Thus, optimizing the reaction conditions can lead to the formation of Rh nanoparticles with a wide variety of shapes [1].

II. Results and Discussion

The Rh NPs were synthesized via a modified polyol method with ethylene glycol (EG) as the polyol solvent. The synthesized Rh NPs were arranged in thin-film geometry and explored as UV-SERS substrates for label-free detection of adenine molecules. The Rh nanocubes were formed with monodispersity and size less than 10 nm. The average edge length of the Rh nanocubes was ~7±1 nm. On the other hand, controlling reaction kinetics through the hot-injection method resulted in the formation of tripods. The tripod nanoparticles maintained an arms length of ~7 nm and width ~3 nm.

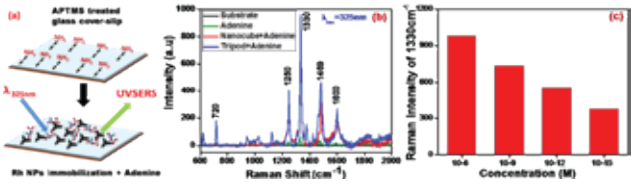

Fig. 1. (i) Schematic representation of SERS substrate preparation, (ii) SERS spectra of adenine molecules under 325 nm excitation for 10^{-9} M and (iii) SERS spectra of adenine on Rh tripod NPs for varying concentrations.

The absorption spectrum reveals a broad response with a plasmonic peak around 278 nm for nanocubes, 326 nm for concave nanocubes and 292 nm for tripods. Further, the LSPR peak red-shifts with size and curvature radius of nannocube as well as with shape alteration of Rh NPs from nanocube to tripod geometry.

Thin films of Rh NPs were prepared on silane (APTMS) treated glass substrate through a self-assembly process. Figure 1 represents SERS substrate preparation, the SERS spectra of adenine molecules adsorbed on SERS substrate with Rh NPs for 10^{-9} M and a linear dependence of SERS enhancement of adenine molecules adsorbed on tripod Rh NPs for varying concentrations. The peak at 1330 cm^{-1} dominates the spectra corresponding to C-N stretching mode of adenine. The large signal enhancement and ultrasensitive detection of adenine molecules demonstrate the high efficacy of UV-active Rh NPs SERS substrates. We observe higher SERS enhancement for analyte molecules adsorbed on tripod NPs compared to nanocube geometry. Several optical and physical factors lead to the enhanced SERS mechanism in the complex metal-molecule systems. The optical properties of metal nanocrystals are significantly modulated due to shape modification from isotropic shapes like a sphere to anisotropic nanostructures like cubes, tripods, stars with sharp corners, edges, or tips [2]. The higher amplified electromagnetic field at the tips of the tripod NPs due to the lightning rod effect serves as better SERS substrate as compared to corners of nanocube. The tripod NPs with tip-localized pronounced electric field augmentation in the nanogaps are arranged in thin-film geometry.

References

[1] S. Xie, X.Y. Liu, Y. Xia, Nano Research. **8(1)**, 82(2015).
[2] Giese, B.; McNaughton, D. J. Phys. Chem. B. **106**, 101 (2002).

Effect of ultrasonic treatment for oxide ceramics preparation with improved luminescent properties

D. Valiev, O. Khasanov, S.Stepanov, E. Dvilis, V.Paygin
School of Advanced Manufacturing technology, National Research Tomsk Polytechnic University, Tomsk, Russia

Abstract—In the present work, treatment by intense ultrasonic was used during dry pressing of an YSZ and YAG:Ce^{3+} nano- and micro- powder. The effect of the ultrasonic treatment on the structural and luminescent performances of oxide ceramics obtained by conventional sintering of the pressed compacts was studied.

Keywords— YAG:Ce, ZrO_2 ceramics; powerful ultrasonic assistance (PUA); structural and luminescent properties

I. INTRODUCTION

Oxide ceramics have found a lot of practical applications in different areas such as laser active media, solid-state lighting, detectors etc. [1]. The luminescent characteristics of phosphor ceramics are determined not only by the initial composition of the sintering components but also by the technological conditions. It is necessary to develop new approaches to the oxide ceramics preparation with improved properties. In the present work, we have used technology for YAG:Ce, ZrO_2 phosphor powder ultrasonic compaction. This approach is applied to the pressed powder material in the axial and transverse directions. Powerful ultrasonic pressing technology produces ceramics with optimum performance and improved luminous efficiency.

II. EXPERIMENTAL DETAILS

Oxide ceramics based on yttrium aluminum garnet (YAG) doped with Ce^{3+} and yttria-stabilized zirconia (YSZ) ceramics were prepared by dry compaction the common uniaxial pressing and under powerful ultrasound assistance (PUA) to the sintering process. The powder was molded using cold static uniaxial pressing in a steel press die under the simultaneous influence of ultrasonic vibrations at pressures of 400 MPa on an IP-500 AVTO automatic press (ZIPO, Russia). The power of the ultrasound waves of the master generator was 800W. Oxide ceramics sintering were performed in a high-temperature LHT 02/18 furnace (Nabertherm, Germany) in an air atmosphere at temperatures of 1400 – 1700 °C with a controlled heating and cooling rate of 200 ºC/min. Holding time at a given sintering temperature was 8 hours. The photo- and electron excitation sources was used for luminescent measurements.

III. EXPERIMENTAL DETAILS

Intense ultrasound applied during dry pressing of the YAG: Ce powder leads to an increase in the relative density and the grain size, a decrease in the pore size of the conventionally sintered YAG: Ce ceramics. The luminous efficiency of YAG:Ce^{3+} ceramics vary from 120 to 219 lm/W (no PUA) and from 120 to 250 lm/W (prepared in PUA conditions) closely related with the phase purity and implicitly with sintering temperature. During the consolidation process of YSZ ceramics using ultrasound treatment the crystal structure defects accumulation, in particular, oxygen vacancies. The oxygen vacancies concentration correlates with the integral intensity of cathodoluminescence values.

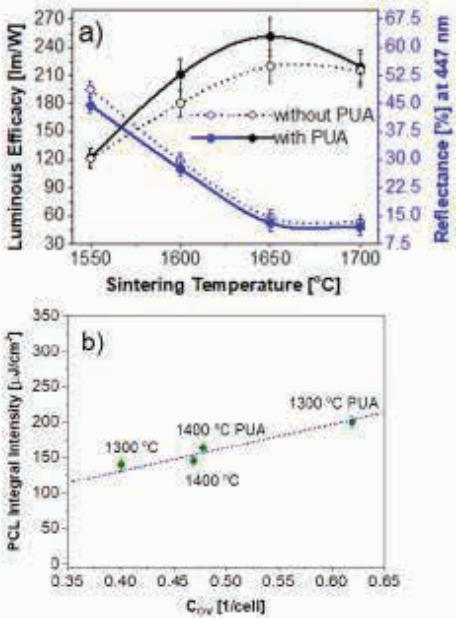

Fig. 1. Effect of PUA on luminescent properties vs. sintering temperature for YAG:Ce^{3+} (a) and concentration of oxygen vacancies of YSZ ceramics (b).

ACKNOWLEDGMENT

This work was funded by Russian Science Foundation No. 21-73-10100. The research was carried out using facilities of the CSU NMNT TPU, supported by the RF MES project #075-15-2021-710

REFERENCES

[1] L. Zhanga, B. Suna, L. Gua, W. Bua, X. Fu, R. Sun, et al.Enhanced light extraction of single-surface textured YAG:Ce transparent ceramics for high power white LEDs, Applied Surface Science vol. 455 pp. 425–432, 2018.

[2] O.L. Khasanov, E.S. Dvilis, Z.G. Bikbaeva, V.D. Paygin, A.O. Khasanov Relationship of optical properties and elastoplastic characteristics of transparent spark-plasma-sintered YSZ ceramics, J. Eur. Ceram. Soc., vol.8, pp. 161-168, 2017.

Manganese concentration effect on spectral properties of lithium-zinc-germanate glass-ceramics

E. Kulpina, A. Babkina, K. Zyryanova, N. Kuzmenko, N. Nikonorov
Research Center for Optical Materials Science, ITMO University, St. Petersburg, Russia

Abstract— The spectral properties of lithium-zinc-germanate glass-ceramics doped with different manganese content are investigated. Luminescence spectra contain two bands at 670 and 535 nm corresponding to Mn^{4+} and Mn^{2+} ions. The maximum quantum yield value of red luminescence is 47% for glass-ceramics with 0.05 mol.% MnO_2.

Keywords— lithium-zinc-germanate glass; luminescent glass-ceramics; tetravalent manganese ions; red phosphor.

I. Introduction

The main requirement for phosphors intended for use in white LED sources (w-LED) based on an ultraviolet / blue LED chip is narrow-band red luminescence. When creating such phosphors, Eu^{2+} and Mn^{4+} ions are most often used; however, the latter has an advantage due it is not rare earth element. As a luminescent center, Mn^{4+} can be successfully introduced into different systems; oxide materials are the most interesting [1].

II. Experimental details

A series of lithium-zinc-germanate glass-ceramics was synthesized by volume thermally induced crystallization of initial glasses of composition (70-x) GeO_2 - 15 Li_2O - 15 ZnO - x MnO_2, where x = 0.01; 0.025; 0.075; 0.1; 0.25 mol%. Initial glass was synthesized by melt-quenching technique at 1150°C in air atmosphere using alumina crucibles Absorption, photoluminescence spectra, decay kinetics and quantum yield (QY) were recorded. The occurrence of nanocrystalline phase in the glass bulk was revealed with XRD method.

III. Results

The absorption spectra of the initial glasses showed broad bands with maxima at 460 and 500 nm typical for Mn^{4+} and Mn^{3+}ions. The weak red luminescence of the initial glasses excited by blue light proved the occurrence of Mn ions in 4+ state. After the isothermal treatment of the initial glasses at a temperature of 560°C, according to the XRD results, Li_2ZnGeO_4 crystals precipitated in the glass matrix.

The luminescence spectra of glass-ceramics consisted of two bands with maxima at 670 and 535 nm, corresponded to Mn^{4+} and Mn^{2+} ions, respectively. For compositions with a low concentration of MnO_2, bands in red and green regions were of comparable values, while in the spectrum of compositions with high MnO_2 concentrations, the luminescence band of Mn^{4+} predominated. Fig. 1 shows the luminescence spectra of glass-ceramics with different concentrations of MnO_2. The spectra are normalized to the luminescence intensity at 670 nm. The maximum QY of red luminescence was 47% for glass-ceramics with 0.05 mol% MnO_2.

Crystalline Li_2ZnGeO_4 phosphors [2], doped with Mn, are known for intense long persistent green luminescence. Here, the same green glow was observed, but of low intensity. Since initially manganese was introduced into the glass composition in a tetravalent form, it was most advantageous for manganese ions to occupy the position of germanium ions in the crystal structure.

Time-lapse spectroscopy showed two-exponential luminescence decay at 670 nm corresponded to the $^4T_2 \rightarrow {}^4A_2$ transition in $3d^3$ ion in octahedral environment. The highest value of luminescence lifetime was 1.39 ms for glass-ceramics with 0.05 mol.% MnO_2. A decrease in the lifetime and QY with a further increase in Mn content was due to concentration quenching.

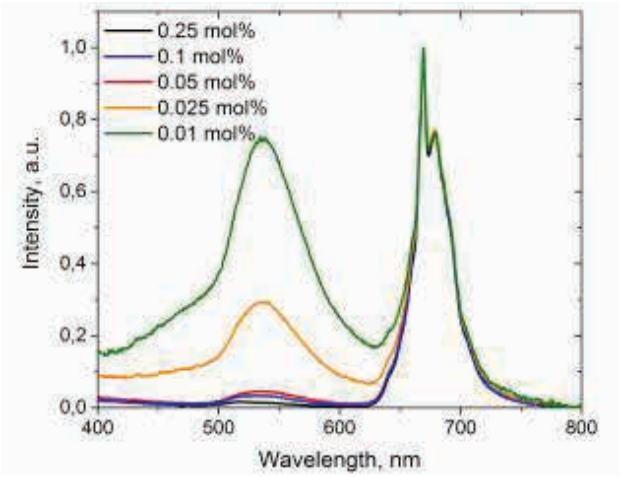

Fig. 1. Luminescence spectra of lithium-zinc-germanate glass ceramics with different MnO_2 content.

The research was funded by the grant of the President of the Russian Federation for young PhD scientists No. MK-4235.2021.1.3.

References

[1] S. Adachi, "Photoluminescence properties of Mn^{4+}-activated oxide phosphors for use in white-LED applications: A review," J. Lumin., vol. 202, pp. 263–281, May 2018.

[2] Y. Jin, Y. Hu, H. Duan, L. Chen, and X. Wang, "The long persistent luminescence properties of phosphors: Li_2ZnGeO_4 and Li_2ZnGeO_4:Mn^{2+}," RSC Adv., vol. 4, no. 22, pp. 11360–11366, 2014.

Synthesis and properties of fluorescent folate modified polymer nanoparticles

D.V. Tsyupka, E.A. Mordovina, A.A. Bakal, A.M. Abramova, I.Yu. Goryacheva

Saratov State University, SSU, Saratov, Russia

Abstract— In the last decade, great scientific interest has been focused on the development of folic acid (FA) modified nanomaterials, which is highly specific for interaction with folate cell receptors. The FA modification of existing nanoparticles is a complex multi-stage process requiring additional purification steps. Therefore, the most promising direction is to obtain the synthesis of fluorescence labels modified by FA in one stage, which can be carried out by the hydrothermal synthesis method.

Keywords— fluorescent nanoparticles, folic acid, polymer, hydrothermal treatment, fluorescent label

I. Introduction

Obtaining folic acid (FA) - based fluorescent labels has several advantages over other biological visualizers due to the ability for specific interaction with folate cell receptors [1]. The activity of folate receptors on most tumor cells is significantly higher than the corresponding values for normal cells [2]; this allows the use of the described materials to visualize cancer cells.

FA molecule consists of three parts: residues of 6-methylpterin, p-aminobenzoic acid and glutamic acid. The first of these fragments are responsible for the fluorescence properties of the FA molecule and are a biologically active component for recognition by folate receptors and specific antibodies, the rest act as internal fluorescence quenchers [3]. In turn, the joint hydrothermal treatment of FA with nitrogen- and oxygen-containing polymers can increase the fluorescence intensity, due to the introduction of additional heteroatoms and a carbon source [4].

II. Results and Discussion

In this work, various polymers (polyethylene glycol (PEG), polyethyleneimine (PEI), polyethylene glycol, and polypropylene glycol block copolymers) were used as a starting material for hydrothermal synthesis. To obtain nanostructures, hydrothermal synthesis in bidistilled water at a constant temperature of 200 °C for one hour was used.

The fluorescent properties of obtained FA-based nanostructures was studied. As a result, of the combined hydrothermal treatment of polymers with FA, an increase in the FA intrinsic fluorescence intensity occurs. The better fluorescence properties are demonstrated by PEG and PEI contained nanostructures with a polymer concentration of 10^{-3} M, whose quantum fluorescence yield is 8%, while the quantum yield for thermally treated FA solution is 2%.

When using Jeffamine to modify FA, the fluorescence intensity increases less, even though this polymer has nitrogen and oxygen heteroatoms. The maximum fluorescence quantum yield is 3% for a concentration of 10^{-2} M. With varying Jeffamine concentrations, the fluorescence intensity does not increase.

TABLE I. Quantum fluorescence yield of samples

		Polymer					
Folic acid		PEG		PEI		Jeffamine	
C, M	***QY, %***	***C, M***	***QY, %***	***C, M***	***QY, %***	***C, M***	***QY, %***
10^{-4}	2	10^{-3}	8	10^{-1}	<1	10^{-2}	3
		10^{-4}	2	10^{-2}	5	10^{-3}	2
		10^{-5}	2	10^{-3}	8	10^{-4}	2

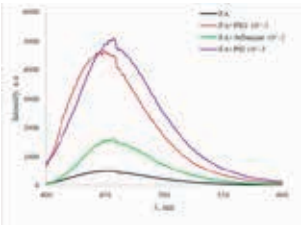

Fig. 1. Fluorescence spectra of nanostructures based on FA modified with various polymers at an excitation wavelength of 350 nm

Acknowledgment

The work supported by Russian Science foundation (project 20-13-00195)

References

[1] Bhunia, S. K., Maity, A. R., Nandi, S., Stepensky, D., & Jelinek, R.. *Imaging Cancer Cells Expressing the Folate Receptor with Carbon Dots Produced from Folic Acid.//* ChemBioChem, 2016, 17(7), 614–619.

[2] Chen C., Ke J., Zhou X.E., Yi W., Brunzelle J.S., Li J., Yong E.L., Xu H.E., Melcher K. *Structural basis for molecular recognition of folic acid by folate receptors //* Nature, 2013, 500, 7463, 486-489

[3] Tsyupka D. V., Mordovina, E. A., Sindeeva, O. A., Sapelkin, A. V., Sukhorukov, G. B., & Goryacheva, I. Y. *High-fluorescent product of folic acid photodegradation: Optical properties and cell effect* //Journal of Photochemistry and Photobiology A: Chemistry, 2021, 407, 113045.

[4] Se-Lim Kim, Hwan-Jeong Jeong and ect. Folate Receptor Targeted Imaging Using Poly (ethylene glycol)-folate: In Vitro and In Vivo Studies// J Korean Med Sci 2007; 22: 405-11.

Non-reactive metal nanoparticles embedded in organic matrix

O.V. Molodtsova [1,2], I.M. Aristova [3], D.V. Potorochin [1,2,4], S.V. Babenkov [1,5], I.I. Khodos [6], S.L. Molodtsov [2,4,7], M. Vorokhta [8], T. Skála [8], and V.Y. Aristov [1,3],

[1]Deutsches Elektronen-Synchrotron DESY, Hamburg, D-22607 Germany,
[2]University ITMO, Saint Petersburg, 197101 Russia,
[3]Institute of Solid State Physics Russian Academy of Sciences, Chernogolovka, 142432 Russia,
[4]Institut für Experimentelle Physik, Freiberg, D-09596 Germany,
[5]Institut für Physik, Johannes Gutenberg-Universität, Mainz, D-55099 Germany,
[6]Institute of Microelectronics Technology and High-Purity Materials RAS, Chernogolovka, 142432 Russia,
[7]European XFEL GmbH, Schenefeld, D-22869 Germany,
[8]Charles University, Faculty of Mathematics and Physics, Prague, 18000 Czech Republic

Abstract— The structure and morphology of nanocomposites created by nanoparticles of non-reactive metals (e.g. gold, silver), which self-assemble in/on a thin organic film of partially fluorinated copper phthalocyanine F_xCuPc (x=0; 4) depending on the amount of deposited metal, were studied in ultrahigh vacuum conditions using measurements HR-TEM and HR-PES.

Keywords— non-reactive nanoparticles, organic matrix, nanocomposite materials, Au, Ag, partially fluorinated copper phthalocyanine F_xCuPc, HR-TEM, HR-PES.

The aim of this work [1-3] is to synthesize and study the properties of nanocomposite structures created by nanoparticles of noble metals (for example, gold, silver), an interesting class of materials with unique properties that differ from both bulk and atomic behavior. Nanoparticles self-assemble in/on a thin organic film of partially fluorinated copper phthalocyanine (F_xCuPc, x=0; 4). The structure and morphology of this material, depending on the amount of deposited metal, was studied in ultrahigh vacuum by transmission electron microscopy (TEM) and photoelectron spectroscopy (PES). Metal atoms deposited on the surface of an organic substrate diffuse into the substrate, forming NPs with a narrow size distribution that correlates with the content of the deposited metal. Using high-resolution TEM [2], the distance between the atomic planes of individual silver nanoparticles was determined (Fig. 1a) and the stable collection of individual nanoparticles into agglomerates and then into nanocrystals with intercrystallite boundaries (Fig. 1b) was observed. PES revealed, on the whole, weak interaction between silver NPs and the organic matrix. However, in an organic film with small coatings of metal atoms, a strong upward bending of the band was observed. Also, we present [3] the fabrication and investigation of the properties of nanocomposite structures consisting of two-dimensional (2D) silver nano-objects self-organized on the surface of the organic molecular thin-film copper tetrafluoro-phthalocyanine ($CuPcF_4$). Metallic atoms, deposited under ultrahigh vacuum (UHV) conditions onto the organic ultrathin film, diffuse along the surface and self-assemble into a system of 2D metallic overlayers. At the same time, the majority of silver atoms diffuse into the organic matrix and self-organize into 3D nanoparticles in a well-defined manner, as shown above. The evolution of the morphology and electronic properties of silver 2D structures as a function of nominal metal content is studied under UHV conditions using also TEM, high-resolution transmission electron microscopy (HR-TEM), and PES techniques. A detailed description of the experiments can be found in [3].

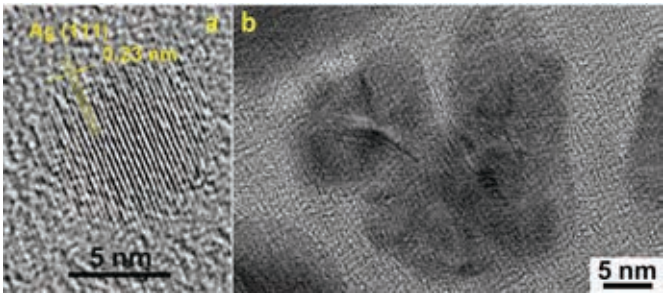

Fig. 1. HR-TEM image of single defect free silver NP surrounded with organic matrix and formed after nominal silver deposition of about 0.4 nm. (b) HR-TEM image of silver NPs observed after nominal silver deposition of about 8.5 nm. The central NP is formed as the result of coalescence of the few ones. The both images were received using JEM 2100 200 keV (JOEL, Japan).

This work was supported by the Russian Foundation for Basic Research (grant no. 20-02-00489).

REFERENCES

[1] S.V. Babenkov, O.V. Molodtsova, I.M. Aristova, M. Tchaplyguine, S.L. Molodtsov, and V.Y. Aristov, Hybrid organic-inorganic systems formed by self-assembled gold nanoparticles in $CuPcF_4$ molecular crystal, Organic electronics 32, 228 (2016), doi: 10.1016/j.orgel.2016.02.038

[2] O.V. Molodtsova, I.M. Aristova, D.V. Potorochin, S.V. Babenkov, I.I. Khodos, S.L. Molodtsov, M. Vorokhta, T. Skála, and V.Y. Aristov, Noble metal nanoparticles in organic matrix, Appl. Surf. Sci. 506, 144980 (8) (2020), doi: 10.1016/j.apsusc.2019.144980

[3] O.V. Molodtsova, I.M. Aristova, D.V. Potorochin, S.V. Babenkov, I.I. Khodos, S.L. Molodtsov, A.A. Makarova, D.A. Smirnov, and V.Yu. Aristov, 2D/3D Metallic Nano-objects Self-Organized in an Organic Molecular Thin Film, ACS Omega 5, 10441 (2020), doi: 10.1021/acsomega.0c00391

Study of In-$CuPcF_4$ nanocomposite by millisecond dynamic XPS and traditional PES and TEM

O.V. Molodtsova [1,2], I.M. Aristova [3], S.V. Babenkov [1,4], I.I. Khodos [5], D.V. Potorochin [1,2,6], S.L. Molodtsov [2,6,7], and V.Y. Aristov [1,3];

[1]Deutsches Elektronen-Synchrotron DESY, Hamburg, D-22607 Germany,
[2]University ITMO, Saint-Petersburg, 197101 Russia,
[3]Institute of Solid-State Physics, Russian Academy of Sciences, Chernogolovka, 142432 Russia,
[4]LIDYL, CEA Saclay, Gif-sur-Yvette, 91191 France,
[5]Institute of Microelectronics Technology and High-Purity Materials RAS, Chernogolovka, 142432 Russia,
[6]Institut für Experimentelle Physik, Freiberg, D-09596 Germany,
[7]European XFEL GmbH, Schenefeld, D-22869, Germany

Abstract— The electronic structure and morphology of nanocomposites created by indium nanoparticles, which self-assemble in a wide-gap $CuPcF_4$ organic semiconductor matrix depending on the amount of deposited metal, were fabricated in situ and investigated using dynamic-XPS method.

Keywords— nanoparticles, organic matrix, nanocomposite materials, In, $CuPcF_4$, dynamic XPS, HR-PES, HR-TEM.

The emergence and development of molecular electronics have drawn particular attention to molecular semiconductors, such as metal phthalocyanines. They have unique properties and are technologically advanced in the production of films. Using ultrathin films as a matrix, it is possible to create organometallic composites containing metal nanoparticles self-assembled in an organic matrix. The technologies for creating the described nanocomposites are quite simple and relatively cheap; therefore, such materials can take a prominent place in practical use in various electronic devices. However, despite the growing interest in hybrid systems, numerous questions about their properties and the processes that occur during their formation still remain unanswered. For example, interfacial phenomena can radically change the electronic properties of organic wide-gap matrices. It should also be noted that the processes of formation of organometallic interfaces in the manufacture of hybrid organo-inorganic systems proceed quickly. Therefore, the recording of experimental data in a dynamic mode could reveal additional properties of these materials that are important for electronics. Thus, Figure 1 shows the evolution of the spectra of core levels C1*s*, N1*s*, and In*3d* $_{5/2}$, recorded directly during the deposition of indium on the $CuPcF_4$ surface under ultrahigh vacuum conditions. A detailed description of the experiments can be found in [1, 2]. When creating a nanocomposite material by indium deposition on a thin film of $CuPcF_4$ organic semiconductor, the recording of photoelectron spectra in the millisecond interval allowed convincing data on the fast-flowing processes of the formation of organometallic In–$CuPcF_4$ interfaces to be obtained. Herewith, the following was established: (i) strong diffusion of indium atoms deep into the organic film was observed; (ii) no chemical interaction of In with carbon atoms of the $CuPcF_4$ molecule was found; (iii) some of the indium atoms, apparently, are located in places close to the pyrrole nitrogen of the $CuPcF_4$ molecule; (iv) during the process of the strong interaction of In atoms and pyrrole nitrogen atoms, a negative charge is transferred from indium to the $CuPcF_4$ molecule; (v) indium atoms self-organize into metal nanoparticles and clusters.

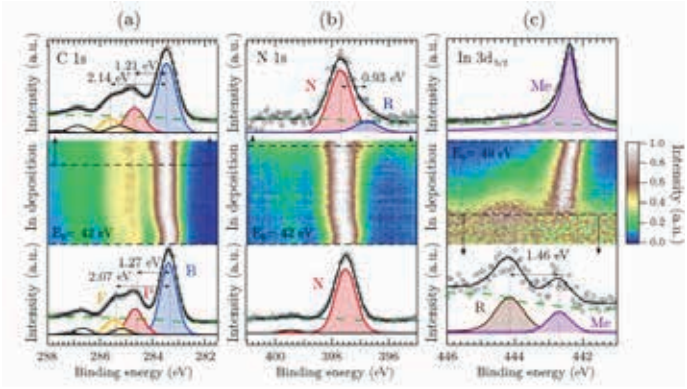

Fig. 1. Evolution of the spectra of core levels (a) C1*s*, (b) N1*s*, and (c) In*3d* $_{5/2}$ recorded in the millisecond interval directly during the deposition of indium on the $CuPcF_4$ surface under ultrahigh vacuum conditions.

This work was supported by the Russian Foundation for Basic Research (grant no. 20-02-00489).

REFERENCES

[1] O.V. Molodtsova, I.M. Aristova, D.V. Potorochin, I.I. Khodos, A. N. Chaika, S.V. Babenkov, S.L. Molodtsov, A.A. Makarova, D.A. Smirnov, and V.Y. Aristov, "In-situ study of multi-phase indium nanoparticle growth on/into CuPcF4 organic thin film in ultra-high vacuum conditions", Appl. Surf. Sci. 546, 149136 (11) (2021), doi: 10.1016/j.apsusc.2021.149136

[2] V.Yu. Aristov, O. V. Molodtsova, I.M. Aristova, S.V. Babenkov, D.V. Potorochin, S.L. Molodtsov, Study of formation and properties of In-CuPcF4 nanocomposite materials in the mode of millisecond recording of photoelectronic spectra, J. Surf. Invest.: X-Ray, Synchrotron Neutron Tech. 15 (6) 1129-1132 (2021), doi: 10.1134/S1027451021060045

Anomalous changes in the band gap of ZnO during the oxidation of zinc nanoparticles

N.B.Leonov[1], M.D.Komissarov[1], T.A.Vartanyan[1]
[1]Laboratory of Surface Photophysics, Center of Information Optical Technologies, ITMO University, St. Petersburg, Russia

Abstract— Granulated zinc metal films on fused quartz and sapphire supports were obtained via pulsed laser deposition and then oxidized in air. We found that the properties of the formed ZnO nanostructured film depend on the oxidation temperature and the nature of the film support in a complicated way. The reduced dimension of the zinc oxide nanoparticles manifests itself in the enhanced optical band gap.

Keywords— laser pulse deposition; oxidation; zinc, zinc oxide; absorbance; luminescence; thin metal film; band gap; exciton

I. INTRODUCTION

Zinc oxide (ZnO) is a semiconductor with a wide band gap Eg = 3.37 eV and relatively large exciton binding energy of 60 meV. It belongs to the group of transparent conducting oxides and is extensively used due to its unique electrophysical and optical properties [1]. Over the past few decades, the properties of ZnO have been well studied. Nevertheless, there are still unresolved questions both in the field of technologies for the preparation of substances and in the field of understanding the processes occurring in ZnO under the influence of various factors. The preparation of the ZnO samples studied in this work contains two stages: (i) pulsed laser deposition of metallic Zn in high vacuum, and (ii) thermal oxidation of the obtained Zn film in air. The purpose of this work is to study the optical properties of thin zinc oxide films obtained by this method and to relate these properties to the composition of the films.

II. RESULTS

Zinc oxide films with thicknesses of more than 7 nm, like zinc films, consist of nanoparticles in contact with each other. In the process of heating and oxidation, the shape of nanoparticles changes greatly, which can be seen from AFM topography of zinc and zinc oxide.

The XPS of oxygen and zinc show that in films oxidized at 400 and 750°C both oxygen and zinc exist in at least two states. Most of the atoms are in the "classical" Zn-O bond and have binding energies of about 529.7 and 1029.9 eV for oxygen and zinc, respectively. Since oxygen deficiency is observed in both of these films (a film oxidized at 400 °C is viewed close to the surface), it can be assumed that excess zinc atoms, being in interstices, affect the nearest oxygen atoms in such a way that the binding energy in these atoms increases. Thus, a "shoulder" is formed at the peak of oxygen and an asymmetry at the peak of zinc.

The properties of the film oxidized at 770°C dramatically change. The valence band spectrum, as well as the extinction spectrum show that the film has changed very strongly. The band gap has increased, and the absorption has sharply decreased. The luminescence has disappeared, which is not surprising: at energies of a quantum of light below 4 eV, no excitation occurs, the absorption is too small. The composition of the film also changed: oxygen deficiency changed to zinc deficiency. However, it is unlikely that only small compositional changes resulted in such changes. A significant increase in the binding energy of both zinc and oxygen suggests that the structure of the ZnO crystal has changed, it has become looser, and the interatomic distances have increased. It is obvious that this behavior of the film is somehow related to the substrate, namely, fused silica. There are no such changes on the sapphire substrate.

The observed growth of the ZnO band gap after high temperature annealing may be explained by mechanical stress and subsequent heat-affected cracking of the zinc oxide nanoparticles on the fused quartz substrate. Fused quartz is unique in possessing extremely small thermal-expansion coefficient 5×10^{-7} K^{-1}, while that of zinc oxide is 1.6×10^{-5} K^{-1}. This large, 30 times, difference in thermal expansion coefficients leads to the cracking and formation of smaller nanoparticles in the course of subsequent cooling of samples to room temperature. Smaller nanoparticles are known to possess larger band gaps as compared to the bulk materials due to quantum confinement.

So, the optical characteristics of zinc oxide films oxidized at 750°C – absorption spectra and luminescence spectra – are similar to those obtained by other authors. The absorption spectra have a pronounced "step" – the absorption edge with a narrow exciton peak. The peak of the green luminescence peak is located at wavelengths of 500 – 520 nm. According to measurements and calculations, such luminescence is caused by oxygen vacancies. In our case, the oxygen deficiency was established by analyzing the XPS. It was found that the composition of the film does not change throughout its depth, as well as the fact that the luminescence intensity depends on the concentration of oxygen vacancies. At an oxidation temperature of 770°C, the bandgap of the obtained zinc oxide nanostructures increases. As a result, absorbance maximum shifts to shorter wavelengths and greatly decreases while luminescence disappears. The XPS show that the composition of the film changes. Instead of oxygen deficiency, zinc deficiency occurs.

REFERENCES

[1] C.F. Klingshirn et al. Zinc oxide: from fundamental properties towards novel applications Springer Series in Materials Science – 2010

Effect of copper doping on the optical and electronic properties of highly ordered TiO_2 nanotubes

A.N.Morozov[1], A.S.Vasil`ev [1], Thant Zin Phyo[1], and I.A.Pochitalkina[1]
[1]Mendeleev University of Chemical Technology of Russia, Moscow, 125047 Russia

Abstract— The effect of copper doping on the optical and electronic properties of highly ordered hexagonal arrays of TiO_2 nanotubes (NTs) has been studied. It was shown that heterovalent cationic doping of TiO_2 NTs with copper ions leads to the appearance of absorption bands in the visible region of the spectrum due to the formation of additional electronic levels near the conduction and valence bands.

Keywords — titanium oxide, doping, copper, highly ordered films, nanotubes, anodization, optical properties, electronic properties

I. Introduction

Highly ordered titanium dioxide nanotube films obtained by the anodization of titanium metal, are among the most promising photoactive materials. Therefore, the development of optical and electronic property control methods for such materials is a necessary and relevant area of research [1].

II. EXPERIMENTAL

Samples of copper-doped highly ordered arrays of titanium dioxide nanotubes were obtained using electrolytic and solvothermal methods [2]. TiO_2 NTs samples with different copper contents were obtained by varying the solvothermal process temperature from 80 to 180°C. The doping process in all experiments was carried out for 1 hour.

III. RESULT AND DISCUSSION

To study the influence of the copper content on the optical and electronic properties of TiO_2 NTs, samples with different copper contents varying from 0 to 3.76 wt % were obtained. By using SEM and TEM, it was found that the newly developed doping procedure does not lead to a change in the highly ordered structure of TiO_2 NT films. Micrographs of the typical morphology of copper-doped TiO_2 NTs are shown in Fig. 1. It can be seen that the films have a high degree of self-organization, and no particles are formed on the surface of the TiO_2 NTs.

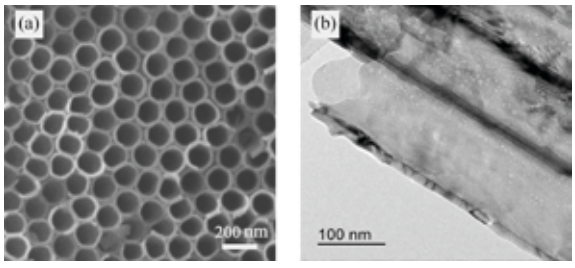

Fig. 1. Micrographs of copper-doped TiO_2 NTs

The incorporation of copper into the TiO_2 crystal structure was confirmed by XRD and Raman spectroscopy. The study of changes in the optical properties of TiO_2 NTs upon the incorporation of various amounts of copper ions was carried out using UV-VIS DRS (Fig. 2).

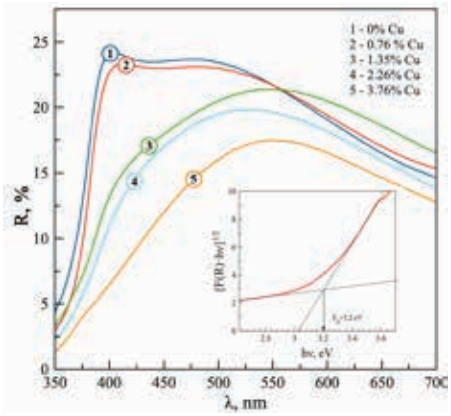

Fig. 2. UV-vis diffuse reflection spectra of the obtained samples

It can be seen that the doping of TiO_2 NTs with copper leads to a significant change in their absorption spectra in the UV and visible range of the solar spectrum. With an increase in the copper content in TiO_2 NT samples, a significant increase in the absorption of light quanta with a wavelength of 400–600 nm is observed. The analysis of the diffuse absorption spectra (Fig. 2) showed that the inclusion of copper does not lead to a change in the titanium dioxide band gap width. It has been established that the appearance of absorption bands in the visible range is associated with the appearance of additional electronic levels near the conduction and valence bands without a change in their position. It has been proven that heterovalent cationic doping of TiO_2 NTs with copper leads to the formation of a large number of oxygen vacancies, which explains the change in the shape of their absorption front (Fig. 2).

Acknowledgment

The authors are grateful to the staff of the Center for Collective Use for studying the samples by the SEM.

References

[1] J. Schneider, M. Matsuoka, M. Takeuchi et al., “Understanding TiO_2 Photocatalysis: Mechanisms and Materials,” Chem. Rev., 2014, V.114, pp. 9919-9986.

[2] A. N. Morozov, Thant Zin Phyo, A. S. Vasil’ev, P. I. Ivanov, A. A. Averin, “Morphology and optical properties of spatially-ordered copper- and fluorine-doped titanium-dioxide films,” Glass and Ceramics, 2020, V.77, №5-6, pp. 231-235

The study is funded by a grant Russian Science Foundation (project No. 19-73-00192)

MBE growth and optical properties of InAs quantum dots in Si

I.Ilkiv[1], V. Lendyashova [2], V.Talalaev[1], B.Borodin[3], D.Mokhov[2], R. Reznik[1], G.Cirlin[2,4]
[1]St. Petersburg State University, St. Petersburg 199034, Russia
[2]Alferov University, St. Petersburg 194021, Russia
[3]Ioffe Institute, St. Petersburg 194021, Russia
[4]Institute for Analytical Instrumentation of the RAS, St. Petersburg, 190103, Russia

Abstract - Fabrication of nanocomposite materials consisting of III–V quantum dots (QDs) embedded in silicon (Si) sustained special attention over years. In this work, we present the formation of InAs QD in Si matrix by molecular beam epitaxy and the study of optical properties.

Keywords— quantum dots, silicon, molecular beam epitaxy

I. Introduction

Monolithic integration of III–V compound materials on silicon platform attracts intense research interest over years due to the promising applications of Si-based photonic integrated circuits. Various strategies, including the growth of the thick buffer with several filter layers, different variations of selective area growth, the utilizing of Si substrates with a 4–6° offcut towards the [110] direction, confined epitaxial lateral overgrowth, as well as migration-enhanced epitaxy growth have been proposed to direct growth of III-V layers on Si. However, the buffer layer cost and process complexity on large-area silicon substrates are still challenging issues. In turn, one-dimensional QDs are well known to be relatively tolerant of defects due to the effective strain relaxation, wherein the strong carrier localization effect in QDs can enhance the quantum efficiency significantly. Therefore, the direct growth III-V QDs on Si with subsequent embedding into silicon matrix is of great interest. Here we report on studies on fabrication of InAs QDs in Si matrix by molecular beam epitaxy.

II. Experiment

Growth experiments were carried out on Si(100)4° using 21EB200 Riber MBE system equipped with solid-state As, In effusion cells and e-beam evaporator for deposition of Si. Prior to growth wet chemical processing followed with degasing and annealing step at 950°C were performed to achieved atomically-clean Si(100) 2x1 surface. Afterwards, temperature was decreased to 600°C and 50 nm Si buffer layer was formed. Then, self-assembled growth of InAs QDs was carried out at 400C. The amount of InAs being deposited onto Si surface corresponded to equivalent film thickness of 0.7-3 monolayer (ML). Further, QDs morphological characterization was carried out by atomic force microscopy (AFM). Optical properties of InAs QDs additionally capped with 30 nm Si layer were investigated using low-temperature photoluminescence (PL) spectroscopy.

Authors gratefully acknowledge financial support of the research grant of St. Petersburg State University No. 75746688.

III. Results and conclusions

We first probed the formation of using by reflection high-energy electron diffraction (RHEED). Formation of InAs QDs was observed by changing the RHEED pattern from streaky to spotty typically after the ~0.7 ML InAs deposition. The AFM investigation revealed the formation of circular QDs with diameter of about 100 nm, 15 nm height and density of $2 \cdot 10^9$ cm^{-2}. The increase in InAs thickness to 3 ML led to increasing in the QD diameter and height up to 120 nm and 23 nm, correspondingly. Low-temperature (10K) PL study of 0.7 Ml InAs QDs capped with 30 nm Si layer revealed band emission at 1.6 µm region (Fig. 1). In turn, InAs QDs with bigger sizes showed no light emission, which is apparently connected with the formation of misfit dislocations.

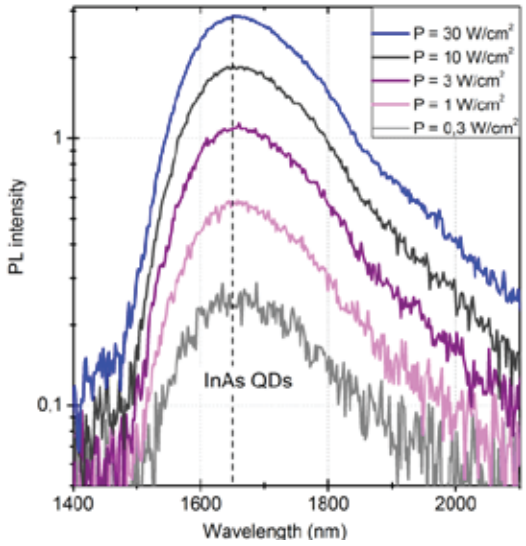

Fig. 1. PL spectra of InAs QDs as a function of excitation power density.

Acknowledgment

This work has been supported by the grant of St. Petersburg State University No. 75746688. The samples were grown under the support of the Ministry of Science and Higher Education of the Russian Federation (0791-2020-0003).

Effective charge transfer within 2D layered nanostructures of PbSe-MoS_2 colloidal nanoplatelets

I.D. Skurlov, P.S. Parfenov, A.V. Sokolova, D.A. Tatarinov, A.A. Babaev, M.A. Baranov, A.P. Litvin,
Center of Informational Optical Technologies, ITMO University, Saint-Petersburg, Russia

Abstract— We report the creation of layered 2D PbSe-MoS2 nanostructures which demostrate efficient electron transfer from PbSe nanoplatelet to MoS2 nanoplatelet. Charge transfer was confirmed by means of Results of the work show that ultrathin layers of transition metal dichalcogenides sensitized by 2D lead chalcogenide nanostructures can be effectively used in photodetectors with a spectral sensitivity extended to the near-IR range.

Keywords— nanoplatelets; transitional metal dichalcogenides; lead selenide, molybdenum disulfide, charge transfer

I. Introduction

Mono or a few-layered transition metal dichalcogenides (TMD) high charge carrier mobility as well as high absorption in the visible range makes them a promising candidate for a photodetection applications. To extend the sensitivity of photodetectors based on TMD to the near IR range sensitizers are often used [1]. One of the promising IR-sensitizers is colloidal lead chalcogenide nanoplatelets (NP). Their unique geometry and high absorption coefficients in the NIR makes them an efficient absorber of the optical radiation and an energy and/or charge donor for more conducting layer [2].

In this work we present the layered structures made from colloidal PbSe nanoplatelets and colloidal MoS_2 NP. We show that the sensitization of MoS2 layers by PbSe NP leads to quenching of PbSe photoluminescence and an increase in the photoresponse when the system is excited by near-IR radiation.

II. Results

Charge transfer between nanoplatelets in a layered structure is possible while distance between nanoplatelets is minimal. Therefore, it is necessary to replace the original long ligand shell of oleic acid molecules with shorter ligands. For this purpose, we employed colloidal exchange with 3-mercaptoropionic acid as well as solid-state post-deposition exchange with ethanedithiol.

To assess the charge transfer we compared photoluminescence spectra and decay kinetics of PbSe and PbSe-MoS_2 complex with excitation at 532 nm (where MoS_2 absorbs) and at 1064 nm (where only PbSe absorbs). Fig. 1 displays absorption normalized spectra and decay curves for 1064 nm excitation. It is clearly seen that PL intensity decreases with the addition of MoS_2 layer, which is accompanied by a reduction in PL decay lifetime. This points out for a presence of an additional recombination channel which we attribute to the charge transfer to MoS_2 layer. In addition we have calculated the efficiency of PL quenching, which was found to be higher than

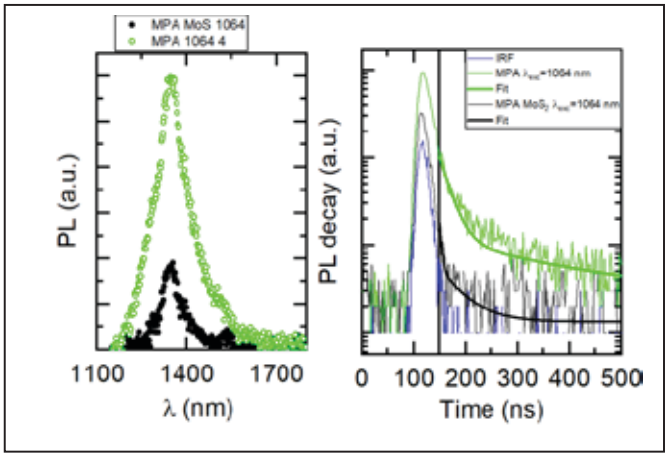

Fig. 1. PL spectra (left) and decay curves (right) of PbSe-MoS_2 layered structure under 1064 nm excitation.

0.5 for each combination of PbSe NP ligand shell and excitation wavelength, and increases for 0.7 and more for 532 nm excitation.

Due to the absence of absorption of MoS2 in the infrared range, it does not react to IR radiation. Photoinduced charge transfer should lead to a photoresponse of the layered structure to infrared radiation. To prove that we performed photo-conductivity measurement with 1050 nm irradiation. Indeed, we observed an increase in the current for the layered structures of PbSe and MoS2 nanoplates, while for the MoS2 layer, the current remains at the same level, irrespective of irradiation. It should be noted that the absolute values of the current strength after the deposition of the layer of PbSe nanoplates decrease, which is probably a consequence of damage to the MoS2 layer during deposition and is still a problem that remains to be solved to employ such structures as an active layer in photodetectors.

Acknowledgments

This work was supported by Russian Foundation for Basic Research, project №20-32-90208

References

[1] C. Mu, J. Xiang, and Z. Liu, "Photodetectors based on sensitized two-dimensional transition metal dichalcogenides—A review," *Journal of Materials Research*, vol. 32, no. 22, pp. 4115–4131, Nov. 2017, doi: 10.1557/jmr.2017.402.

[2] B. Guzelturk and H. V. Demir, "Near-Field Energy Transfer Using Nanoemitters For Optoelectronics," *Advanced Functional Materials*, vol. 26, no. 45, pp. 8158–8177, Dec. 2016, doi: 10.1002/adfm.201603311.

Colloidal magnetic photonic crystals: synthesis and modification*

A.S. Drozdov[1,2], Y. A. Andreeva[2]
[1]Laboratory of Nanotechnologies , Moscow Institute of Physics and Thechnology, Dolgoprudny, Moscow Region, Russia.
[2]SCAMT Institute, ITMO University, Saint Petersburg, Russia

***Abstract*—Colloidal magnetic photonic crystals are an emerging class of responsive colloidal systems with unique variable optical properties. Here we describe a novel example of polyelectrolyte-based magnetic photonic crystals produced by layer-by-layer adsorption of polymeric molecules onto magnetite cores producing particles with a mean diameter of 180 nm. The surface of the synthesized particles was modified by *in situ* polymerization of dopamine derivatives.**

***Index Terms*—magnetic photonic crystals, surface modification, polydopamine**

Magnetically-responsive nanosystems are among the most rapidly developing topics in modern nanotechnology and nanoscience. Susceptibility of such systems to external physical stimuli dictates their protectiveness in various areas of applications ranging from electronics and microfluidics to optics and biomedicine. One of such systems are colloidal magnetic photonic crystals which are the colloids that form chain-like structures with regular interparticle spacing so that the system strongly diffracts light, and the diffraction wavelength can be tuned across the entire visible spectrum by simply changing the strength of the magnetic field. Typical synthetic procedures leading to magnetic photonic colloids are based on autoclave conditions using ethylene glycol or diethylene glycol as solvents, which may potentially limit the application of such systems due to the high toxicity of the solvents and used reagents [1], [2]. To overcome this issue soft chemistry approaches may be utilized.

Recently we have developed a new green and convenient synthetic approach to the synthesis of magnetic colloidal aggregates based on multi-step procedure [3], [4]. The synthetic protocol involved the synthesis of magnetite from a non-stochiometric mixture of Fe^{2+} and Fe^{3+} by co-precipitation procedure with a subsequent washing to neutral pH level and ultrasonication giving stable hydrosols of nanoparticles with a diameter of 50-60 nm and zeta potential values up to +34 mV at pH 7. Neutral pH level and absence of any surfactants or pepticizers made the synthesized colloids an ideal candidate for further synthetic applications. The magnetic colloid was destabilized in a controlled manner by the addition of varying amounts of citric acid and glycerol, leading to partial aggregation of nanoparticles into magnetic clusters Fig. 1a, . It was found that the size of the produced aggregates could be tuned in the range 40-650 nm, and the value of zeta potential from +30 mV to 43 mV, by changing the ratio of reagents [5]. Due to excellent colloidal stability, high magnetization value, and low size polydispersity the colloid solution of the synthesized particles demonstrated the properties of magnetic photon liquids and showed a blue-shift of its reflection maximum from 720 nm to 445 nm upon application of magnetic fields from 200 G to 680 G Fig. 1. The surface of the synthesized clusters can be modified with a variety of molecules by biomimetic strategy and *in situ* polymerization of dopamine derivatives. Thus, modification of the surface with dopamine-CY7 conjugate rendered the produced clusters fluorescent with a peak of emission at 780 nm. The synthesized systems can find their application in biomedicine for targeted drug delivery or *in vitro* analysis.

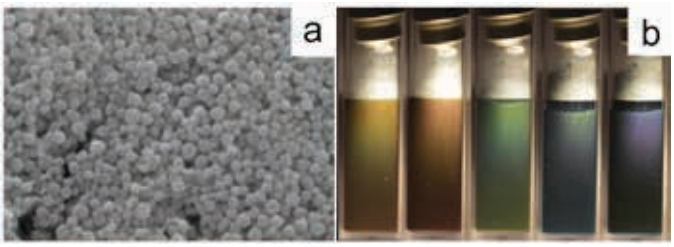

Fig. 1. a: SEM image of the magnetic clusters; b: visual appearance of the colloid under the influence of magnetic field varied from 200 to 650 G.

This work was supported by the Russian Science Foundation, grant No. 20-73-00001.

REFERENCES

[1] Ge, Jianping, and Yadong Yin. "Magnetically responsive colloidal photonic crystals." J. Mat. Chem. vol. 18, 2008: pp. 5041-5045.
[2] Wang, Hui, et al. "Size-and solvent-dependent magnetically responsive optical diffraction of carbon-encapsulated superparamagnetic colloidal photonic crystals." J. Phys. Chem. C vol. 115, 2011,: pp. 11427-11434.
[3] Dikansky, Yury I., et al. "Temperature Dependences of the Magnetic Susceptibility of Water-Based Magnetic Fluids." J. Nanofluids vol. 9, 2020,: pp. 90-97.
[4] Anastasova, Elizaveta I., et al. "Magnetically-assisted synthesis of porous sol-gel magnetite matrices with structural anisotropy." J. Magn. Magn. Mater. vol. 503, 2020.: pp. 166619.
[5] Andreeva, Yulia I., et al. "The controllable destabilization route for synthesis of low cytotoxic magnetic nanospheres with photonic response." Sci. Rep. vol. 7, 2017.: pp. 1-9.
[6] Andreeva, Y. I., et al. "Polyelectrolyte-based magnetic photonic crystals with anticoagulant activity." Mater. Today Chem., vol. 17, 2020: pp. 100292.

Plasmon Structures on Gold Surface Induced by Femtosecond Laser Radiation

A.V. Tcibulnikova [1], A.A.Khankaev[1], V.V.Bryukhanov[1],I.G.Samusev[1], I.I.Lyatun[1], V.A.Slezhkin[2],
[1]REC "Fundamental and applied photonics. Nanophotonics", Immanuel Kant Baltic Federal University, IKBFU, Kaliningrad, Russia
[2]Kaliningrad State Technical University, KSTU, Kaliningrad, Russia

Abstract— the method of femtosecond laser structuring of the gold surface is presented in order to study the morphological features of the formed structures, as well as the plasmonic-optical properties.

Keywords— LIPSS; plasmon resosnance; gold

I. INTRODUCTION

LIPSS, laser-induced periodic surface structures, is a surface morphology formed as a result of exposure to short-pulse laser radiation (from several fs to hundreds of ns).

LIPSS is an easily reproducible, commercially profitable way to change the surface properties.

The presented work shows a method of structuring the surface of a thin film of gold fs laser exposure in order to study the optical properties of the obtained structures by ellipsometry methods. Also the dependence of the influence of laser radiation parameters on the formation of surface structures is investigated. By the method of scanning electron microscopy the size and shape of the surface structures were evaluated.

II. EXPERIMENT RESULTS

Laser structuring of the surface was performed using the Theta-25 laser unit (Avesta, Russia). Structuring parameters are presented in Table 1. The surface was displaced relative to a motorized positioner 8 MTF-102LS05 (Standa, Lithuania). The sample was displaced perpendicularly to the vector of p-polarization of the laser beam at a relative velocity of 500 μm/s.

The results of scanning electron microscopy of the gold surface are shown in Figure 1. The result of surface structuring is the formation of laser-induced periodic surface structures on the width of the order of 30 microns. It is shown that the structures are homogeneous in width, their cross-sectional size is 300 nm, however, it is worth noting that due to the initial heterogeneity of the surface craters were also formed, shown in Fig. 1.a. The surface of LIPSS is covered with nanometer gold particles, formed as a result of ablation and resuspension of material, which is seen in Figure 1.b.

TABLE I. LASER STRUCTURING PARAMETERS

Wavelength λ, nm	*Pulse duration τ, фс*	*Pulse repetition rate f, кГц*	*Processing speed v, μm/s*
1030	230	25	500

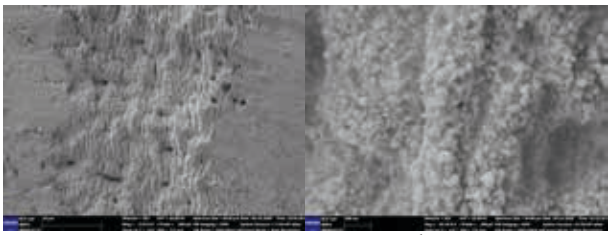

a b

Fig. 1. SEM-images of structured gold surface

A further goal of the study is to investigate the plasmonic-optical properties of the surface by ellipsometry in order to determine the absorption regions of the material, to determine the possibility of generating surface plasmon resonance when exposed to electromagnetic radiation by analyzing the spectra of the dielectric permittivity and reflection of the surface. .

ACKNOWLEDGMENT

This work was carried out within the framework of the project supported by the Ministry of Science and Higher Education of the Russian Federation No. FZWM-2020-0003.

Diffraction and selective properties of one-dimensional and two-dimensional periodic structures in a wide range of angles of incidence

P.P.Sokolov[1], N.D. Vorzobova[1]
[1]Faculty of Photonics, ITMO University, St. Petesburg, Russia
Sokol7858@yandex.ru

Abstract — The diffraction and selective properties of various types of periodic nanostructures in promising photopolymer materials at radiation incidence in a wide range of angles are presented for the creation on their basis of effective deflectors and laser beam splitters, as well as diffractive elements for solar energy.

Keywords—periodic nanostructures, diffraction efficiency, angular selectivity

In previous years, interest in volume holographic gratings was determined by their high angular and spectral selectivity and the possibility of using them as selective elements of laser systems. In recent years, problems have emerged that require a combination of high diffraction properties with a wide range of incident angles. In this work, we present the results of experimental studies of the diffraction and selective properties of various types of nanostructures - one-dimensional volume non-slanted and slanted gratings, hybrid structures, as well as two-dimensional gratings in promising photopolymer materials, with radiation incidence in a wide range of angles in three-dimensional space, which are of interest for solving practical problems of diffractive optics and solar energy.

Transmitting structures were recorded by the holographic method using helium-neon, helium-cadmium and DPSS lasers with wavelengths of 0.63, 0.44, and 0.53 μm. The diffraction efficiency (DE) was determined at a wavelength of 0.65 nm.

The following new regularities and properties are revealed. For volume non-slanted and slanted gratings, when radiation is incident in the Bragg plane, the maximum diffraction efficiency (about 80%) remains in a wide range of angles - about 80°. In contrast to volume gratings for slanted gratings, Bragg planes are located on one side of the normal to surface. With a deviation from the Bragg plane, a shift in the position of the DE maxima towards large angles - up to 70° is observed (Fig.1), while the contours of the angular selectivity remain rather wide It is shown that there are directions of radiation incidence on the grating, different from the classical Bragg direction and corresponding to the oblique transmission of radiation through the grating structure, providing the maximum diffraction efficiency. For hybrid structures - volume gratings, on the surface of which relief gratings are formed, the conditions for obtaining a surface relief corresponding to the maximum DE, the mechanism of relief formation, as well as the contribution of the relief component to the diffraction properties of the hybrid structure are determined. An advantage in the angular range (for β angles) compared to volume gratings is revealed.

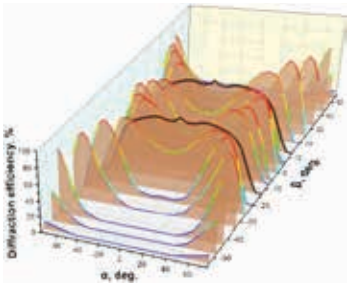

Fig. 1. Dependence of the diffraction efficiency of a non-slanted volume grating on the angles α and β.

For two-dimensional periodic structures obtained by sequential recording of one-dimensional volume structures, the optimal recording conditions and regularities of DE change in the main diffraction orders are determined with changing angles of radiation incidence over a wide range.

The revealed diffraction and selective properties of the structures determine the possibility of obtaining effective deflectors, as well as multichannel controlled laser beam splitters, which make it possible to change the radiation intensity in the channels without imposing high requirements for their positioning. The established properties of the structures are also of great interest for solving problems of solar energy - obtaining effective diffractive deflectors that redirect solar radiation in a wide range of angles in one direction with the advantages of expansion of the angular range compared to existing solutions[1-3], including the possibility of obtaining a high DE and the use of solar radiation at large angles of incidence and the possibility of excluding complex technical solutions based on the use of stacked volume gratings.

REFERENCES

[1] Akbari, H.; Naydenova, I.; Martin, S. Using acrylamide-based photopolymers for fabrication of holographic optical elements in solar energy applications. Appl. Opt. **2014**, 53, 1343–1363.

[2] Pen, E.F. Energy Efficiency of Photovoltaic Panels when Using Holographic Gratings as Passive Solar Trackers. Optoelectron.Instrum. Data Process. **2019**, 55, 271–279.

[3] Keshri, S.; Marín-Sáez, J.; Naydenova, I.; Murphy, K.; Atencia, J.; Chemisana, D.; Garner, S.; Collados, M.V.; Martin, S. Stacked volume holographic gratings for extending the operational wavelength range in LED and solar applications. Appl. Opt. **2020**, 59,2569–2579.

Synthesis of silver iodide and copper oxide nanowires in nanoporous glasses for photocatalytic water splitting

P.A.Bezrukov[1], A.I.Sidorov [1], N.V.Nikonorov[1]
[1] ITMO University, Saint-Petersburg, Russian Federation
[2] Saint-Petersburg Electrotechnical University "LETI", Saint-Petersburg, Russian Federation

Abstract— Methods of silver iodide and copper oxide nanowires in nanoporous glasses synthesis are described. Methods consist in electrolysis of metal salts in nanoporous glasses with interconnecting pores, with the following iodizing or oxidizing of metal nanowires. The transformation of metal nanowires can be carried out as fully, or partially. The cross-section of synthesized semiconductor nanowires is less than 25 nm. Optical properties of synthesized semiconductor nanowires are presented. It is shown that silver iodide nanowires possess luminescence in visible spectral range and phase transition. The synthesized nanocomposites can be used for photocatalytic water splitting for hydrogen generation

Keywords— silver iodide; copper oxide; nanowires; nanoporous glasses; photocatalytic; water splitting; luminescence.

This work was financially supported by Russian Science Foundation (Project № 20-19-00559).

Investigation of the characteristics of a microresonator with carbon nanotubes deposited on its surface

I.K.Gorelov[1], A.A.Mkrtchan[2], A.E.Shitikov[1], V.E.Lobanov[1], I.A.Bilenko[1]

[1]Russian Quantum Center, Skolkovo, Russia
[2]Skolkovo Institute of Science and Technology, Skolkovo, Russia

Abstract - Nonlinearity of carbon nanotubes significantly exceeds nonlinearity of the materials of crystal. Deposition of carbon nanotubes to the surface of the microresonator may enhance its nonlinearity. In this paper, the characteristics of high-quality factor microresonators with whispering gallery modes with single walled carbon nanotubes deposited on the surface are experimentally investigated.

Keywords— microresonator, laser, carbon nanotubes, whispering gallery modes

High-quality optical dielectric resonators with whispering gallery modes (WGM) are widely used at present, both for conducting fundamental research and for creating advanced radiophotonic devices. Their advantages are small dimensions (from tens of microns to several millimeters), Q-factor reaching values of 10^11, multimode structure, high concentration of the field in a small volume and, as a consequence, low thresholds for observing nonlinear effects. This allows to create narrow-line lasers, radiophotonic microwave generators, narrow-band optical filters, high-speed modulators based on them.

One of the promising areas of research is the use of nanomaterials to improve the characteristics of microresonators [1, 2]. Promising nanomaterials are single-walled carbon nanotubes (SWCNTs), since their nonlinearity significantly exceeds the nonlinearity of materials of microresonators and waveguides. The coefficient of cubic nonlinearity of SWCNT is 10^{-12}-10^{-13} m^2/W, which is 7 orders of magnitude higher than the nonlinearity of MgF2 – 10^{-20} m^2/W. SWCNT can be transferred to the surface of both crystalline and integrated microresonators.

The purpose of this work is an experimental study of the characteristics of the microresonator after the application of SWCNT, in particular, the quality factor and the nonlinearity coefficient of the resulting hybrid structure. The experiment used a crystalline microresonator made of MgF2, with Q= 6*10^8, and carbon nanotubes, with a semiconductor interband transition at 1550 nm. The thickness of the SWCNTs was 4 nm, and the coating area was 2x2 mm^2.

The application of SWCNT took place without the use of special devices: a nitrocellulose film with nanotubes was brought to the resonator, pressed to the side surface of the resonator, then it was moistened with acetone, after which the nanotubes moved from the filter to the resonator. Immediately after the above procedure, the Q-factor of the resonator deteriorated to Q=3*10^5. Further, cleaning was carried out, which does not damage the surface of the resonator and the nanotube film from the remnants of the nitrocellulose filter. The resonator was washed with acetone, isopropanol, distilled water, followed by blowing the resonator with nitrogen. After all the stages of purification, the Q-factor of a pure resonator with nanotubes was measured: Q=10^7. Further, the nanotubes were removed from the side surface of the resonator with lint-free wipes moistened with isopropanol. The measured Q-factor after this procedure was Q= 6*10^8, which coincided with the Q-factor value before the nanotube film was applied.

As a result of this study, a technique for applying SWCNTs to a crystalline microresonator was developed, a technique for cleaning the resonator after applying nanotubes, the lower limit of the Q-factor of the resonator with nanotubes was determined and it was shown that after removing the nanotubes, the Q-factor of the resonator is restored.

The work is supported by the Russian Science Foundation (Project No. 20-12-00344).

References

[1] Tomoki S. L., et al, "Design of a passively mode-locking whispering-gallery-mode microlaser," J. Opt. Soc. Am. B 38, 3172-3178 (2021).

[2] Yamashita S., "Nonlinear optics in carbon nanotube, graphene, and related 2D materials." Apl Photonics 4.3, 034301 (2019).

[3] Nasibulin A. G., et al. "Multifunctional free-standing single-walled carbon nanotube films." *ACS nano* 5.4: 3214-3221 (2011).

[4] Gladush Y., et al. "Ionic liquid gated carbon nanotube saturable absorber for switchable pulse generation." *Nano letters* 19.9: 5836-5843 (2019).

[5] Kondratiev N. M. et al. Self-injection locking of alaser diode to a high-q wgm microresonator. OpticsExpress, (2017).

[6] Shitikov, A. E., et al. "Microresonator and Laser Parameter Definition via Self-Injection Locking." *Physical Review Applied* 14.6: 064047 (2020).